AD-A031 361 MASSACHUSETTS INST OF TECH CAMBRIDGE AEROELASTIC AND--ETC F/G 20/11
USE OF THE HYBRID-STRESS FINITE-ELEMENT MODEL FOR THE STATIC AN--ETC(U)
SEP 76 R L SPILKER, O ORRINGER, E A WITMER DAAG46-75-C-0055

UNCLASSIFIED ASRL-TR-181-2 AMMRC-CTR-76-29 NL

1 OF 3
AD A031361

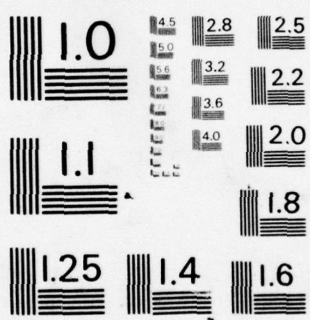

MICROCOPY RESOLUTION TEST CHART
NATIONAL BUREAU OF STANDARDS-1963-A

2

FC

AD

AMMRC CTR 76-29
ASRL TR 181-2

USE OF THE HYBRID-STRESS FINITE-ELEMENT MODEL FOR THE STATIC AND DYNAMIC ANALYSIS OF MULTILAYER COMPOSITE PLATES AND SHELLS

September 1976

Robert L. Spilker
Oscar Orringer
Emmett A. Witmer
Samuel Verbiese
Susan E. French
Alex Harris

Aeroelastic and Structures Research Laboratory
Department of Aeronautics and Astronautics
Massachusetts Institute of Technology
Cambridge, Massachusetts 02139

FINAL REPORT CONTRACT NUMBER DAAG46-75-C-0055

Prepared for
ARMY MATERIALS AND MECHANICS RESEARCH CENTER
Watertown, Massachusetts 02172

UNCLASSIFIED

SECURITY CLASSIFICATION OF THIS PAGE (When Data Entered)

(19) REPORT DOCUMENTATION PAGE		READ INSTRUCTIONS BEFORE COMPLETING FORM
1. REPORT NUMBER (18) AMMRC CTR-76-29	2. GOVT ACCESSION NO.	3. RECIPIENT'S CATALOG NUMBER
4. TITLE (and Subtitle) (6) USE OF THE HYBRID-STRESS FINITE-ELEMENT MODEL FOR THE STATIC AND DYNAMIC ANALYSIS OF MULTILAYER COMPOSITE PLATES AND SHELLS.		5. TYPE OF REPORT & PERIOD COVERED (9) Final Report.
		6. PERFORMING ORG. REPORT NUMBER (14) ASRL-TR-181-2
7. AUTHOR(s) (10) Robert L. Spilker, Oscar Orringer, Emmett A. Witmer, Samuel Verbiese, Susan E. French, Alex Harris		8. CONTRACT OR GRANT NUMBER(s) (15) DAAG46-75-C-0055 NEW
9. PERFORMING ORGANIZATION NAME AND ADDRESS Aeroelastic and Structures Research Laboratory, Department of Aeronautics and Astronautics, Massachusetts Institute of Technology, Cambridge, Massachusetts 02139		10. PROGRAM ELEMENT, PROJECT, TASK AREA & WORK UNIT NUMBERS D/A Proj. 1W362306AH72 AMCMS Code: 632306.11.117200
11. CONTROLLING OFFICE NAME AND ADDRESS Army Materials and Mechanics Research Center, Watertown, Massachusetts 02172		12. REPORT DATE (11) September 1976
		13. NUMBER OF PAGES 214
14. MONITORING AGENCY NAME & ADDRESS (if different from Controlling Office) (12) 220p.		15. SECURITY CLASS. (of this report) Unclassified
		15a. DECLASSIFICATION/DOWNGRADING SCHEDULE

16. DISTRIBUTION STATEMENT (of this Report)

Approved for public release; distribution unlimited.

(16) DA-1-W-362306-AH-72

17. DISTRIBUTION STATEMENT (of the abstract entered in Block 20, if different from Report)

18. SUPPLEMENTARY NOTES

19. KEY WORDS (Continue on reverse side if necessary and identify by block number)

Finite-element method
Static response
Dynamic response
Elastic behavior
Structural mechanics
Stress analysis
Laminated plates
Fiber composites
Shell structures

20. ABSTRACT (Continue on reverse side if necessary and identify by block number)

This report presents the results of an investigation into the formulation and application of assumed-stress hybrid finite-elements for bending of multi-layer laminated plates and shells. Two families of hybrid-stress-based multi-layer plate elements are considered; these elements are denoted as thick plate and moderately-thick plate elements. In the development of the thick plate elements, transverse shear deformation effects are included by allowing lines normal to the plate midsurface in the undeformed state to be piecewise linear from layer to layer in the deformed state. Transverse shear deformation effects

DD FORM 1 JAN 73 1473 EDITION OF 1 NOV 65 IS OBSOLETE

UNCLASSIFIED

SECURITY CLASSIFICATION OF THIS PAGE (When Data Entered)

006 850 LB-

20 . Abstract (Continued)

are included in an average sense in the moderately-thick plate element family by assuming that straight lines normal to the plate midsurface prior to deformation remain straight but not necessarily normal to the plate midsurface after deformation. Comparison of the results obtained by using the thick plate and moderately-thick plate elements with independent analytical results shows that the moderately-thick plate elements are more efficient and practical for the analysis of multilayer structures having a large number of elastically dissimilar layers.

For dynamic analyses, the Modal Superposition Method (MSM) is employed to obtain the timewise solution, and the Subspace Iteration Method (SIM) is adopted as an efficient scheme for calculation of the lowest few eigenvalues and eigenvectors of the assembled structure. Both the SIM and MSM are programmed as modules to be compatible with a general modular finite-element computer code for static and dynamic analysis. The advantages of this modular approach are demonstrated in a series of static and dynamic applications analyses.

FOREWORD

This research has been conducted by the Aeroelastic and Structures Research Laboratory, Department of Aeronautics and Astronautics, Massachusetts Institute of Technology, Cambridge, Massachusetts under Contract No. DAAG46-75-C-0055 from the Army Materials and Mechanics Research Center, Watertown, Massachusetts. Mr. J.F. Dignam of the AMMRC was project manager and Dr. S.C. Chou of the AMMRC served as technical monitor. The advice and guidance of Mr. Dignam and Dr. Chou in this research are much appreciated.

TABLE OF CONTENTS

Section		Page
1	INTRODUCTION	1
2	DESCRIPTION OF MATERIAL ELASTIC CONSTANTS	4
	2.1 Introduction	4
	2.2 Tensor and Engineering Stress and Strain	4
	2.3 Transformation of Stress and Strain	5
	2.4 Stress-Strain Relations	7
	2.5 Stress-Strain Relations for Moderately-Thick Plates and Shells	11
	2.6 Transformation of Elastic Constants	12
3	DEVELOPMENT OF THICK MULTILAYER PLATE ELEMENTS	16
	3.1 Introduction	16
	3.2 Review of Mau's Quadrilateral Element	16
	3.2.1 Derivation of the Element Stiffness Matrix	17
	3.2.2 Element Stress and Displacement Assumptions	21
	3.2.3 Derivation of the Element Mass Matrix	22
	3.3 Adaptation of the Mau Element to Triangular Shape	26
	3.4 Development of a Quadrilateral Element with a Traction-Free Edge	27
	3.5 Discussion	30
4	DEVELOPMENT OF MODERATELY-THICK MULTILAYER PLATE ELEMENTS	33
	4.1 Introduction	33
	4.2 Derivation of Stiffness and Mass Matrices for a Quadrilateral Element	34
	4.3 Modification to a Triangular Element	43
	4.4 Comparison of Alternate Formulations	45
5	ELEMENT PERFORMANCE TESTS	48
	5.1 Cylindrical Bending of a Three-Layer Infinite Strip	48
	5.2 A Square Two-Layer Plate Under Uniform Transverse Loading	51

Section		Page
6	INTEGRALLY-STIFFENED PLATES AND SHELLS	58
	6.1 Introduction	58
	6.2 Integrally-Stiffened Quadrilateral Element	59
	6.3 Example Problem and Results	64
7	DYNAMIC ANALYSIS	67
	7.1 Introduction	67
	7.2 Eigenvalue Solution Method	67
	7.3 Eigenvalue Solution in the Subspace	71
	7.4 Transient Response Analysis	76
	7.5 Software Verification and Performance Tests	80
	7.5.1 Verification of Jacobi Iteration Method	80
	7.5.2 Verification and Assessment of SIM	83
	7.5.3 Verification of Transient Response Analysis	86
8	APPLICATIONS PROGRAMS	89
	8.1 Introduction	89
	8.2 Subroutine AMMRC and AMMRC2	89
	8.3 Subroutines AMMRC3 and AMMRC4	93
	8.4 Update Requirements	100
	8.5 Subroutine VIBEPT	100
9	DISCUSSION AND CONCLUSIONS	102
	9.1 Summary	102
	9.2 Discussion of Results	104
	9.3 Conclusions and Recommendations	108
REFERENCES		111
TABLES		113
FIGURES		127
APPENDICES		
	A - Subroutine AMMRC2	168
	B - Subroutine AMMRC3	179
	C - Subroutine AMMRC4	188
	D - Subroutine VIBEPT	200

LIST OF TABLES

Table		Page
1	Comparison of Predicted Values for (Normalized) Center Deflection, $\bar{w}$, for Cylindrical Bending Problem	113
2	Effect of Fiber Orientation Angle, $\pm\theta$, on the Accuracy of Finite-Element Results, Using Element MLP3K(Q), for a 2 Layer Square Plate Under Uniform Load (10x10 Mesh)	114
3	A Comparison of Analyses for the Stiffened Simply Supported Plate	115
4	Effect of Arithmetic Precision on the Jacobi Iteration Method	116
5	Effect of Modelling Detail on the Jacobi Iteration Method	117
6	Effect of Plate Model Detail on Convergence of Eigenvalues	118
7	Theoretical Effect of Subspace Size on Eigenvalue Convergence Rates	119
8	Effect of Subspace Size on Convergence of Eigenvectors	120
9	Input Conventions for Subroutine AMMRC2	121
10	Input Conventions for Subroutine AMMRC3	122
11	Input Conventions for Subroutine AMMRC4	123
12	Variation of Required Core Storage with Problem Size for Subroutine VIBEPT	124
13	Input Conventions for Subroutine VIBEPT	125

LIST OF ILLUSTRATIONS

Figure		Page
1	Positive Convention for Single-Rotation Axis Transformation	127
2	Physical Symmetries in a Typical Fiber-Composite Ply	127
3	Positive Convention for Transformation of Typical Ply Properties	127
4	Possible Severe Cross-Sectional Warping Effect in Thick Multilayer Plates	128
5	Definition of Nodal Degrees of Freedom for a Thick Laminated Plate Element	128
6	Deformation of Normal to the Plate Midsurface for Moderately-Thick Laminate	129
7	Definition of Nodal Degrees of Freedom for a Moderately-Thick Laminated Plate Element	129
8	Nomenclature and Property Definitions for 3-Layer Cross Ply Cylindrical Bending Problem	130
9	Analytic Solutions and Finite-Element Results for the Problem of the Cylindrical Bending of a Three-Layer (Cross-Ply) Infinite Strip	132
10	Analytic Solutions and Finite-Element Results for the Problem of the Cylindrical Bending of a Seven-Layer (Cross-Ply) Infinite Strip	135
11	Nomenclature and Property Defintions for 2-Layer Angle Ply Under Uniform Transverse Loading	138
12	Finite-Element Results for a Two-Layer Laminate of Angle-Ply ($\pm\theta$) Construction	139
13	Example Problem - Simply Supported Isotropic Stiffened Plate	144
14	Perspective View of Typical Integrally Stiffened Plate Element (Viewed from Below)	145
15	Assumed-Displacement Element for Engineering Beam Theory	146
16	Finite-Element Model of Simply Supported Square Plate	146
17	Eigenvalue Convergence Rates for Simply Supported Square Plate	147

LIST OF ILLUSTRATIONS (Concluded)

Figure		Page
18	Limiting Effect of Element Mode-Shape Reproduction Capability on Solution Convergence	149
19	Correlation of Computing Efficiency with Convergence Rate	150
20	Example of Computed Response of Plate to Steady Sinusoidal Load	151
21	Example of Computed Response of Plate to Initial Deflection	152
22	Example of Computed Response of Plate to Initial Velocity	153
23	Summary of FEABL-2 and FEABL-5 Software Modules	154
24	Four-Point Bending Experiment on Plate with Circular Hole	155
25	Scale Planes of Typical Meshes Generated by Subroutine AMMRC2	156
26	Division of Quadrant into Regions for Automatic Mesh Generation	157
27	Modular Organization for Execution of Subroutine AMMRC2	158
28	Bending Stresses Computed by Subroutine AMMRC2 for a Single-Layer Isotropic Plate	159
29	Comparison of Computed and Experimental Stress Concentration Factors	160
30	Comparison of Computed and Experimental Results for Bending Strain	161
31	Laminated Conical Shell and Finite-Element Model	162
32	Modular Organization for Execution of Subroutines AMMRC3 and AMMRC4	163
33	Stress and Ply Angle Conventions for Conical Shell	164
34	Conventions for Element STIF2	165
35	Orientation of Grip Ring Stiffeners Assumed in Subroutine AMMRC4	165
36	Flow Diagram for Subroutine VIBEPT	166
37	Modular Organization for Execution of Subroutine VIBEPT	167

SECTION 1

INTRODUCTION

This report summarizes the results of an investigation of the assumed-stress hybrid finite-element method [1]* for applications involving bending-stretching behavior of multilayer laminated composite plates and shells. The present investigation took as its starting point the results of a previous investigation in which a quadrilateral multilayer thick-plate element was developed and incorporated in a specialized computer code for analysis of flat plates and shell segments [2,3]. These results were extended to the case of a triangular element, and the possibility of including special-purpose assumed-stress distributions to satisfy traction-free conditions along one element edge was examined [4].

The thick-plate elements were found to be computationally inefficient, and, hence, were replaced with moderately-thick elements which were developed by extension of a concept from an earlier investigation [5]. The data reviewed in this report demonstrate that the new elements are both computationally efficient and as accurate as the thick-plate elements for analyses of thin and moderately-thick structures, i.e. for plates with span/thickness ratios greater than 10 and for shells with similar ratios of radius-of-curvature to thickness. These elements were programmed to be compatible with a general modular finite-element analysis code [6].

A review of the material property matrices and their transformations required by the new element is given in Section 2. Sections 3 and 4 review the formulations of the thick and moderately-thick elements, respectively. The performances of both types of elements in static stress analyses are compared with independent analytical solutions in Section 5.

The investigation of the new elements was also extended to a formulation for an integrally-stiffened quadrilateral element, in which the stiffener is treated simply as an extra layer which covers only a part of the element's surface. Presented in Section 6 is a comparative evaluation of this concept with the traditional approach in which stiffeners are modelled separately as assumed-displacement beam-theory elements.

---

*Numbers in square brackets [ ] denote references listed at the end of the text.

Both lumped and consistent mass matrices were formulated for the new elements (Section 4) and were tested by means of dynamic analysis procedures which were adopted from the previous codes [3]. The subspace iteration method for eigenvalue analysis and the modal superposition method for transient response analysis were selected on the basis of computational efficiency. These procedures were reprogrammed to be compatible with a general modular finite-element analysis code [6]. The original formulation of the modal superposition method permitted only analyses of undamped transient response [3], but has been extended in the present investigation to allow damped response with prescribed modal damping factors less than critical. Verification tests of the dynamic analysis procedures, together with some dynamic performance tests of the new elements, are presented in Section 7.

One phase of the present research effort was the development of a modular dynamic analysis finite-element-based computer code. This has been accomplished by modification and extension of an existing modular static analysis finite-element program [6]. A modular code is arranged as a library of subroutines, each of which performs a series of computations which, taken together, form a single logical step in the context of the analysis. The user responsibility now shifts from the routine input preparation associated with "black-box" codes to the writing of a MAIN controlling program which generates the desired geometrical configuration and sequences the required analysis steps. The use of a modular approach thus requires additional user-interaction, but in turn, provides the user with increased flexibility in comparison with the use of "black-box" codes.

Incorporation of the dynamic analysis capability in the existing modular code required that some modifications be made in the original subroutines. A fully updated user's guide will be published in the near future to document the modified code, which has been designated as FEABL-5. Some preliminary documentation is presented in Section 8 of this report, which describes in detail four applications programs. The static applications programs combine the new elements with the existing FEABL-2 software for automatically generated analyses of a plate with a circular hole subjected to four-point bending, and stiffened and unstiffened laminated conical shells. One dynamic application, vibration of a simply-supported

flat plate, is presented to illustrate the new FEABL-5 software. Some of the applications programs are intended for stress and strain predictions which will be compared with experimental results to be obtained under other current AMMRC investigations.

SECTION 2

DESCRIPTION OF MATERIAL ELASTIC CONSTANTS

2.1 Introduction

Each ply of a composite laminate may be treated as a homogeneous orthotropic material for the purpose of stress analysis. With homogeneity assumed, there are at most 9 independent elastic constants for a general orthotropic material. This number may be reduced to 6, of which 5 constants are absolutely necessary, for the description of bending-stretching behavior in thin and moderately thick laminates including transverse shear deformation. Also, two methods of description are possible. One, based on a tensor formulation of the equations of elasticity, is convenient for the derivation of axis-rotation transformations necessary to translate the material properties to general elastic matrices associated with arbitrarily oriented reference axes. The second is a matrix formulation which is convenient for the computer-programming of finite-element stiffness matrix computations, and which also corresponds to the data usually found in materials handbooks. The purpose of this section is to review the relationship between the two methods of description and their relations to the finite-element formulations discussed in Sections 3 and 4.

2.2 Tensor and Engineering Stress and Strain

The key to the relation between elastic constants is the relationship which exists between the tensor and "engineering" components of stress and strain. The two systems are physically identical for stress (within the theory of linear elasticity), the only difference being the various notations which have been adopted. The stress tensor is represented by:

$$\underset{\sim}{\tau} = \begin{bmatrix} \tau_{11} & \tau_{12} & \tau_{13} \\ \tau_{21} & \tau_{22} & \tau_{23} \\ \tau_{31} & \tau_{32} & \tau_{33} \end{bmatrix} \qquad (\tau_{ji} = \tau_{ij}) \tag{1}$$

Equivalent "engineering" or vector descriptions of stress are given by:

$$\underset{\sim}{\bar{\sigma}} = \{\sigma_1\ \sigma_2\ \sigma_3\ \tau_{23}\ \sigma_{31}\ \sigma_{12}\} = \{\sigma_1\ \sigma_2\ \sigma_3\ \sigma_4\ \sigma_5\ \sigma_6\} = \{\tau_{11}\ \tau_{22}\ \tau_{33}\ \tau_{23}\ \tau_{31}\ \tau_{12}\} \tag{2*}$$

*The braces { } denote a column vector, here arranged horizontally to save space.

The notations in Eq. 2 are commonly used in the literature on composite materials.

In a similar manner, the strain tensor is represented by:

$$\underset{\sim}{\gamma} = \begin{bmatrix} \gamma_{11} & \gamma_{12} & \gamma_{13} \\ \gamma_{21} & \gamma_{22} & \gamma_{23} \\ \gamma_{31} & \gamma_{32} & \gamma_{33} \end{bmatrix} \qquad (\gamma_{ji} = \gamma_{ij}) \tag{3}$$

where the components γ_{ij} satisfy the continuum strain-displacement relations:

$$\gamma_{ij} = \frac{1}{2}(\partial u_i/\partial x_j + \partial u_j/\partial x_i) \tag{4}$$

and where $u_i = u_i(x_1, x_2, x_3)$ is the component of the continuum displacement field parallel to axis x_i. However, the "engineering" strains ε_{ij} are defined in a slightly different manner:

$$\bar{\underset{\sim}{\varepsilon}} = \{\varepsilon_1\ \varepsilon_2\ \varepsilon_3\ \varepsilon_{23}\ \varepsilon_{31}\ \varepsilon_{12}\} = \{\varepsilon_1\ \varepsilon_2\ \cdots\ \varepsilon_6\} = \{\gamma_{11}\ \gamma_{22}\ \gamma_{33}\ 2\gamma_{23}\ 2\gamma_{31}\ 2\gamma_{12}\} \tag{5}$$

with *corresponding strain-displacement relations:*

$$\varepsilon_i = \partial u_i/\partial x_i \quad (i = 1, 2, 3) \qquad \varepsilon_{ij} = \partial u_i/\partial x_j + \partial u_j/\partial x_i \quad (i \neq j) \tag{6}$$

The difference arises from a convenience in the traditional description of shear stress-strain relations for isotropic materials, i.e. $\sigma_{ij} = G\varepsilon_{ij}$ instead of $\tau_{ij} = 2G\gamma_{ij}$, where $G = E/[2(1+\nu)]$ is the material shear modulus. This convention has been carried over to the description of the orthotropic properties of a composite laminate, as will be seen in Subsection 2.4.

2.3 Transformation of Stress and Strain

Consider now two Cartesian axis systems $x_1x_2x_3$ and $\tilde{x}_1\tilde{x}_2\tilde{x}_3$ with different spatial orientations. Let the direction cosines between the two systems be given by:

$$\begin{bmatrix} \cos(\tilde{x}_1, x_1) & \cos(\tilde{x}_1, x_2) & \cos(\tilde{x}_1, x_3) \\ \cos(\tilde{x}_2, x_1) & \cos(\tilde{x}_2, x_2) & \cos(\tilde{x}_2, x_3) \\ \cos(\tilde{x}_3, x_1) & \cos(\tilde{x}_3, x_2) & \cos(\tilde{x}_3, x_3) \end{bmatrix} = \begin{bmatrix} m_{\tilde{1}1} & m_{\tilde{1}2} & m_{\tilde{1}3} \\ m_{\tilde{2}1} & m_{\tilde{2}2} & m_{\tilde{2}3} \\ m_{\tilde{3}1} & m_{\tilde{3}2} & m_{\tilde{3}3} \end{bmatrix} \tag{7}$$

Then the transformation between stress (strain) components in the $x_1x_2x_3$ system and stress (strain components in the $\tilde{x}_1\tilde{x}_2\tilde{x}_3$ system can be expressed

concisely with the indicial notation and summation conventions of tensor analysis:

$$\tilde{\tau}_{ij} = m_{\tilde{i}k} m_{\tilde{j}\ell} \tau_{k\ell} \qquad \tilde{\gamma}_{ij} = m_{\tilde{i}k} m_{\tilde{j}\ell} \gamma_{k\ell} \tag{8}$$

Expressions like Eqs. 8 are convenient for compact presentation of formulations, but a matrix notation is more practical for computations. Of most interest in the present study is the special case in which axes $x_3, \tilde{x}_3$ coincide, while there is a rotation between $x_1 x_2$ and $\tilde{x}_1 \tilde{x}_2$ (Fig. 1). If Eqs. 8 are applied to this case and "engineering" notations are used, it is easy to show that $\tilde{\sigma}_3 = \sigma_3$, $\tilde{\varepsilon}_3 = \varepsilon_3$ and:

$$\{\sigma_1 \ \ \sigma_2 \ \ \sigma_{23} \ \ \sigma_{31} \ \ \sigma_{12}\} = \underset{\sim}{M} \{\tilde{\sigma}_1 \ \ \tilde{\sigma}_2 \ \ \tilde{\sigma}_{23} \ \ \tilde{\sigma}_{31} \ \ \tilde{\sigma}_{12}\} \tag{9}$$

$$\{\varepsilon_1 \ \ \varepsilon_2 \ \ \tfrac{1}{2}\varepsilon_{23} \ \ \tfrac{1}{2}\varepsilon_{31} \ \ \tfrac{1}{2}\varepsilon_{12}\} = \underset{\sim}{M} \{\tilde{\varepsilon}_1 \ \ \tilde{\varepsilon}_2 \ \ \tfrac{1}{2}\tilde{\varepsilon}_{23} \ \ \tfrac{1}{2}\tilde{\varepsilon}_{31} \ \ \tfrac{1}{2}\tilde{\varepsilon}_{12}\} \tag{10}$$

where

$$\underset{\sim}{M} = \begin{bmatrix} m^2 & n^2 & 0 & 0 & 2mn \\ n^2 & m^2 & 0 & 0 & -2mn \\ 0 & 0 & m & n & 0 \\ 0 & 0 & -n & m & 0 \\ -mn & mn & 0 & 0 & m^2-n^2 \end{bmatrix} \qquad \begin{matrix} m = \cos\theta \\ n = \sin\theta \end{matrix} \tag{11}$$

and where θ (positive CCW) is the angle from $\tilde{x}_1$ to x_1. Also of interest is the inverse transformation matrix:

$$\underset{\sim}{M}^{-1} = \begin{bmatrix} m^2 & n^2 & 0 & 0 & -2mn \\ n^2 & m^2 & 0 & 0 & 2mn \\ 0 & 0 & m & -n & 0 \\ 0 & 0 & n & m & 0 \\ mn & -mn & 0 & 0 & m^2-n^2 \end{bmatrix} \tag{12}$$

Equations 11 and 12 contain the familiar Mohr circle transformations for the components $\sigma_1, \sigma_2, \sigma_{12}$ ($\varepsilon_1, \varepsilon_2, \frac{1}{2}\varepsilon_{12}$) in the $x_1 x_2$ plane, as well as the corresponding information for transverse shears σ_{23}, σ_{31} ($\frac{1}{2}\varepsilon_{23}, \frac{1}{2}\varepsilon_{31}$). It is particularly important to note the factors of 1/2 applied to the "engineering" shear strains in Eq. 10: the transformation is valid *only* for tensor components,

a fact which must be reflected when "engineering" notation is employed.

2.4 Stress-Strain Relations

The stress-strain relations for a linear elastic material are conventionally given in "engineering" form, either in terms of compliance constants:

$$\begin{Bmatrix} \varepsilon_1 \\ \varepsilon_2 \\ \vdots \\ \varepsilon_6 \end{Bmatrix} = \begin{bmatrix} \bar{S}_{11} & \bar{S}_{12} & \cdots & \bar{S}_{16} \\ \bar{S}_{21} & \bar{S}_{22} & \cdots & \bar{S}_{26} \\ \vdots & \vdots & \ddots & \vdots \\ \bar{S}_{61} & \bar{S}_{62} & \cdots & \bar{S}_{66} \end{bmatrix} \begin{Bmatrix} \sigma_1 \\ \sigma_2 \\ \vdots \\ \sigma_6 \end{Bmatrix} \tag{13}$$

or in terms of stiffness constants:

$$\begin{Bmatrix} \sigma_1 \\ \sigma_2 \\ \vdots \\ \sigma_6 \end{Bmatrix} = \begin{bmatrix} \bar{C}_{11} & \bar{C}_{12} & \cdots & \bar{C}_{16} \\ \bar{C}_{21} & \bar{C}_{22} & \cdots & \bar{C}_{26} \\ \vdots & \vdots & \ddots & \vdots \\ \bar{C}_{61} & \bar{C}_{62} & \cdots & \bar{C}_{66} \end{bmatrix} \begin{Bmatrix} \varepsilon_1 \\ \varepsilon_2 \\ \vdots \\ \varepsilon_6 \end{Bmatrix} \tag{14}$$

The matrices $\bar{\underset{\sim}{S}}$ and $\bar{\underset{\sim}{C}}$ are symmetric, and $\bar{\underset{\sim}{S}}=\bar{\underset{\sim}{C}}^{-1}$. For an isotropic material,

$$\bar{\underset{\sim}{S}} = \begin{bmatrix} 1/E & -\nu/E & -\nu/E & 0 & 0 & 0 \\ -\nu/E & 1/E & -\nu/E & 0 & 0 & 0 \\ -\nu/E & -\nu/E & 1/E & 0 & 0 & 0 \\ 0 & 0 & 0 & 1/G & 0 & 0 \\ 0 & 0 & 0 & 0 & 1/G & 0 \\ 0 & 0 & 0 & 0 & 0 & 1/G \end{bmatrix} \tag{15}$$

A general orthotropic material possess 9 independent elastic constants [7], such that:

$$\bar{\underset{\sim}{S}} = \begin{bmatrix} \bar{S}_{11} & & & \text{(Symmetric)} & & \\ \bar{S}_{21} & \bar{S}_{22} & & & & \\ \bar{S}_{31} & \bar{S}_{32} & \bar{S}_{33} & & & \\ 0 & 0 & 0 & \bar{S}_{44} & & \\ 0 & 0 & 0 & 0 & \bar{S}_{55} & \\ 0 & 0 & 0 & 0 & 0 & \bar{S}_{66} \end{bmatrix} \tag{16}$$

However, Eq. 16 may be simplified for a fiber-composite ply, which possesses more symmetries than does a general orthotropic material. The additional symmetries are physical in nature and arise from consideration of the role played by the fibers in stiffening the surrounding resin material.

The conventions adopted for the description of a typical ply and its symmetries are illustrated in Fig. 2. The axes $x_1x_2x_3$ are defined as the material axes. Axis x_1 is oriented parallel to the fibers, axis x_2 occupies the in-plane transverse orientation, and axis x_3 is oriented perpendicular to the ply. As shown in the figure, the fibers tend to behave somewhat like layers in their effects upon elastic response of the material in the x_1x_2 and x_3x_1 planes, but in the x_2x_3 plane the fibers tend to behave as small circular inclusions. Thus, there is good reason to assume that the elastic cross-coupling terms related to the x_1x_2 and x_3x_1 planes are identical, while those related to the x_2x_3 plane have different values, i.e.:

$$\bar{S}_{31} = \bar{S}_{21} \qquad \bar{S}_{33} = \bar{S}_{22} \qquad \bar{S}_{55} = \bar{S}_{66} \tag{17}$$

Equation (16) is thus reduced to 6 independent elastic constants:

$$\bar{\underset{\sim}{S}} = \begin{bmatrix} \bar{S}_{11} & & & \text{(Symmetric)} & & \\ \bar{S}_{21} & \bar{S}_{22} & & & & \\ \bar{S}_{21} & \bar{S}_{32} & \bar{S}_{22} & & & \\ 0 & 0 & 0 & \bar{S}_{44} & & \\ 0 & 0 & 0 & 0 & \bar{S}_{66} & \\ 0 & 0 & 0 & 0 & 0 & \bar{S}_{66} \end{bmatrix} \tag{18}$$

The general notation in Eq. 18 is commonly replaced with a notation which follows the conventions for isotropic materials (see Eq. 15). Longitudinal and transverse Young's moduli are defined by:

$$\bar{S}_{11} = 1/E_1 \qquad \bar{S}_{22} = 1/E_2 \tag{19}$$

The shear moduli (unrelated to E_1, E_2) are defined by:

$$\bar{S}_{44} = 1/G_{23} \qquad \bar{S}_{66} = 1/G_{12} \tag{20}$$

Poisson's ratios are also defined by following the traditional method, for example:

$$\nu_{12} = -\varepsilon_2/\varepsilon_1 \qquad \text{when} \quad \sigma_1 \neq 0, \quad \sigma_2 = \sigma_3 = 0$$

$$\nu_{21} = -\varepsilon_1/\varepsilon_2 \qquad \text{when} \quad \sigma_2 \neq 0, \quad \sigma_3 = \sigma_1 = 0 \tag{21}$$

$$\nu_{23} = -\varepsilon_3/\varepsilon_2 \qquad \text{when} \quad \sigma_2 \neq 0, \quad \sigma_3 = \sigma_1 = 0$$

Combination of Eqs. 18, 19, and 21 finally leads to the following expression for the stress-strain relations in the material axis system of a composite ply:

$$\begin{Bmatrix} \varepsilon_1 \\ \varepsilon_2 \\ \varepsilon_3 \\ \varepsilon_{23} \\ \varepsilon_{31} \\ \varepsilon_{12} \end{Bmatrix} = \begin{bmatrix} 1/E_1 & -\nu_{21}/E_2 & -\nu_{21}/E_2 & 0 & 0 & 0 \\ -\nu_{12}/E_1 & 1/E_2 & -\nu_{23}/E_2 & 0 & 0 & 0 \\ -\nu_{12}/E_1 & -\nu_{23}/E_2 & 1/E_2 & 0 & 0 & 0 \\ 0 & 0 & 0 & 1/G_{23} & 0 & 0 \\ 0 & 0 & 0 & 0 & 1/G_{12} & 0 \\ 0 & 0 & 0 & 0 & 0 & 1/G_{12} \end{bmatrix} \begin{Bmatrix} \sigma_1 \\ \sigma_2 \\ \sigma_3 \\ \sigma_{23} \\ \sigma_{31} \\ \sigma_{12} \end{Bmatrix} \tag{22}$$

where

$$\nu_{12}/E_1 = \nu_{21}/E_2 \tag{23}$$

The elastic constants in Eq. 22 are commonly identified as indicated below. An alternate system of subscript notation found in much of the literature on composite materials is also shown:

$E_1 = E_L$ = Longitudinal modulus

$E_2 = E_T$ = Transverse modulus

$\nu_{12} = \nu_{LT}$ = Major Poisson ratio

$\nu_{21} = \nu_{TL}$ = Minor Poisson ratio

$\nu_{23} = \nu_T$ = Transverse Poisson ratio

$G_{12} = G_{LT}$ = In-plane shear modulus

$G_{23} = G_T$ = Transverse shear modulus

Note that ν_{21} and ν_{12} are not independent quantities, in view of Eq. 23. The major Poisson ratio ν_{12} is usually reported when material properties

are measured. Values for ν_{23} and G_{23} are seldom reported because of the difficulty in measuring these quantities, and because stress analyses of composite laminates have focussed in the past on stretching behavior or on bending of thin plates for which transverse shear effects can safely be neglected. However, reasonable estimates for ν_{23} and G_{23} can be made by assuming that these properties in the laminate are close to unreinforced resin properties, i.e.:

$$\nu_{23} \cong \nu_R \qquad G_{23} \cong E_R / 2(1+\nu_R) \tag{24}$$

where

ν_R = Resin Poisson ratio

E_R = Resin Young's modulus

and where the resin is assumed to be isotropic. Some handbook data for unreinforced resin properties are available. Generally, $\nu_R \cong 0.35$ and $E_R \cong 10^6$ psi for many epoxy resins currently used in composite materials.

If the compliance matrix $\bar{\underset{\sim}{S}}$ in Eq. 22 is inverted, the resulting stiffness matrix may be expressed as:

$$\bar{\underset{\sim}{C}} = \begin{bmatrix} \frac{(1-\nu_{23})E_1}{1-2\nu_{12}\nu_{21}-\nu_{23}} & \frac{\nu_{12}E_2}{1-2\nu_{12}\nu_{21}-\nu_{23}} & \frac{\nu_{12}E_2}{1-2\nu_{12}\nu_{21}-\nu_{23}} & 0 & 0 & 0 \\ \frac{\nu_{21}E_1}{1-2\nu_{12}\nu_{21}-\nu_{23}} & \frac{(1-\nu_{12}\nu_{21})E_2}{(1+\nu_{23})(1-2\nu_{12}\nu_{21}-\nu_{23})} & \frac{(\nu_{23}+\nu_{12}\nu_{21})E_2}{(1+\nu_{23})(1-2\nu_{12}\nu_{21}-\nu_{23})} & 0 & 0 & 0 \\ \frac{\nu_{21}E_1}{1-2\nu_{12}\nu_{21}-\nu_{23}} & \frac{(\nu_{23}+\nu_{12}\nu_{21})E_2}{(1+\nu_{23})(1-2\nu_{12}\nu_{21}-\nu_{23})} & \frac{(1-\nu_{12}\nu_{21})E_2}{(1+\nu_{23})(1-2\nu_{12}\nu_{21}-\nu_{23})} & 0 & 0 & 0 \\ 0 & 0 & 0 & G_{23} & 0 & 0 \\ 0 & 0 & 0 & 0 & G_{12} & 0 \\ 0 & 0 & 0 & 0 & 0 & G_{12} \end{bmatrix} \tag{25}$$

Eq. 25 may be compared with the corresponding expression for isotropic material to further illustrate the similarity of the notation:

$$
\bar{\underset{\sim}{C}} = \begin{bmatrix} \frac{(1-\nu)E}{(1+\nu)(1-2\nu)} & & & & & \text{(Symmetric)} \\ \frac{\nu E}{(1+\nu)(1-2\nu)} & \frac{(1-\nu)E}{(1+\nu)(1-2\nu)} & & & & \\ \frac{\nu E}{(1+\nu)(1-2\nu)} & \frac{\nu E}{(1+\nu)(1-2\nu)} & \frac{(1-\nu)E}{(1+\nu)(1-2\nu)} & & & \\ 0 & 0 & 0 & G & & \\ 0 & 0 & 0 & 0 & G & \\ 0 & 0 & 0 & 0 & 0 & G \end{bmatrix} \tag{26}
$$

2.5 Stress-Strain Relations for Moderately-Thick Plates and Shells

Moderately thick plates and shells subjected to combined bending-stretching loads may be analyzed in terms of 5 components of stress. The sixth component (the stress σ_3 normal to the plate or shell midsurface) is at most of the order of the applied pressure loading, and can be neglected in comparison with the in-plane components $\sigma_1, \sigma_2, \sigma_{12}$ and the transverse shear stresses σ_{23}, σ_{31}. The compliance and stiffness elastic matrices for a fiber-composite ply (Eqs. 22 and 25) then reduce to the following forms:

$$
\underset{\sim}{S} = \begin{bmatrix} 1/E_1 & -\nu_{21}/E_2 & 0 & 0 & 0 \\ -\nu_{12}/E_1 & 1/E_2 & 0 & 0 & 0 \\ 0 & 0 & 1/G_{23} & 0 & 0 \\ 0 & 0 & 0 & 1/G_{12} & 0 \\ 0 & 0 & 0 & 0 & 1/G_{12} \end{bmatrix} \tag{27}
$$

$$
\underset{\sim}{C} = \begin{bmatrix} \frac{E_1}{1-\nu_{12}\nu_{21}} & \frac{\nu_{12}E_2}{1-\nu_{12}\nu_{21}} & 0 & 0 & 0 \\ \frac{\nu_{21}E_1}{1-\nu_{12}\nu_{21}} & \frac{E_2}{1-\nu_{12}\nu_{21}} & 0 & 0 & 0 \\ 0 & 0 & G_{23} & 0 & 0 \\ 0 & 0 & 0 & G_{12} & 0 \\ 0 & 0 & 0 & 0 & G_{12} \end{bmatrix} \tag{28}
$$

where

$$
\begin{gathered} \underset{\sim}{\sigma} = \underset{\sim}{C}\,\underset{\sim}{\varepsilon} \qquad \underset{\sim}{\varepsilon} = \underset{\sim}{S}\,\underset{\sim}{\sigma} \\ \underset{\sim}{\sigma} = \{\sigma_1\ \sigma_2\ \sigma_4\ \sigma_5\ \sigma_6\} = \{\sigma_1\ \sigma_2\ \sigma_{23}\ \sigma_{31}\ \sigma_{12}\} \\ \underset{\sim}{\varepsilon} = \{\varepsilon_1\ \varepsilon_2\ \varepsilon_4\ \varepsilon_5\ \varepsilon_6\} = \{\varepsilon_1\ \varepsilon_2\ \varepsilon_{23}\ \varepsilon_{31}\ \varepsilon_{12}\} \end{gathered} \tag{29}
$$

The compliance matrix $\underset{\sim}{S}$ in Eq. 27 is in the form which is used for the computation of assumed-stress hybrid element stiffness matrices (Sections 3 and 4). Also, the in-plane portion of the elastic stiffnesses:

$$\underset{\sim}{C}_{IP} = \begin{bmatrix} \dfrac{E_1}{1-\nu_{12}\nu_{21}} & \dfrac{\nu_{12}E_2}{1-\nu_{12}\nu_{21}} & 0 \\ \dfrac{\nu_{21}E_1}{1-\nu_{12}\nu_{21}} & \dfrac{E_2}{1-\nu_{12}\nu_{21}} & 0 \\ 0 & 0 & G_{12} \end{bmatrix} \tag{30}$$

is used to compute assumed stress field information in the elements which are discussed in Section 4. Note that neither $\underset{\sim}{S}$ nor $\underset{\sim}{C}_{IP}$ require the transverse Poisson ratio ν_{23}.

2.6 Transformation of Elastic Constants

The computation of a finite-element stiffness matrix requires application of rotation transformations to the ply elastic constants $\underset{\sim}{S}$ and $\underset{\sim}{C}$, as indicated in Fig. 3. The figure illustrates a typical ply whose material reference axes x_1x_2 are in general rotated with respect to the global reference axes xy. The properties $\underset{\sim}{S}$ and $\underset{\sim}{C}$ are associated with stress and strain components $\underset{\sim}{\sigma}$ and $\underset{\sim}{\varepsilon}$ referred to the material axes x_1x_2. However, it is necessary to describe the behavior of the finite element in terms of the global stress and strain components:

$$\underset{\sim}{\sigma}^G = \{\sigma_x \;\; \sigma_y \;\; \sigma_{yz} \;\; \sigma_{zx} \;\; \sigma_{xy}\} \qquad \underset{\sim}{\varepsilon}^G = \{\varepsilon_x \;\; \varepsilon_y \;\; \varepsilon_{yz} \;\; \varepsilon_{zx} \;\; \varepsilon_{xy}\} \tag{31}$$

Therefore, global elastic constants:

$$\underset{\sim}{S}^G = \begin{bmatrix} S^G_{11} & S^G_{12} & 0 & 0 & S^G_{16} \\ S^G_{21} & S^G_{22} & 0 & 0 & S^G_{26} \\ 0 & 0 & S^G_{44} & S^G_{45} & 0 \\ 0 & 0 & S^G_{54} & S^G_{55} & 0 \\ S^G_{61} & S^G_{62} & 0 & 0 & S^G_{66} \end{bmatrix} \qquad \underset{\sim}{C}^G = \begin{bmatrix} C^G_{11} & C^G_{12} & 0 & 0 & C^G_{16} \\ C^G_{21} & C^G_{22} & 0 & 0 & C^G_{26} \\ 0 & 0 & C^G_{44} & C^G_{45} & 0 \\ 0 & 0 & C^G_{54} & C^G_{55} & 0 \\ C^G_{61} & C^G_{62} & 0 & C & C^G_{66} \end{bmatrix} \tag{32}$$

$$(S^G_{ji} = S^G_{ij}\,, \quad C^G_{ji} = C^G_{ij})$$

must be obtained. The additional nonzero terms (subscripts 61,62,54) will appear as a result of the transformation.

Expressions for $\underset{\sim}{S}^G$ and $\underset{\sim}{C}^G$ may be derived by first recasting the matrices $\underset{\sim}{S}$ and $\underset{\sim}{C}$ to give the stress-strain relations in terms of tensor components and then applying the Mohr circle transformations presented in Subsection 2.3. For example, $\underset{\sim}{\varepsilon}=\underset{\sim}{S}\underset{\sim}{\sigma}$ is replaced by:

$$\underset{\sim}{\gamma} = \left\{\varepsilon_1 \ \varepsilon_2 \ \tfrac{1}{2}\varepsilon_{23} \ \tfrac{1}{2}\varepsilon_{31} \ \tfrac{1}{2}\varepsilon_{12}\right\} = \underset{\sim}{S}^{\star}\underset{\sim}{\sigma} \tag{33}$$

where $\underset{\sim}{\Delta}$ and $\underset{\sim}{S}$ are related by:

$$\underset{\sim}{S} = \begin{bmatrix} S_{11} & S_{12} & 0 & 0 & 0 \\ S_{21} & S_{22} & 0 & 0 & 0 \\ 0 & 0 & S_{44} & 0 & 0 \\ 0 & 0 & 0 & S_{55} & 0 \\ 0 & 0 & 0 & 0 & S_{66} \end{bmatrix} \qquad \underset{\sim}{S}^{\star} = \begin{bmatrix} S_{11} & S_{12} & 0 & 0 & 0 \\ S_{21} & S_{22} & 0 & 0 & 0 \\ 0 & 0 & S_{44}/2 & 0 & 0 \\ 0 & 0 & 0 & S_{55}/2 & 0 \\ 0 & 0 & 0 & 0 & S_{66}/2 \end{bmatrix} \tag{34}$$

In a similar manner,

$$\underset{\sim}{\sigma} = \underset{\sim}{C}^{\star}\underset{\sim}{\gamma} \qquad \underset{\sim}{C}^{\star} = \begin{bmatrix} C_{11} & C_{12} & 0 & 0 & 0 \\ C_{21} & C_{22} & 0 & 0 & 0 \\ 0 & 0 & 2C_{44} & 0 & 0 \\ 0 & 0 & 0 & 2C_{55} & 0 \\ 0 & 0 & 0 & 0 & 2C_{66} \end{bmatrix} \tag{35}$$

while in the global reference frame:

$$\underset{\sim}{\gamma}^G = \underset{\sim}{S}^{G\star}\underset{\sim}{\sigma}^G \qquad \underset{\sim}{S}^{G\star} = \begin{bmatrix} S^G_{11} & S^G_{12} & 0 & 0 & S^G_{16} \\ S^G_{21} & S^G_{22} & 0 & 0 & S^G_{26} \\ 0 & 0 & S^G_{44}/2 & S^G_{45}/2 & 0 \\ 0 & 0 & S^G_{54}/2 & S^G_{55}/2 & 0 \\ S^G_{61}/2 & S^G_{62}/2 & 0 & 0 & S^G_{66}/2 \end{bmatrix} \tag{36}$$

$$\underset{\sim}{\sigma}^{G} = \underset{\sim}{C}^{G\star} \underset{\sim}{\gamma}^{G} \qquad \underset{\sim}{C}^{G\star} = \begin{bmatrix} C_{11}^{G} & C_{12}^{G} & 0 & 0 & 2C_{16}^{G} \\ C_{21}^{G} & C_{22}^{G} & 0 & 0 & 2C_{26}^{G} \\ 0 & 0 & 2C_{44}^{G} & 2C_{45}^{G} & 0 \\ 0 & 0 & 2C_{54}^{G} & 2C_{55}^{G} & 0 \\ C_{61}^{G} & C_{62}^{G} & 0 & 0 & 2C_{66}^{G} \end{bmatrix} \tag{37}$$

$$\underset{\sim}{\gamma}^{G} = \left\{ \varepsilon_x \quad \varepsilon_y \quad \tfrac{1}{2}\varepsilon_{yz} \quad \tfrac{1}{2}\varepsilon_{zx} \quad \tfrac{1}{2}\varepsilon_{xy} \right\} \tag{38}$$

Note that the matrices $\underset{\sim}{S}^{G\star}$ and $\underset{\sim}{C}^{G\star}$ are not symmetric. However, these matrices are merely used to compute appropriate values for the symmetric matrices $\underset{\sim}{S}^{G}$ and $\underset{\sim}{C}^{G}$ from which the final calculations are made to obtain the element stiffness matrix.

Comparison of Fig. 3 with Fig. 1 now shows that the Mohr circle transformations which were presented in subsection 2.3 apply to the present case, with $\underset{\sim}{\sigma}^{G}, \underset{\sim}{\gamma}^{G}$ playing the roles of $\underset{\sim}{\tilde{\sigma}}, \underset{\sim}{\tilde{\gamma}}$ in Eqs. 9 and 10; i.e.,

$$\underset{\sim}{\sigma} = \underset{\sim}{M}\,\underset{\sim}{\sigma}^{G} \qquad \underset{\sim}{\gamma} = \underset{\sim}{M}\,\underset{\sim}{\gamma}^{G} \tag{39}$$

where $\underset{\sim}{M}, \underset{\sim}{M}^{-1}$ are given by Eqs. 11 and 12, respectively. Substitution of Eqs. 39 into Eqs. 33 and 35 now leads to:

$$\underset{\sim}{M}\,\underset{\sim}{\gamma}^{G} = \underset{\sim}{S}^{\star}\underset{\sim}{M}\,\underset{\sim}{\sigma}^{G} \qquad \underset{\sim}{M}\,\underset{\sim}{\sigma}^{G} = \underset{\sim}{C}^{\star}\underset{\sim}{M}\,\underset{\sim}{\gamma}^{G}$$

$$\underset{\sim}{\gamma}^{G} = \underset{\sim}{M}^{-1}\underset{\sim}{S}^{\star}\underset{\sim}{M}\,\underset{\sim}{\sigma}^{G} \qquad \underset{\sim}{\sigma}^{G} = \underset{\sim}{M}^{-1}\underset{\sim}{C}^{\star}\underset{\sim}{M}\,\underset{\sim}{\gamma}^{G}$$

Therefore:

$$\underset{\sim}{S}^{G\star} = \underset{\sim}{M}^{-1}\underset{\sim}{S}^{\star}\underset{\sim}{M} \qquad \underset{\sim}{C}^{G\star} = \underset{\sim}{M}^{-1}\underset{\sim}{C}^{\star}\underset{\sim}{M} \tag{40}$$

Substitution of Eqs. 27 and 28 for the components of $\underset{\sim}{S}^{\star}$ and $\underset{\sim}{C}^{\star}$ and of Eqs. 11 and 12 into Eqs. 40 then leads to the following expressions for the components of $\underset{\sim}{S}^{G}$ and $\underset{\sim}{C}^{G}$, after the matrix multiplications have been carried out:

$$
\begin{aligned}
S_{11}^G &= m^4/E_1 + n^4/E_2 + m^2n^2\left(1/G_{12} - 2\nu_{12}/E_1\right)\\
S_{21}^G &= m^2n^2\left(1/E_1 + 1/E_2 - 1/G_{12}\right) - (m^4+n^4)\,\nu_{12}/E_1\\
S_{22}^G &= n^4/E_1 + m^4/E_2 + m^2n^2\left(1/G_{12} - 2\nu_{12}/E_1\right)\\
S_{44}^G &= m^2/G_{23} + n^2/G_{12}\\
S_{54}^G &= mn\left(1/G_{23} - 1/G_{12}\right)\\
S_{55}^G &= n^2/G_{23} + m^2/G_{12}\\
S_{61}^G &= 2mn\left(m^2/E_1 - n^2/E_2\right) - mn\left(m^2-n^2\right)/G_{12}\\
S_{62}^G &= 2mn\left(n^2/E_1 - m^2/E_2\right) + mn\left(m^2-n^2\right)/G_{12}\\
S_{66}^G &= 4m^2n^2\left(1/E_1 + 1/E_2 + 2\nu_{12}/E_1\right) + \left(m^2-n^2\right)^2/G_{12}
\end{aligned}
\tag{41}
$$

$$
\begin{aligned}
C_{11}^G &= \left[m^4E_1 + 2m^2n^2\nu_{12}E_2 + n^4E_2\right]/(1-\nu_{12}\nu_{21}) + 4m^2n^2G_{12}\\
C_{21}^G &= \left[m^2n^2(E_1+E_2) + (m^4+n^4)\nu_{12}E_2\right]/(1-\nu_{12}\nu_{21}) - 4m^2n^2G_{12}\\
C_{22}^G &= \left[n^4E_1 + 2m^2n^2\nu_{12}E_2 + m^4E_2\right]/(1-\nu_{12}\nu_{21}) + 4m^2n^2G_{12}\\
C_{61}^G &= mn\left[m^2E_1 - n^2E_2 - (m^2-n^2)\nu_{12}E_2\right]/(1-\nu_{12}\nu_{21}) - 2mn(m^2-n^2)G_{12}\\
C_{62}^G &= mn\left[n^2E_1 - m^2E_2 + (m^2-n^2)\nu_{12}E_2\right]/(1-\nu_{12}\nu_{21}) + 2mn(m^2-n^2)G_{12}\\
C_{66}^G &= m^2n^2\left[E_1 + (1-2\nu_{12})E_2\right]/(1-\nu_{12}\nu_{21}) + (m^2-n^2)^2G_{12}
\end{aligned}
\tag{42}
$$

Only the in-plane elastic constants $\underset{\sim}{C}_{IP}^{G}$ have been given in Eqs. 42, since the transverse shear stiffnesses are not required in the finite-element formulation.

SECTION 3

DEVELOPMENT OF THICK MULTILAYER PLATE ELEMENTS

3.1 Introduction

An essential ingredient in the development of an effective multilayer plate transient analysis capability is the choice of an accurate and efficient finite-element model. In general, one may choose from the assumed-displacement model, assumed-stress model, assumed-stress hybrid model, or other mixed models, but the choice must be governed by the ease of application, and the ability of the model to represent accurately the type(s) of behavior characteristic of the structure and material being considered. Earlier studies by Spilker [5] and Mau and Witmer [2] suggest that the assumed-stress hybrid model is the appropriate choice for multilayer composite plate structures, and this model has been chosen for the present effort. In particular, two alternate hybrid-stress-based multilayer plate elements will be considered, one based on the approach suggested by Mau and Witmer [2] (presented in this section) and the other based on an improvement of the approach suggested by Spilker [5] (presented in Section 4).

3.2 Review of Mau's Quadrilateral Element

One phase of the present research effort involves the adaptation of the general quadrilateral multilayer plate element developed by Mau [2]. In his formulation, Mau obtained a model which includes transverse shear effects and which is capable of representing the severe cross-sectional warping effects often observed in relatively thick laminated plates. This is accomplished by assuming that straight lines normal to the plate midsurface prior to deformation need not be straight or normal to the midsurface of the plate following deformation, but that the post-deformation length of a normal line is the same as its pre-deformation length. Mau has shown that the resulting element model gives accurate displacement and stress predictions even for relatively thick laminated plates where severe cross-sectional warping is present. It is believed that this approach is the most general approach (with the exception of a complete three-dimensional analysis) for multilayer plate analyses and was thus chosen for the present study.

3.2.1 Derivation of the Element Stiffness Matrix

The assumed-stress hybrid finite-element model is based on a modified complementary energy principle in which the requirements of inter-element traction compatibility and boundary traction compatibility (mechanical boundary conditions) have been relaxed. The resulting hybrid-stress functional, π_{mc}, may be stated in matrix form as

$$\pi_{mc} = \sum_n \left\{ \frac{1}{2} \int_{V_n} \underset{\sim}{\sigma}^T \underset{\sim}{S}\, \underset{\sim}{\sigma}\, dV - \int_{\partial V_n} \underset{\sim}{T}^T \underset{\sim}{u}\, ds + \int_{S_{\sigma_n}} \underset{\sim}{\bar{T}}^T \underset{\sim}{u}\, ds \right\} \tag{43}$$

where

$\underset{\sim}{\sigma}$ = stress vector

$\underset{\sim}{S}$ = material properties matrix

$\underset{\sim}{T}$ = element boundary traction vector

$\underset{\sim}{u}$ = element boundary displacement vector

$\underset{\sim}{\bar{T}}$ = prescribed boundary traction vector

V_n = volume of the nth element

∂V_n = boundary of the nth element

S_{σ_n} = portion of ∂V_n over which tractions are prescribed.

and the summation in Eq. 43 is over all elements.

The application of Eq. 43 requires the assumption of a stress field, $\underset{\sim}{\sigma}$, in each element which satisfies the homogeneous equilibrium equations, and the assumption of a displacement field, $\underset{\sim}{u}$, along the element boundary which satisfies interelement displacement compatibility. For the present multilayer element the stresses in the mth layer, $\underset{\sim}{\sigma}^m$, are expressed in terms of a set of stress parameters, $\underset{\sim}{\beta}^m$, for the mth layer, in the form

$$\underset{\sim}{\sigma}^m = \underset{\sim}{P}\, \underset{\sim}{\beta}^m \tag{44}$$

where $\underset{\sim}{P}$ is a function of the Cartesian coordinates x,y,z. The boundary tractions for the mth layer, $\underset{\sim}{T}^m$, can be related to the stress parameters, $\underset{\sim}{\beta}^m$, using the direction cosines of the boundary, and can be expressed as

$$\underset{\sim}{T}^m = \underset{\sim}{R}\, \underset{\sim}{\beta}^m \tag{45}$$

The displacements, $\underset{\sim}{u}$, along the boundary of the element are then expressed in terms of a finite number of generalized nodal displacement parameters (degrees of freedom), $\underset{\sim}{q}$, such that interelement displacement continuity is satisfied, in the form

$$\underset{\sim}{u} = \underset{\sim}{L}\,\underset{\sim}{q} \tag{46}$$

where $\underset{\sim}{L}$ is a function of position on the element boundary. Substituting Eqs. 44, 45, and 46 into Eq. 43 yields the following expression for π_{mc}:

$$\pi_{mc} = \sum_n \left\{ \frac{1}{2} \underset{\sim}{\beta}^T \underset{\sim}{H} \underset{\sim}{\beta} - \underset{\sim}{\beta}^T \underset{\sim}{G}\, \underset{\sim}{q} + \underset{\sim}{q}^T \underset{\sim}{Q} \right\} \tag{47}$$

where

$$\underset{\sim}{H} = \begin{bmatrix} \underset{\sim}{H}^1 & & & \\ & \underset{\sim}{H}^2 & & \\ & & \ddots & \\ & & & \underset{\sim}{H}^M \end{bmatrix} \tag{48a}$$

$$\underset{\sim}{H}^m = \int_{V_n^m} \underset{\sim}{P}^T \underset{\sim}{S}^m \underset{\sim}{P}\, dV \tag{48b}$$

$$\underset{\sim}{G} = \begin{bmatrix} \underset{\sim}{G}^1 \\ \underset{\sim}{G}^2 \\ \vdots \\ \underset{\sim}{G}^M \end{bmatrix} \tag{48c}$$

$$\underset{\sim}{G}^m = \int_{\partial V_n^m} \underset{\sim}{R}^T \underset{\sim}{L}\, ds \tag{48d}$$

$$\underset{\sim}{Q} = \int_{S_{\sigma_n}} \underset{\sim}{L}^T \bar{\underset{\sim}{T}}\, ds \tag{48e}$$

$$\underset{\sim}{\beta} = \begin{Bmatrix} \underset{\sim}{\beta}^1 \\ \underset{\sim}{\beta}^2 \\ \vdots \\ \underset{\sim}{\beta}^M \end{Bmatrix} \tag{48f}$$

It should be noted that the integrations in Eqs. 48b and 48d extend over the volume of the mth layer, V_n^m, and the boundary surface of the mth layer, ∂V_n^m, respectively, for the nth element. The matrix $\underset{\sim}{S}^m$ is the material property matrix for the mth layer in the x,y,z coordinate system (see Section 2). In addition, it should be noted that the element $\underset{\sim}{H}$ and $\underset{\sim}{G}$ matrices are "supermatrices" composed of contributions from each of the M layers, and $\underset{\sim}{\beta}$ is a column vector composed of the $\underset{\sim}{\beta}^m$ vectors from each of the M layers.

The choice of independent stress assumptions within each layer implies that stresses on interlayer surfaces are not compatible in general. For present purposes, it will be assumed that perfect bonding exists between layers and thus the following stress compatibility requirements should be satisfied at the (m+1)st interface (between layers m and m+1):

$$\sigma_{xz}^m, \sigma_{yz}^m, \sigma_z^m \Big|_{z=\frac{h^m}{2}} = \sigma_{xz}^{m+1}, \sigma_{yz}^{m+1}, \sigma_z^{m+1} \Big|_{z=-\frac{h^{m+1}}{2}} \tag{49}$$

where h^m is the thickness of the mth layer and a reference z=0 axis is chosen at the midsurface of <u>each</u> layer. In addition to the stress compatibility at interlayer boundaries given by Eq. 49, the requirement that the stresses σ_{xz}, σ_{yz}, and σ_z be zero on the top and bottom surfaces of the plate will also be imposed, i.e.

$$\sigma_{xz}^1, \sigma_{yz}^1, \sigma_z^1 \Big|_{z=-\frac{h^1}{2}} = 0 \tag{50a}$$

$$\sigma_{xz}^M, \sigma_{yz}^M, \sigma_z^M \Big|_{z=\frac{h^M}{2}} = 0 \tag{50b}$$

Equation 50a corresponds to the bottom of the plate (i.e. bottom surface of the first layer) and Eq. 50b corresponds to the top of the plate (i.e. upper surface of the Mth layer). Equations 49 and 50 may be viewed as constraint conditions on the full set of stress parameters, $\underset{\sim}{\beta}$, and these constraint equations can be expressed as

$$\underset{\sim}{A}\,\underset{\sim}{\beta} = 0 \tag{51}$$

Using the Lagrange Multiplier technique, Eq. 51 (premultiplied by a vector

of Lagrange multipliers, $\boldsymbol{\lambda}$) is substituted into the hybrid functional π_{mc} (Eq. 47) to yield a modified hybrid functional, π'_{mc}, in the form

$$\pi'_{mc} = \sum_n \left\{ \frac{1}{2} \boldsymbol{\beta}^T \mathbf{H} \boldsymbol{\beta} - \boldsymbol{\beta}^T \mathbf{G} \mathbf{q} + \mathbf{q}^T \mathbf{Q} + \boldsymbol{\lambda}^T \mathbf{A} \boldsymbol{\beta} \right\} \tag{52}$$

At this point it is perhaps worthwhile to discuss briefly the nature and meaning of π'_{mc}. Consider a *typical multilayer element as a region* composed of a number of subregions (in this case layers). The application of Eq. 52 can be shown [8] to be equivalent to the use of the stress model of Fraeijs de Veubeke [9] for each subregion (layer) boundary and the use of the hybrid-stress model for the boundary of the whole region (element). The implication is that stress equilibrium must be satisfied in each subregion (layer), but that stress compatibility along the boundaries of subregions is satisfied only in an average (or integral) sense.

The expression for the element stiffness matrix, $\mathbf{k}$, can now be obtained from Eq. 52 by setting the first variation of π'_{mc} with respect to $\boldsymbol{\beta}$ equal to zero, yielding

$$\mathbf{H} \boldsymbol{\beta} - \mathbf{G} \mathbf{q} + \mathbf{A}^T \boldsymbol{\lambda} = 0 \tag{53}$$

from which

$$\boldsymbol{\beta} = \mathbf{H}^{-1} \mathbf{G} \mathbf{q} - \mathbf{H}^{-1} \mathbf{A}^T \boldsymbol{\lambda} \tag{54}$$

Substituting Eq. 54 into Eq. 51 and solving for the Lagrange multipliers, $\boldsymbol{\lambda}$, gives

$$\boldsymbol{\lambda} = (\mathbf{A} \mathbf{H}^{-1} \mathbf{A}^T)^{-1} (\mathbf{A} \mathbf{H}^{-1} \mathbf{G} \mathbf{q}) \tag{55}$$

The expression which relates the stress parameters, $\boldsymbol{\beta}$, to the nodal displacements, $\mathbf{q}$, is then obtained by substituting Eq. 55 into Eq. 54;

$$\boldsymbol{\beta} = [\mathbf{H}^{-1} \mathbf{G} - \mathbf{H}^{-1} \mathbf{A}^T (\mathbf{A} \mathbf{H}^{-1} \mathbf{A}^T)^{-1} \mathbf{A} \mathbf{H}^{-1} \mathbf{G}] \mathbf{q} = \mathbf{B} \mathbf{q} \tag{56}$$

when Eqs. 55 and 56 are substituted into Eq. 52, the resulting expression for π'_{mc} can be written in the familiar form

$$\pi'_{mc} = \sum_n \left\{ \frac{1}{2} \mathbf{q}^T \mathbf{k} \mathbf{q} - \mathbf{q}^T \mathbf{Q} \right\} \tag{57}$$

where $\mathbf{k}$ is the element stiffness matrix and is given by

$$\underset{\sim}{k} = \underset{\sim}{G}^T \underset{\sim}{H}^{-1} \underset{\sim}{G} - \underset{\sim}{G}^T \underset{\sim}{H}^{-1} \underset{\sim}{A}^T (\underset{\sim}{A} \underset{\sim}{H}^{-1} \underset{\sim}{A}^T)^{-1} \underset{\sim}{A} \underset{\sim}{H}^{-1} \underset{\sim}{G} \tag{58}$$

and $\underset{\sim}{Q}$ is the element nodal loading vector. It should be noted that the first term in Eq. 58 is the same as that obtained for the conventional hybrid-stress model, and the second term is present because of the introduction of stress continuity (in an approximate sense) at interlayer boundaries.

3.2.2 Element Stress and Displacement Assumptions

In Ref. 2, Mau considered various combinations of linear and quadratic interpolations for the stresses in the interior of the element and displacements along the element boundary. Based on the results of several performance tests, he concluded that the optimum choice for both stress and displacement is a linear interpolation in x and y.

Mau used the following linear interpolation for stresses (which satisfies the homogeneous equilibrium equations for the mth layer):

$$\begin{aligned}
\sigma_x^m &= \beta_1^m + \beta_4^m x + \beta_7^m y + z(\beta_{10}^m + \beta_{13}^m x + \beta_{16}^m y) \\
\sigma_y^m &= \beta_2^m + \beta_5^m x + \beta_8^m y + z(\beta_{11}^m + \beta_{14}^m x + \beta_{17}^m y) \\
\sigma_z^m &\equiv 0 \\
\sigma_{yz}^m &= \beta_{20}^m - z(\beta_6^m + \beta_8^m) - \frac{z^2}{2}(\beta_{15}^m + \beta_{17}^m) \\
\sigma_{xz}^m &= \beta_{19}^m - z(\beta_4^m + \beta_9^m) - \frac{z^2}{2}(\beta_{13}^m + \beta_{18}^m) \\
\sigma_{xy}^m &= \beta_3^m + \beta_6^m x + \beta_9^m y + z(\beta_{12}^m + \beta_{15}^m x + \beta_{18}^m y)
\end{aligned} \tag{59}$$

Thus, 20 stress parameters are required for each layer so that a laminate composed of M layers would require a total of 20M stress parameters. It should be noted that the zero normal stress, σ_z, is a consequence of the linear assumption for σ_x, σ_y, and σ_{xy}; if quadratic terms in x and y were added, then σ_z would be nonzero. The $\underset{\sim}{P}$ and $\underset{\sim}{R}$ matrices for each layer are obtained from Eqs. 59 and the $\underset{\sim}{A}$ matrix for the laminate can be obtained from Eqs. 59 by applying the constraint conditions of Eqs. 49 and 50 (for σ_{xz} and σ_{yz} since σ_z is zero everywhere).

The boundary displacement assumption should be chosen in such a way that a severe cross-sectional warping behavior, such as that shown in Fig. 4, can be approximately represented. This can be accomplished by defining the inplane displacement behavior in terms of translational nodal

displacements u and v (in the x and y directions, respectively) at each interlayer boundary including the top and bottom of the laminate. Thus, the inplane displacement behavior is assumed to be linear along each side of the element and piecewise linear in the z direction. The transverse displacement, w, is assumed to be linear along each side of the element but constant in the z direction for all layers. Therefore, the total number of degrees of freedom at a node consists of one w and 2(M+1) inplane displacements u and v, where M is the total number of layers. The total number of degrees-of-freedom for the present four-node general quadrilateral element is thus 8M+12.

For a typical layer, m, the displacement interpolation along side 1-2 (between nodes 1 and 2 -- see Fig. 5), for example, is given by

$$
\begin{aligned}
u_{1-2}^{m} &= \frac{1}{2}\left(u_1^{m+1}+u_1^{m}\right)(1-s)+\frac{1}{2}\left(u_2^{m+1}+u_2^{m}\right)s+\frac{z}{h^m}\left[\left(u_1^{m+1}-u_1^{m}\right)(1-s)+\left(u_2^{m+1}-u_2^{m}\right)s\right] \\
v_{1-2}^{m} &= \frac{1}{2}\left(v_1^{m+1}+v_1^{m}\right)(1-s)+\frac{1}{2}\left(v_2^{m+1}+v_2^{m}\right)s+\frac{z}{h^m}\left[\left(v_1^{m+1}-v_1^{m}\right)(1-s)+\left(v_2^{m+1}-v_2^{m}\right)s\right] \qquad (60) \\
w_{1-2}^{m} &= w_1(1-s)+w_2 s
\end{aligned}
$$

where s is a nondimensional parameter which takes on the values s=0 at node 1 and s=1 at node 2. Expressions similar to Eqs. 60 can be obtained for each layer and each side of the element.

In practice, the supermatrices $\underset{\sim}{H}$ and $\underset{\sim}{G}$ are obtained by forming the matrices $\underset{\sim}{H}^m$ and $\underset{\sim}{G}^m$ for the mth layer and inserting the appropriate terms in $\underset{\sim}{A}$ corresponding to the mth layer. When all layers have been processed, the $\underset{\sim}{H}$, $\underset{\sim}{G}$, and $\underset{\sim}{A}$ matrices are complete. The element $\underset{\sim}{B}$ matrix can now be obtained from Eq. 56 and the element stiffness matrix can be obtained from Eq. 58. In subsequent discussions, the 4-node general quadrilateral multilayer plate element based on Eq. 52 and utilizing the stress assumption of Eq. 59 and displacement assumption of Eq. 60 will be termed element ELEMZ.

3.2.3 Derivation of the Element Mass Matrix

As was shown in the previous subsections, the use of the hybrid-stress finite-element model for static analysis is equivalent to the use of the conventional assumed-displacement model in the sense that the resulting matrix equations are expressed in terms of unknown nodal displacement parameters. The hybrid-stress model thus represents an alternate way of obtaining an element

stiffness matrix. For dynamic analysis, the corresponding element mass matrix is required.

The derivation of the element mass matrix is most conveniently seen by considering a functional in the form of a Hellinger-Reissner principle [10,11] for the free vibration of a continuum,

$$\pi_{mR} = \sum_n \left\{ \int_{V_n} \left[-\tfrac{1}{2} S_{ijk\ell}\, \sigma_{ij}\, \sigma_{k\ell} + \tfrac{1}{2} \sigma_{ij} (u_{i,j} + u_{j,i}) - \tfrac{1}{2} \rho\, \dot{u}_i \dot{u}_i \right] dV - \int_{\partial V_n} T_i (u_i - \bar{u}_i)\, ds \right\} \tag{61}$$

In Eq. 61, tensor notation and the summation convention have been employed. Also, ρ is the material density, u_i is the displacement field in the <u>interior</u> of the element, $\bar{u}_i$ is the displacement field on the boundary of the element (note that u_i need not be equal to $\bar{u}_i$ on ∂V_n), $\dot{u}_i$ is the velocity field in the interior of the element, and a comma denotes partial differentiation. The reduction of π_{mR} to correspond to the hybrid-stress model is accomplished by assuming that the boundary tractions, T_i, are related to the stress, σ_{ij}, by

$$T_i = \sigma_{ij} \nu_j \qquad \text{on} \quad \partial V_n \tag{62}$$

where ν_j is the direction cosine tensor on the element boundary, ∂V_n. Then the Divergence theorem

$$\int_{V_n} \tfrac{1}{2} \sigma_{ij} (u_{i,j} + u_{j,i})\, dV = \int_{\partial V_n} T_i u_i\, ds - \int_{V_n} \sigma_{ij,j}\, u_i\, dV \tag{63}$$

is applied to Eq. 61 to yield

$$\pi_{mR} = \sum_n \left\{ \int_{V_n} \left[-\tfrac{1}{2} S_{ijk\ell}\, \sigma_{ij}\, \sigma_{k\ell} - \sigma_{ij,j}\, u_i - \tfrac{1}{2} \rho\, \dot{u}_i \dot{u}_i \right] dV + \int_{\partial V_n} T_i \bar{u}_i\, ds \right\} \tag{64}$$

If the stress field within each element exactly satisfies the homogeneous portion of the equilibrium equations, i.e.

$$\sigma_{ij,j} = 0 \tag{65}$$

then Eq. 64 can be rewritten as

$$\pi_{mR} = \sum_n \left\{ \frac{1}{2} \int_{V_n} S_{ijkl}\, \sigma_{ij}\, \sigma_{kl}\, dV + \frac{1}{2} \int_{V_n} \rho \dot{u}_i \dot{u}_i\, dV - \int_{\partial V_n} T_i \bar{u}_i\, ds \right\} \tag{66}$$

Equation 66 may be viewed as a modified hybrid-stress functional so that the governing functional for dynamic analysis can be written in matrix form as

$$\pi_{mc} = \sum_n \left\{ \frac{1}{2} \int_{V_n} \underset{\sim}{\sigma}^T \underset{\sim}{S}\, \underset{\sim}{\sigma}\, dV + \frac{1}{2} \int_{V_n} \rho \dot{\underset{\sim}{u}}^T \dot{\underset{\sim}{u}}\, dV - \int_{\partial V_n} \underset{\sim}{T}^T \bar{\underset{\sim}{u}}\, ds + \int_{S_{\sigma_n}} \bar{\underset{\sim}{T}}^T \bar{\underset{\sim}{u}}\, ds \right\} \tag{67}$$

Equation 67 is the dynamic equivalent of Eq. 43, and it should be clear that the second term in Eq. 67 will yield the desired element mass matrix. As is done for static applications, the stresses are expressed in terms of unknown stress parameters, $\underset{\sim}{\beta}$, and the <u>boundary</u> displacements, $\bar{\underset{\sim}{u}}$, are expressed in terms of unknown nodal displacement parameters, $\underset{\sim}{q}$. In addition, a displacement assumption for $\underset{\sim}{u}$ in the interior of the element is now required in terms of the nodal displacement parameters, $\underset{\sim}{q}$,

$$\underset{\sim}{u} = \underset{\sim}{N}\, \underset{\sim}{q} \quad \text{in } V_n \tag{68}$$

It should be recalled that the interior displacement assumption need not be equal to the boundary displacement assumption (i.e. $\underset{\sim}{u}$ need not be equal to $\bar{\underset{\sim}{u}}$ on ∂V_n). Then Eqs. 44, 45, 46, and 68 are substituted into Eq. 67, and the constraint condition (Eq. 51) on stresses at interlayer boundaries is introduced. Finally, the stress parameters, $\underset{\sim}{\beta}$, and Lagrange multiplier, $\underset{\sim}{\lambda}$, are eliminated in favor of the nodal displacement parameters, $\underset{\sim}{q}$, the resulting expression for π'_{mc} being given by

$$\pi'_{mc} = \sum_n \left\{ \frac{1}{2} \underset{\sim}{q}^T \underset{\sim}{k}\, \underset{\sim}{q} + \frac{1}{2} \dot{\underset{\sim}{q}}^T \underset{\sim}{m}\, \dot{\underset{\sim}{q}} - \underset{\sim}{q}^T \underset{\sim}{Q} \right\} \tag{69}$$

where $\underset{\sim}{k}$ is the element stiffness matrix given by Eq. 58 and $\underset{\sim}{m}$ is the element mass matrix given by

$$\underset{\sim}{m} = \int_{V_n} \rho\, \underset{\sim}{N}^T \underset{\sim}{N}\, dV \tag{70}$$

It should be noted that the use of Eq. 67 is not fully consistent with the hybrid-stress model. This is because the hybrid-stress model requires that the equilibrium equations be satisfied. However, for dynamic analysis, the equilibrium equations include an inhomogeneous portion corresponding to

inertia terms, and are thus not satisfied by the stress assumptions in the present formulation. Since only the homogeneous equilibrium equations are satisfied, it is more appropriate to view Eq. 67 as a modified Hellinger-Reissner functional or a modified hybrid-stress functional. For convenience, the element mass matrix derived from Eq. 67 will be termed a "hybrid rational" mass matrix.

Now consider the development of a hybrid-rational mass matrix corresponding to element ELEMZ. Since the element boundary displacements for ELEMZ are assumed to be linear, a convenient and suitable interpolation for $\tilde{N}$ would be a bilinear expansion in terms of a pair of transformed coordinates (ξ,η):

$$u^m = \sum_{i=1}^{4} \left\{ \left[\frac{1}{2}\left(u_i^{m+1} + u_i^m\right) + \frac{z}{h^m}\left(u_i^{m+1} - u_i^m\right) \right] N_i \right\} \tag{71}$$

$$v^m = \sum_{i=1}^{4} \left\{ \left[\frac{1}{2}\left(v_i^{m+1} + v_i^m\right) + \frac{z}{h^m}\left(v_i^{m+1} - v_i^m\right) N_i \right\} \right.$$

$$w^m = \sum_{i=1}^{4} \left\{ w_i N_i \right\}$$

where

$$\begin{aligned} N_1 &= (1-\xi)(1-\eta) \\ N_2 &= (1-\eta)\xi \\ N_3 &= \xi\eta \\ N_4 &= (1-\xi)\eta \end{aligned} \tag{72}$$

Equations 71 have been written for the mth layer of the multilayer element, and it should be noted that the original coordinates (x,y) are related to the transformed coordinates (ξ,η) by

$$\begin{aligned} x &= \sum_{i=1}^{4} x_i N_i \\ y &= \sum_{i=1}^{4} y_i N_i \end{aligned} \tag{73}$$

where (x_i, y_i) are the coordinates of the ith node of the element. The element mass matrix is obtained from Eq. 70 by integration over the volume of each

layer of the laminate, with $\underset{\sim}{N}$ and ρ in Eq. 70 replaced by the particular $\underset{\sim}{N}^m$ and ρ^m corresponding to the mth layer.

3.3 Adaptation of the Mau Element to Triangular Shape

In many structural problems of interest, there are regions of the structure in which high stress gradients may exist, and other regions where stress gradients are low. In practice it is most advantageous to be able to use a refined finite-element mesh in regions of high stress gradients and/or other regions of interest, and a more coarse mesh arrangement in regions of low stress gradients. To do this, a suitable element must be available which can be used as a transition element between the refined and coarse mesh regions, and which is compatible with the elements in these regions. The transition element which will be employed in the present effort is a triangular-shaped multilayer plate element.

Because this triangular element is to be used in conjunction with the quadrilateral element ELEMZ described in Subsection 3.2, the primary restriction is that the displacement assumption along the element boundary and the number of generalized displacement parameters at a node, for the triangular element, must be identical to those used for ELEMZ. Thus, the development of the present triangular plate element is based on the same boundary displacement and interior stress assumptions as used in ELEMZ. Because of this, only straightforward modifications of the volume and surface integrations used to generate ELEMZ are necessary to obtain the triangular element.

Mau has included in Ref. 2 a comparison of results obtained for a single-layer isotropic plate problem by using several different element types (quadrilateral and triangular, with a variety of different stress and displacement assumptions) including single-layer versions of the present quadrilateral and triangular multilayer plate elements. Based on these initial comparisons, Mau concluded that the present quadrilateral element yields reasonably accurate solutions, whereas the present triangular element yields results which are too stiff for practical use of the triangular element to model the entire plate. However, when used solely as a transition (mesh expander) element, the stiffening effects of the triangular element should be less pronounced in terms of determining the overall structural behavior.

3.4 Development of a Quadrilateral Element with a Traction-Free Edge

When the finite-element method is employed for the analysis of structures containing cutouts, it is often necessary to use a highly refined mesh in the region of the cutout so that the stress gradient near the cutout and the traction-free condition at the surface of the cutout may be more closely approximated. Pian has presented some results for single layer, isotropic materials which suggest that improved results may be obtained near traction-free boundaries by using a special assumed-stress hybrid element which exactly satisfies the traction-free condition [12]. Thus, one phase of the present effort was the investigation and evaluation of a quadrilateral shaped, multilayer plate element for which the traction-free condition is exactly satisfied on one of the element boundaries. In order for such an element to be of practical use in engineering analyses it must be computationally efficient and it must yield displacement and stress results near a cutout which are significantly better than the results which could be obtained by using conventional elements.

In practice, because this special element may be linked to ELEMZ, the boundary displacement assumption employed for the traction-free element must be identical to the boundary displacement assumption employed in ELEMZ. The stress assumption chosen for the traction-free element must satisfy the equilibrium equations and, in addition, must yield zero surface tractions (not necessarily zero stresses) when evaluated on the traction-free boundary of the element. In essence, the only difference between the formulation of the traction-free element and the formulation of ELEMZ is in the choice of an appropriate stress field in the interior of the element.

Several different stress assumptions were considered in a study reported in Ref. 4. For the sake of completeness, the essence of this study will be summarized here. For convenience, the notation $A_1A_2A_3A_4$ will be adopted to describe the order of the stress assumption. In this notation, A_1, will denote the highest order of z included in the stress assumption (either linear, L, or quadratic, Q). A_2 will denote the highest order (either L or Q) of x and y contained in the portion of the stress assumption of order z^o (constant). A_3 will denote the highest order (either L or Q) of x and y contained in the portion of the stress assumption of order z^1 (linear). If

A_1=Q, then A_4 will denote the highest order (either L or Q) of x and y contained in the portion of the stress assumption of order z^2 (quadratic). It should be noted that this notation applies only to the inplane stress assumption ($\sigma_x, \sigma_y, \sigma_{xy}$), and it is assumed that the interpolation is complete up to the order stated (i.e. L implies that terms of the order 1, x, and y are present, and Q implies that terms of the order $1, x, y, xy, x^2$, and y^2 are present). For example, the stress assumption used for ELEMZ (Eq. 59) would be denoted by LLL (i.e. linear in z, and linear in x and y in the z^0 and z^1 terms).

In order to obtain the required stress assumption, an assumption is made for the inplane stress components ($\sigma_x, \sigma_y, \sigma_{xy}$) and the remaining stress components ($\sigma_{xz}, \sigma_{yz}, \sigma_z$) are obtained by solving the equilibrium equations. The resulting stress assumption thus satisfies the homogeneous equilibrium equations as required. Next the traction-free conditions must be satisfied. For convenience, a local (element) axis system is adopted in such a way that the traction-free edge coincides with the x axis; this simplifies the traction-free conditions to

$$\left.\begin{aligned} T_x &= -\sigma_{xy} = 0 \\ T_y &= -\sigma_y = 0 \\ T_z &= -\sigma_{yz} = 0 \end{aligned}\right\} \text{ at } y = 0 \tag{74}$$

The conditions given by Eqs. 74 are then imposed on the stress distribution and appropriate stress parameters (β's) are eliminated so that Eqs. 74 are exactly satisfied. The resulting stress assumption has a reduced number of stress parameters and satisfies both equilibrium and the traction-free condition exactly. It should be noted that the resulting number of β's following reduction cannot be arbitrarily small. Tong and Pian [13] have shown that the number of stress parameters, n_β, must be greater than or equal to the number of nodal displacement parameters, n_q, minus the number of rigid body modes, n_R (=6 for the present elements), i.e.

$$n_\beta \geq n_q - n_R \tag{75}$$

Equation 75 is a necessary but not sufficient condition to guarantee the existence of a solution. Even when Eq. 75 is satisfied, so-called "additional

kinematic modes" may be present [5,8]. These modes behave in a fashion similar to rigid-body modes; if they are not properly constrained*, the assembled stiffness matrix will either be singular or so poorly conditioned that reliable results cannot be obtained. A more thorough discussion of this phenomenon as well as procedures for determining these modes, if present, may be found in Refs. 5 and 8.

Initially, attempts were made to choose stress assumptions which had a minimum number of stress parameters. The first assumption attempted, LLL, coresponds to that used in ELEMZ. However, after Eqs. 74 were satisfied, it was found that Eq. 75 was not satisfied; thus the LLL assumption could not be used. Next, the order of the bending stress behavior was increased to yield a LLQ assumption which contained 36 stress parameters. After application of Eqs. 74, the number of stress parameters was reduced to 21 (which satisfies Eq. 75 even for a single layer). However, numerical difficulties were encountered; after assembly, the $\underset{\sim}{A}\,\underset{\sim}{H}^{-1}\,\underset{\sim}{A}^{T}$ supermatrix was found to be singular and thus could not be inverted as needed to obtain the element stiffness matrix (see Eq. 58). By tracing the origin of this ill behavior, it was found that a linear stretching part in the assumed stress field does not furnish the odd powers of z necessary to make the interlayer conditions $\underset{\sim}{A}\underset{\sim}{\beta}=0$ linearly independent. The lack of odd-power terms gives an identical relation for the top and the bottom of each layer. In other words, the shear stresses appear to be the same at the bottom and the top of each layer and from layer to layer, which is too restrictive.

Another way to increase the number of β's is to use an in-plane stress field linear in x and y as in ELEMZ (computationally a good bargain) but quadratic in z. This third formulation (QLLL) satisfies the "odd powers" condition and Eq. 75 for two or more layers, but is found to contain additional kinematic modes. Here, the approximation is probably too crude; only 13 β's, no σ_z, no σ_y, no σ_{yz}. In addition, increasing the order in z while keeping the x y behavior linear does not appear logical, since the xy dimensions of the element are generally larger than its thickness. Moreover, Pagano's results [14] for the cylindrical bending of multilayer plates show a quasi-linear behavior of the in-plane stresses in the z direction.

---

*The structure must be constrained in such a way that all deformation modes of the structure corresponding to the additional kinematic mode are constrained. For most cases, this is accomplished simply by imposing the physical boundary condition of the problem.

The final stress assumption attempted contained quadratic expansions in x and y in both the stretching and bending portions of the inplane stress assumption (i.e. LQQ). After reduction, the stress assumption contained 25 β's. However, the assembled stiffness matrix was found to be singular when a simple plate analysis was performed. The source of this difficulty (currently under investigation) appears to be the presence of a single additional kinematic mode.

In view of the various difficulties encountered in the development of a traction-free element, no further stress assumptions were attempted. However, this was not the sole reason for abandoning the search for a traction-free element. In particular, it was found that the use of ELEMZ was impractical for engineering analysis because of restrictions on the number of layers which can be accommodated, as explained in the next subsection. In addition, performance tests (Section 5) indicated that an alternate multilayer plate element (Section 4) would prove to be more practical for use in engineering analysis, and could also yield reasonable estimates of stress distribution near a cutout.

In summary, it is believed that a stress assumption of higher order than the LQQ assumption will be required, which suggests that the number of stress parameters after reduction will exceed 25 β's per layer. Because of core storage requirements associated with the ELEMZ formulation, such an element would be restricted to structures having few layers. It is believed that such an element would be of little use in practical engineering analyses.

3.5 Discussion

The elements developed in this section are based on the assumption of an independent set of stress parameters, $\underset{\sim}{\beta}$, in each layer and nodal displacement parameters, $\underset{\sim}{q}$, which, in effect, allow for piecewise linear rotation of the cross-section of each layer. This level of generality may be necessary for thick laminated plates exhibiting severe cross-sectional warping. The purpose of this subsection is to discuss the price to be paid for including these generalities. The discussion will center on element ELEMZ, but the observations are valid for the other elements based on the same formulation.

The first penalty is in terms of computer core storage requirements. Assuming a laminate composed of n layers, the total number of stress parameters required would be 20n and the total number of nodal degrees of freedom would be (8n+12) for a single element ELEMZ. The $\underset{\sim}{G}$ supermatrix (Eq. 48c) would require $(160n^2+240n)$ words of storage, the $\underset{\sim}{H}$ supermatrix (Eq. 48a) would

require (210n) words of storage (storing only the lower triangle of each of the symmetric $\tilde{H}^m$ matrices), the element $\tilde{B}$ matrix (Eq. 56) would require $(160n^2+240n)$ words of storage, and the element stiffness matrix, $\tilde{k}$ (Eq. 58), would require $(32n^2+100n+72)$ words of storage (storing only the lower triangle of the symmetric stiffness matrix). The storage of all of these arrays in core would require $(352n^2+790n+72)$ words of storage. Tabulated below are the storage requirements in words and BYTES (assuming 4 BYTES/word for single precision arithmetic) for several values of n:

n	Storage (words)	Storage (bytes)
1	1,214	4,856
3	5,610	22,440
6	17,484	69,936
9	35,694	142,776
15	91,122	364,488
20	156,672	626,688
30	340,572	1,362,288

Thus, based solely on in-core storage requirements for the generation of a stiffness matrix, certain limitations will exist on the maximum number of layers which can be accommodated.

In many engineering analyses, the largest single block of storage required is for the assembled stiffness matrix (and mass matrix, if consistent mass matrices, rather than lumped mass matrices, are employed). For illustrative purposes, assume that ELEMZ is to be used to analyze a square flat plate which is modeled by a uniform mesh having m elements in the x-direction and m elements in the y-direction (i.e. a total of m^2 elements, and $(m+1)^2$ nodes). Assume that the nodes are numbered optimally to yield the smallest bandwidth in the assembled stiffness matrix, and that the lower triangle of the assembled stiffness matrix is stored row by row (in a vector) starting in each row with the first nonzero term. The storage requirements can be estimated as the total number of degrees of freedom times the average semi-bandwidth. For ELEMZ, each node has (2n+3) degrees-of-freedom (n=number of layers), so that the total number of degrees-of-freedom would be $(m+1)^2(2n+3)$ and the average semi-bandwidth can be estimated as (m+2)(2n+3). Thus, the total number of

words of storage required for the assembled stiffness matrix is given approximately by $(m+1)^2(m+2)(2n+3)^2$. Tabulated below are the storage requirements (in thousands of words) for several values of n and m:

		m				
		2	4	6	8	10
n	1	0.9	3.75	9.80	20.25	36.30
	5	6.08	25.35	66.25	136.89	245.39
	10	19.04	29.35	207.37	428.49	768.11
	15	39.20	163.35	426.89	882.09	1581.23

These requirements would double for dynamic analyses if both the assembled stiffness and mass matrices were stored in core simultaneously. As a result of these storage requirements, use of ELEMZ may, in practice, be limited to laminated plates composed of fewer than five layers if a complete in-core solution is desired.

The second penalty for using element ELEMZ is in terms of computation time. Typically, the most time consuming operation in the formation of an element stiffness matrix by the hybrid-stress method is the inversion of the $\underset{\sim}{H}$ matrix. For element ELEMZ the 20 by 20 $\underset{\sim}{H}^m$ matrix (associated with the mth layer) must be inverted for each of the n layers in the laminate. In addition, a single inversion of the $(\underset{\sim}{A}\ \underset{\sim}{H}^{-1}\ \underset{\sim}{A}^T)$ supermatrix is required. The computation time required to process the assembled matrix equations will increase rapidly as the total number of degrees of freedom increases, which is, in turn, related to the total number of layers.

In view of these considerations, an alternate element formulation may be required for which the storage requirements are less severe, while maintaining an acceptable degree of accuracy. Such a formulation is presented in the next section.

SECTION 4

DEVELOPMENT OF MODERATELY-THICK MULTILAYER PLATE ELEMENTS

4.1 Introduction

In this section, an alternate formulation will be presented for a multilayer plate element based on the hybrid-stress model. In the formulation of element ELEMZ (Section 3), the number of degrees of freedom per element was dependent on the number of layers so that severe cross-sectional warping effects from layer to layer could be approximately represented. This, in turn, dictated that the number of stress parameters per element also be dependent on the number of layers so that the β-q relation, discussed in Subsection 3.4, would be satisfied for an arbitrary number of layers. As a result, the computer storage requirements when using ELEMZ may become prohibitively large even for relatively few layers. To alleviate these difficulties, a less general deformation behavior is incorporated in the present alternate element formulation. In particular, it is assumed that straight lines normal to the plate midsurface prior to deformation remain straight (but not necessarily normal to the plate midsurface) after deformation (Fig. 6). By utilizing this more restrictive assumption, transverse shear deformation effects are still included (because of the assumption of non-normal rotations of the cross-section), but the layer to layer cross-sectional warping will be modeled only in an average sense. It is believed that such an assumption is adequate for thin or moderately thick laminates.

Such an element, based on the hybrid-stress model, was developed by Spilker [5]. In the earlier element, the number of degrees of freedom was fixed at five per node (independent of the number of layers) and the number of stress parameters for the laminate was 18+2n, where n is the total number of layers. The calculation of the element stiffness matrix uses the same expression (Eq. 58) as used for ELEMZ. Element performance tests cited in Ref. 5 (displacement results only) suggest that reliable results can be obtained for thin and moderately-thick plates where transverse shear deformation effects are present.

The present alternate element is based on an improvement of the formulation given in Ref. 5. As will be shown, the number of stress parameters and

nodal degrees of freedom in the resulting element are independent of the number of layers in the laminate, and the expression for the element stiffness matrix is identical to that employed in the conventional assumed-stress hybrid model.

4.2 Derivation of Stiffness and Mass Matrices for a Quadrilateral Element

The derivation of the stiffness and mass matrices for the present four-node general quadrilateral multilayer plate element follows the development given in Section 3 with the following key simplifications:

1. The stresses within each layer are assumed in terms of a set of stress parameters, $\underset{\sim}{\beta}$, which are the same for each layer, and thus correspond to the laminate as a whole.

2. In addition to satisfying the homogeneous equilibrium equations, the stress assumption must exactly satisfy the interlayer stress compatibility relations given by Eqs. 49 and 50.

3. The displacement behavior of the laminate is defined in terms of translational displacements, u,v, and w (in the x,y, and z directions, respectively) of the plate midsurface and rotations θ_x and θ_y of lines normal to the midsurface prior to deformation. The rotations θ_x and θ_y correspond, but are not identical to $\partial w/\partial y$ and $\partial w/\partial x$, respectively.

The introduction of the second simplification implies that Eq. 51 is exactly satisfied and need not be introduced into the hybrid functional. As a result, the conventional form of π_{mc} (Eq. 43) can be used and the relation between stress parameters, $\underset{\sim}{\beta}$, and nodal displacement parameters, $\underset{\sim}{q}$, (Eq. 56) reduces to

$$\underset{\sim}{\beta} = \underset{\sim}{H}^{-1} \underset{\sim}{G} \underset{\sim}{q} = \underset{\sim}{B} \underset{\sim}{q} \tag{76}$$

The expression for the element stiffness matrix, $\underset{\sim}{k}$, (Eq. 58) then reduces to

$$\underset{\sim}{k} = \underset{\sim}{G}^T \underset{\sim}{H}^{-1} \underset{\sim}{G} \tag{77}$$

Equations 76 and 77 are the same as those obtained in the conventional hybrid-stress model. For the present element, the stresses in the mth layer are expressed in terms of an interpolation matrix for the mth layer, $\underset{\sim}{P}^m$, and a set of stress parameters, $\underset{\sim}{\beta}$, which are the same for each layer. Thus, the stresses, $\underset{\sim}{\sigma}^m$, and boundary tractions, $\underset{\sim}{T}^m$, in the mth layer will be assumed in the form:

$$\underset{\sim}{\sigma}^m = \underset{\sim}{P}^m \underset{\sim}{\beta} \tag{78a}$$

$$\underset{\sim}{T}^m = \underset{\sim}{R}^m \underset{\sim}{\beta} \tag{78b}$$

The element $\underset{\sim}{H}$ and $\underset{\sim}{G}$ matrices are then defined as

$$\underset{\sim}{H} = \underset{\sim}{H}^1 + \underset{\sim}{H}^2 + \cdots + \underset{\sim}{H}^M \tag{79a}$$

$$\underset{\sim}{G} = \underset{\sim}{G}^1 + \underset{\sim}{G}^2 + \cdots + \underset{\sim}{G}^M \tag{79b}$$

where

$$\underset{\sim}{H}^m = \int_{V_n^m} \underset{\sim}{P}^{m^T} \underset{\sim}{S}^m \underset{\sim}{P}^m \, dV \tag{80a}$$

$$\underset{\sim}{G}^m = \int_{\partial V_n^m} \underset{\sim}{R}^{m^T} \underset{\sim}{L} \, ds \tag{80b}$$

the integration extending over the volume, V_n^m, and boundary, ∂V_n^m, of the mth layer of the nth element. Because of the first and third simplifications, the dimensions of these matrices are fixed (i.e. independent of the number of layers). The method for determining the $\underset{\sim}{P}^m$ matrices will now be discussed.

It is required that the stress assumption in each layer be related to a set of stress parameters, $\underset{\sim}{\beta}$, which correspond to the entire laminate. To accomplish this, the inplane <u>strains</u> for the <u>entire laminate</u> are first expressed in terms of a set of parameters, $\underset{\sim}{\beta}$, using a linear interpolation:

$$\begin{aligned} \varepsilon_x &= \beta_1 + \beta_4 x + \beta_7 y + z(\beta_{10} + \beta_{13} x + \beta_{16} y) \\ \varepsilon_y &= \beta_2 + \beta_5 x + \beta_8 y + z(\beta_{11} + \beta_{14} x + \beta_{17} y) \\ \gamma_{xy} &= \beta_3 + \beta_6 x + \beta_9 y + z(\beta_{12} + \beta_{15} x + \beta_{18} y) \end{aligned} \tag{81}$$

where a reference axis z=0 defines the midsurface of the laminate. The inplane stresses in the mth layer are related to the inplane strains by

$$\begin{Bmatrix} \sigma_x \\ \sigma_y \\ \sigma_{xy} \end{Bmatrix}^m = \begin{bmatrix} C_{11} & C_{12} & C_{16} \\ C_{12} & C_{22} & C_{26} \\ C_{16} & C_{26} & C_{66} \end{bmatrix}^m \begin{Bmatrix} \varepsilon_x \\ \varepsilon_y \\ \gamma_{xy} \end{Bmatrix} \tag{82}$$

or

$$\begin{aligned} \sigma_x^m = {} & C_{11}^m \left[\beta_1 + \beta_4 x + \beta_7 y + z\left(\beta_{10} + \beta_{13} x + \beta_{16} y \right) \right] \\ & + C_{12}^m \left[\beta_2 + \beta_5 x + \beta_8 y + z\left(\beta_{11} + \beta_{14} x + \beta_{17} y \right) \right] \\ & + C_{16}^m \left[\beta_3 + \beta_6 x + \beta_9 y + z\left(\beta_{12} + \beta_{15} x + \beta_{18} y \right) \right] \end{aligned} \tag{83a}$$

$$\begin{aligned} \sigma_y^m = {} & C_{12}^m \left[\beta_1 + \beta_4 x + \beta_7 y + z\left(\beta_{10} + \beta_{13} x + \beta_{16} y \right) \right] \\ & + C_{22}^m \left[\beta_2 + \beta_5 x + \beta_3 y + z\left(\beta_{11} + \beta_{14} x + \beta_{17} y \right) \right] \\ & + C_{26}^m \left[\beta_3 + \beta_6 x + \beta_9 y + z\left(\beta_{12} + \beta_{15} x + \beta_{18} y \right) \right] \end{aligned} \tag{83b}$$

$$\begin{aligned} \sigma_{xy}^m = {} & C_{16}^m \left[\beta_1 + \beta_4 x + \beta_7 y + z\left(\beta_{10} + \beta_{13} x + \beta_{16} y \right) \right] \\ & + C_{26}^m \left[\beta_2 + \beta_5 x + \beta_8 y + z\left(\beta_{11} + \beta_{14} x + \beta_{17} y \right) \right] \\ & + C_{66}^m \left[\beta_3 + \beta_6 x + \beta_9 y + z\left(\beta_{12} + \beta_{15} x + \beta_{18} y \right) \right] \end{aligned} \tag{83c}$$

The C_{ij} (i,j=1,2,6) terms are the inplane material stiffness coefficients transformed into the global x,y,z coordinate system, as given in Section 2 (Eqs. 42). The remaining stress components for the mth layer are obtained from the equilibrium equations as:

$$\begin{aligned} \sigma_{xz}^m & = - \int \left(\sigma_{x,x}^m + \sigma_{xy,y}^m \right) dz \\ & = -z \left[C_{11}^m \beta_4 + C_{12}^m \beta_5 + C_{16}^m \beta_6 + C_{16}^m \beta_7 + C_{26}^m \beta_8 + C_{66}^m \beta_9 \right] \\ & \quad - \frac{z^2}{2} \left[C_{11}^m \beta_{13} + C_{12}^m \beta_{14} + C_{16}^m \beta_{15} + C_{16}^m \beta_{16} + C_{26}^m \beta_{17} + C_{66}^m \beta_{18} \right] + D_1^m \end{aligned} \tag{83d}$$

$$\sigma_{yz}^m = -\int (\sigma_{y,y}^m + \sigma_{xy,x}^m)\, dz$$

$$= -z \left[C_{12}^m \beta_7 + C_{22}^m \beta_8 + C_{26}^m \beta_9 + C_{16}^m \beta_4 + C_{26}^m \beta_5 + C_{66}^m \beta_6 \right] \tag{83e}$$

$$- \frac{z^2}{2} \left[C_{12}^m \beta_{16} + C_{22}^m \beta_{17} + C_{26}^m \beta_{18} + C_{16}^m \beta_{13} + C_{26}^m \beta_{14} + C_{66}^m \beta_{15} \right] + D_2^m$$

$$\sigma_z^m = -\int (\sigma_{xz,x}^m + \sigma_{yz,y}^m)\, dz \equiv 0 \tag{83f}$$

where D_1^m and D_2^m are the constants of integration for the mth layer. The stress assumption for the mth layer given by Eqs. 83a through 83f satisfies equilibrium as required. Also, it should be noted that the zero σ_z^m is a consequence of the linear (in x and y) assumptions chosen for the inplane stresses.

For the present formulation, the stress assumption is required to satisfy exactly the interlayer stress compatibility conditions given by Eqs. 49, 50a, and 50b. (Note that the condition on σ_z is identically satisfied in this case since σ_z=0 everywhere.) The conditions may be satisfied by appropriate choice of the constants of integration, D_1^m and D_2^m, for each layer. Specifically, D_1^1 and D_2^1 are chosen so that Eq. 50a is satisfied (zero transverse shear stress at the bottom of the laminate). Then D_1^m and D_2^m (m=2,3...M) are chosen so that Eq. 49 is satisfied at the interface between layers m-1 and m. This process is repeated until the constants D_1^M and D_2^M have been determined. The resulting expressions for σ_{xz}^m and σ_{yz}^m are given by:

$$\sigma_{xz}^m = K_4^m \beta_4 + K_5^m \beta_5 + K_6^m \beta_6 + K_6^m \beta_7 + K_8^m \beta_8 + K_9^m \beta_9$$
$$+ K_{13}^m \beta_{13} + K_{14}^m \beta_{14} + K_{15}^m \beta_{15} + K_{15}^m \beta_{16} + K_{17}^m \beta_{17} + K_{18}^m \beta_{18} \tag{84a}$$

$$\sigma_{yz}^m = K_6^m \beta_4 + K_8^m \beta_5 + K_9^m \beta_6 + K_5^m \beta_7 + A_8^m \beta_8 + K_8^m \beta_9$$
$$+ K_{15}^m \beta_{13} + K_{17}^m \beta_{14} + K_{18}^m \beta_{15} + K_{14}^m \beta_{16} + A_{17}^m \beta_{17} + K_{17}^m \beta_{18} \tag{84b}$$

where the coefficients of the β's are given by

$$K_4^m = \sum_{i=1}^{m} h_i C_{11}^i - \sum_{i=2}^{m} h_i C_{11}^{i-1} - z C_{11}^m \tag{85a}$$

$$K_5^m = \sum_{i=1}^{m} h_i C_{12}^i - \sum_{i=2}^{m} h_i C_{12}^{i-1} - z C_{12}^m \tag{85b}$$

$$K_6^m = \sum_{i=1}^{m} h_i C_{16}^i - \sum_{i=2}^{m} h_i C_{16}^{i-1} - z C_{16}^m \tag{85c}$$

$$K_8^m = \sum_{i=1}^{m} h_i C_{26}^i - \sum_{i=2}^{m} h_i C_{26}^{i-1} - z C_{26}^m \tag{85d}$$

$$K_9^m = \sum_{i=1}^{m} h_i C_{66}^i - \sum_{i=2}^{m} h_i C_{66}^{i-1} - z C_{66}^m \tag{85e}$$

$$K_{13}^m = \frac{1}{2}\left[\sum_{i=1}^{m} h_i^2 C_{11}^i - \sum_{i=2}^{m} h_i^2 C_{11}^{i-1} - z^2 C_{11}^m \right] \tag{85f}$$

$$K_{14}^m = \frac{1}{2}\left[\sum_{i=1}^{m} h_i^2 C_{12}^i - \sum_{i=2}^{m} h_i^2 C_{12}^{i-1} - z^2 C_{12}^m \right] \tag{85g}$$

$$K_{15}^m = \frac{1}{2}\left[\sum_{i=1}^{m} h_i^2 C_{16}^i - \sum_{i=2}^{m} h_i^2 C_{16}^{i-1} - z^2 C_{16}^m \right] \tag{85h}$$

$$K_{17}^m = \frac{1}{2}\left[\sum_{i=1}^{m} h_i^2 C_{26}^i - \sum_{i=2}^{m} h_i^2 C_{26}^{i-1} - z^2 C_{26}^m \right] \tag{85i}$$

$$K_{18}^m = \frac{1}{2}\left[\sum_{i=1}^{m} h_i^2 C_{66}^i - \sum_{i=2}^{m} h_i^2 C_{66}^{i-1} - z^2 C_{66}^m \right] \tag{85j}$$

$$A_8^m = \sum_{i=1}^{m} h_i C_{22}^i - \sum_{i=2}^{m} h_i C_{22}^{i-1} - z C_{22}^m \tag{85k}$$

$$A_{17}^m = \frac{1}{2}\left[\sum_{i=1}^{m} h_i^2 C_{22}^i - \sum_{i=2}^{m} h_i^2 C_{22}^{i-1} - z^2 C_{22}^m \right] \tag{85l}$$

where h_i is the z-coordinate of the ith surface (see Fig. 7).

The stress assumption given by Eqs. 83a-83c, 84a, and 84b now satisfies the zero transverse shear stress requirement at the bottom surface of the laminate, and the transverse shear stress compatibility requirement at each interlayer surface in the laminate. The only remaining requirement is that the transverse shear stresses be zero on the upper surface of the laminate. This condition may be stated as

$$\sigma_{xz}^{M}\left(z=h_{M+1}\right)=0 \tag{86a}$$

$$\sigma_{yz}^{M}\left(z=h_{M+1}\right)=0 \tag{86b}$$

The expressions for σ_{xz}^{M} and σ_{yz}^{M} contain no undetermined constants of integration so that Eqs. 86a and 86b may be viewed as constraint conditions on the stress parameters requiring elimination of two of the β's in favor of the remaining sixteen β's. For the present element, β_4 and β_8 will be determined in terms of the remaining β's. Thus, Eqs. 84a and 84b are substituted into Eqs. 86a and 86b and the resulting two equations are solved to yield, in matrix form,

$$\begin{Bmatrix} \beta_4 \\ \beta_8 \end{Bmatrix} = -\frac{1}{D}\begin{bmatrix} \bar{A}_8^M & -\bar{K}_8^M \\ -\bar{K}_6^M & \bar{K}_4^M \end{bmatrix}\begin{bmatrix} \bar{K}_5^M & \bar{K}_6^M & \bar{K}_6^M & \bar{K}_9^M & \bar{K}_{13}^M & \bar{K}_{14}^M & \bar{K}_{15}^M & \bar{K}_{15}^M & \bar{K}_{17}^M & \bar{K}_{18}^M \\ \bar{K}_8^M & \bar{K}_9^M & \bar{K}_5^M & \bar{K}_8^M & \bar{K}_{13}^M & \bar{K}_{17}^M & \bar{K}_{18}^M & \bar{K}_{14}^M & \bar{A}_{17}^M & \bar{K}_{17}^M \end{bmatrix}\begin{Bmatrix} \beta_5 \\ \beta_6 \\ \beta_7 \\ \beta_9 \\ \beta_{13} \\ \vdots \\ \beta_{18} \end{Bmatrix} \tag{87}$$

where D is the determinant of the 2 by 2 matrix coefficient of the vector $\lfloor \beta_4 \ \beta_8 \rfloor$ and is given by

$$D = \bar{K}_4^M \bar{A}_8^M - \bar{K}_6^M \bar{K}_8^M \tag{88}$$

and where the barred notation has been employed to indicate that the coefficient of the β's are evaluated at the upper surface of the laminate (e.g. $\bar{K}_5^M = K_5^M$ evaluated at $z=h_{M+1}$). It is important to note that the choice of which β's to eliminate is not arbitrary; they must be chosen in such a way that the determinant of the coefficient matrix of the β's chosen is never zero (i.e. D in Eq. 88, or its equivalent if other β's are chosen for elimination). An appropriate choice for the present element is β_4 and β_8 because the coefficients $\bar{K}_4^M$ and $\bar{A}_8^M$ of β_4 and β_8, respectively, will always be nonzero.

The matrix multiplication indicated in Eq. 87 can be performed and the resulting expressions for β_4 and β_8 can then, in principle, be substituted into Eqs. 83a, 83b, 83c, 84a, and 84b to yield a stress assumption, in terms of 16 stress parameters, which satisfies equilibrium and which also satisfies the interlayer transverse shear stress compatibility conditions and the

requirement of zero transverse shear stress on the lower and upper surfaces of the laminate. However, in practice, it is more convenient to form the laminate $\underset{\sim}{H}$ (Eq. 79a) and $\underset{\sim}{G}$ (Eq. 79b) matrices based on the full set of 18 β's with the matrix $\underset{\sim}{P}^m$ for the mth layer being determined from Eqs. 83a-83c, 84a, and 84b (denote these matrices by $\underset{\sim}{H}^{(18)}$, $\underset{\sim}{G}^{(18)}$, and $\underset{\sim}{\beta}^{(18)}$). A relation between the set of 18 β's and the final set of 16 β's (denoted by $\underset{\sim}{\beta}^{(16)}$) can be obtained, using Eq. 87 for β_4 and β_8, in the form

$$\underset{\sim}{\beta}^{(18)} = \underset{\sim}{T}_{18-16}\ \underset{\sim}{\beta}^{(16)} \tag{89}$$

Equation 89 can be viewed as a transformation relation between sets of stress parameters; the final laminate $\underset{\sim}{H}$ and $\underset{\sim}{G}$ matrices (denoted by $\underset{\sim}{H}^{(16)}$ and $\underset{\sim}{G}^{(16)}$) based on the final set of 16 stress parameters, $\underset{\sim}{\beta}^{(16)}$, are calculated from:

$$\underset{\sim}{H}^{(16)} = \underset{\sim}{T}_{18-16}^{T}\ \underset{\sim}{H}^{(18)}\ \underset{\sim}{T}_{18-16} \tag{90a}$$

$$\underset{\sim}{G}^{(16)} = \underset{\sim}{T}_{18-16}^{T}\ \underset{\sim}{G}^{(18)} \tag{90b}$$

The element $\underset{\sim}{B}$ and $\underset{\sim}{k}$ matrices can then be calculated from Eqs. 76 and 77, respectively, using the matrices $\underset{\sim}{H}^{(16)}$ and $\underset{\sim}{G}^{(16)}$.

The displacement behavior of the laminate is represented by translational displacements u,v, and w (in the x,y, and z directions, respectively) of the midsurface of the laminate, and rotations θ_x and θ_y of the cross-section normal lines about the x and y axes respectively. The rotations θ_x and θ_y correspond to $\partial w/\partial y$ and $\partial w/\partial x$ but are not equal to these quantities because θ_x and θ_y are assumed independent of w. Lines normal to the plate midsurface prior to deformation need not be normal to the plate midsurface after deformation. Thus, average laminate transverse shear deformation effects are included. The displacements, u,v, and w along side i (between nodes i and i+1) are expressed in terms of generalized nodal degrees of freedom u,v,w,θ_x, and θ_y (see Fig. 7) at nodes i and i+1 by the following linear interpolation

$$u = u_i(1-s) + u_{i+1}s + z\left[\theta_{y_i}(1-s) + \theta_{y_{i+1}}s\right] \tag{91a}$$

$$v = v_i(1-s) + v_{i+1}s - z\left[\theta_{x_i}(1-s) + \theta_{x_{i+1}}s\right] \tag{91b}$$

$$w = w_i(1-s) + w_{i+1}s \tag{91c}$$

where s is a nondimensional parameter taking on values s=0 at node i and s=1 at node i+1. Note that the inplane displacements u and v vary linearly in the z direction, but the transverse displacement w is constant through the thickness of the laminate. The calculation of the matrix $\underset{\sim}{G}^m$ for the mth layer is performed by obtaining the boundary displacement interpolation matrix, $\underset{\sim}{L}$, from Eqs. 91, and the boundary traction interpolation matrix, $\underset{\sim}{R}^m$, for the mth layer from the stress assumption by

$$\underset{\sim}{R}^m \Big|_{\text{side } i} = \underset{\sim}{\nu}\,\underset{\sim}{P}^m \Big|_{\text{side } i} \tag{92}$$

where $\underset{\sim}{\nu}$ is the matrix of direction cosines on the ith side of the element and is obtained from the relations

$$T_x = \sigma_x \nu_x + \sigma_{xy} \nu_y \tag{93a}$$

$$T_y = \sigma_{xy} \nu_x + \sigma_y \nu_y \tag{93b}$$

$$T_z = \sigma_{xz} \nu_x + \sigma_{yz} \nu_y \tag{93c}$$

where

$$\nu_x = \cos\alpha \tag{94a}$$

$$\nu_y = \sin\alpha \tag{94b}$$

and where α is the angle (CCW) from the x-axis to the outward normal direction for the ith side of the element.

For dynamic analyses, the element mass matrix is required. Because of the linear interpolation of displacements on the boundary of the element, the appropriate choice for a displacement interpolation in the interior of the present quadrilateral element is a bilinear assumption:

$$u = \sum_{i=1}^{4} \left[(u_i + z\,\theta_{y_i}) N_i \right] \tag{95a}$$

$$v = \sum_{i=1}^{4} \left[(v_i - z\,\theta_{x_i}) N_i \right] \tag{95b}$$

$$w = \sum_{i=1}^{4} \left[w_i N_i \right] \tag{95c}$$

where the N_i terms are given by Eqs. 72. The hybrid-rational element mass matrix, $\underset{\sim}{m}_{HR}$, is then obtained from

$$\underset{\sim}{m}_{HR} = \sum_{i=1}^{M} \int_{V_n^i} \rho^i \underset{\sim}{N}^T \underset{\sim}{N}\, dV \tag{96}$$

where ρ^i is the mass density of the ith layer, V_n^i is the volume of the ith layer of the nth element, and where the interpolation matrix, $\underset{\sim}{N}$, is obtained from Eqs. 95. It is important to note again that for the present element formulation a reference surface z=0 is chosen for the laminate, in contrast to element ELEMZ where a reference surface z=0 was chosen for each layer.

The resulting hybrid-rational mass matrix is in general fully populated and thus the storage requirements for the assembled mass matrix will be the same as those for the assembled stiffness matrix. An alternate approach often used in dynamic analyses is to define the mass properties of an element in terms of generalized nodal lumped masses. In effect, the mass properties of the entire element are assumed to be equally portioned to each of the four nodes. The resulting lumped mass matrix, $\underset{\sim}{m}_L$, is a diagonal matrix (i.e. nonzero contributions only on the diagonal) and is given by

$$\underset{\sim}{m}_L = \begin{bmatrix} \left[{}^{\backslash}d_{\backslash} \right] & & & 0 \\ & \left[{}^{\backslash}d_{\backslash} \right] & & \\ & & \left[{}^{\backslash}d_{\backslash} \right] & \\ 0 & & & \left[{}^{\backslash}d_{\backslash} \right] \end{bmatrix} \tag{97}$$

where

$$[d_\diagdown] = \begin{bmatrix} d_1 & & & & 0 \\ & d_1 & & & \\ & & d_1 & & \\ & & & d_2 & \\ 0 & & & & d_2 \end{bmatrix} \tag{98}$$

and the quantities d_1 and d_2 are given by

$$d_1 = \frac{A}{4} \sum_{m=1}^{M} \rho^m (h_{m+1} - h_m) \tag{99a}$$

$$d_2 = \frac{A}{12} \sum_{m=1}^{M} \rho^m (h_{m+1}^3 - h_m^3) \tag{99b}$$

where A is the area of the plate midsurface, ρ^m is the mass density of the mth layer, h_m is the z coordinate of the mth interface (h_1=z coordinate of the bottom surface of the laminate), and M is the total number of layers in the laminate. The terms d_1 and d_2 correspond, respectively, to the translational and rotational degrees of freedom in the element.

Because of the diagonal form of the lumped mass matrix, the assembled mass matrix can be stored as a vector of length equal to the total number of degrees of freedom in the assembled structure, requiring significantly less computer storage than the assembled mass matrix corresponding to the hybrid-rational element mass matrix. However, the more important consideration in this case is the relative accuracy of the two approaches for predict- the frequencies and mode shapes of the assembled structure (as discussed in Section 7).

In subsequent discussions, the present multilayer plate four-node quadrilateral element will be referred to as element MLP3K(Q). Corresponding to the present development, computer subroutines MLP3K and MLP3M have been written to calculate the element stiffness and mass matrices, respectively, and subroutine MLP3S has been written to calculate the stresses and strains, given the calculated nodal displacements. These modules can then be utilized in a static or dynamic structural analysis package.

4.3 Modification to a Triangular Element

Because of the need to utilize refined mesh arrangements in regions of expected high stress or strain gradients and more coarse mesh arrangements

in regions of the structure where less severe stress and strain gradients are expected, a transition element is required. For present purposes, a three-node triangular element will be used.

The requirement of displacement compatibility on interelement boundaries dictates that the boundary displacement interpolation used for the triangular element be identical to that used for element MLP3K(Q). In addition, the same stress interpolation used for element MLP3K(Q) can be used for the triangular element (termed element MLP3K(T) in subsequent discussions). Thus, the development of element MLP3K(T) follows exactly the development of element MLP3K(Q) with the exceptions that the area integrals now extend over a triangular planform, and that the boundary integrals now extend over a three-sided boundary.

In applications of the hybrid-stress model to static analysis, the accuracy of the element is often dependent on how well the stress and displacement assumptions are matched. Because the hybrid-stress model is a mixed model, the element becomes more stiff as the order of the stress assumption is increased (holding the displacement assumption fixed) and the element becomes more flexible as the order of the displacement assumption is increased (holding the stress assumption fixed). Although no rigid guidelines are available for determining the appropriate balance between stress and displacement assumptions, experience to date with the quadrilateral multilayer plate elements suggests that a reasonable guideline is that the number of stress parameters, $\underset{\sim}{\beta}$, should be as close to the minimum number (corresponding to be $\underset{\sim}{\beta}$-$\underset{\sim}{q}$ relation of Eq. 75) as possible. For element MLP3K(Q) the minimum number of β's is 14 (20 q's minus 6 rigid-body modes) and 16 β's are actually used for that element; as will be shown in Section 5, good convergence behavior is obtained for element MLP3K(Q). For element MLP3K(T) the minimum number of β's is 9 (15 q's minus 6 rigid-body modes), and 16 β's are used. Convergence studies given in Section 5 will show, as expected, that element MLP3K(T) is significantly stiffer than element MLP3K(Q).

The present triangular element is intended for use solely as a transition element and it is expected that the accuracy of the analysis will be governed primarily by the accuracy of the quadrilateral elements in the mesh. However, even in the role of transition element, the

triangular element MLP3K(T) could have a degrading effect on the solution by introducing bands of excessively stiff elements in the finite-element mesh. To alleviate this potential stiffening effect, a more flexible triangular element is required. The only alternative for obtaining a more flexible element is to reduce the stress assumption. The displacement assumption cannot be increased because of the displacement compatibility required between the triangular element and element MLP3K(Q). Such an element has been developed in the present study by deleting $\beta_4, \beta_6, \beta_8, \beta_9$, β_{15}, and β_{18} from the strain assumption of Eq. 81. The resulting 12β stress assumption is obtained from Eqs. 83a-83c, 84a, and 84b by deleting the above β's. In order to satisfy the zero transverse shear stress requirements on the upper surface of the laminate, β_5 and β_7 are eliminated (these stress parameter numbers correspond to the original numbering used in Eq. 81). After reduction, the element contains 10 independent stress parameters, one more than the minimum number required. In subsequent discussions, this element will be referred to as element MLTPK.

4.4 Comparison of Alternate Formulations

The fomulation of a multilayer plate element (ELEMZ) applicable for thick-plate structures has been given in Section 3, and an alternate formulation (element MLP3K(Q)) for applications to moderately-thick plate structures has been given in the present section. The purpose of the present subsection is to compare the two formulations in terms of applicability, computer core storage requirements, and computation time requirements. The question of relative accuracy of the two approaches will be addressed in the next section.

In terms of applicability, it should be expected that element ELEMZ will be capable of adequately representing the severe cross-sectional warping often observed in thick laminated plates, whereas element MLP3K(Q) will represent this behavior only in an average sense. Results presented by Mau [2] and Spilker [5] suggest that accurate answers will be obtained by using element ELEMZ for structures having typical thickness ratios (defined as the ratio of the spanwise dimension to the thickness dimension) as low as 4 (thick plate), whereas the accuracy of element MLP3K(Q) will degenerate noticeably for aspect ratios less than 8 to 10 (moderately-thick plate).

Most multilayer structures of interest will be no more than moderately thick, but will be made up of a large number of layers (i.e. more than 20). For such structures, similar accuracy should be expected from both elements. However, only element MLP3K(Q) will be applicable for such problems in practice because of the excessive storage requirements associated with element ELEMZ.

The clear superiority of MLP3K(Q) over ELEMZ is found in terms of computational efficiency. As discussed in Subsection 3.5, the storage requirements for element ELEMZ may be prohibitively large if the number of layers is large. This is a consequence of the choice of a set of independent stress parameters for each layer, and the fact that the number of nodal degrees of freedom depends on the number of layers. For element MLP3K(Q) the number of stress parameters (16) and the number of degrees of freedom (20) for an element are fixed and thus the storage requirements for the generation of the MLP3K(Q) element stiffness matrix and, on a global level, for the assembled stiffness matrix are independent of the number of layers. In principle, there is no limitation on the number of layers which can be accommodated by element MLP3K(Q).

In terms of computation time, element MLP3K(Q) will again be superior to element ELEMZ. The generation of the ELEMZ stiffness matrix requires an inversion of the 20x20 $\underset{\sim}{H}^{m}$ matrix for each layer, whereas MLP3K(Q) requires only a single conversion of the 16x16 $\underset{\sim}{H}$ matrix for the entire laminate. In addition, element ELEMZ requires an additional inversion of the matrix product $\underset{\sim}{A}\,\underset{\sim}{H}^{-1}\,\underset{\sim}{A}^{T}$ and the expression for $\underset{\sim}{k}$ requires significantly more matrix multiplications than for element MLP3K(Q). When element ELEMZ is used, the solution time for the assembled matrix equations for the structure will depend on both the number of elements and the number of layers because the total number of degrees of freedom in the assembled system depends on both. However, the solution time for element MLP3K(Q) will depend only on the number of elements in the finite-element mesh.

As discussed in Subsection 3.4, it is possible in principle to develop a traction-free-edge element based on the formulation used for element ELEMZ. However, it appears that no such traction-free-edge element can be developed based on the formulation used for element MP3K(Q). It should be recalled that the stress assumption used for element MLP3K(Q) is based on a fixed set

of stress parameters. However, the stresses σ_x, σ_y, and σ_{xy} need not be continuous at interlayer boundaries. In effect, these stresses are independent from layer to layer because the interpolation matrix $\underset{\sim}{P}^m$ depends on layer material properties which vary from layer to layer. As a result, in order to satisfy the traction-free condition in each layer, a reduction of the total number of β's would be required for each layer processed. Clearly, this layer-dependent reduction of β's is not acceptable for an element in which the number of stress parameters is independent of the number of layers. Such an argument is not limited to the linear stress assumption employed for element MLP3K(Q); it also applies to any higher order assumption.

Finally, some comments on the advantages of the assumed-stress hybrid model over the conventional assumed-displacement model should be made. In general, the plate and/or shell elements are more easily formulated by the hybrid-stress model because compatible displacement assumptions need be made only along the element <u>boundaries</u>; formulations by the assumed-displacement model require the assumption of a displacement field in the <u>interior</u> of the element which yields displacement continuity along interelement boundaries. In many cases, assumed-stress hybrid elements yield improved displacement and stress distribution results by comparison with assumed-displacement elements with similar-order interpolation. In particular, the present MLP3K(Q) element has been shown in Ref. 5 to yield more accurate displacement results than an assumed-displacement multilayer plate element (which also includes transverse shear effects) for identical meshes; however, element MLP3K(Q) has five degrees of freedom per node by comparison to the seven degrees of freedom per node for the assumed-displacement element.

SECTION 5

ELEMENT PERFORMANCE TESTS

5.1 Cylindrical Bending of a Three-Layer Infinite Strip

The problem of a strip of width ℓ in the y-direction and infinite length in the x-direction, of cross-ply construction, total thickness h, and loaded by a sinusoidal load in the transverse direction has been chosen as a first test of the multilayer plate elements. The exact elasticity solution and the classical lamination theory solution have been obtained by Pagano [14]. The geometry, material properties, coordinate directions, and loading function are given in Fig. 8a. The finite strip is assumed to be simply supported along the boundaries $y=0$ and $y=\ell$.

Because the plate is infinitely long in the x-direction and the laminate constuction is balanced, the finite-element analysis may be performed by analyzing a strip of finite width, a, in the x-direction, and of length $\ell/2$ because of symmetry in the y-direction (see Fig. 8b). Ten equally sized square elements, with side length $a=\ell/20$, are employed in the finite-element analysis. Simply-supported boundary conditions are imposed on the side $y=0$, and symmetry conditions are imposed on the other three sides. Elements ELEMZ and MLP3K(Q) are employed in the present analysis to obtain a comparison of their performances.

The following quantities of interest have been chosen to obtain a comparison of the results obtained by using each of the above elements: (1) the normal stress σ_y at $y=\ell/2$; (2) the transverse shear stress τ_{yz} at the boundary $y=0$; (3) the inplane displacement v in the y-direction at the boundary $y=0$; and (4) the midplane transverse displacement w in the z-direction at the center of the plate $y=\ell/2$. For convenience, the results will be presented in terms of normalized quantities (barred) which are given by

$$\bar{\sigma}_y = \frac{\sigma_y}{q_o} \qquad \bar{\tau}_{yz} = \frac{\tau_{yz}}{q_o}$$

$$\bar{v} = \frac{E_{22} v}{h q_o} \qquad \bar{w} = \frac{100\, E_{22} h^3 w}{q_o \ell^4} \tag{100}$$

$$s = \frac{\ell}{h} \qquad \bar{z} = \frac{z}{h}$$

where q_o is the amplitude of the sinuisoidal loading and E_{22} is the elastic modulus perpendicular to the fiber direction. It should be noted that the quantity S is a measure of the thickness ratio of the plate (S=4 is considered to be a thick plate, S=50 is considered to be a thin plate).

Results are presented for a three-layer ($90^o/0^o/90^o$) laminate (N=3) and a seven-layer ($90^o/0^o/90^o/0^o/90^o/0^o/90^o$) laminate (N=7). Two subcases are then considered for each of the above laminates: one in which the plate is thick (S=4) and one in which the plate is moderately thick (S=10). For each case, and in the corresponding tables and figures, results are presented which were obtained by an exact solution [14], classical lamination theory [14], and by using elements ELEMZ and MLP3K(Q). Table 1 gives the results obtained for the transverse displacement, $\bar{w}$, at $y=\ell/2$. The results obtained by using element ELEMZ are in excellent agreement with the exact solution for all cases (0.8% error for S=4, N=3, 0.003% error for S=10, N=3, 0.63% error for S=4, N=7, and 0.15% error for S=10, N=7). The results obtained by using element MLP3K(Q) for the three-layer cases are too flexible for the case S=4 (9.51% error), but are in excellent agreement with the exact solution for the case S=10 (0.96% error). The results obtained by using element MLP3K(Q) for the seven layer laminate are in good agreement with the exact solution for both S=4 (1.81% error) and S=10 (0.08% error), which suggests that for increasing number of layers the average cross-sectional rotation behavior incorporated in element MLP3K(Q) more closely models the exact behavior. Note that the lamination theory solution is in poor agreement with the exact solution even for moderately-thick laminates (S=10) which suggests that transverse shear effects (neglected in lamination theory) play a significant role in the calculation of transverse deflection.

The results obtained for the stresses $\bar{\sigma}_y$ and $\bar{\tau}_{yz}$ for the three-layer cases are plotted in Figs. 9a and 9b as a function of the nondimensionalized thickness parameter $\bar{z}$. Note that the results are plotted only from $\bar{z}=0$ to 0.5 because the quantities $\bar{\sigma}_y$ and $\bar{\tau}_{yz}$ are odd and even functions of $\bar{z}$, respectively. As is shown in Fig. 9a, the results obtained for $\bar{\sigma}_y$ by using element ELEMZ are in excellent agreement with the exact solution, whereas the results obtained by using element MLP3K(Q) are in essential agreement with the classical lamination theory solution. Note that the lamination

theory solution gives poor agreement with the exact solution for S=4, but much better agreement for S=10.

The results for the transverse shear stress, $\bar{\tau}_{yz}$ for the three-layer laminate (Fig. 9b) obtained by using element ELEMZ are in reasonable agreement with the exact solution for both S=4 and S=10, although the tendency appears to be to underestimate slightly the interlaminar shear stress value at the interface between the top and middle layers, and to overestimate slightly the value at the center ($\bar{z}$=0) of the laminate. The results obtained by using element MLP3K(Q) are in general agreement with the lamination theory solution in the top layer, but tend more toward the exact solution in the center layer. For the case S=10, the MLP3K(Q) results are actually slightly more accurate than the ELEMZ results.

The inplane displacement $\bar{v}$, given in Fig. 9c, demonstrates the degree of cross-sectional warping present in the three-layer laminate. For the case S=4, severe warping is present, but for the case S=10, only moderate warping is present. For both cases, the results obtained by using element ELEMZ are in excellent agreement with the exact solution, whereas the results obtained by using element MLP3K(Q) are in essential agreement with the lamination theory solution. The lamination theory solution gives a good approximation to the exact solution for S=10, but a poor approximation to the exact solution for S=4.

The results obtained for the stresses $\bar{\sigma}_y$ and $\bar{\tau}_{yz}$ and the inplane displacement, $\bar{v}$, for the seven-layer laminate are shown in Figs. 10a through 10c. The observations made about the element behavior for the three-layer laminate also hold for the seven-layer laminate. The results obtained by using element ELEMZ are found to be in good agreement with the exact solution for all cases, and are clearly superior to the results obtained by using element MLP3K(Q) for the cases corresponding to a thick laminate (S=4). For the moderately thick cases (S=10), the accuracy of the MLP3K(Q) results is comparable to or slightly better than the ELEMZ results.

For the present ten-element (3-layer) finite element solutions, approximately 215,000 BYTES of computer core storage (in double precision) were required for the ELEMZ solutions, whereas only 106,000 BYTES of computer core storage were required for the MLP3K(Q) solution. For the seven-layer laminate cases, using the same 10 element mesh, 430,000 BYTES of storage were required

for the ELEMZ solutions, whereas the MLP3K(Q) solution still required only 106,000 BYTES of storage. When the 4 cases (3 layers, 7 layers, S=4, and S=10) were run together, the ELEMZ solution required approximately 0.461 CPU minute, and the MLP3K(Q) solution required approximately 0.040 CPU minute. Thus, significant savings in computer core storage and in computation time were found when using element MLP3K(Q).

A comparison of the results obtained by using elements ELEMZ and MLP3K(Q) shows element ELEMZ to be (as expected) the more accurate element, particularly for the case S=4 (thick laminate). However, for the case S=10, the superiority of element ELEMZ over element MLP3K(Q) becomes much less significant, and the MLP3K(Q) results are well within the accuracy limits of engineering analysis. In view of the large storage requirements associated with ELEMZ as the number of layers is increased, it may be expected that the use of ELEMZ must be restricted to cases where the number of layers is small and the laminate is thick (e.g. the case S=4). For cases where a representative thickness aspect ratio such as S is greater than 10, element MLP3K(Q) can be used with confidence regardless of the number of layers. Based on the results of the present example, it may be expected that if applied to thick laminated plate problems, element MLP3K(Q) will yield transverse normal displacement results which are significantly more accurate than lamination theory, all other results tending toward lamination theory. However, it should be recalled that element MLP3K(Q) is not, strictly speaking, based on lamination theory. Transverse shear stresses, strains, and strain energy are included automatically in element MLP3K(Q), but transverse shear strain energy is not included in lamination theory. Finally, for thick laminates of few layers (e.g. S=4, N=3), it appears that the accuracy of the stress distribution through the thickness is most strongly influenced by the cross-sectional warping behavior of the laminate.

5.2 A Square Two-Layer Plate Under Uniform Transverse Loading

The example problem to be considered here is a square plate of side length, a, of two-layer angle-ply construction ($\pm\theta$ fiber orientations with respect to the global x axis), loaded by a uniform pressure load of magnitude q_o. The plate has total thickness h, and each layer is of equal thickness, h/2. The plate is simply supported on all four edges such that displacements transverse and normal to the edge are not permitted, but motion in a direction parallel to the boundaries is permitted. Each layer is composed of the same material; the material properties, dimensions, and geometry are given in Fig. 11.

A solution for the present problem based on classical lamination theory has been presented by Whitney [15] using a Fourier series approach. The equations required to calculate the Fourier coefficients, displacements, stress resultants, and moment resultants are given in Ref. 15. However, the expressions given for the moment resultants, M_x and M_y, appear to be in error. For convenience, the correct expressions for M_x and M_y will be derived here.

The inplane displacements, u^o and v^o, at the laminate midsurface, and transverse displacement, w, are expressed as a Fourier series in the form

$$u^o = \sum_{m=1}^{\infty} \sum_{n=1}^{\infty} E_{mn} \sin \frac{m\pi x}{a} \cos \frac{n\pi y}{b} \tag{101a}$$

$$v^o = \sum_{m=1}^{\infty} \sum_{n=1}^{\infty} F_{mn} \cos \frac{m\pi x}{a} \sin \frac{n\pi y}{b} \tag{101b}$$

$$w = \sum_{m=1}^{\infty} \sum_{n=1}^{\infty} G_{mn} \sin \frac{m\pi x}{a} \sin \frac{n\pi y}{b} \tag{101c}$$

where a and b are the dimensions of the plate in the x and y directions, respectively, and the Fourier coefficients, E_{mn}, F_{mn}, and G_{mn} are obtained by expressions given in Ref. 15. From the laminate constitutive relations, the stress resultants, N_x, N_y, and N_{xy}, and moment resultants, M_x, M_y, and M_{xy}, can be related to the midsurface strains, ε_x^o, ε_y^o, and ε_{xy}^o, and curvatures, k_x, k_y, and k_{xy} by

$$\begin{Bmatrix} N_x \\ N_y \\ N_{xy} \\ M_x \\ M_y \\ M_{xy} \end{Bmatrix} = \begin{bmatrix} A_{11} & A_{12} & A_{16} & B_{11} & B_{12} & B_{16} \\ & A_{22} & A_{26} & B_{12} & B_{22} & B_{26} \\ & & A_{66} & B_{16} & B_{26} & B_{66} \\ & & & D_{11} & D_{12} & D_{16} \\ & & & & D_{22} & D_{26} \\ & & & & & D_{66} \end{bmatrix} \begin{Bmatrix} \varepsilon_x^o \\ \varepsilon_y^o \\ \varepsilon_{xy}^o \\ k_x \\ k_y \\ k_{xy} \end{Bmatrix} \tag{102}$$

where the A_{ij}, B_{ij}, and D_{ij} terms are given for the present two-layer laminate by

$$
\left.
\begin{aligned}
A_{ij} &= \sum_{m=1}^{2} C_{ij}^{m} \left(h_m - h_{m-1} \right) \\
B_{ij} &= \sum_{m=1}^{2} \frac{1}{2} C_{ij}^{m} \left(h_m^2 - h_{m-1}^2 \right) \\
D_{ij} &= \sum_{m=1}^{2} \frac{1}{3} C_{ij}^{m} \left(h_m^3 - h_{m-1}^3 \right)
\end{aligned}
\right\} \quad i,j = 1,2,6 \tag{103}
$$

and where C_{ij}^{m} are the reduced (plane-stress) stiffness material properties of the mth layer (Eqs. 42) and h_m and h_{m-1} are the z-coordinates of the upper and lower surface of the mth layer. For $\pm\theta$ angle-plies, it can be shown that the terms $B_{11}, B_{12}, B_{22}, D_{16}$, and D_{26} are zero, so that the expressions for the moment resultants, M_x and M_y, are obtained from Eq. 102 as

$$
M_x = B_{16}\, \varepsilon_{xy}^{o} + D_{11} k_x + D_{12} k_y \tag{104a}
$$

$$
M_y = B_{26}\, \varepsilon_{xy}^{o} + D_{12} k_x + D_{22} k_y \tag{104b}
$$

The necessary inplane strain and curvature terms can be obtained by differentiation of Eqs. 101a through 101c:

$$
\varepsilon_{xy}^{o} = \frac{\partial u^{o}}{\partial y} + \frac{\partial v^{o}}{\partial x} = -\sum_m \sum_n \left(\frac{n\pi}{b} E_{mn} + \frac{m\pi}{a} F_{mn} \right) \sin\frac{m\pi x}{a} \sin\frac{m\pi y}{b} \tag{105a}
$$

$$
k_x = -\frac{\partial^2 w}{\partial x^2} = \sum_m \sum_n \left(\frac{m\pi}{a} \right)^2 G_{mn} \sin\frac{m\pi x}{a} \sin\frac{n\pi y}{b} \tag{105b}
$$

$$
k_y = -\frac{\partial^2 w}{\partial y^2} = \sum_m \sum_n \left(\frac{n\pi}{b} \right)^2 G_{mn} \sin\frac{m\pi x}{a} \sin\frac{n\pi y}{b} \tag{105c}
$$

Substituting Eqs. 105a through 105c into Eqs. 104a and 104b yields the final expression for M_x and M_y:

$$
M_x = -\frac{\pi}{a^2} \sum_m \sum_n \left\{ a B_{16} \left[nRE_{mn} + mF_{mn} \right] - \pi G_{mn} \left[D_{11} m^2 + D_{12} n^2 R^2 \right] \right\} \sin\frac{m\pi x}{a} \sin\frac{n\pi y}{b} \tag{106a}
$$

$$
M_y = -\frac{\pi}{a^2} \sum_m \sum_n \left\{ a B_{26} \left[nRE_{mn} + mF_{mn} \right] - \pi G_{mn} \left[D_{12} m^2 + D_{22} n^2 R^2 \right] \right\} \sin\frac{m\pi x}{a} \sin\frac{n\pi y}{b} \tag{106b}
$$

where R is the spanwise aspect ratio and is given by

$$R = \frac{a}{b} \tag{106c}$$

The exact solutions for the present example problem have been numerically generated by using Whitney's expression (except for M_x and M_y where Eqs. 106a and 106b have been substituted) and retaining 400 terms* in the Fourier series.

Because the results presented in the previous subsection suggest that element MLP3K(Q) may be the more widely useful element, the present example problem has been chosen to obtain additional performance information for element MLP3K(Q). Because of the bending/extensional coupling in the present unbalanced laminate, symmetry conditions cannot be invoked, and the entire plate must be modeled in the finite-element analysis. A K-by-K mesh of square elements is employed, where K is the number of elements in each direction.

The first case to be considered is a plate of side length a=10", thickness h=0.2", fiber orientation angles $\theta=\pm 45^{\circ}$, and a uniform load q_o=100 psi. The quantities of interest are: (1) the transverse deflection w at the center of the plate; (2) the in-plane x-direction displacement $u^o(z=0)$ at x=a/2, y=0; and (3) the moment M_x at the center of the plate. The percent errors (compared to Whitney's Fourier series approach) in the finite-element results (using element MLP3K(Q)) for these quantities are plotted in Fig. 12a versus the total number of degrees of freedom in the finite-element solution. The points correspond, respectively, to values of K=4,6,8,10, and 12 (K-by-K mesh). The results for u^o converge very rapidly to the exact solution. The convergence of the results for w is much slower, but for the 12-by-12 mesh, the w solution is in error by only 1.5%. The results for M_x are converging rapidly, but have not yet reached the exact solution for the 12-by-12 mesh (0.7% error). Because the stress (and, thus, moment) solution is dependent upon both in-plane and out-of-plane displacements for the present unbalanced laminate, this solution should not converge to the exact solution until <u>both</u> u^o and w have converged. Note that for all cases, the moment is calculated from the finite-element solution by integrating the average stress distribution

---

*Significantly more terms than required to obtain a converged solution.

(obtained by nodal averaging at the center of the plate). Note also that for the present example ($\theta=\pm 45^{\circ}$), u^{o} at $x=a/2$, $y=0$ is the same as v^{o} (in-plane displacement in the y-direction) at $x=0$, $y=a/2$, and $M_x=M_y$ at the center of the plate.

To assess the effects of the fiber orientation angle, θ, on the finite-element solution, a second case has been considered. In this case the plate dimensions and loading are identical to the first case (a=10", h=0.2", and $q_o=100$ psi), and a 10-by-10 mesh has been used to model the entire plate. A series of results was obtained for the fiber orientation angles, $\pm\theta=5^{\circ}$, 15°, 25°, 35°, and 45°. The quantities of interest for the present case are those defined for the first case and, in addition, the in-plane displacement v^{o} in the y-direction at $x=0$, $y=a/2$, and the moment M_y at the center of the plate. The percent errors in the finite-element solution for these quantities versus the fiber orientation angle, $\pm\theta$, are plotted in Fig. 12b. The exact solution finite-element solution, and error in the finite-element solution for each of these values of θ are also tabulated in Table 2. Figure 12b shows that the absolute value of the error for these quantities is less than 3 percent for all values of θ. The mild fluctuations in the error as θ is varied may be attributed to the increase (or decrease) in the relative significance of a particular quantity (see Table 2). For example, a comparison of the exact solutions for u^{o} and v^{o} shows that u^{o} is small compared with v^{o} for $\pm\theta=5^{\circ}$ and 15°, and the finite-element solution for u^{o} is less accurate until the values of u^{o} and v^{o} are quite close. A similar observation can be made for M_x and M_y. This kind of behavior is typical of most numerical procedures requiring the solution of a large number of simultaneous equations; the dominant terms are predicted more accurately. However, it should be noted again that the fluctuations in the error for the quantities of interest as θ is varied are quite small and all quantities of interest are predicted to within 3 percent error regardless of the value of θ.

The final performance test for element MLP3K(Q) is the effect of element spanwise aspect ratio. For this case, a rectangular plate of two-layer $\pm 45^{\circ}$ angle-ply construction is considered with material properties and loading identical to case 1. The plate dimension in the y direction, b, is fixed at 10" and the plate dimension in the x direction, a, is increased to give values of the spanwise aspect ratio, R (Eq. 106c), of 1,2,3,4,5,6,8, and 10.

A 10x10 mesh is used for all values of R to model the entire structure, so that in all cases R is also the spanwise aspect ratio of each element.

Shown in Fig. 12c are the percent errors in the quantities u^o at $x=a/2$, $y=0$, v^o at $x=0$, $y=b/2$, and w, M_x, and M_y at the center of the plate ($x=a/2$, $y=b/2$) as functions of R. As shown, the effect of increased aspect ratio is to stiffen the predicted response. A very mild stiffening effect is observed for the quantities u^o, w, M_x, and M_y, with very little degeneration of the solution even for the extreme case of R=10. However, a severe stiffening effect is observed for the quantity v^o. The increasing error in the quantity v^o may be viewed largely as a modeling error rather than ill-conditioning of the element as a function of aspect ratio. Fixing the number of elements in the x direction and then increasing the plate dimension in the x direction is analogous to fixing the dimension and then decreasing the number of elements, and the effects of either approach are the same. In effect, fewer elements are available to model the distribution of v^o along the x direction of the plate. In contrast, the dimension in the y direction and number of elements in the y direction are fixed in the present example and the percent error in the quantity u^o at $x=a/2$, $y=0$ increases only slightly as R increases (i.e. the accuracy in the modeling of the distribution of u^o along the y direction is nearly independent of R). Difficulties associated with the use of large element aspect ratio are usually manifested by severe ill-conditioning of the assembled matrix equations resulting in large numerical errors in all quantities of interest. No such difficulties have been observed for the present test problem which utilizes rectangular elements only. However, in an application example described in Subsection 8.2, the $\underset{\sim}{H}$ matrix for a quadrilateral element of spect ratio, R=7, could not be inverted. Because of this, the use of element aspect ratios greater than 5 is not recommended.

Limited results have been obtained by using the triangular shaped elements MLP3K(T) and MLTPK. The example chosen is identical to the first case presented in this subsection (i.e. 2 layers, $\theta=\pm45^o$, square plate). The entire plate is modelled with a K-by-K uniform mesh where each square contains two triangular elements. The results of a convergence study using element MLP3K(T) are shown in Fig. 12d for K=4,6,8, and 10. The finite element solution for the quantities of interest (v^o at $x=0$, $y=a/2$, w at the

center of the plate, and M_x at the center of the plate) is in error by more than 35% even for the 10x10 mesh (200 triangular elements). This element is clearly unacceptable for use in modeling the entire structure, and is also felt to be too stiff for use as a transition (mesh expander) element. It should be recalled that element MLP3K(T) is based on the same stress assumption used in element MLP3K(Q). The results of a convergence study using element MLTPK (based on a reduction of the stress assumption used in element MLP3K(Q)) are shown in Fig. 12e. Although the convergence behavior is not monotonic, it is substantially better than that observed for element MLP3K(T). The use of element MLTPK to model the entire structure is not recommended, but this element is suitable for use as a transition element. Consequently, element MLTPK should be used for all multilayer plate/shell problems requiring a transition element.

The example problems in the present subsection have been chosen to verify the accuracy and range of applicability of element MLP3K(Q). The application of element MLP3K(Q) to the static analysis of a finite rectangular plate with a circular cutout subjected to four-point bending is discussed in Subsection 8.2. Additional performance tests of element MLP3K(Q) for dynamic analyses are given in Subsection 8.5.

SECTION 6

INTEGRALLY-STIFFENED PLATES AND SHELLS

6.1 Introduction

Stiffeners are of interest in plates and shells since they are commonly used to reduce stress concentrations in panels around cutouts or to increase the buckling strength of webs. There are two ways to model stiffened plates.

The first approach is the nonintegrally stiffened method which divides the stiffeners and plate into separate elements, using beam elements to model the stiffeners. Both elements are easy to formulate, but sometimes displacement incompatibility exists between the stiffener and plate interfaces. This occurs in the present study, which uses the quadrilateral element developed in Section 4 and beam elements based on the displacement model. The boundary transverse displacement for the quadrilateral plate element is linear and this is incompatible with the cubic interpolation of the beam stiffener. This approach is also inefficient when the stiffeners are closely spaced, since nodal lines must fall along stiffeners and hence the number of plate elements increases.

The second approach is the integrally-stiffened method which avoids some of the difficulties mentioned above by formulating the plate-stiffener combination as a single element. Nodal lines can then be spaced conveniently without regard to stiffener locations and displacement compatibility is satisfied. A formulation for an integrally-stiffened element based on the displacement model is developed in Ref. 16. An equivalent element based on the hybrid model is developed in Subsection 6.2. In the latter formulation it is difficult to satisfy stress compatibility at the stiffener-plate interface. Also, the stress-free conditions are not satisfied at the stiffener sides and at one free surface of the plate.

A test problem of an isotropic simply-supported stiffened plate under uniform transverse loading is analyzed by the above two methods. These results are compared in Subsection 6.3 with a Ritz analysis of the plate. Kirk [17] has shown that the Ritz method is extremely accurate, and, thus, it provides an independent standard for assessment of the finite-element methods.

6.2 Integrally-Stiffened Quadrilateral Element

The integrally-stiffened multilayer plate element is based on the hybrid model and follows the same basic formulation as the quadrilateral element MLP3K(Q) discussed in Subsection 4.2. The stiffener is treated as a finite layer attached to the plate (Fig. 14) and the following approximations are made:

1. The hybrid element is based on the Principle of Modified Complementary Energy which requires that the stresses be in equilibrium in the element. Thus, stress compatibility must be satisfied at layer interfaces. This is done in the present MLP3K(Q) element with stress assumptions that include transverse shear stresses which vary only through the plate thickness. However, at the plate-stiffener interface, which represents only a portion of the plate area, the fact that the transverse shear stresses are constant over the plate surface implies that only shear force rather than stress compatibility is satisfied, i.e., the equilibrium condition is met in an integral sense rather than exactly. The above approximation is chosen to be consistent with the present MLP3K(Q) stress assumption. It is not the only possible choice, but other assumptions could not be investigated within the scope of the present study. The stresses assumed also violate certain stress-free boundary conditions. The stress-free condition on the surface of the plate outside of the stiffener is violated. On the stiffener itself the stress-free conditions on the lateral sides are violated. (However, note that these stress-free conditions apply to surfaces which are not a part of the inter-layer boundary, and therefore, they are not required to be satisfied by the modified complementary energy principle.)

2. The entire stiffener property is lumped on a plane perpendicular to the plate. Hence, no variation of stress across the width of the stiffener is considered.

3. It is assumed that the neutral surface of the plate remains unaffected by the stiffener.

4. Stiffeners are modelled on the lower surface of the plate only (Fig. 14). This is an arbitrary restriction; equivalent formulations are possible with stiffeners on the upper surface or on both surfaces.

These approximations limit the stiffened plate element. Since the stiffener is lumped, the element is restricted to stiffeners which are narrow relative to the dimensions of the plate element. The stiffeners are also restricted to small moments of inertia, such that the neutral surface of the plate is not significantly altered.

The strain assumption used in the quadrilateral element (Eq. 81) is also assumed in the integrally-stiffened plate element. However, the resulting equations for transverse shear stresses and the $\underset{\sim}{H}$ and $\underset{\sim}{G}$ matrices (Subsection 4.2) change slightly as a result of the above approximations. Since the stiffeners are treated as layers, Eqs. 79 become

$$\underset{\sim}{H} = H_p^1 + H_p^2 + \quad \cdots \quad + H_p^M + H_s^1 + \quad \cdots \quad + H_s^N \tag{107a}$$

$$\underset{\sim}{G} = G_p^1 + G_p^2 + \quad \cdots \quad + G_p^M + G_s^1 + \quad \cdots \quad + G_s^N \tag{107b}$$

where the subscript 'p' refers to the plate and 's' to the stiffeners and where

$$\underset{\sim}{H}{}_{p,s}^{i} = \int_{V_{n_{p,s}}^{i}} \underset{\sim}{P}{}_{p,s}^{i\,T} \underset{\sim}{S}{}_{p,s}^{i} \underset{\sim}{P}{}_{p,s}^{i} \, dv \tag{108a}$$

$$\underset{\sim}{G}{}_{p,s}^{i} = \int_{\partial V_{n_{p,s}}^{i}} \underset{\sim}{R}{}_{p,s}^{i\,T} \underset{\sim}{L} \, ds \tag{108b}$$

The boundary surface $\partial V_{n_s}^i$ (Fig. 14) includes only the interelement boundaries of the ith stiffener.

The transverse shear stresses exactly satisfy the stress-free condition at the bottom surface of the stiffener. However, the constraints on the shear stresses change slightly from Subsection 4.2 due to the approximation

of shear force compatibility. The shear stress in the ith stiffener is given by

$$[\sigma_{xz}]_s^i = K_{s_4}^i \beta_4 + K_{s_5}^i \beta_5 + K_{s_6}^i (\beta_6 + \beta_7) + K_{s_8}^i \beta_8 + K_{s_9}^i \beta_9 + K_{s_{13}}^i \beta_{13} + K_{s_{14}}^i \beta_{14} + K_{s_{15}}^i (\beta_{15} + \beta_{16}) + K_{s_{17}}^i \beta_{17} + K_{s_{18}}^i \beta_{18} \tag{109a}$$

$$[\sigma_{yz}]_s^i = K_{s_6}^i \beta_4 + K_{s_8}^i \beta_5 + K_{s_9}^i \beta_6 + K_{s_5}^i \beta_7 + A_{s_8}^i \beta_8 + K_{s_8}^i \beta_9 + K_{s_{15}}^i \beta_{13} + K_{s_{17}}^i \beta_{14} + K_{s_{18}}^i \beta_{15} + K_{s_{14}}^i \beta_{16} + A_{s_{17}}^i \beta_{17} + K_{s_{17}}^i \beta_{18} \tag{109b}$$

where the coefficients of the β's are given by

$$K_{s_4}^i = h_s^i C_{s_{11}}^i - z C_{s_{11}}^i \tag{110a}$$

$$K_{s_5}^i = h_s^i C_{s_{12}}^i - z C_{s_{12}}^i \tag{110b}$$

$$K_{s_6}^i = h_s^i C_{s_{16}}^i - z C_{s_{16}}^i \tag{110c}$$

$$K_{s_8}^i = h_s^i C_{s_{26}}^i - z C_{s_{26}}^i \tag{110d}$$

$$K_{s_9}^i = h_s^i C_{s_{66}}^i - z C_{s_{66}}^i \tag{110e}$$

$$K_{s_{13}}^i = \frac{1}{2}\left[h_s^{i\,2} C_{s_{11}}^i - z^2 C_{s_{11}}^i \right] \tag{110f}$$

$$K_{s_{14}}^i = \frac{1}{2}\left[h_s^{i\,2} C_{s_{12}}^i - z^2 C_{s_{12}}^i \right] \tag{110g}$$

$$K_{s_{15}}^{i} = \frac{1}{2}\left[h_s^{i^2} C_{s_{16}}^{i} - z^2 C_{s_{16}}^{i}\right] \tag{110h}$$

$$K_{s_{17}}^{i} = \frac{1}{2}\left[h_s^{i^2} C_{s_{26}}^{i} - z^2 C_{s_{26}}^{i}\right] \tag{110i}$$

$$K_{s_{18}}^{i} = \frac{1}{2}\left[h_s^{i^2} C_{s_{66}}^{i} - z^2 C_{s_{66}}^{i}\right] \tag{110j}$$

$$A_{s_8}^{i} = \left[h_s^{i} C_{s_{22}}^{i} - z\, C_{s_{22}}^{i}\right] \tag{110k}$$

$$A_{s_{17}}^{i} = \frac{1}{2}\left[h_s^{i^2} C_{s_{22}}^{i} - z^2 C_{s_{22}}^{i}\right] \tag{110ℓ}$$

and where i=1,2,...,N.

Similarly, for the mth layer of the plate, the transverse shear stresses are

$$\begin{aligned}[\sigma_{xz}]_p^m = {} & K_{p_4}^i \beta_4 + K_{p_5}^i \beta_5 + K_{p_6}^i (\beta_6 + \beta_7) + \\ & K_{p_8}^i \beta_8 + K_{p_9}^i \beta_9 + K_{p_{13}}^i \beta_{13} + K_{p_{14}}^i \beta_{14} + \\ & K_{p_{15}}^i (\beta_{15} + \beta_{16}) + K_{p_{17}}^i \beta_{17} + K_{p_{18}}^i \beta_{18}\end{aligned} \tag{111a}$$

$$\begin{aligned}[\sigma_{ys}]_p^m = {} & K_{p_6}^i \beta_4 + K_{p_8}^i \beta_5 + K_{p_9}^i \beta_6 + K_{p_5}^i \beta_7 + \\ & A_{p_8}^i \beta_8 + K_{p_8}^i \beta_9 + K_{p_{15}}^i \beta_{13} + K_{p_{17}}^i \beta_{14} + \\ & K_{p_{18}}^i \beta_{15} + K_{p_{14}}^i \beta_{16} + A_{p_{17}}^i \beta_{17} + K_{p_{17}}^i \beta_{18}\end{aligned} \tag{111b}$$

where the coefficients of the β's are given by

$$K_{p_4}^m = \sum_{i=1}^{m} h_p^i C_{p_{11}} - \sum_{i=2}^{m} h_p^i C_{p_{11}}^{i-1} - z\, C_{p_{11}}^m + \sum_{i=1}^{N} \left[AR_s^i\, K_{s_4}^i\right]_{z=h_p^1} \tag{112a}$$

$$K{p_5}^m = \sum_{i=1}^{m} h_p^i C_{p_{12}}^i - \sum_{i=2}^{m} h_p^i C_{p_{12}}^{i-1} - z C_{p_{12}}^m + \sum_{i=1}^{4} \left[AR_s^i \, K_{s_5}^i \right]_{z=h_p^1} \tag{112b}$$

$$K{p_6}^m = \sum_{i=1}^{m} h_p^i C_{p_{16}}^i - \sum_{i=2}^{m} h_p^i C_{p_{16}}^{i-1} - z C_{p_{16}}^m + \sum_{i=1}^{4} \left[AR_s^i \, K_{s_6}^i \right]_{z=h_p^1} \tag{112c}$$

$$K{p_8}^m = \sum_{i=1}^{m} h_p^i C_{p_{26}}^i - \sum_{i=2}^{m} h_p^i C_{p_{26}}^{i-1} - z C_{p_{26}}^m + \sum_{i=1}^{4} \left[AR_s^i \, K_{s_8}^i \right]_{z=h_p^1} \tag{112d}$$

$$K{p_9}^m = \sum_{i=1}^{m} h_p^i C_{p_{66}}^i - \sum_{i=2}^{m} h_p^i C_{p_{66}}^{i-1} - z C_{p_{66}}^m + \sum_{i=1}^{4} \left[AR_s^i \, K_{s_9}^i \right]_{z=h_p^1} \tag{112e}$$

$$K{p_{13}}^m = \frac{1}{2}\left[\sum_{i=1}^{m} {h_p^i}^2 C_{p_{11}}^i - \sum_{i=2}^{m} {h_p^i}^2 C_{p_{11}}^{i-1} - z^2 C_{p_{11}}^m \right] + \sum_{i=1}^{4} \left[AR_s^i \, K_{s_{13}}^i \right]_{z=h_p^1} \tag{112f}$$

$$K{p_{14}}^m = \frac{1}{2}\left[\sum_{i=1}^{m} {h_p^i}^2 C_{p_{12}}^i - \sum_{i=2}^{m} {h_p^i}^2 C_{p_{12}}^i - z^2 C_{p_{12}}^m \right] + \sum_{i=1}^{4} \left[AR_s^i \, K_{s_{14}}^i \right]_{z=h_p^1} \tag{112g}$$

$$K{p_{15}}^m = \frac{1}{2}\left[\sum_{i=1}^{m} {h_p^i}^2 C_{p_{16}}^i - \sum_{i=2}^{m} {h_p^i}^2 C_{p_{16}}^{i-1} - z^2 C_{p_{16}}^m \right] + \sum_{i=1}^{4} \left[AR_s^i \, K_{s_{15}}^i \right]_{z=h_p^1} \tag{112h}$$

$$K{p_{17}}^m = \frac{1}{2}\left[\sum_{i=1}^{m} {h_p^i}^2 C_{p_{26}}^i - \sum_{i=2}^{m} {h_p^i}^2 C_{p_{26}}^{i-1} - z^2 C_{p_{26}}^m \right] + \sum_{i=1}^{4} \left[AR_s^i \, K_{s_n}^i \right]_{z=h_p^1} \tag{112i}$$

$$K{p_{18}}^m = \frac{1}{2}\left[\sum_{i=1}^{m} {h_p^i}^2 C_{p_{66}}^i - \sum_{i=2}^{m} {h_p^i}^2 C_{p_{66}}^{i-1} - z^2 C_{p_{66}}^m \right] + \sum_{i=1}^{N} \left[AR_s^i \, K_{s_{18}}^i \right]_{z=h_p^1} \tag{112j}$$

$$A{p_8}^m = \sum_{i=1}^{m} h_p^i C_{p_{22}}^i - \sum_{i=2}^{m} h_p^i C_{p_{22}}^{i-1} - z C_{p_{22}}^m + \sum_{i=1}^{N} \left[AR_s^i \, A_{s_8}^i \right]_{z=h_p^1} \tag{112k}$$

$$A{p_{17}}^m = \frac{1}{2}\left[\sum_{i=1}^{m} {h_p^i}^2 C_{p_{22}}^i - \sum_{i=2}^{m} {h_p^i}^2 C_{p_{22}}^{i-1} - z^2 C_{p_{22}}^m \right] + \sum_{i=1}^{N} \left[AR_s^i \, A_{s_{17}}^i \right]_{z=h_p^1} \tag{112ℓ}$$

In the above equations, AR_s^i represents the area ratio for the ith stiffener, defined by:

$$AR_s^i = \frac{\text{Interface area of the ith stiffener}}{\text{Lower surface area of plate.}}$$

Except for the foregoing changes in the transverse shear stresses and the $\underset{\sim}{H}$ and $\underset{\sim}{G}$ matrices, the remaining formulation for the quadrilateral element stiffness matrix follows that of Subsection 4.2.

6.3 Example Problem and Results

The example problem is a simply supported square isotropic plate stiffened symmetrically by four stiffeners (Fig. 13). The plate is loaded by a uniform transverse pressure p_o. The problem is analyzed by using three methods.

Since the plate has two axes of symmetry only a quarter of the plate will be considered for finite-element analysis. In the first analysis, the plate is modelled by element MLP3K(Q) developed in Section 4 and the stiffeners are modelled separately by a beam element based on the displacement model with shear effects included. The displacement interpolation in the beam is cubic for bending and linear for torsion and extension. It has two nodes and six degrees of freedom per node (three translations and three rotations). Since the boundary displacements of the plate element are linearly interpolated between nodes, the transverse displacements will be incompatible. Four different meshes are used: 2x2, 4x4, 6x6, and 8x8. These same meshes are again modelled in the second analysis which uses the integrally stiffened element developed in Subsection 6.2.

The third analysis applies the Ritz method by modelling the deflection behavior of the plate as

$$\omega(x,y) = A_{11} \sin\frac{\pi x}{a} \sin\frac{\pi y}{a} + A_{12}\left[\sin\frac{\pi x}{a} \sin\frac{3\pi y}{a} + \sin\frac{3\pi x}{a} \sin\frac{\pi y}{a}\right] + A_{22} \sin\frac{3\pi x}{a} \sin\frac{3\pi y}{a} \tag{113}$$

here 'a' is the length of the plate. The assumed displacement field satisfies the prescribed force and displacement boundary conditions for a simply-supported square plate.

The total potential energy of the structure can be evaluated from the assumed deflection in terms of the unknown coefficients A_{11}, A_{12} and A_{22}. The minimization of the potential energy with respect to these coefficients then gives a set of simultaneous linear equations in these unknowns which can be solved to evaluate them.

The total potential energy π_p of the structure can be written as

$$\pi_p = U - W \tag{114a}$$

where

$$U = \text{strain energy of the structure} \tag{114b}$$

$$W = \text{work done by applied loads} \tag{114c}$$

The strain energy can be evaluated for the plate and stiffener and the total strain energy is written as

$$U = U_s + U_p \tag{115a}$$

where

$$U_p = \frac{1}{2}\int_0^a\int_0^a D\left[\left(\frac{\partial^2 w}{\partial x^2}\right)^2 + \left(\frac{\partial^2 w}{\partial y^2}\right)^2 + 2\nu\frac{\partial^2 w}{\partial x^2}\frac{\partial^2 w}{\partial y^2} + 2(1-\nu)\left(\frac{\partial^2 w}{\partial x \partial y}\right)^2\right] dx\,dy \tag{115b}$$

$$U_s = \sum_{i=1}^{4}\left[\frac{EI}{2}\int_0^{\ell}\left(\frac{d^2 w}{ds^2}\right)^2 dA\right]_i \tag{115c}$$

Under a uniform transverse pressure loading the work done is given by

$$W = p_o \int_0^a\int_0^a w\,dx\,dy \tag{116}$$

since the plate is thin, transverse shear deformation effects have been neglected.

The transverse center deflection of the plate evaluated by the three methods has been tabulated in Table 3 for comparison. It is apparent that the nonintegrally stiffened method is acceptably accurate. The center deflections computed by this method are slightly greater than those computed by the Ritz method since the finite element formulation includes transverse shear deformation effects. However, for the integrally-stiffened element, the error is about 14 percent with t_s = 0.1 in. and w_s = 0.03 in. (Fig. 13). For the 2x2 mesh the area ratio AR = 0.01 and with an 8x8 mesh, AR = 0.04 (the area ratio is the same for both stiffeners). Thus, the nonintegrally stiffened method has provided an accurate analysis, but the integrally-stiffened element is poor and hence this particular formulation should be rejected.

In any case, it must be recognized that the use of beam-like behavior in the stiffener model restricts the analysis to the regime of small stiffeners, i.e. with area ratio $AR \leq 0.1$. Stiffeners which exceed this size may begin to have a plate-like influence upon the structure in either of two ways. If w_s is large, then the structure should really be treated as an assembly of plates having different thicknesses. On the other hand, if t_s is large, then a three-dimensional model is required, with the stiffeners represented by plate elements perpendicular to the primary structure.

SECTION 7

DYNAMIC ANALYSIS

7.1 Introduction

New modules for dynamic analysis were added to the existing static-analysis FEABL-2 software [6] during the present investigation. The new software consists of a collection of subroutines for solution of the undamped free-vibration eigenvalue problem:

$$(\underset{\sim}{K} - \omega^2 \underset{\sim}{M})\underset{\sim}{q} = \underset{\sim}{0} \tag{117}$$

and one subroutine which combines the eigen-solutions with load time histories for transient response calculations. The eigen-analysis procedure is based upon the same approach used in an earlier computer code [2,3], but it has been re-programmed to achieve modularization and hardware-independence. The transient response procedure has been programmed to permit analyses of damped structures (a feature not included in the earlier code), as well as undamped structures.

During development of the above software, it was determined that some modifications were required in the existing FEABL-2 code in order to achieve inter-subroutine compatibility. These modifications were made and were exercised as part of the software verification program (Subsection 7.5.3). The resulting modified software has been designated FEABL-5* and will be documented separately in a self-contained user's guide. Only the numerical analysis methodology, general software organization, and verification tests are reviewed in this report.

7.2 Eigenvalue Solution Method

The free-vibration eigenvalue problem is posed in the following form for numerical solution:

$$\underset{\sim}{K}\,\underset{\sim}{U} = \underset{\sim}{M}\,\underset{\sim}{U}\,\underset{\sim}{\lambda} \tag{118}$$

where

$$\underset{\sim}{U} = \left[\{\underset{\sim}{U}_1\} \{\underset{\sim}{U}_2\} \cdots \{\underset{\sim}{U}_N\} \right] \tag{119}$$

---

*The capabilities of the FEABL-5 software include both static and dynamic analysis; FEABL-5 will be described in an ASRL TR in preparation.

$$\underset{\sim}{\lambda} = \begin{bmatrix} \lambda_1 & & & \\ & \lambda_2 & & \\ & & \ddots & \\ (\text{Diag.}) & & & \lambda_N \end{bmatrix} \tag{120}$$

$\underset{\sim}{U}_j = \{U_{1j} \; U_{2j} \; \ldots \; U_{Nj}\}$ = jth eigenvector (mode shape).

λ_j = jth eigenvalue = $(\omega_j)^2$.

ω_j = jth natural frequency (rad/sec).

N = Total number of unconstrained degrees of freedom in the assembled finite-element model.

Note that only the unconstrained degrees of freedom are included in the assembled equation system. If the constrained degrees of freedom were also assembled, the solutions would include spurious eigenvalues and mode shapes associated with the constraints. The necessary modifications to avoid this condition have been made to FEABL-2 by establishing an internal renumbering system which assigns negative numbers to all constrained degrees of freedom and which skips assembly of the corresponding stiffnesses and masses.

The free-vibration eigenvalue problem is solved by the Subspace Iteration Method (SIM), generally following the earlier code [2,3] and developments by other investigators [18]. The SIM has previously been proposed as a computationally efficient method for analyses in which only the lowest few modes in the structure are sought [18]. Let p be the actual number of eigenvalues wanted. Then, generally, the first P eigenvectors are included in the numerical iteration, where:

$$p + 3 \leq P \leq 2p \tag{121}$$

Equations 119 and 120 are replaced by their truncated forms:

$$\underset{\sim}{U}_{(N \times P)} = \left[\{\underset{\sim}{U}_1\} \; \{\underset{\sim}{U}_2\} \; \cdots \; \{\underset{\sim}{U}_P\} \right] \tag{122}$$

$$\underset{\sim (P\times P)}{\lambda} = \begin{bmatrix} \lambda_1 & & & \\ & \lambda_2 & & \\ & & \ddots & \\ (\text{Diag.}) & & & \lambda_P \end{bmatrix} \tag{123}$$

However, note that each eigenvector $\underset{\sim}{U}_j$ in Eq. 122 still retains its full set of N components.

The SIM algorithm begins with an initial guess $\underset{\sim}{U}^{(o)}$ for the collection of P eigenvectors. The eigenvectors are then recomputed in each major iteration step in accordance with the following procedure. Let $\underset{\sim}{U}^{(i)}$ be the results for the eigenvectors at the end of the ith iteration step. Then stiffnesses $\underset{\sim}{k}$ and masses $\underset{\sim}{m}$ in the solution subspace are computed for step (i+1) by a similarity transformation from the assembled equations:

$$\underset{\sim}{k} = \underset{\sim}{U}^{(i)T} \underset{\sim}{K} \underset{\sim}{U}^{(i)} \qquad \underset{\sim}{m} = \underset{\sim}{U}^{(i)T} \underset{\sim}{M} \underset{\sim}{U}^{(i)} \tag{124}$$

Within the subspace, the auxiliary eigenvalue problem:

$$\underset{\sim}{k}\,\underset{\sim}{u} = \underset{\sim}{m}\,\underset{\sim}{u}\,\underset{\sim}{\lambda} \tag{125}$$

is now solved by double Jacobi iteration (Subsection 7.3). The subspace matrices $\underset{\sim}{k}$ and $\underset{\sim}{m}$ are in general fully populated, even if $\underset{\sim}{M}$ in the assembled equation system is a diagonal (lumped-mass) matrix. The collection of subspace eigenvectors $\underset{\sim}{u}$ is a PxP matrix, i.e.:

$$\begin{aligned} \underset{\sim}{u} &= \left[\{\underset{\sim}{u}_1\} \; \{\underset{\sim}{u}_2\} \; \cdots \; \{\underset{\sim}{u}_P\} \right] \\ \underset{\sim}{u}_j &= \left\{ u_{1j} \; u_{2j} \; \cdots \; u_{Pj} \right\} \end{aligned} \tag{126}$$

At the end of step (i+1), the full-space eigenvectors are recomputed according to:

$$\underset{\sim}{U}^{(i+1)} = \underset{\sim}{K}^{-1} \underset{\sim}{M} \underset{\sim}{U}^{(i)} \underset{\sim}{u} \tag{127}$$

The matrix operation $\underset{\sim}{U}^{(i)}\underset{\sim}{u}$ can be recognized as a vector projection in which each eigenvector $\underset{\sim}{U}_j^{(i)}$ is aligned with its corresponding subspace eigenvector $\underset{\sim}{u}_j$:

$$\{\underset{\sim}{U}^{(i)}\underset{\sim}{u}\}_j = \sum_{k=1}^{P} \underset{\sim}{U}_k^{(i)} \cdot \underset{\sim}{u}_j \tag{128}$$

The remainder of Eq. 127 is analogous to the principal operation found in the simpler Matrix Iteration Method [19] which is often used for computation of the first eigenvalue only, i.e.:

$$\underset{\sim}{U}_1^{(i+1)} = \underset{\sim}{K}^{-1}\underset{\sim}{M}\,\underset{\sim}{U}_1^{(i)}\,\lambda_1 \tag{129}$$

The steps outlined in Eqs. 124 through 127 are repeated until one of two conditions occurs. The iteration will be stopped after some maximum number of iterations specified by the user, or when some specified number of eigenvalues n ($p \le n \le P$) have converged. The convergence criterion is taken as:

$$|\lambda_j^{(i)} - \lambda_j^{(i+1)}| \,/\, |\lambda_j^{(i)}| < \varepsilon \tag{130}$$

where the tolerance parameter ε is specified by the user. (A value $\varepsilon = 10^{-4}$ will assure convergence of the natural frequencies $\omega_j = \sqrt{\lambda_j}$ to 10^{-2}.) If, during the iteration, some of the eigenvalues $\lambda_1, \lambda_2, \ldots, \lambda_j$ ($j<n$) have already converged, then the corresponding eigenvectors $\underset{\sim}{U}_1, \underset{\sim}{U}_2, \ldots, \underset{\sim}{U}_j$ are "frozen" while iteration of $\underset{\sim}{U}_{j+1}, \ldots, \underset{\sim}{U}_P$ proceeds. The process is such that the eigenvalues computed in the subspace converge to the eigenvalues $\underset{\sim}{\lambda}$ of the assembled equation system. Hence, no distinction has been made in the notation for these quantities.

The SIM algorithm outlined by Eqs. 124 through 127 is not the most efficient possible procedure, since it requires three coefficient matrices from the assembled equation system: $\underset{\sim}{K}$, $\underset{\sim}{M}$, and $\underset{\sim}{K}^{-1}$ in terms of its factored triple product $\underset{\sim}{K} = \underset{\sim}{L}\underset{\sim}{D}\underset{\sim}{L}^T$ for simultaneous solution [6]. However, the need

for the unfactored stiffness matrix $\underset{\sim}{K}$ can be eliminated by the following revised algorithm. Let $\underset{\sim}{V}^{(i)}$ be a collection of auxiliary vectors formed at the end of the ith iteration step, such that $\underset{\sim}{K}\,\underset{\sim}{U}^{(i)} = \underset{\sim}{V}^{(i)}$. Then the current eigenvectors $\underset{\sim}{U}^{(i)}$ are first calculated from:

$$\underset{\sim}{U}^{(i)} = \underset{\sim}{K}^{-1}\underset{\sim}{V}^{(i)} \tag{131}$$

Equations 124 can now be replaced with the following seris of computations which never require $\underset{\sim}{K}$ directly:

$$\underset{\sim}{k} = \underset{\sim}{U}^{(i)T}\underset{\sim}{V}^{(i)} \quad \left(= \underset{\sim}{U}^{(i)T}\underset{\sim}{K}\,\underset{\sim}{U}^{(i)} \text{ as in Eqs. 124}\right) \tag{132}$$

$$\bar{\underset{\sim}{V}}^{(i)} = \underset{\sim}{M}\,\underset{\sim}{U}^{(i)} \tag{133}$$

$$\underset{\sim}{m} = \underset{\sim}{U}^{(i)T}\bar{\underset{\sim}{V}}^{(i)} \quad \left(= \underset{\sim}{U}^{(i)T}\underset{\sim}{M}\,\underset{\sim}{U}^{(i)} \text{ as in Eqs. 124}\right) \tag{134}$$

The eigenvalue problem in the subspace is then solved in the manner mentioned previously, and the iteration cycle is completed with:

$$\underset{\sim}{V}^{(i+1)} = \bar{\underset{\sim}{V}}^{(i)}\underset{\sim}{u} \quad \left(= \underset{\sim}{M}\,\underset{\sim}{U}^{(i)}\underset{\sim}{u}\right) \tag{135}$$

It is now easy to see that the definitions are consistent, i.e. $\underset{\sim}{V}^{(i+1)} = \underset{\sim}{K}\,\underset{\sim}{U}^{(i+1)}$, by comparing Eq. 135 with Eq. 127.

The procedure outlined by Eqs. 131 through 135 requires only the assembled mass matrix $\underset{\sim}{M}$ and "$\underset{\sim}{K}^{-1}$" (in the form $\underset{\sim}{L}\,\underset{\sim}{D}\,\underset{\sim}{L}^T$), and is thus more efficient than the simpler iteration procedure which was presented in the first part of this subsection. However, note that since both procedures require $\underset{\sim}{K}^{-1}$, the SIM is restricted to analyses of finite-element models to which displacement boundary condtions have been properly applied to restrain all rigid-body modes.

7.3 Eigenvalue Solution in the Subspace

The eigenvalue problem in the subspace (Eq. 125) is solved by means of a two-stage iteration scheme in which each stage treats a standard eigenvalue

problem with one coefficient matrix. The eigenvalues and eigenvectors of the mass matrix $\underset{\sim}{m}$ alone are computed first, and these quantities are then used to transform Eq. 125 to a standard problem [20]. Let the first eigenvalue problem be represented by:

$$\underset{\sim}{m}\,\underset{\sim}{z} = \underset{\sim}{z}\,\underset{\sim}{\gamma} \qquad (136)$$

where

$$\begin{aligned} \underset{\sim}{z} &= \left[\{\underset{\sim}{z}_1\}\ \{\underset{\sim}{z}_2\}\ \cdots\ \{\underset{\sim}{z}_p\} \right] \\ \underset{\sim}{z}_j &= \{ z_{1j}\ \ z_{2j}\ \ \cdots\ \ z_{pj} \} \end{aligned} \qquad (137)$$

$$\underset{\sim}{\gamma} = \begin{bmatrix} \gamma_1 & & & \\ & \gamma_2 & & \\ & & \ddots & \\ (\text{Diag.}) & & & \gamma_p \end{bmatrix} \qquad (138)$$

γ_j = jth eigenvalue of $\underset{\sim}{m}$

After $\underset{\sim}{z}$ and $\underset{\sim}{\gamma}$ have been computed, the mass matrix may be expressed in the form

$$\underset{\sim}{m} = \underset{\sim}{z}\,\underset{\sim}{\gamma}\,\underset{\sim}{z}^T \qquad (139)$$

Also, powers of $\underset{\sim}{m}$ can be expressed in simple form, in particular [20]:

$$\underset{\sim}{m}^{1/2} = \underset{\sim}{z}\,\underset{\sim}{\gamma}^{1/2}\,\underset{\sim}{z}^T \qquad \underset{\sim}{m}^{-1/2} = \underset{\sim}{z}\,\underset{\sim}{\gamma}^{-1/2}\,\underset{\sim}{z}^T \qquad (140)$$

where

$$\underset{\sim}{\gamma}^{1/2} = \begin{bmatrix} \sqrt{\gamma_1} & & & \\ & \sqrt{\gamma_2} & & \\ & & \ddots & \\ (\text{Diag.}) & & & \sqrt{\gamma_p} \end{bmatrix} \qquad \underset{\sim}{\gamma}^{-1/2} = \begin{bmatrix} 1/\sqrt{\gamma_1} & & & \\ & 1/\sqrt{\gamma_2} & & \\ & & \ddots & \\ (\text{Diag.}) & & & 1/\sqrt{\gamma_p} \end{bmatrix} \qquad (141)$$

The validity of Eqs. 140 can be proved in a straightforward manner by verifying that the matrix products $\underset{\sim}{m}^{1/2}\underset{\sim}{m}^{1/2}$ and $\underset{\sim}{m}^{-1/2}\underset{\sim}{m}^{-1/2}$ are equal to $\underset{\sim}{m}$ and $\underset{\sim}{m}^{-1}$, respectively. The proof proceeds by substitution and carrying out the matrix multiplications, recognizing that the collection of eigenvectors are orthonormal, i.e. $\underset{\sim}{z}\,\underset{\sim}{z}^T = \underset{\sim}{z}^T\underset{\sim}{z}$ = identity matrix.

In order to transform the subspace eigenvalue problem to a standard problem, let $\underset{\sim}{v} = \underset{\sim}{m}^{1/2}\underset{\sim}{u}$ and premultiply Eq. 125 by $\underset{\sim}{m}^{-1/2}$ to obtain:

$$\underset{\sim}{m}^{-1/2}\left(\underset{\sim}{k}\,\underset{\sim}{m}^{-1/2}\underset{\sim}{m}^{1/2}\underset{\sim}{u}\right) = \underset{\sim}{m}^{-1/2}\left(\underset{\sim}{m}^{1/2}\underset{\sim}{m}^{1/2}\underset{\sim}{u}\,\underset{\sim}{\lambda}\right)$$

$$\left(\underset{\sim}{m}^{-1/2}\underset{\sim}{k}\,\underset{\sim}{m}^{-1/2}\right)\underset{\sim}{v} = \underset{\sim}{v}\,\underset{\sim}{\lambda} \tag{142}$$

Thus, the second standard problem consists of forming the coefficient matrix $\underset{\sim}{m}^{-1/2}\underset{\sim}{k}\,\underset{\sim}{m}^{-1/2}$ and computing the eigenvalues $\underset{\sim}{\lambda}$ and transformed eigenvectors $\underset{\sim}{v}$. When the problem has been solved, the proper eigenvectors $\underset{\sim}{u}$ are obtained from the definition of $\underset{\sim}{v}$, i.e.:

$$\underset{\sim}{u} = \underset{\sim}{m}^{-1/2}\underset{\sim}{v} \tag{143}$$

The two standard eigenvalue problems represented by Eqs. 136 and 142 are solved by the well known Jacobi Iteration Method [19]. The fundamental operation in the Jacobi method is a rotation transformation which is used to diagonalize the coefficient matrix. Only one such operation is required for a 2x2 matrix. Using the mass matrix $\underset{\sim}{m}$ as an example,

$$\begin{bmatrix} \cos\theta & \sin\theta \\ -\sin\theta & \cos\theta \end{bmatrix} \begin{bmatrix} m_{11} & m_{12} \\ m_{21} & m_{22} \end{bmatrix} \begin{bmatrix} \cos\theta & -\sin\theta \\ \sin\theta & \cos\theta \end{bmatrix} = \begin{bmatrix} \gamma_1 & 0 \\ 0 & \gamma_2 \end{bmatrix} \tag{144}$$

where

$$\theta = \frac{1}{2}\tan^{-1}\left(\frac{2m_{12}}{m_{11} - m_{22}}\right) \tag{145}$$

For larger matrices, the procedure is approximate. Successive rotation transformations must be applied to reduce the sum of squares of the off-diagonal terms. Let $\underset{\sim}{m}$ represent the current matrix and suppose that the

term $m_{k\ell}$ is to be reduced to zero during the current step. This is accomplished by replacing $\underset{\sim}{m}$ with $\bar{\underset{\sim}{m}} = \underset{\sim}{R}^T \underset{\sim}{m}\, \underset{\sim}{R}$, where:

$$\underset{\sim}{R} = \begin{array}{c} \\ \\ \text{row } k \\ \\ \text{row } \ell \\ \\ \end{array} \begin{array}{c} \begin{array}{ccccc} & \text{col. } k & & \text{col. } \ell & \end{array} \\ \left[\begin{array}{c|c|c|c|c} \begin{matrix} 1 & & \\ & \ddots & \\ & & 1 \end{matrix} & & & & \\ \hline & \cos\theta & & -\sin\theta & \\ \hline & & \begin{matrix} 1 & & \\ & \ddots & \\ & & 1 \end{matrix} & & \\ \hline & \sin\theta & & \cos\theta & \\ \hline & & & & \begin{matrix} 1 & & \\ & \ddots & \\ & & 1 \end{matrix} \end{array} \right] \end{array} \tag{146}$$

$$\theta = \frac{1}{2} \tan^{-1} \left(\frac{2 m_{k\ell}}{m_{kk} - m_{\ell\ell}} \right)$$

The replacement operations implied by the product $\underset{\sim}{R}^T \underset{\sim}{m}\, \underset{\sim}{R}$ are as follows:

$$\begin{aligned} &\left.\begin{aligned} \bar{m}_{kj} &= \bar{m}_{jk} = m_{kj} \cos\theta + m_{\ell j} \sin\theta \\ \bar{m}_{\ell j} &= \bar{m}_{j\ell} = -m_{kj} \sin\theta + m_{\ell j} \cos\theta \end{aligned}\right\} \quad (j = 1, 2, \ldots, P \;;\; j \neq k, \ell) \\ &\bar{m}_{kk} = m_{kk} \cos^2\theta + 2 m_{k\ell} \sin\theta\cos\theta + m_{\ell\ell} \sin^2\theta \\ &\bar{m}_{\ell\ell} = m_{kk} \sin^2\theta - 2 m_{k\ell} \sin\theta\cos\theta + m_{\ell\ell} \cos^2\theta \\ &\bar{m}_{k\ell} = \bar{m}_{\ell k} = 0 \end{aligned} \tag{147}$$

It can be shown [19] that:

$$\sum_{j=1}^{P} (\bar{m}_{jj})^2 = 2 (m_{k\ell})^2 + \sum_{j=1}^{P} (m_{jj})^2 \tag{148}$$

In other words, the sum of squares of the diagonal terms in $\bar{\underset{\sim}{m}}$ increases by $2(m_{k\ell})^2$ as a result of the Jacobi rotation and hence, the sum of squares of the off-diagonal terms must decrease by that amount. However, other off-diagonal terms ($\bar{m}_{kj}$, $\bar{m}_{\ell j}$) which may have been reduced to zero by previous

operations are made non-zero by the current operation which reduces $m_{k\ell}$. Thus, the entire process involves a series of sweeps through the coefficient matrix, each sweep consisting of successive reduction operations applied to all off-diagonal terms, until either a maximum allowed number of iterations is reached or until:

$$\Sigma\ (\text{Current off-diagonal terms})^2/\Sigma\ (\text{Original off-diagonal terms})^2 < \varepsilon \qquad (149)$$

where the number of iterations and the tolerance parameter ε are specified by the user. The series of Jacobi rotations which reduce $\underset{\sim}{m}$ to a nearly diagonal matrix can also be used to compute the eigenvectors directly, as shown by the following identity. Suppose that J such rotations were required in the order $\underset{\sim}{R}_1, \underset{\sim}{R}_2, \ldots, \underset{\sim}{R}_J$. Then (see Eq. 136):

$$\underset{\sim}{R}_J^T \underset{\sim}{R}_{J-1}^T \cdots \underset{\sim}{R}_2^T \underset{\sim}{R}_1^T \underset{\sim}{m} \underset{\sim}{R}_1 \underset{\sim}{R}_2 \cdots \underset{\sim}{R}_{J-1} \underset{\sim}{R}_J \cong \underset{\sim}{\gamma} = \underset{\sim}{z}^T \underset{\sim}{m} \underset{\sim}{z}$$

Therefore:

$$\underset{\sim}{z} \cong \underset{\sim}{R}_1 \underset{\sim}{R}_2 \cdots \underset{\sim}{R}_J \qquad (150)$$

The product for $\underset{\sim}{z}$ is accumulated as the individual Jacobi rotations are applied.

The Jacobi method outlined in Eqs. 144 through 150 is applied in exactly the same manner to the second standard problem, in which the eigenvalues of $\underset{\sim}{m}^{-1/2} \underset{\sim}{k}\ \underset{\sim}{m}^{-1/2}$ are sought. The entire procedure has been programmed as FEABL-5 subroutine JACKM1, which employs IBM Scientific Subroutine Package subroutine EIGEN for the Jacobi iteration computations. Double-precision arithmetic is used within the subspace to obtain the necessary accuracy in the computations for the rotation angles θ (Eq. 146). Single-precision calculations were tried, but were found to make the convergence process slower, in agreement with the conclusions reached by other investigators [19]. The inefficiencies of double-precision arithmetic and fully populated matrices are acceptable within the subspace, which will usually be of the order 20x20 or less. This has no effect upon the global computations, since $\underset{\sim}{K}$ and $\underset{\sim}{M}$ are kept as single-precision band-matrices.

7.4 Transient Response Analysis

The Modal Superposition Method (MSM) has been chosen for transient response analysis in order to avoid the time-step limitations which are imposed by stability criteria, frequency distortion, and false damping associated with finite-difference time operators employed in direct time-integration schemes [21,22]. In the direct time-integration approach, the assembled transient equation system

$$\underset{\sim}{M}\,\ddot{\underset{\sim}{q}}(t) + \underset{\sim}{K}\,\underset{\sim}{q}(t) = \underset{\sim}{Q}(t) \tag{151}$$

is replaced by a finite-difference equivalent, e.g.:

$$\frac{1}{(\Delta t)^2}\,\underset{\sim}{M}\left(\underset{\sim}{q}_{i+1} - 2\underset{\sim}{q}_i + \underset{\sim}{q}_{i-1}\right) + \underset{\sim}{K}\,\underset{\sim}{q}_i = \underset{\sim}{Q}_i \qquad (152)^*$$

where the subscripts i-1, i, i+1 denote quantities evaluated at the times $t=t_{i-1}$, $t=t_i=t_{i-1}+\Delta t$, $t=t_{i+1}=t_i+\Delta t$. The displacement solution $\underset{\sim}{q}_{i+1}$ can then be estimated from current and prior information:

$$\underset{\sim}{q}_{i+1} = 2\underset{\sim}{q}_i - \underset{\sim}{q}_{i-1} + (\Delta t)^2\,\underset{\sim}{M}^{-1}\underset{\sim}{K}\,\underset{\sim}{q}_i + \underset{\sim}{Q}_i \tag{153}$$

(Equation 152 applies to the second and all succeeding time steps. For the first step, $\underset{\sim}{q}_1$ is calculated from $\underset{\sim}{q}_o$, $\underset{\sim}{Q}_o$ and $\dot{\underset{\sim}{q}}_o$.) Direct time-integration has the advantage of not requiring the assembled equation eigenvalue solutions for the transient response calculations. However, the integration stability boundary does require knowledge of the highest frequency ω_N in the finite-element model, since $\Delta t < 2/\omega_N$ is the stability criterion [23] for the central difference operator. Thus, even direct time-integration must be preceded by at least the simple inverse iteration scheme:

$$\underset{\sim}{U}_N^{(i+1)} = \underset{\sim}{M}^{-1}\underset{\sim}{K}\,\underset{\sim}{U}_N^{(i)}\,(1/\lambda_N) \tag{154}$$

(Compare Eq. 154 with Eq. 129.)

Since some knowledge about the frequencies and mode shapes of a structure is usually sought anyway, the MSM offers, potentially, a much more efficient

---

*The central difference operator is used here as a simple illustrative example.

solution scheme. In this approach, the assembled transient system (Eq. 151) is first decoupled by means of the system eigenvectors. The transient displacement vector $\underset{\sim}{q}(t)$ can be represented approximately as a linear combination of the first few eigenvectors:

$$\underset{\sim}{q}(t) \cong \sum_{j=1}^{p} \underset{\sim}{U}_j \, \alpha_j(t) = \underset{\sim}{U} \, \underset{\sim}{\alpha}(t) \tag{155}$$

where $\underset{\sim}{\alpha}(t) = \{\alpha_1 \; \alpha_2 \; \ldots \; \alpha_p\}$ is the modal amplitude vector. It is assumed that only the p modes actually sought in the eigenvalue analysis (see Subsection 7.2) are retained in the modal solution. This illustrates immediately the inherent disadvantage of the MSM, that the quality of the solution degrades rapidly for transient load-histories whose power content for frequencies $\omega > \omega_p$ is significant. If Eq. 155 is now substituted in Eq. 151 and the result is premultiplied by $\underset{\sim}{U}^T$ the following decoupled equation system is obtained:

$$\underset{\sim}{U}^T \underset{\sim}{M} (\underset{\sim}{U} \, \ddot{\underset{\sim}{\alpha}}) + \underset{\sim}{U}^T \underset{\sim}{K} (\underset{\sim}{U} \, \underset{\sim}{\alpha}) = \underset{\sim}{U}^T \underset{\sim}{Q}$$

$$\underset{\sim}{m} \, \ddot{\underset{\sim}{\alpha}} + \underset{\sim}{k} \, \underset{\sim}{\alpha} = \underset{\sim}{f}(t) \tag{156}$$

where

$\underset{\sim}{m} = \underset{\sim}{U}^T \underset{\sim}{M} \underset{\sim}{U}$ = subspace mass matrix (diagonal)

$\underset{\sim}{k} = \underset{\sim}{U}^T \underset{\sim}{K} \underset{\sim}{U}$ = subspace stiffness matrix (diagonal)

$\underset{\sim}{f}(t) = \underset{\sim}{U}^T \underset{\sim}{Q}(t)$ = generalized subspace force vector

The subspace mass and stiffness matrices are diagonal in the present case because they result from computations with a converged set of eigenvectors. For practical purposes, the diagonal matrices $\underset{\sim}{m}$ and $\underset{\sim}{k}$ are obtained simultaneously with $\underset{\sim}{U}$ at the conclusion of the SIM algorithm (Subsection 7.2). Note that while $\underset{\sim}{m}$ and $\underset{\sim}{k}$ are in general fully populated matrices during execution of the SIM, they become diagonalized as a part of the convergence process. Equation 156 may now be rewritten as the collection of scalar equations:

$$m_j \ddot{\alpha}_j(t) + k_j \alpha_j(t) = f_j(t) \qquad (j = 1, 2, \cdots, p) \tag{157}$$

or since $\omega_j^2 = k_j/m_j$ (and dropping the subscript j without loss of generality):

$$\ddot{\alpha}(t) + \omega^2 \alpha(t) = f(t)/m \tag{158}$$

Damping should be added to the transient response equation in order to permit realistic solutions to be calculated. This is done most conveniently in the MSM by directly assuming nondimensional modal damping factors:

$$\zeta_j = c_j / 2\sqrt{k_j m_j} \tag{159}$$

rather than assuming the physical damping coefficients c_j. Equation 158 for the typical modal amplitude response is thus replaced by:

$$\ddot{\alpha}(t) + 2\zeta\omega\dot{\alpha}(t) + \omega^2 \alpha(t) = f(t)/m \tag{160}$$

A general solution of Eq. 160 can be derived by analytical integration if a specific assumption is made about the generalized force history f(t). A piece-wise linear representation for f(t) is a simple approximation which is also useful, since it is unlikely that the force time-history is known to an accuracy which would justify higher-order representation. Therefore, during the ith time step the generalized force is taken as:

$$f(t) = \left(\frac{t_i - t}{t_i - t_{i-1}}\right) f_{i-1} + \left(\frac{t - t_{i-1}}{t_i - t_{i-1}}\right) f_i \tag{161}$$

where $f_{i-1} = f(t_{i-1})$ and $f_i = f(t_i)$. With Eq. 161 substituted for f(t) in Eq. 160, the following general solution may be derived:

$$\begin{aligned} \alpha(t_i) = \alpha_i = e^{-\zeta\omega(t_i - t_{i-1})} &\Big\{ \left[\alpha_{i-1} + 2\zeta C/\omega - f_{i-1}/k\right] \cos\omega_D (t_i - t_{i-1}) + \\ &+ \left[\dot{\alpha}_{i-1} + \zeta\omega\alpha_{i-1} - (1-2\zeta^2)C - \zeta\omega f_{i-1}/k\right] \frac{1}{\omega_D} \sin\omega_D (t_i - t_{i-1}) \Big\} + \\ &+ (t_i - t_{i-1} - 2\zeta/\omega) C + f_{i-1}/k \end{aligned} \tag{162}$$

$$\begin{aligned} \dot{\alpha}(t_i) = \dot{\alpha}_i = e^{-\zeta\omega(t_i - t_{i-1})} &\Big\{ \left[\omega^2 f_{i-1}/k - \omega^2\alpha_{i-1} - \zeta\omega\dot{\alpha}_{i-1} - \zeta\omega C\right] \frac{1}{\omega_D} \sin\omega_D (t_i - t_{i-1}) + \\ &+ \left[\dot{\alpha}_{i-1} - C\right] \cos\omega_D (t_i - t_{i-1}) \Big\} + C \end{aligned} \tag{163}$$

where

$\alpha_{i-1} = \alpha(t_{i-1})$ = amplitude at beginning of time step

$\dot{\alpha}_{i-1} = \dot{\alpha}(t_{i-1})$ = amplitude velocity at beginning of time step

$\omega_D = \omega\sqrt{1-\zeta^2}$ = damped natural frequency

and where

$$C = \frac{1}{k}\left(\frac{f_i - f_{i-1}}{t_i - t_{i-1}}\right) \tag{164}$$

Equations 162 and 163 give the modal amplitude α_i and its velocity $\dot{\alpha}_i$ at the end of the time step $t=t_i$, in terms of the associated generalized force history (f_{i-1}, f_i) prior information (α_{i-1}, $\dot{\alpha}_{i-1}$) and system properties (ζ,ω,k). It should be noted that this solution applies only to underdamped systems, i.e. $\zeta < 1$.

The MSM solution scheme is quite straightforward. Vectors of initial modal amplitudes and modal amplitude velocities $\underset{\sim}{\alpha}_o$, $\dot{\underset{\sim}{\alpha}}_o$ are prescribed and the set of discrete force vectors:

$$\left[\underset{\sim}{f}_0 \ \underset{\sim}{f}_1 \ \underset{\sim}{f}_2 \ \cdots \ \right] = \underset{\sim}{U}^T \left[\underset{\sim}{Q}(0) \ \underset{\sim}{Q}(t_1) \ \underset{\sim}{Q}(t_2) \ \cdots\right] \tag{165}$$

is computed. Equations 162 and 163 are then employed for each time step in succession, and the physical displacement solutions

$$\left[\underset{\sim}{q}_1 \ \underset{\sim}{q}_2 \ \cdots \ \right] = \underset{\sim}{U}\left[\underset{\sim}{\alpha}_1 \ \underset{\sim}{\alpha}_2 \ \cdots \ \right] \tag{166}$$

are calculated during the transient solution. The scheme presented in Eqs. 162 and 163 has the advantage that the size of each time step may be arbitrarily chosen. The most economical choice of times t_1, t_2, ... is such that each interval is as long as possible while still maintaining a reasonably accurate piece-wise linear approximation for the force history. Specific choices are, of course, dependent upon the specific problem under

analysis. The transient solution algorithm has been programmed as FEABL-5 subroutines TSTEP and ELAPSE.

7.5 Software Verification and Performance Tests

Several test analyses were run, in which the computed results were compared with independent analytical solutions, both to verify the basic software and to assess the performance of the SIM. The verification tests included validations of subroutine MLP3M, the element mass matrix generator which is the companion to element stiffness matrix subroutine MLP3K. Results of the tests are presented here approximately in chronological order, i.e. following the actual development work.

7.5.1 Verification of Jacobi Iteration Method

The accuracy of the Jacobi Iteration Method (subroutines JACKM1 and EIGEN, Subsection 7.3) was assessed in the first series of tests by computing the first few natural frequencies for both cantilever and unrestrained slender beams. The purpose of this series of tests was two-fold: first to reassess the sensitivity of the Jacobi method to arithmetic precision [19] and second, to verify the code in subroutine EIGEN. Some doubt had been cast upon the validity of parts of the IBM Scientific Subroutine Package because it is no longer supported [24]. However, the verification tests did demonstrate the validity of subroutine EIGEN, as will be seen below.

Independent analytical solutions of the slender-beam vibration problem [20] give the following results for the first few natural frequencies of a cantilever beam with uniform section properties:

$$\begin{aligned} \omega_1 &= (1.875)^2 \sqrt{EI/mL^4} \\ \omega_2 &= (4.694)^2 \sqrt{EI/mL^4} \\ \omega_3 &= (7.855)^2 \sqrt{EI/mL^4} \end{aligned} \tag{167}$$

where the frequencies are in units of rad/sec, and where:

E = material Young's modulus (psi)

I = cross section bending inertia (in^4)

m = mass per unit length ($lb\ sec^2/in^2$)

L = total length of the beam (in.)

Similarly, the solutions for an unrestrained beam are:

$$
\begin{aligned}
\omega_1 &= \omega_2 = 0 \\
\omega_3 &= (1.506\pi)^2 \sqrt{EI/mL^4} \\
\omega_4 &= (2.500\pi)^2 \sqrt{EI/mL^4}
\end{aligned}
\tag{168}
$$

The first two solutions in Eq. 168 correspond to the rigid-body modes of vertical translation and rotation of the beam about its center.

A cubic-interpolation assumed-displacement beam element was programmed to provide element software to implement the tests. The beam element (Fig. 15) is of length ℓ, such that the total beam length L is a multiple of the element length. The element stiffness matrix, which is easily derived by substituting the displacement interpolation into the strain-energy equivalence:

$$
\frac{1}{2}\int_0^{\ell} EI\,(d^2w/dx^2)^2\,dx = \frac{1}{2}\,\underset{\sim}{q}^T\,\underset{\sim}{k}\,\underset{\sim}{q}
\tag{169}
$$

is given by:

$$
\underset{\sim}{k} = \frac{EI}{\ell^3}\begin{bmatrix} 12 & & \text{(Symmetric)} & \\ 6\ell & 4\ell^2 & & \\ -12 & -6\ell & 12 & \\ 6\ell & 2\ell^2 & -6\ell & 4\ell^2 \end{bmatrix}
\tag{170}
$$

The representation is "exact", in the sense that the engineering beam theory solutions for static deflections of a cantilever under a tip load or tip moment (for example) can be obtained exactly with models in which the entire beam is represented by a single element. In other words, the beam element introduces no convergence error due to discretization of a continuum. However, some convergence error in the higher eigenvalues can still be expected, even with several elements modelling the beam, as will be explained subsequently. The element consistent mass matrix is derived by substituting the interpolation function into the kinetic energy equivalence:

$$\frac{1}{2}\int_0^{\ell} m(\dot{w})^2\,dx = \frac{1}{2}\dot{\underset{\sim}{q}}^T \underset{\sim}{m}\,\dot{\underset{\sim}{q}} \tag{171}$$

from which there results:

$$\underset{\sim}{m} = \frac{m\ell}{420}\begin{bmatrix} 156 & & (\text{Symmetric}) & \\ 22\ell & 4\ell^2 & & \\ 54 & 13\ell & 156 & \\ -13\ell & -3\ell^2 & -22\ell & 4\ell^2 \end{bmatrix} \tag{172}$$

Analytical and computed results are compared for both the cantilever and unrestrained beams in Table 4. Computed values are shown for both single- and double-precision arithmetic. It is evident that the arithmetic precision has not affected the results except* in the case of the rigid-body modes of the unrestrained beam. Therefore, single-precision arithmetic could be used when subroutines JACKM1 and EIGEN are coupled with the SIM software, since the SIM can be applied only to structures which are restrained against any rigid-body motion. However, the results for the unrestrained beam do indicate that accuracy problems might occur for structures which possess a very low first natural frequency, or for structures which possess one or more closely grouped frequencies. The arithmetic in subroutines JACKM1 and EIGEN has been left in double-precision for the above reason and to permit their use as an independent module for eigenvalue analyses of unrestrained structures. The apparent "improvement" in the single-precision results, in comparison with the earlier investigation which gave rise to the warning about precision [19], is most probably due to the transition from 12- and 16-BIT hardware in the late 1950's to today's 32-BIT hardware.

The errors in both computed solutions for the higher modes serve to illustrate another form of convergence error which is specifically associated with eigenvalue analysis. As higher natural frequencies are sought for the beams, the corresponding exact mode shapes exhibit higher

---

*It was also noted that more iterations were required in single-precision to achieve a given error tolerance ε.

spatial frequency distributions of transverse displacement as a function of distance along the beam. The ability of the finite-element model to reproduce mode shapes and frequencies is thus limited, through the element displacement interpolation function, by the number of elements in the model. This point is further illustrated by the results in Table 5, which compares two solutions for the cantilever beam. Here, the arithmetic precision has been kept constant, but one model contains only 12 degrees of freedom (5 elements) while the other contains 50 degrees of freedom (24 elements). The improvements are apparent in the third and higher frequencies.

7.5.2 Verification and Assessment of SIM

The SIM software was first verified by conducting another series of tests in which SIM solutions of the cantilever beam problem were compared with analytical results outlined in Subsection 7.5.1. A 50 degree-of-freedom model was used to generate the assembled equation system. The size of the subspace was set at P=12, while convergence was sought for p=6 eigenvalues. The results presented in Subsection 7.5.1 were reproduced.

In a second series of tests, the SIM software was coupled with element MLP3K and its mass matrix MLP3M (Section 4) to provide further verification while simultaneously validating subroutine MLP3M. The single-layer, isotropic, simply supported square plate illustrated in Fig. 16 was chosen as a test problem. One quadrant of the plate, shown in the lower part of the figure, was isolated for analysis by applying symmetry boundary conditions along the centerlines. Eigenvalue analysis of a model of this type will compute only those frequencies corresponding to mode shapes which are symmetric in both the X and Y directions. Independent analytical solutions for the symmetric frequencies were obtained from a Fourier analysis [25] for comparison. A 3x3 mesh is shown in Fig. 16, but 5x5, 7x7 and 9x9 meshes were also analyzed to obtain information about solution convergence rates.

In the first test, the subspace size was set at P=9, the error tolerance parameter was set at $\varepsilon = 10^{-2}$, and convergence was sought for p=6 eigenvalues. The results are summarized in terms of percent errors:

$$\%\ \text{Error} = 100\ (1-\omega_{\text{Computed}}/\omega_{\text{Exact}}) \qquad (173)$$

and are shown in Table 6 and Fig. 17. Analyses were run using both hybrid-rational and lumped element mass matrices. Surprisingly, the lumped-mass matrix appears to converge as fast as or faster than the hybrid-rational mass matrix for the higher frequencies, while the hybrid-rational mass matrix converges faster for the first natural frequency. This result is opposite to what one would expect from a comparison of a lumped-mass matrix with a consistent-mass matrix for an assumed-displacement element. In either case, the convergence is quite rapid after enough detail has been placed in the finite-element model.

A more interesting conclusion may be drawn from the erroneous predictions associated with the combinations of higher frequency and coarser mesh. Here reappears the problem of mesh convergence error which was mentioned in Subsection 7.5.1. The results are dramatic in the present case because of the linear interpolation which is used in element MLP3K for the plate's transverse displacement, w. The convergence effect is illustrated schematically in Fig. 18, which compares the spatial distributions of the first few natural modes with the abilities of the finite-element models to mimic these shapes. For example, the 3x3 mesh is able to reproduce the first and third harmonics without spatial distortion, but can not do so for the fifth harmonic. Thus (considering the lumped-mass results in Table 6), low errors appear for f_{11}, f_{13} and f_{31}. The next eigenvalue, f_{33}, should also have a low error, but it is apparently "infected" by its next neighbors f_{15} and f_{51}. A similar argument can be made about the 5x5 mesh, which is capable of reproducing harmonics up to the fifth, but which severely distorts the seventh harmonic.

A second test was conducted to investigate the effect of subspace size, P, on the rates of convergence of the six lowest eigenvalues. The finite-element mesh was fixed at 9x9 for this test, in order to eliminate as nearly as possible the effects of modelling convergence error. As can be seen in Table 6, the worst errors with a 9x9 mesh and P=9 were 7.08 percent with the hybrid-rational mass matrix and 2.29 percent with the lumped-mass matrix. Subspace sizes P=6,8,10 and 12 were investigated in the second test, for comparison with the case P=9. The tolerance parameter was kept fixed at $\varepsilon = 10^{-2}$.

According to the mathematical theory of eigenvalue analysis [18], the principal reason for the potential efficiency of the SIM as a numerical method is that the SIM algorithm causes eigenvalues λ_j to converge at rates proportional to λ_j/λ_{P+1}, while the rates for other numerical methods may only be proportional to λ_j/λ_{j+1}. Thus, for example, if 6 eigenvalues are sought and if:

$$\lambda_{12} = \lambda_{13} > \lambda_9 = \lambda_{10} = \lambda_{11} \tag{174}$$

then the choice P=12 should be superior to P=10 because $\lambda_j/\lambda_{13} < \lambda_j/\lambda_{11}$ (j=1,2,..., 6). This situation occurs for the present plate analysis, as illustrated by the analytical eigenvalue solutions in the second column of Table 7. The remainder of the table gives the nondimensional convergence rate factors λ_j/λ_{P+1} (j=1,2,..., 6) for the various choices of P which were investigated. Theoretically, the error in a computed eigenvalue at any iteration step may be expressed as:

$$\text{Error} \sim (\lambda_j/\lambda_{P+1})^I = (R_j)^I \tag{175}$$

where I represents the cumulative number of iterations which have been completed. Taking the logarithm of Eq. 175 and recognizing that

$$I \sim \text{Elapsed CPU Time}$$

then leads to the relation:

$$\frac{\log_{10}(\text{Error})}{(\text{CPU Time})} = \text{Constant} \times \log_{10}(R_j) \tag{176}$$

The results of the test are summarized in Table 8 in terms of percent errors in the predictions for the first 6 eigenvalues. The CPU times varied approximately from 0.38 to 0.66 minute per case, as indicated in the bottom row of the table. Shown below each error is a figure in parentheses equal to the quantity $\log_{10}$(Error)/(CPU Time) in arbitrary units. A cross-plot

of the data in Tables 7 and 8 should lead to a linear relationship for each type of element mass matrix on semi-logarithmic paper if Eq. 176 is valid. Such a plot is given in Fig. 19, and it indicates that the simple convergence theory outlined above is not obeyed by the present case. The probable cause of the discrepancy is that the theoretical convergence rates are asymptotic values [18], i.e. rates which are realized near the end of the entire SIM iteration process, while a significant portion of the CPU time is expended upon iterations for which the convergence rates are not asymptotic. However, the actual CPU times of less than one minute for eigenvalue analyses of 500 degree-of-freedom models still demonstrate that the SIM is an efficient computing algorithm.

7.5.3 Verification of Transient Response Analysis

The transient response software (subroutines TSTEP and ELAPSE, and Eqs. 162 and 163; see Subsection 7.4) was verified by four test analyses of the 3x3-mesh finite-element model of one quadrant of a simply supported square plate having the following properties:

$$
\begin{aligned}
&E = 10^7 \text{ psi} && \nu = 0.3 \\
&\text{Single layer,} && h = 0.01 \text{ inch} \\
&\text{Mass density,} && \rho = 0.1 \text{ lb sec}^2/\text{inch} \\
&\text{Edge dimension,} && L = 10 \text{ inches}
\end{aligned}
\tag{177}
$$

The first two tests attempted to reproduce the correct response to a steady-state sinusoidal forcing function given by the pressure distribution:

$$p(X, Y, t) = p_0 \sin\left(\frac{\pi X}{L}\right) \sin\left(\frac{\pi Y}{L}\right) \sin(\Omega t) \tag{178}$$

with p_o=0.5 psi. The above distribution is designed to excite the first natural mode of the plate, for which the transverse displacement shape function is given by

$$\bar{w}_1(X, Y) = \alpha_1 \sin\left(\frac{\pi X}{L}\right) \sin\left(\frac{\pi Y}{L}\right) \tag{179}$$

AD-A031 361 MASSACHUSETTS INST OF TECH CAMBRIDGE AEROELASTIC AND--ETC F/G 20/11
USE OF THE HYBRID-STRESS FINITE-ELEMENT MODEL FOR THE STATIC AN--ETC(U)
SEP 76 R L SPILKER, O ORRINGER, E A WITMER DAAG46-75-C-0055
UNCLASSIFIED ASRL-TR-181-2 AMMRC-CTR-76-29 NL

2 OF 3
AD
A031361

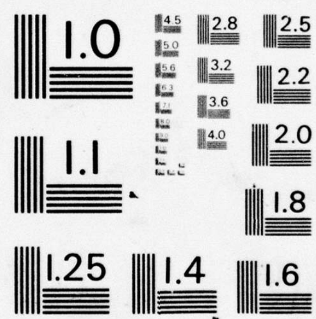

MICROCOPY RESOLUTION TEST CHART

NATIONAL BUREAU OF STANDARDS-1963-A

The corresponding values for the generalized force and the generalized mass are then:

$$f_1(t) = \int_0^L \int_0^L p(X,Y,t)\,\bar{w}_1(X,Y)\,dX\,dY = \frac{1}{4} p_o L^2 \sin(\Omega t) \tag{180}$$

$$m_1 = \int_0^L \int_0^L \rho h\,\bar{w}_1(X,Y)\,dX\,dY = \frac{4L^2}{\pi^2}\rho h \tag{181}$$

The steady-state solution of Eq. 160 gives the following result for the modal amplitude α_1, which is also numerically equal to the amplitude of the center deflection of the plate:

$$\alpha_1 = \frac{f_1 / m_1 \omega_1^2}{\left[(1-\Omega^2/\omega_1^2)^2 + (2\zeta\Omega/\omega_1)^2\right]^{1/2}} \tag{182}$$

where, for the properties given by Eqs. 177, the first natural frequency is:

$$\omega_1 \cong 6.11 \quad \text{rad/sec} \tag{183}$$

The first test was run at $\Omega = 0.5\omega_1$ and $\zeta = 0.1$, for which $\alpha_1 \cong 10.88$ in. according to Eq. 182. In this case, the computed center deflection amplitude was found to be 10.33 in., giving an error of 5.05 percent. The second test was run at $\Omega = \omega_1$ and $\zeta = 0.05$, for which $\alpha_1 \cong 82.4$ in. according to Eq. 182. In this case, the computed center deflection amplitude was found to be 80.9 in., giving an error of 1.82 percent. Plots of both runs indicated that the center deflection amplitude built up to its steady-state value, as should be expected. Figure 20 illustrates the computed center deflection time history from the second test.

The third and fourth tests were run to verify the initial-condition portions of the software. With the damping factor kept constant at $\zeta = 0.1$, the plate was subjected to the initial conditions:

$$w(X,Y,0) = 0.5\,\bar{w}_1(X,Y) \qquad \dot{w}(X,Y,0) = 0 \tag{184}$$

in the third test, and

$$w(X,Y,0) = 0 \qquad \dot{w}(X,Y,0) = 0.5\,\bar{w}_1(X,Y) \tag{185}$$

in the fourth test, with the forcing function p(X,Y,t) = 0 in both tests, in order to simulate damped free vibration. Time histories of the computed center deflections from these runs are illustrated in Figs. 21 and 22, respectively. The behavior has the proper appearance, and the calculations summarized in the figures show that the input damping factor $\zeta = 0.1$ has been reproduced by the computed results with about 3 to 4 percent error. The solutions are probably somewhat better than these results indicate, since the estimations of ζ have been based upon roughly sketched decay envelopes.

SECTION 8

APPLICATIONS PROGRAMS

8.1 Introduction

Several applications programs were prepared during the investigation in order to verify software integration and to address some specific problems of current interest. Each applications program is written in the form of a primary subroutine, which controls mesh generation and execution of the analysis, and a dummy main program which simply calls the primary subroutine. The purpose of the dummy main program is to permit the re-dimensioning of certain FORTRAN vectors and arrays, when required, without the need for recompilation of the more extensive code in the primary subroutine.

Each applications program is tailored to employ only those general software modules specifically required for the particular analysis task. Block diagrams of the individual general modules are illustrated in Fig. 23.

Those application programs which are expected to be useful in the future are described in this section. The appendices contain listings of the dummy main and primary subroutine for each program described below. Modular block diagrams in each subsection summarize the general software required by each applications program.

8.2 Subroutine AMMRC and AMMRC2

One of the objectives of the present investigation was to assess the need for special traction-free-edge versions of the hybrid plate elements for the purpose of obtaining accurate stress solutions at free edges of structural details. Hybrid elements without this special feature are usually capable of reproducing the traction-free condition in geometrically simple situations, e.g., zero bending and shear stresses at the edges of a simply supported rectangular plate subjected to transverse pressure loading [2,3]. The situation is less clear for more complex situations, e.g. the bending of a rectangular plate which contains a circular cutout. Therefore, two applications programs were prepared to provide analyses of this situation. Subroutine AMMRC was intended to model the structure with thick-plate elements, using either regular or traction-free elements along

the free edges. This program was discontinued because of the problems encountered in computing efficiency and derivation of the special traction-free stress distribution (see Section 3). Subroutine AMMRC2 (listed in Appendix A) models the structure with moderately thick quadrilateral plate elements (MLP3K), for which the traction-free formulation of assumed stresses is not possible (see Section 4).

A brief literature search failed to provide any independent analytical solutions for this problem. Therefore, the finite-element model was designed to simulate structure and loading which could easily be reproduced in the laboratory, in order to obtain experimental data for comparison with the computed stresses. The configuration, illustrated in Fig. 24, is a rectangular plate with a symmetrically placed circular hole. The plate is subjected to four-point bending by four knife edges, so that the bending moment is constant in the test section. A quadrant of the plate is isolated for analysis, as shown in the lower part of the figure. This model is restricted to analyses of isotropic plates and $0^{\circ}/90^{\circ}$ balanced crossplies because of its symmetry boundary conditions, which are not valid for other laminates possessing bending-twisting coupling. The dimensions A, A_1, A_2, B, and R constitute the geometrical input, from which the finite-element mesh is automatically generated. Scale mesh plans from typical runs are illustrated in Fig. 25.

The mesh-generation algorithm is summarized schematically in Fig. 26, which shows the model divided into four regions. The first region is sized to have a square outer boundary, so that a 45° ray subdivides the region into two equal areas. There are always 8 elements placed circumferentially around the quarter-circle boundary, a condition which determines that the other regions always have four rows of elements from the plate centerline to the lateral free edge. The edge length of a typical element along the quarter-circle boundary is $\pi/16$, and the number of elements allowed radially (NER) in the first region is computed to make the aspect ratios of the boundary elements as close to unity as possible* (see Fig. 25). The second,

---

*It is sometimes necessary to reprogram this part of the code to increase the aspect ratios of these elements, in order to reduce aspect ratios in other parts of the mesh. For example, an aspect ratio of 2 was used for the comparison with experimental results discussed at the end of this subsection.

third and fourth regions are filled with rectangular meshes, with the number of elements between the bounding lines of each region computed to make the element aspect ratios as close as possible to being between 1 and 2. A few of the key element and node numbers are given in Fig. 26. Also, the element numbering sequences are represented by arrows, and the DO loop in the code which generates each region is noted to provide a reference to the program listing.

The following user actions are required to execute the analysis. First, vector and array dimensions must be properly defined in the dummy main program. A dimension of 50,000 words is suggested for the FEABL-2 data vector names (RE,IN) as a starting point. Whatever dimension is chosen must also be defined in the DATA statement:

```
DATA LENGTH, NLY,NLY1/ xxx, y, z/
```

where

xxx = length of the data vector

y = total number of distinct layers in the laminated plate.

z = y+1

Also, the auxiliary arrays and vectors must be dimensioned as follows to agree with the DATA statement:

```
DIMENSION  XEL2(y,6), XR(y), CMC(y,3,3), HI(z), H(y)
```

Second, job control instructions external to the FORTRAN code must be provided to establish two temporary sequential-access datasets on system disk or tape storage. The first dataset must be allocated 10 single-precision words per record and must be assigned FORTRAN unit number* 20. The second data set must be allocated 352+9y words per record and must be assigned FORTRAN unit number 21. Each data set must be allocated a number

---

*The FORTRAN unit number (sometimes referred to as a hardware device code) is used to control input/output operations. The unit numbers 5 and 6 are commonly assigned to the card reader and line printer, respectively, on IBM and CDC systems.

of records sufficient to provide one record per plate element. Job control instructions must also be provided to access the pre-compiled codes, or the source decks must be provided for the general software modules shown in Fig. 27.

Third, the user must prepare input data cards in accordance with the conventions given in Table 9. The geometrical data must satisfy the restrictions:

$$A - A_2 > B > R \qquad A_2 > A_1 \tag{186}$$

The program automatically places the neutral axis at the geometrical midplane of the plate. If a multilayer laminate is to be analyzed, the laminate must be of balanced construction (distribution of layer angles and thicknesses symmetric about the mid-plane) because of the symmetry boundary conditions imposed in the analysis. The program places a line load of 1 lb/inch along the knife edges.

Two preliminary analyses of single-layer isotropic aluminum plates were conducted with subroutine AMMRC2 to assess the ability of element MLP3K to reproduce stresses and strains properly near the cutout. Stress results are summarized in Fig. 28 for the case of a 1-inch-thick x 16-inch x 21-inch plate with an 8-inch-diameter hole and with the knife edges placed 3 inches apart. Thus, the applied line bending moment per unit plate width is:

$$M = 3.0 \text{ in-lb/in.}$$

in the gage section, and the maximum bending stress to be expected at locations remote from the hole is given by

$$\sigma_x = 6M/H^2 = 18 \text{ psi} \tag{187}$$

The stress contours shown in Fig. 28 demonstrate that Eq. 187 is obeyed remote from the hole, and also that the bending stress decreases linearly to zero between the knife edges, as it should. More significantly, the bending stress approaches zero in the region near the hole and the X-axis, i.e., reproducing the traction-free condition at the hole. Along the Y-axis, a stress concentration appears in σ_x, as should be expected. An extrapolation of these results to the edge of the hole is compared with independent experimental

results obtained from a handbook [26] in Fig. 29. Although the handbook data do not cover the range of parameters used in the present analysis, it is apparent that the finite-element results are somewhat stiff, i.e. the computed stresses are lower than the probable experimental values.

An experiment was run by AMMRC personnel in order to obtain better confirmation. The test specimen was an aluminum plate with the following properties and dimensions:

$E = 10^7$ psi and $\nu = 0.3$
Length (2A) = 10 inches
Width (2B) = 4 inches
Hole Diameter (2R) = 1 inch
Thickness = 0.26 inch

The computed and measured strains along the Y axis are shown in Fig. 30.

8.3 Subroutines AMMRC3 and AMMRC4

One of the verification tasks which was defined during the investigation involves analysis of laminated conical shells subjected to axial compression, shear and bending, as shown schematically in Fig. 31. This analysis provides a test of the ability of the flat-plate MLP3K(Q) elements to model curved shells. Subroutines AMMRC3 (Appendix B) and AMMRC4 (Appendix C) were programmed for this purpose.

The lower part of Fig. 31 summarizes the conventions which were adopted for the automatic mesh-generation scheme in subroutine AMMRC3. A half-model of the shell is used, since the applied loads and shell geometry are symmetric with respect to the XZ plane. The half-model is a faceted surface consisting of a number of equi-angular gores; the lateral edges of the gores are coincident with generators in the true cone surface. Each gore is then subdivided into a number of MLP3K elements.

Several systems of axes must be dealt with in order to generate the problem data and assemble the final equation system. Coordinates of points on the true cone surface are described in the reference axis system XYZ. For example, points on the generators AB, CD (Fig. 31) are described by:

$$R = R_1 (Z/L) + R_2 (1 - Z/L) \tag{188}$$

$$X = R\cos\theta_1 \quad Y = R\sin\theta_1 \quad (\text{Edge } AB)$$
$$X = R\cos\theta_2 \quad Y = R\sin\theta_2 \quad (\text{Edge } CD) \tag{189}$$

However, the MLP3K elements must be given nodal coordinates in the local gore plane system xyz (common for all gores), and the computed element stiffnesses must then be transformed to the collection of systems $x_1y_1z_1$, $x_2y_2z_2$ before assembly of the final equations. The latter systems are oriented such that the axes z_1, z_2 are locally normal to the true cone surface. Thus, the local plate-element degrees of freedom $u, v, w, \theta_x, \theta_y$ are transformed to $u_1, v_1, w_1, \theta_{x_1}, \theta_{y_1}$ along AB and $u_2, v_2, w_2, \theta_{x_2}, \theta_{y_2}$ along CD to permit consistent assembly to adjacent gores.

The required transformations are three-dimensional rotations governed by the geometrical relationships between the various axis systems. It is easy to show that:

$$\{x\ y\ z\} = \underset{\sim}{D}\,\{X\ Y\ Z\} \qquad \{x_i\ y_i\ z_i\} = \underset{\sim}{D}_i\,\{X\ Y\ Z\} \tag{190}$$

where i=1,2 and where

$$\underset{\sim}{D} = \begin{bmatrix} (R_2-R_1)\cos\alpha\cos\beta/A & (R_2-R_1)\sin\alpha\cos\beta/A & -L/A \\ (\cos\theta_2-\cos\theta_1)/2\sin\beta & (\sin\theta_2-\sin\theta_1)/2\sin\beta & 0 \\ L(\sin\theta_2-\sin\theta_1)/2A\sin\beta & -L(\cos\theta_2-\cos\theta_1)/2A\sin\beta & (R_2-R_1)\cos\beta/A \end{bmatrix} \tag{191}$$

$$A = \sqrt{(R_2-R_1)^2\cos^2\beta + L^2} \qquad \alpha = (\theta_1+\theta_2)/2 \qquad \beta = (\theta_2-\theta_1)/2$$

$$\underset{\sim}{D}_i = \begin{bmatrix} (R_2-R_1)\cos\theta_i/B & (R_2-R_1)\sin\theta_i/B & -L/B \\ -\sin\theta_i & \cos\theta_i & 0 \\ L\cos\theta_i/B & L\sin\theta_i/B & (R_2-R_1)/B \end{bmatrix} \tag{192}$$

$$B = \sqrt{(R_2-R_1)^2 + L^2}$$

Equations 190 are combined to provide a transformation from the local axis system xyz, in which the element stiffnesses are computed, to the axes $x_iy_iz_i$ for assembly:

$$\{x\ y\ z\} = \underset{\sim}{D}\,\underset{\sim}{D}_i^{-1}\{x_i\ y_i\ z_i\} = \underset{\sim}{T}_i\{x_i\ y_i\ z_i\} \tag{193}$$

The corresponding degree-of-freedom transformation is:

$$\begin{Bmatrix} u \\ v \\ w \\ \theta_x \\ \theta_y \end{Bmatrix} = \begin{bmatrix} T_{11} & T_{12} & T_{13} & 0 & 0 \\ T_{21} & T_{22} & T_{23} & 0 & 0 \\ T_{31} & T_{32} & T_{33} & 0 & 0 \\ 0 & 0 & 0 & T_{11} & T_{12} \\ 0 & 0 & 0 & T_{21} & T_{22} \end{bmatrix} \begin{Bmatrix} u_i \\ v_i \\ w_i \\ \theta_{x_i} \\ \theta_{y_i} \end{Bmatrix} = \underset{\sim}{R}_i \begin{Bmatrix} u_i \\ v_i \\ w_i \\ \theta_{x_i} \\ \theta_{y_i} \end{Bmatrix} \tag{194}$$

where

$$\begin{bmatrix} T_{11} & T_{12} & T_{13} \\ T_{21} & T_{22} & T_{23} \\ T_{31} & T_{32} & T_{33} \end{bmatrix} = \underset{\sim}{T}_i \tag{195}$$

and where i=1 or 2 according to whether the node considered lies on the edge AB or CD, respectively (see Fig. 31). Recognizing that element nodes 1, 2 are on edge AB and nodes 3, 4 are on edge CD according to the numbering convention given in Fig. 31 and formally substituting Eq. 194 in a strain-energy expression, one obtains for the global stiffness matrix of a typical element:

$$\underset{\sim}{k}_G = \begin{bmatrix} \underset{\sim}{R}_1^T & & & \\ & \underset{\sim}{R}_1^T & & \\ & & \underset{\sim}{R}_2^T & \\ & & & \underset{\sim}{R}_2^T \end{bmatrix} \underset{\sim}{k} \begin{bmatrix} \underset{\sim}{R}_1 & & & \\ & \underset{\sim}{R}_1 & & \\ & & \underset{\sim}{R}_2 & \\ & & & \underset{\sim}{R}_2 \end{bmatrix} \tag{196}$$

where $\underset{\sim}{k}$ is the stiffness matrix computed by subroutine MLP3K, and where the transformation matrices in Eq. 196 are 20x20 super-diagonal matrices. Note that the foregoing procedure is programmable directly from the geometrical relationships between the various coordinate systems and that it selects directly the best set of coordinate systems for assembly of the final equations (z_i coordinate normal to the true cone surface). Also, the element matrices $\underset{\sim}{k}$ need be computed only once, since all gores are geometrically identical when viewed in their own local planes. However, the matrices $\underset{\sim}{k}_G$ must be recomputed for each gore, since the transformation matrices $\underset{\sim}{R}_1$, $\underset{\sim}{R}_2$ are functions of the angular position of the gore on the cone surface. Finally, note that the mesh subdivision is done most conveniently in the reference coordinate system XYZ (Eqs. 188 and 189), but that local coordinates are obtained easily from the XYZ nodal coordinates by means of the second of Eqs. 190.

The applied loads are treated in a similar manner, except that it is most convenient to express the loads initially as stress distributions in the reference system XYZ. The applied bending moment is assumed as an axial stress distribution which varies linearly with X:

$$\sigma_Z = -MX/I = -MR_1\cos\theta/I \tag{197}$$

where

$$I \cong \pi R_1^3 H \tag{198}$$

is the tip cross section moment of inertia, and where H is the total thickness of the shell. This distribution is only an approximation when the shell is a multilayer laminate, but St. Venant's Principle insures that the computed stresses in elements away from the tip of the shell will quickly conform to the proper distribution for the laminate. Equations 197 and 198 may be combined to give the following expression for the average axial stress due to bending which acts upon a typical gore bounded by edges at angles θ_1,θ_2:

$$\bar{\sigma}_Z = -M\left(\cos\theta_1 + \cos\theta_2\right)/2\pi R_1^2 H \tag{199}$$

Equation 199 is statically equivalent to a pair of nodal forces:

$$F_1 = -M(\cos\theta_1 + \cos\theta_2)\beta/2\pi R_1 \quad ; \quad \beta = (\theta_2 - \theta_1)/2 \tag{200}$$

which are applied at the two tip nodes of the gore (points A and D in Fig. 31). In a similar manner, the nodal forces:

$$F_2 = -F\beta/2\pi \qquad F_3 = V(\sin^2\theta_1 + \sin^2\theta_2)\beta/2\pi \tag{201}$$

are derived, corresponding respectively to a constant distribution of compression stress σ_z and a parabolic distribution of shear stress σ_{ZX} with maximum at X=0. The typical nodal force vector is then given by:

$$\underset{\sim}{Q} = \{Q_X \; Q_Y \; Q_Z\} = \{F_3 \quad 0 \quad F_1 + F_2\} \tag{202}$$

However, vector $\underset{\sim}{Q}$ is aligned with the reference axes XYZ, and

$$\underset{\sim}{Q}_1 = \underset{\sim}{D}_1 \underset{\sim}{Q} \qquad \underset{\sim}{Q}_2 = \underset{\sim}{D}_2 \underset{\sim}{Q} \tag{203}$$

must be computed for assembly at points A and D, respectively, where $\underset{\sim}{D}_1$, and $\underset{\sim}{D}_2$ are given by Eq. 192. *The details of these computations*, as well as the stiffness transformations, can be followed in the program code (Appendix B).

The following user actions are required to execute the analysis. First, vector and array dimensions must be properly defined in the dummy main program. The FEABL-2 data vector (variables RE, IN) should be given the dimension:

$$xxx \cong (25N_e^2 + 45)(N_g + 1) + 86\, N_e N_g + 69 N_e \tag{204}$$

where N_g, N_e are respectively the maximum number of gores and the maximum number of elements per gore to be specified in any case included in the run. Values of N_e up to and including 10 elements per gore are permitted. The dimension, as determined from Eq. 204 must also be defined in the DATA statement:

```
DATA LENGTH,NLY,NLYP1/xxx,y,z/
```

where also:

y = total number of distinct layers in the laminated plate

z = y+1

The auxiliary arrays and vectors must then be dimensioned as follows to agree with the DATA statement:

```
DIMENSION CM(y,3,3,10), CMC(y,3,3), H(y), XEL(y,6), XR(y), Z(z)
```

Second, a job control instruction external to the FORTRAN code must be provided to establish a temporary sequential-access dataset on system disk or tape storage. The dataset must be allocated 418 single-precision words per record and a number of records at least equal to N_g, the maximum number of gores to be used in any case in the run. The dataset must be assigned FORTRAN unit number* 20. Job control instructions must also be provided to access the pre-compiled codes, or the source decks must be provided for the general software modules shown in Fig. 32.

Third, the user must prepare input data cards in accordance with the conventions given in Table 10. Note that cases with different amounts of mesh refinement (NGOR $\leq N_g$, NEPG $\leq N_e$) may be stacked together, and that various combinations of loading may be applied to the models. Also, note that the correct ply angle θ for a layer of the laminate is opposite in sign to the wrapping angle ϕ which would be specified for a filament-winding operation to fabricate the cone. The sign difference results from the arrangement of coordinate systems, as shown in Fig. 33. The figure also shows how the stress solution printout $\{\sigma_x\ \sigma_y\ \sigma_{xy}\ \sigma_{xz}\ \sigma_{yz}\}$ in each local gore plane may be interpreted approximately as shell stresses $\{\sigma_s\ \sigma_\theta\ \sigma_{s\theta}\ \sigma_{s\zeta}\ \sigma_{\theta\zeta}\}$, where $s\theta\zeta$ represents the shell surface coordinate system.

Subroutine AMMRC4 (Appendix C) is a modification of subroutine AMMRC3 in which two options have been added to the code. First, a fourth mode of applied loading is permitted, in the form of a total side-force S which is distributed over that portion of the shell surface in the region X<0, i.e. $\pi/2 < \theta < 3\pi/2$ (see Fig. 31). The distribution is assumed to be a pressure loading normal to the shell surface, uniform with respect to Z and varying sinusoidally with θ:

$$p(R,\theta,Z) = p_0 \cos\theta \tag{205}$$

*See footnote on page 91 for definition of FORTRAN unit number.

where

$$p_o = \frac{2S\sqrt{(R_2-R_1)^2+L^2}}{(R_1+R_2)L^2} \tag{206}$$

The side-force is intended to simulate local aerodynamic or blast loading on the shell.

Second, a ring of stiffeners may be added to the free tip of the shell ($Z=L$, $R=R_1$) to simulate the presence of a metal grip fixture such as would be used in experimental apparatus to introduce the tip loads M,F,V into the shell structure. Subroutine STIF2, a standard assumed-displacement engineering beam theory element, is used for this purpose. Element STIF2 incorporates cubic bending behavior in two planes, linear axial stretching, and linear axial twisting in its displacement field. Figure 34 illustrates the element, together with definitions of the section properties which are required to describe it. In the present case, the element cross section is oriented as shown in Fig. 35 for the purpose of calculating inputs for the cross section inertias I_{yy}, I_{zz} and I_{yz}. The element nodal coordinates, together with addition of a sixth degree of freedom at each node coupled to a stiffener, are programmed internally in the AMMRC4 code.

Subroutine AMMRC4 is prepared for execution in the same manner as subroutine AMMRC3, with the following exceptions. First, a slightly larger dimension for the FEABL-2 data vector may be needed if the stiffener option is exercised. Second, the conventions for input data cards have been modified slightly, as shown in Table 11.

Only limited verification tests of subroutines AMMRC3 and AMMRC4 were conducted because the performance of all basic modules used by these codes had previously been verified (see Section 7). Hence, only a brief test problem of an isotropic cylinder was run simply to verify the mesh- and load-generation algorithms. After verification, a few runs of laminated conical shells were made for demonstration purposes. Subroutines AMMRC3 and AMMRC4 are intended primarily for future verifications involving the comparison of computed stresses and strains with experimental data currently being sought by AMMRC under another program.

8.4 Update Requirements

Subroutines AMMRC2, AMMRC3 and AMMRC4 have been programmed to be compatible with the existing FEABL-2 software [6]. However, these codes may be modified easily for compatibility with FEABL-5. The following actions are required to modify each subroutine. First labelled COMMON area SIZE must be expanded to:

```
COMMON /SIZE/ NET,NDT,NUT,NSP,IODYN
```

Second, the statement IODYN=0 must be placed near the beginning of the subroutine. The other added parameters NUT,NSP need not be defined for the static analyses executed by the AMMRC subroutines. Finally, all instructions which generate prescribed displacements and prescribed nodal forces must be moved from their present locations into positions between the calls to subroutines SETUP and ORK, and this must be done without changing the order in which these instructions occur relative to each other.

8.5 Subroutine VIBEPT

Subroutine VIBEPT was programmed to verify integration of the FEABL-5 dynamic analysis software. The code generates and computes eigenvalues for a quarter-model of a simply supported rectangular plate. After the eigenvalue analysis has been completed, a transient response analysis problem is executed. Subroutine VIBEPT was used to perform the test analyses described in Subsections 7.5.2 and 7.5.3. The general flow chart given in Fig. 36 illustrates the complete sequence of operations required in a FEABL-5 dynamic analysis. Subroutine VIBEPT is listed in Appendix D.

The following user actions are required to execute the analysis. First, vector and array dimensions must be properly defined in the dummy main program. Suggested dimensions for the FEABL-5 data vector range from 2,500 words for a 3x3-element mesh, to 52,800 words for a 9x9-element mesh, as detailed in Table 12. Whatever dimension is chosen must also be defined in the DATA statement:

```
DATA NLY, NSPACE,LENGTH/y,P,xxx/
```

where

y = total number of distinct layers in the laminated plate.

P = total number of degrees of freedom to be included in the subspace for eigenvalue iteration (see Subsection 7.2).

xxx = length of the data vector.

Also, the auxiliary arrays and vectors must be dimensioned as follows to agree with the DATA statement:

```
DIMENSION CMC(y,3,3), H(y), DENS(y), XR(y), XEL(y,6), Z(z)
DIMENSION ELK(q), EMS(q), DELK(q), DEMS(q)
DIMENSION EV(P²), T(P,P), AM(P,P), ICONV(P), ASQ(P)
```

where $z=y+1$ and $q=P(P+1)/2$. Second, the user must prepare input data cards in accordance with the conventions given in Table 13. Subroutine VIBEPT does not require any temporary datasets. However, job control instructions must be provided to access the pre-compiled codes, or the source decks must be provided for the general software modules shown in Fig. 37.

Results of the transient response verification which were run with subroutine VIBEPT were presented in Subsection 7.5.3. Analyses of a 3x3-element model were conducted for two cases of sinusoidally varying transverse load, one case in which the plate was given initial displacement, and one case in which the plate was given an initial velocity. These various conditions are established by subroutine INPUT, which was programmed as a temporary code to establish load time-history and initial condition data for FEABL-5 subroutines TSTEP and ELAPSE. These subroutines are listed in Appendix E. The version of subroutine INPUT given in the appendix establishes zero initial conditions and the sinusoidal load time-history with a spatial distribution corresponding to the first natural mode of the plate. Subroutine TSTEP will be modified to accept general load time-histories prior to its documentation in the FEABL-5 user's guide.

SECTION 9

DISCUSSION AND CONCLUSIONS

9.1 Summary

This report has presented the results of an extension of previous investigations into the formulation of assumed-stress hybrid finite elements for bending of multilayer laminated plates and shells. The previous investigations resulted in a quadrilateral thick-plate element capable of reproducing the severe cross-section warping which results when an extremely thick plate consisting of only a few elastically dissimilar layers is subjected to bending. During the current investigation, a triangular version of this element was formulated, and attempts were made to modify the existing quadrilateral element by incorporating an assumed stress distribution which would exactly satisfy traction-free boundary conditions along one of the element's lateral edges. The candidate traction-free stress distributions which were investigated in this study were unsuccessful in that they led to internal kinematic instabilities in the element stiffness matrix. Also, study of the practical aspects of this element family revealed that its employment for analysis of typical advanced fiber composite laminates (which generally consist of ten or more elastically distinct layers) would require more core memory than is generally available, even in today's large digital computer systems.

A second family of multilayer plate bending elements was subsequently investigated in order to provide similar analysis capabilities without the storage penalty. The new family is based on stress distributions derived from assumed in-plane strains, and thus does not reproduce severe cross section warping. However, the transverse shear effects associated with the behavior of moderately-thick plates are included, and these elements are thus applicable to both thin and moderately-thick plates. The software which resulted from this part of the study has been programmed in the form of independent modules: subroutines MLP3K(Q/T) and MLTPK which compute the stiffness matrices for, respectively, one quadrilateral and two triangular elements, subroutine MLP3S which computes element stresses and strains from given nodal displacements, and subroutine MLP3M which computes both lumped and hybrid-rational element mass matrices for dynamic analyses.

The modularity of these subroutines permits them to be adapted to any finite-element code with little or no reprogramming required. In the present investigation, the subroutines were combined with the existing ASRL FEABL-2 code, which contains the global algorithms for assembly and solution of finite-element equation systems and which is also modular. In the course of the investigation, FEABL-2 was modified for compatibility for several additional dynamic analysis modules which were adapted from concepts presented in the previous investigations. The modified software, designated FEABL-5, will be documented in detail in a separate user's guide. The dynamic analysis software consists of two major modules. The first executes an eigenvalue analysis to compute the natural frequencies and mode shapes associated with an assembled finite-element model of a structure. This module is based on the Subspace Iteration Method, which has proved to be an efficient approach to modal analysis where the primary interest is to obtain the first few modes (say up to 20 percent of the total number represented in the model). The second module executes a transient response analysis based on the Modal Superposition Method (MSM). Arbitrary damping factors (up to critical) for each mode, arbitrary initial displacement and velocity conditions, and arbitrary applied force time-histories may be input. The MSM was chosen rather than a direct time-integration finite-difference approach for the following reasons:

1. The natural frequencies and mode shapes required for the MSM are likely to be of interest anyway for various engineering purposes.

2. Because an analytic solution is used in the MSM, one can elect to calculate response information at any time instant or sequence of time instants apart, spaced evenly or unevenly. There is, in principle, no restriction on the size of the time interval between "sampling" instants, except for that cited next in item 3. Further, this type of solution does not introduce frequency distortion or false damping; such detrimental effects are often encountered in direct timewise finite-difference solution methods.

3. In the MSM, the time-step size or sampling interval can easily be varied arbitrarily from one step to the next. This is particularly

convenient for modelling load time-histories in which periods of slowly and rapidly changing loads are interspersed. Of course, one must insure that an adequate number of modes has been included.

It should be realized, however, that if the spatial distribution of the externally-applied loading varies significantly with time, one is faced with a considerable amount of calculation in order to evaluate the generalized force acting on each mode; this type of added computational burden is not nearly as severe when one employs the generalized-displacement direct time-wise solution procedure.

A further modification of the new family of plate elements was also studied. In this case, an extra partial layer was added to the laminate to simulate the presence of an integral stiffener offset from the plate neutral axis. This formulation was compared with the conventional approach to stiffened plates by means of another existing module, subroutine STIF2 which is a separate assumed-displacement model of a stiffener.

Finally, the various modules described above were put together in several combinations to form applications programs for different purposes. These applications programs included analyses of a rectangular plate with circular hole, subjected to four-point bending; a conical shell subjected to tip shear, axial load, and bending and a distributed side-force; and an eigenvalue and transient response analysis of a simply-supported flat plate.

9.2 Discussion of Results

Comparative performance tests of the thick and moderately-thick plate elements were conducted to assess the abilities of these elements to reproduce the bending-stretching behavior which is expected to occur in multilayer laminated plates and shells. The assessments were made by comparison with independent analytical solutions obtained by other investigators. The thick-plate elements were found to represent accurately the severe cross sectional warping which occurs in short-span laminates (span/thickness ratio $S/t < 10$) which have less than 4 distinct layers. Accurate results were obtained for very thick plates ($S/t = 4$). On the other hand, these elements exhibited the distinct disadvantage that the requirements for total degrees of freedom, core memory and computation time rose extremely rapidly as the number of

layers in the laminate increased. Four layers appeared to constitute a practical upper limit, given the capabilities of current large digital computing facilities (e.g., IBM S-370/168 with 125,000 decimal words of core memory or CDC-6600 with 300,000 octal words).

The moderately-thick plate elements were observed to be much more efficient in this respect. For these elements, the total number of degrees of freedom in a model is independent of the number of layers in the laminate, as is the core memory requirement, while the computation time was observed to increase insignificantly as the number of layers was increased. Demonstration analyses of conical shells with several hundred degrees of freedom and up to 25 distinct layers required only on the order of 1 CPU minute for mesh generation and a complete static stress/strain solution. The technical performance of these elements was observed to be poor for thick plates ($S/t=4$) with few layers, as expected. However, the results for thick, many-layered plates ($S/t=4$, 7 layers) and the results for moderately thick to thin plates ($S/t \geq 10$) were observed to be accurate. (In these cases, the exact stress solutions tend strongly to approach lamination theory, and the cross-sectional warping effects become much less significant.) It is important to recall that advanced composite plates and shells generally consist of ten or more distinct layers and have $S/t>10$.

The attempt to formulate a special traction-free-edge (TFE) thick-plate element was motivated by a concern about solution accuracy in the vicinity of free lateral edges of plates and shells. Past experience with assumed-stress hybrid elements has shown that the TFE modification is sometimes (but not always) required to obtain accurate stresses near free edges associated with geometrical details (e.g., a circular hole in a rectangular plate). As has been mentioned, the attempt to formulate a TFE thick-plate element proved unsuccessful. A TFE moderately-thick plate element was also considered briefly. However, an investigation of the formulation of this element quickly revealed that such a modification was mathematically impossible. The applications program mentioned previously (analysis of a plate with circular hole in four-point bending) was put together specifically to assess the potential inaccuracies which might occur when the non-specialized hybrid elements were used to model geometrical details of this type. Fortunately, the

computed solutions were observed to reproduce all free-edge conditions with good accuracy, for both the thick and moderately-thick plate elements. The computed solutions were also observed to reproduce accurately the bending stress concentration near the hole, as was shown by comparison with independently obtained experimental data.

Attention was then focussed strictly on the moderately-thick plate elements, since these appeared to be the more practical analysis tools for composite laminates. Parametric analyses of unbalanced two-layer ($\pm\theta$) simply supported rectangular plates were conducted and compared with an independent analytical solution to obtain additional performance data. The quadrilateral element, MLP3K(Q), was observed to produce results within 3 percent of the exact solutions for stresses and displacements with the ply angle varied parametrically, $15^{\circ} \leq \theta \leq 75^{\circ}$. On the other hand, the triangle element MLP3K(T) proved to be too stiff. Errors of 30 percent were observed when this element was subjected to a convergence tests for the case of a $\pm 45^{\circ}$ square plate. These results led to the creation of element MLTPK, a triangle element similar to MLP3K(T), but with fewer assumed-stress parameters to give the element additional flexibility. The convergence study with element MLTPK resulted in errors of 10 percent, i.e. within the bounds of reasonable engineering accuracy.

In another series of tests of element MLP3K(Q), the ply angle was fixed at $\theta=45^{\circ}$, while the plate shape and number of elements in each direction were varied to produce different aspect ratios (length/width). The results of these tests indicated that no apparent inaccuracies resulted from aspect ratios as large as 10. These tests were conducted with the critical element stiffness computations carried out in double-precision arithmetric (approximately 15 significant decimal figures). However, severe aspect ratio degradations were observed in MLP3K(Q) elements with aspect ratios of 7 when these calculations were carried out in single-precision (approximately 7 decimal significant figures). The latter results were obtained during some of the trail analyses of the plate with a circular hole.

In another series of tests, element MLP3K(Q) was modified to incorporate an extra partial layer simulating offset integral stiffeners. The modified MLP3K(Q) and the unmodified MLP3K(Q) combined with separate assumed-displacement

stiffener elements were used to analyze a simply supported square plate with two integral stiffeners parallel to each pair of edges. A Fourier analysis was also carried out to provide an independent analytical solution for comparison. The results of these tests showed that the combination of separate stiffeners with unmodified MLP3K(Q) elements gave accurate answers, while the modified MLP3K(Q) gave poor answers. The latter result was, tentatively, attributed to the violation of traction-free conditions on the lower surface of the plate, a situation caused by the modified stress assumptions.

Tests of the dynamic analysis modules were conducted primarily for verification and demonstration of software compatibility. The conclusions of previous investigators about the efficiency of the Subspace Iteration Method of eigenvalue analysis were reconfirmed, with all tests limited to the simplest of three previously proposed methods for generating initial estimates of the natural mode shapes. However, three additional interesting observations resulted from these tests. First, the converged eigenvalues were found to be quite sensitive to modelling detail. Errors which could not be reduced by continued iteration were observed for eigenvalues corresponding to mode shapes with spatial distributions having variations more rapid than the capability of the MLP3K(Q) element interpolation functions. Second, the rates of convergence of the eigenvalues were found to have some sensitivity to the number of modes included in the subspace. However, the asymptotic convergence rate theory developed by other investigators was found to give poor predictions for required computation times. Third, comparisons of analyses performed with lumped and hybrid-rational mass matrices showed that the hybrid-rational approach gave better results for the first mode, while the lumped-mass approach gave better results for the second and higher modes. Although the errors in both cases were well within reasonable engineering accuracy, this result is a surprising reversal of the behavior commonly found when lumped and consistent mass models are compared in analyses based upon assumed-displacement elements.

The Modal Superposition Method software module was verified in a brief series of tests in which a simply supported square plate was modelled. Accurate results were obtained in four test problems: free vibration of the

plate with a prescribed initial displacement field, free vibration with a prescribed initial velocity field, and two cases of steady-state sinusoidal forced vibration.

Finally, an informal assessment of the effectiveness of the modular concept was conducted during the applications program phase of the study. This phase of the work involved several analysis modifications which were requested by AMMRC, and which were performed with a minimum amount of reprogramming by ASRL personnel. More significantly, other similar modifications were carried out by AMMRC personnel in parallel with learning to use the various modules. These latter modifications were generally accomplished rapidly, after receipt of brief advice and suggestions from ASRL. One such modification has resulted in the coupling of the FEABL software with an AMMRC in-house program for automatic generation of finite-element grids for structures with boundaries of arbitrary shape.

9.3 Conclusions and Recommendations

Several useful conclusions can be drawn from the results discussed above, as follows:

1. The family of moderately-thick plate elements appears to suit the analysis needs for practical advanced fiber composite plates and shells better than does the family of thick-plate elements. It is recommended that element MLP3K(Q) be retained in a primary role, with element MLTPK serving a secondary role as a mesh-expander.

2. A traction-free-edge special-purpose element does not appear to be required for plates with circular cutouts; numerical accuracy of the unmodified elements has been demonstrated in tests with free-edge geometrical details.

3. The family of moderately-thick plate elements appears to have some performance limitations in terms of aspect ratio (length/width). Element aspect ratios of less than 5 are recommended for the elements in present (single-precision) form, while aspect ratios of 7 to 10 appear to be acceptable if the element stiffness subroutines are converted to double-precision arithmetic.

4. The current procedure of modelling integrally stiffened plates by combining separate plate and stiffener elements is acceptable for

engineering results. Modification of the plate elements to incorporate integral stiffeners proved to be unsatisfactory. However, all of the possible approaches to the latter type of formulation have not yet been exhausted.

5. The combination of the Subspace Iteration Method and the Modal Superposition Method appears to be the most efficient approach for the type of dynamic analysis required to evaluate the small displacement linear-elastic transient responses of advanced composite plates and shells.

6. Modularization of the finite-element software has proved to be of great benefit in terms of both ease of transfer from the developing to the using organization and flexibility in modification for future analysis tasks.

In addition to the above conclusions, several recommendations for possible future developments are presented. First, additional carefully-controlled tests of combinations of elements MLP3K(Q) and MLTPK should be carried out. Element MLTPK has been identified as a good "mesh-expander", i.e. an element which can be used to transist between coarse grids of quadrilaterals in regions with low stress gradients to fine grids in regions with high stress gradients. The numerical errors in such analyses will probably be lower than the 10 percent level observed in tests of models consisting only of MLTPK elements. However, this is merely a conjecture until confirmed by numerical experiment.

Second, it appears to be worthwhile to investigate the possibility of modifying element MLP3K(Q) to incorporate the laminate edge effects which are known to occur near free lateral edges. The edge effects spoken of here do not refer to the TFE-type modifications discussed previously. Rather, the intent is to model properly the peaks in the interlaminar peel and shear stresses which appear near the lateral edges of laminates. These stresses constitute a departure from simple lamination theory, and the presence of the peel stress requires displacement interpolations which permit the transverse displacement to vary through the laminate thickness. Hence, extra degrees of freedom are required along one edge of the modified

element, as well as revised interpolations for the assumed stress field. This possibility is judged to be worth investigation because it offers the potential of a natural incorporation of the important edge effects within the finite-element method.

Third, it is recommended that additional alternatives for integrally stiffened plate elements be investigated. Although the present method of combining assumed-displacement stiffeners with unstiffened plate elements is workable, it introduces the practical inconvenience that finite-element grids must be arranged so that all stiffeners lie along edges of plate elements. This can result in an over-refined mesh in areas of low stress gradient where many stiffeners are placed. The principal alternatives to be examined are other modified plate stress assumptions and rational transformations of separate stiffener elements based on the plate element displacement interpolation.

Fourth, the development of other special-purpose elements based on the assumed-stress hybrid method may be useful for advanced analyses of real composite structures. One possible example is an element which includes within its interior a fastener detail or cutout. An element of this type has already been developed and applied successfully to problems involving plane stress analysis and fracture mechanics analysis of single-layer isotropic media.

Finally, it must be recognized that even the Subspace Iteration Method will tax the capacity of current digital computers for eigenvalue analyses of the very detailed finite-element models which may be required to assess the dynamic behavior of real composite structures. Therefore, it is recommended that application of the Component Mode Synthesis Method [27] to these analyses be investigated. The Component Mode Synthesis Method is a rational approach to substructuring a finite-element model for dynamic analysis. The necessary global software for these computations is currently being developed under another contract, and will be implemented in the near future as an additional FEABL-5 module.

REFERENCES

1. Pian, T.H.H., "Derivation of Element Stiffness Matrices by Assumed Stress Distributions", AIAA J, Vol. 2, July 1964, pp. 1333-1336.

2. Mau, S.T. and Witmer, E.A., "Static, Vibration, and Thermal Stress Analyses of Laminated Plates and Shells by the Hybrid-Stress Finite-Element Method, With Transverse Shear Deformation Effects Included", AMMRC CTR 72-24 (also MIT ASRL TR 169-2), October 1972.

3. Mau, S.T. and Pian, T.H.H., "Linear Dynamic Analyses of Laminated Plates and Shells by the Hybrid-Stress Finite-Element Method", AMMRC CTR 73-40 (also MIT ASRL TR 172-2), October 1973.

4. Verbiese, S., "Hybrid-Stress Multilayer Quadrilateral Plate Element With a Traction-Free Edge", Aeroelastic and Structures Research Laboratory, MIT, ASRL TR 181-1, September 1975.

5. Spilker, R.L., "A Finite Element Model for Laminated Plates Including Transverse Shear Deformation", AMMRC CTR 72-12 (also MIT ASRL TR 169-1), July 1972.

6. Orringer, O. and French, S.E., "FEABL (Finite Element Analysis Basic Library) User's Guide", AFOSR-TR-72-2228 (also MIT ASRL TR 162-3), August 1972.

7. Bisplinghoff, R.L., Mar, J.W. and Pian, T.H.H., Mechanics of Deformable Solids, Addison-Wesley, 1967.

8. Pian, T.H.H. and Mau, S.T., "Some Recent Studies in Assumed Stress Hybrid Models", Advances in Computational Methods in Structural Mechanics and Design, edited by R.W. Clough, Y. Yamamoto, and J.T. Oden, University of Alabama in Huntsville Press, 1972, pp. 87-106.

9. Fraeijs de Veubeke, B., "Displacement and Equilibrium Models in the Finite Element Method", Stress Analysis, O.C. Zienkiewicz and G.S. Holister (eds.), John Wiley and Sons, 1965, pp. 145-197.

10. Tong, P., Mau, S.T. and Pian, T.H.H., "Derivation of Geometric Stiffness and Mass Matrices for Finite Element Hybrid Models", Int. J. Solids and Str., Vol. 10, 1974, pp. 919-932.

11. Pian, T.H.H., "Finite Element Methods by Variational Principles with Relaxed Continuity Requirements", Paper presented at the International Conference on Variational Methods in Engineering, Southampton, England, Sept. 25-29, 1972.

12. Pian, T.H.H., "Element Stiffness Matrices for Boundary Compatibility and for Prescribed Boundary Stresses", Proc. First Conf. on Matrix Methods in Structural Mechanics, AFFDL-TR-66-80, WPAFB, 1966, pp. 457-477.

13. Tong, P. and Pian, T.H.H., "A Variational Principle and the Convergence of a Finite-Element Method Based on Assumed Stress Distribution", Int. J. of Solids and Structures, Vol. 5, 1969, pp. 463-472.

14. Pagano, N.J., "Exact Solutions for Composite Laminates in Cylindrical Bending", J. Composite Materials, Vol. 3, 1969, pp. 398-411.

15. Whitney, J.M., "Bending-Extensional Coupling in Laminated Plates Under Transverse Loading", J. Comp. Materials, Vol. 3, Jan. 1969, pp. 20-28.

16. Wu, R.W-H. and Witmer, E.A., "Finite-Element Predictions of Transient Elastic-Plastic Large Deflections of Stiffened and/or Unstiffened Rings and Cylindrical Shells", AMMRC CTR 74-31 (also MIT ASRL TR 171-4), April 1974.

17. Kirk, C.L., "Natural Frequencies of Stiffened Rectangular Plates", J. Sound and Vibration, Vol. 13, No. 4, December 1970, pp. 375-388.

18. Bathe, K.J., "Solution Methods for Large Generalized Eigenvalue Problems in Structural Engineering", UC SESM 71-20, Structural Engineering Laboratory, Univ. of California, Berkeley, November 1971.

19. Wilkinson, J.H., <u>The Algebraic Eigenvalue Problem</u>, Clarendon Press, Oxford, 1965.

20. Meirovitch, L., <u>Analytical Methods in Vibrations</u>, Macmillan Co., New York, 1967.

21. Nickell, R.E., "On the Stability of Approximation Operators in Problems of Structural Dynamics", International Journal of Solids and Structures, Vol. 7, 1971, pp. 301-319.

22. Park, K.C., "An Improved Stiffly Stable Method for Direct Integration of Nonlinear Strucutral Dynamics Equations", Journal of Applied Mechanics, June 1975, pp. 464-470.

23. Leech, J.W., Hsu, P.T. and Mack, E.W., "Stability of a Finite-Difference Method for Solving Matrix Equations", AIAA Journal, Vol. 3, No. 11, Nov. 1965, pp. 2172-2173.

24. Private communication, Programming Assistance and Information Office, MIT Information Processing Center, 1975.

25. Timoshenko, S.P. and Young, D.H., <u>Vibration Problems in Engineering</u>, Van Nostrand Reinhold Co., New York, 1961.

26. Peterson, R.E., <u>Stress Concentration Design Factors</u>, Wiley, New York, 1953, p. 102.

27. Hurty, W.C., "Dynamic Analysis of Structural Systems by Component Mode Synthesis", Tech. Rept. No. 32-530, Jet Propulsion Laboratory, Pasadena, California, January 1964.

TABLE 1

COMPARISON OF PREDICTED VALUES FOR (NORMALIZED) CENTER DEFLECTION, $\bar{w}$, FOR CYLINDRICAL BENDING PROBLEM

			ANALYTIC SOLUTIONS		FINITE ELEMENT SOLUTIONS	
N	S		EXACT	LAMINATION THEORY	ELEMZ	MLP3K(Q)
3	4	$\bar{w}$	2.8872	.50966	2.9102	3.1617
		% Error	--	82.35	-.80	-9.51
3	10	$\bar{w}$	.93164	.50966	.93167	.94054
		% Error	--	45.29	-.003	-.96
7	4	$\bar{w}$	3.1110	.67993	3.1306	3.1673
		% Error	--	78.14	-.63	-1.81
7	10	$\bar{w}$	1.0798	.67993	1.0814	1.0789
		% Error	--	37.03	-.15	.08

N = Number of Layers

$S = \frac{\ell}{h}$ (thickness ratio)

$\%\ \text{Error} = \left(1 - \frac{\bar{w}_{Approx}}{\bar{w}_{Exact}}\right) \times 100\%$

Note:

% Error > 0 => $\bar{w}_{Approx} < \bar{w}_{Exact}$ (Approx. too stiff)

% Error < 0 => $\bar{w}_{Approx} > \bar{w}_{Exact}$ (Approx. too flexible)

TABLE 2

EFFECT OF FIBER ORIENTATION ANGLE, $\pm\theta$, ON THE ACCURACY OF FINITE-ELEMENT RESULTS, USING ELEMENT MLP3K(Q), FOR A 2 LAYER SQUARE PLATE UNDER UNIFORM LOAD (10x10 MESH)

QUANTITY	SOLN. TECHNIQUE	FIBER ORIENTATIONS, $\pm\theta$				
		$\pm 5^o$	$\pm 15^o$	$\pm 25^o$	$\pm 35^o$	$\pm 45^o$
In-plane displ. v^o at x=0, y=b/2	Exact	.01871	.03281	.02502	.01610	.01481
	Finite Elem.	.0186	.0326	.0249	.0160	.0148
	% Error	0.59	0.64	0.48	0.62	0.0
Normal displacement w, at the center of the plate	Exact	.5920	.8927	.9838	.9451	.9152
	Finite Elem.	.609	.909	.999	.960	.930
	% Error	-2.87	-1.83	-1.53	-1.58	-1.64
Moment, M_x, at the center of the plate	Exact	$1.318x10^3$	$1.142x10^3$	$8.436x10^2$	$5.646x10^2$	$3.681x10^2$
	Finite Elem.	$1.331x10^3$	$1.150x10^3$	$8.470x10^2$	$5.695x10^2$	$3.722x10^2$
	% Error	-.99	-.70	-.40	-.87	-1.11
In-plane Displ. u^o at x=a/2, y=0	Exact	$.2649x10^{-2}$	$.7710x10^{-2}$	.01135	.01465	.01481
	Finite Elem.	$.258x10^{-2}$	$.753x10^{-2}$	.0112	.0146	.0148
	% Error	2.60	2.33	1.32	.34	0.0
Moment, M_y, at the center of the plate	Exact	34.25	$1.234x10^2$	$2.260x10^2$	$3.041x10^2$	$3.681x10^2$
	Finite Elem.	35.03	$1.255x10^2$	$2.283x10^2$	$3.075x10^2$	$3.722x10^2$
	% Error	-2.28	-1.70	-1.02	-1.12	-1.11

TABLE 3

A COMPARISON OF ANALYSES FOR THE STIFFENED SIMPLY SUPPORTED PLATE

			CENTER LATERAL DEFLECTION		
t_s	ω_s	MESH	RITZ METHOD	INTEGRALLY STIFFENED	NONINTEGRALLY STIFFENED
0.0	0.0	2x2	0.296	0.300	0.300
		4x4		0.297	0.297
		6x6		0.297	0.297
		8x8		0.297	0.297
0.01	0.03	2x2	0.296	0.299	0.300
		4x4		0.297	0.297
		6x6		0.297	0.297
		8x8		0.297	0.297
0.03	0.03	2x2	0.295	0.298	0.299
		4x4		0.295	0.297
		6x6		0.295	0.297
		8x8		0.294	0.297
0.1	0.03	2x2	0.293	0.291	0.297
		4x4		0.284	0.295
		6x6		0.270	0.295
		8x8		0.251	0.295

TABLE 4

EFFECT OF ARITHMETIC PRECISION ON THE

JACOBI ITERATION METHOD

ANALYTICAL SOLUTION (1)		JIM SOLUTION IN SINGLE PRECISION (2)		JIM SOLUTION IN DOUBLE PRECISION (2)	
		VALUE	% ERROR	VALUE	% ERROR
CANTILEVER:					
$\omega_1 = (1.875)^2 \sqrt{EI/mL^4}$	249.4	249.4	0	249.4	0
$\omega_2 = (4.694)^2 \sqrt{EI/mL^4}$	1,563	1,564	.064	1,564	.064
$\omega_3 = (7.855)^2 \sqrt{EI/mL^4}$	4,376	4,392	.366	4,392	.366
$\omega_4 = (11.00)^2 \sqrt{EI/mL^4}$	8,576	8,676	1.17	8,676	1.17
$\omega_5 = (14.14)^2 \sqrt{EI/mL^4}$	14,180	14,400	3.12	14,400	3.12
$\omega_6 = (17.28)^2 \sqrt{EI/mL^4}$	21,180	23,920	12.96	23,920	12.96
$\omega_7 = (20.42)^2 \sqrt{EI/mL^4}$	29,580	34,990	18.32	34,990	18.32
$\omega_8 = (23.56)^2 \sqrt{EI/mL^4}$	39,380	50,740	28.90	50,740	28.90
$\omega_9 = (26.70)^2 \sqrt{EI/mL^4}$	50,580	72,080	42.50	72,080	42.50
$\omega_{10} = (29.85)^2 \sqrt{EI/mL^4}$	63,180	106,000	67.70	106,000	67.70
UNRESTRAINED:					
$\omega_1 = 0$	0	32.46	--	0.00184	--
$\omega_2 = 0$	0	-56.02	--	0.0348	--
$\omega_3 = (1.506\pi)^2 \sqrt{EI/mL^4}$	1,587	1,587	.063	1,588	.063
$\omega_4 = (2.500\pi)^2 \sqrt{EI/mL^4}$	4,375	4,388	.298	4,388	.298

Notes: (1) Analytical solutions from Ref. 20. Numerical values are for the case $\sqrt{EI/m} = 1.134901 \times 10^5$ in^2/sec and L = 40 inches. Solutions are in units of rad/sec.

(2) JIM solutions obtained from 12-DOF finite-element model (5 elements) and with tolerance $\varepsilon = 10^{-4}$. Arithmetic precisions for IBM S-370/168 are: Single = 32 BITS $\cong$ 7.2 decimal significant figures, Double = 64 BITS $\cong$ 15 decimal significant figures.

TABLE 5

EFFECT OF MODELLING DETAIL ON THE JACOBI ITERATION METHOD

ANALYTICAL SOLUTION (1)		JIM SOLUTION (2) 12-DOF MODEL		JIM SOLUTION (2) 50-DOF MODEL	
		VALUE	% ERROR	VALUE	% ERROR
$\omega_1 = (1.875)^2 \sqrt{EI/mL^4}$	249.4	249.4	0	249.4	0
$\omega_2 = (4.694)^2 \sqrt{EI/mL^4}$	1,563	1,564	.064	1,563	0
$\omega_3 = (7.855)^2 \sqrt{EI/mL^4}$	4,376	4,392	.366	4,376	0
$\omega_4 = (11.00)^2 \sqrt{EI/mL^4}$	8,576	8,676	1.17	8,576	0
$\omega_5 = (14.14)^2 \sqrt{EI/mL^4}$	14,180	14,400	3.12	14,180	0
$\omega_6 = (17.28)^2 \sqrt{EI/mL^4}$	21,180	23,920	12.96	21,180	0

Notes: (1) Analytical solutions from Ref. 20. Numerical values are for the case $\sqrt{EI/m} = 1.134901 \times 10^5$ in^2/sec and L =40 inches. Solutions are in units of rad/sec.

(2) JIM solutions in double-precision arithmetic (64 BITS $\cong$ 15 decimal significant figures) on IBM S-370/168.

TABLE 6

EFFECT OF PLATE MODEL DETAIL ON CONVERGENCE OF EIGENVALUES

		HYBRID-RATIONAL MASS MATRIX				LUMPED (DIAGONAL MASS MATRIX			
	MESH*	3x3	5x5	7x7	9x9	3x3	5x5	7x7	9x9
	TOTAL* DOF	80	180	320	500	80	180	320	500
% ERROR IN PLATE NATURAL FREQ. NUMBER	1(f_{11})	-2.28	-0.75	-0.06	0.12	2.29	0.89	0.77	0.62
	2(f_{13})	-22.28	-7.69	-3.85	-2.30	2.42	0.80	0.42	0.26
	3(f_{31})	-22.28	-7.69	-3.85	-2.31	2.42	0.80	0.42	0.26
	4(f_{33})	-16.23	-7.21	-3.74	-2.27	44.12	9.16	3.80	2.29
	5(f_{15})	-2.35	-24.35	-11.95	-7.08	46.37	35.97	13.10	-0.25
	6(f_{51})	-49.03	-24.35	-11.96	-7.08	25.22	-1.04	-0.45	-0.27

SIMPLY SUPPORTED PLATE (10"x10")

$$\left.\begin{aligned} NOEIG &= 6 \\ \varepsilon &= 0.01 \\ NSPACE &= 9 \end{aligned}\right\} \text{CONVERGENCE}$$

$$\%\ ERROR = \left(1 = \frac{APPROX}{EXACT}\right) \times 100\%$$

*MODELED QUARTER PLATE INCLUDING IN-PLANE DEGREES OF FREEDOM

TABLE 7

THEORETICAL EFFECT OF SUBSPACE SIZE ON

EIGENVALUE CONVERGENCE RATES

j	$\lambda_j (rad^2/sec^2)$*	SIZE OF SUBSPACE, P =				
		6	8	9	10	12
1	0.90381	.00346	.00160	.00160	.00160	.00119
2	22.595	.0865	.0400	.0400	.0400	.0297
3	22.595	.0865	.0400	.0400	.0400	.0297
4	73.209	.280	.130	.130	.130	.0963
5	152.74	.585	.270	.270	.270	.201
6	152.74	.585	.270	.270	.270	.201
7	261.21					
8	261.21	CONVERGENCE RATES:				
9	564.87	$R_j \sim \lambda_j / \lambda_{p+1}$				
10	564.87					
11	564.87					
12	760.10					
13	760.10					

*Analytical solutions from Ref. 25.

TABLE 8

EFFECT OF SUBSPACE SIZE ON CONVERGENCE OF EIGENVECTORS

		HYBRID-RATIONAL MASS MATRIX NO. OF EIGENVECTORS IN SUBSPACE, P=					LUMPED (DIAGONAL) MASS MATRIX NO. OF EIGENVECTORS IN SUBSPACE, P=				
	p=	6	8	9	10	12	6	8	9	10	12
% ERROR[1] IN PLATE NATURAL FREQUENCY ($\bar{\varepsilon}^{(4)}$)	1(f_{11})	0.12 (.208)	-0.63 (1.60)	0.12 (.120)	0.12 (.120)	-0.63 (1.60)	0.62 (2.08)	0.77 (1.77)	0.62 (1.20)	0.62 (1.20)	0.77 (1.77)
	2(f_{13})	2.34 (3.60)	-3.85 (3.17)	-2.30 (2.06)	-2.34 (2.08)	-3.85 (3.17)	0.26 (1.09)	0.42 (1.25)	0.26 (0.63)	0.26 (0.63)	0.42 (1.25)
	3(f_{31})	2.34 (3.60)	-3.85 (3.17)	-2.31 (2.07)	-2.34 (2.08)	-3.85 (3.17)	0.26 (1.09)	0.42 (1.25)	0.26 (.063)	0.26 (0.63)	0.42 (1.25)
	4(f_{33})	-2.28 (3.57)	-3.74 (3.15)	-2.27 (2.06)	-2.27 (2.06)	-3.74 (3.15)	2.28 (3.67)	3.80 (3.16)	2.29 (2.06)	2.30 (2.06)	3.80 (3.16)
	5(f_{15})	-7.08 (4.86)	-12.00 (4.16)	-7.08 (2.80)	-7.08 (2.80)	-11.90 (4.15)	-0.35 (1.43)	-13.10 (4.24)	-0.25 (0.60)	-0.24 (0.58)	-13.10 (4.24)
	6(f_{51})	-7.34 (4.91)	-12.00 (4.16)	-7.08 (2.80)	-7.08 (2.80)	-12.00 (4.16)	-11.20 (5.39)	-0.53 (1.45)	-0.27 (0.66)	-0.25 (0.60)	-0.41 (1.23)
	CPU[5]	0.38	0.50	0.66	0.66	0.50	0.38	0.50	0.66	0.66	0.50

Notes:

(1) % Error = $100\ (1 - \omega_{computed}/\omega_{exact})$

(2) Convergence sought for p=6 eigenvalues with $\varepsilon = 10^{-2}$

(3) Finite-element model: 9x9 mesh for one quadrant of plate

(4) $\bar{\varepsilon} = [\log 1000\ |1 - \omega_{computed}/\omega_{exact}|]$/CPU Time

(5) Approximate CPU times in minutes

AEROELASTIC AND STRUCTURES RESEARCH LABORATORY

JOB TITLE SUBROUTINE AMMRC2 — ENGINEER ORRINGER

JOB NO. 82619 — PROGRAMMER ORRINGER /FRENCH — DATE 12 MAY 1976 — SHEET 1 OF 1

CARD #	Columns 1–72	Format
①	NCASES ← KT1 →	2I5
	NCASES = TOTAL NO. OF CASES TO BE RUN	
	KT1 = FORTRAN UNIT NO. FOR LINE PRINTER TO SUPRESS NORMAL FEABL-2 OUTPUT, LEAVING ONLY STRESS SOLUTION	
②	← R → ← A → ← B → ← A_1 → ← A_2 →	5E10.3
	SEE FIGURE FOR DEFINITIONS OF GEOMETRICAL PARAMETERS AND EQUATIONS FOR RESTRICTIONS	
③	← θ → ← h → ← E_1 → ← E_2 → ← ν_{12} → ← ν_{23} → ← G_{12} → ← G_{23} →	8E10.3
	θ = PLY ANGLE IN DEGREES (SEE FIGURE 3)	
	h = LAYER THICKNESS	
	SEE SECTION II FOR DEFINITIONS OF ELASTIC CONSTANTS	
	GENERAL NOTES: CARD # ③ - ONE CARD PER LAYER; BOTTOM LAYER FIRST, TOP LAYER LAST	
	REPEAT CARD # ② AND CARD SET # ③ FOR SUCCEEDING CASES	
	E10.3 FORMATS MAY BE OVERRIDDEN BY F10 FORMATS	

TABLE 9

INPUT CONVENTIONS FOR SUBROUTINE AMMRC2

AEROELASTIC AND STRUCTURES RESEARCH LABORATORY

JOB TITLE: SUBROUTINE AMMRC3 — ENGINEER: ORRINGER

JOB NO. 82619 — PROGRAMMER: ORRINGER/FRENCH — DATE: 12 MAY 1976 — SHEET 1 OF 1

CARD #	Fields	Format
①	NCASES	I5
②	NGØR | NEPG	2I5
③	R_1 (cols 1–10) | R_2 (cols 11–20) | L (cols 21–30)	3E10.3
④	M | F | V	3E10.3
⑤	h | θ | E_1 | E_2 | ν_{12} | ν_{23} | G_{12} | G_{23}	8E10.3

① NCASES = TOTAL NO. OF CASES TO BE RUN

② NGØR = TOTAL NO. OF GORES IN HALF-MODEL
NEPG = TOTAL NO. OF ELEMENTS PER GORE ($\leq$ 10 ELEMENTS)

③ R_1 = TIP RADIUS R_2 = ROOT RADIUS L = AXIAL LENGTH (SEE FIGURE)

④ M = BENDING MOMENT F = AXIAL FORCE V = SHEAR FORCE (SEE FIGURE)

⑤ h = LAYER THICKNESS
θ = PLY ANGLE = $-\phi$ (SEE FIGURE) IN DEGREES
SEE SECTION II FOR DEFINITIONS OF ELASTIC CONSTANTS

GENERAL NOTES: CARD #⑤ - ONE CARD PER LAYER; INSIDE LAYER FIRST, OUTSIDE LAYER LAST
REPEAT CARDS #②, ③, ④ AND CARD SET #⑤ FOR SUCCEEDING CASES
E10.3 FORMATS MAY BE OVERRIDDEN BY F10 FORMATS

TABLE 10

INPUT CONVENTIONS FOR SUBROUTINE AMMRC3

AEROELASTIC AND STRUCTURES RESEARCH LABORATORY

JOB TITLE: SUBROUTINE AMMRC4 — ENGINEER: ORRINGER

JOB NO. 82619 — PROGRAMMER: FRENCH — DATE: 12 MAY 1976 — SHEET 1 OF 1

CARD #	Fields / Description	Format
①	NCASES	I5
	NCASES = TOTAL NO. OF CASES TO BE RUN	
②	NGØR | NEPG | ← NS →	3I5
	NGØR = TOTAL NO. OF GORES IN HALF-MODEL	
	NEPG = TOTAL NO. OF ELEMENTS PER GORE ($\leq$ 10 ELEMENTS)	
	NS = 0 FOR SHELL WITHOUT STIFFENERS	
	NS = 1 FOR SHELL WITH STIFFENERS	
③	← R_1 → | ← R_2 → | ← L →	3E10.3
	R_1 = TIP RADIUS R_2 = ROOT RADIUS L = AXIAL LENGTH (SEE FIGURE)	
④	← M → | ← F → | ← V → | ← S →	4E10.3
	M = BENDING MOMENT F = AXIAL FORCE V = SHEAR FORCE S = SIDE FORCE (SEE FIGURE)	
⑤	← h → | ← θ → | ← E_1 → | ← E_2 → | ← ν_{12} → | ← ν_{23} → | ← G_{12} → | ← G_{23} →	8E10.3
	h = LAYER THICKNESS	
	θ = PLY ANGLE = $-\phi$ (SEE FIGURE) IN DEGREES	
	SEE SECTION II FOR DEFINITIONS OF ELASTIC CONSTANTS	
⑥	← E → | ← G → | ← A → | ← J → | ← I_{yy} → | ← I_{zz} → | ← I_{yz} →	7E10.3
	STIFFENER PROPERTIES (USE ONLY IF NS = 1 ON CARD #②):	
	E = YOUNG'S MODULUS G = SHEAR MODULUS	
	A = CROSS SECTION AREA J = CROSS SECTION TORSION CONSTANT	
	I_{yy}, I_{zz}, I_{yz} = CROSS SECTION INERTIAS (SEE FIGURES AND)	

GENERAL NOTES: CARD #⑤ - ONE CARD PER LAYER; INSIDE LAYER FIRST, OUTSIDE LAYER LAST

REPEAT CARDS #②, ③, ④, CARD SET #⑤ (AND CARD #⑥ IF NS = 1) FOR SUCCEEDING CASES

E10.3 FORMATS MAY BE OVERRIDDEN BY F10 FORMATS

TABLE 11

INPUT CONVENTIONS FOR SUBROUTINE AMMRC4

TABLE 12

VARIATION OF REQUIRED CORE STORAGE WITH

PROBLEM SIZE FOR SUBROUTINE VIBEPT

MESH SIZE	TOTAL DOF	NUMBER OF DOF INCLUDED IN SUBSPACE (P)	LENGTH OF FEABL-% DATA VECTOR (xxx)	REGION SIZE SIZE*
3x3	80	9	2,500	120K
5x5	180	9	9,900	148K
7x7	320	9	24,700	206K
9x9	500	9	49,300	302K
9x9	500	10	50,500	310K
9x9	500	12	52,800	320K

*Region size: total core storage required for problem data and object code on IBM S-370/168, using IBM FORTRAN-Gl and FORTRAN-H(0) compilers Region sizes are given in KBYTES (1 KBYTE = $1,024_{10}$ single-precision words).

AEROELASTIC AND STRUCTURES RESEARCH LABORATORY

JOB TITLE: SUBROUTINE VIBEPT ENGINEER: SPILKER / ORRINGER

JOB NO. 82619 PROGRAMMER: FRENCH DATE: 12 MAY 1976 SHEET 1 OF 2

CARD #	Columns 1–72	Format
①	NCASES	I5
	NCASES = TOTAL NO. OF CASES TO BE RUN	
②	IØDYN | NW | NL | NLAY | ← WIDTH → | ← EL →	4I5,2E15.5
	IØDYN = 2 FOR HYBRID-RATIONAL MASS MATRIX	
	IØDYN = 3 FOR LUMPED MASS MATRIX	
	NW = NO. OF ELEMENTS ALONG WIDTH OF QUARTER-PLATE MODEL (X DIRECTION)	
	NL = NO. OF ELEMENTS ALONG LENGTH OF QUARTER-PLATE MODEL (Y DIRECTION)	
	NLAY = TOTAL NO. OF LAYERS IN THE LAMINATE ($\leq$ NLY, MAXIMUM NO. ALLOWED IN RUN BY PROGRAM DIMENSIONS)	
	WIDTH = WIDTH OF QUARTER-PLATE MODEL (= HALF-WIDTH OF PLATE)	
	EL = LENGTH OF QUARTER-PLATE MODEL (= HALF-LENGTH OF PLATE)	
	(SEE FIGURE FOR GEOMETRY)	
③	MAXIT | NØEIG | ← EPS →	2I5,E15.5
	MAXIT = MAXIMUM NO. OF ITERATIONS ALLOWED DURING SUBSPACE ITERATION	
	NØEIG = MINIMUM NO. OF EIGENVALUES WHICH ARE TO BE CONVERGED; ALSO = NO. OF MODES USED IN TRANSIENT ANALYSIS	
	EPS = CONVERGENCE TOLERANCE CRITERION $\lvert\lambda_i - \lambda_{i-1}\rvert / \lambda_{i-1} < \varepsilon \equiv$ CONVERGENCE	
④	← H → | ← DENS → | ← XR →	3E15.5
	H = LAYER THICKNESS	
	DENS = LAYER MASS DENSITY	
	XR = PLY ANGLE IN DEGREES (POSITIVE FROM X AXIS TO FIBER DIRECTION)	
⑤	← E_1 → | ← E_2 → | ← ν_{12} → | ← ν_{23} → | ← G_{12} → | ← G_{23} →	6E10.5
	SEE SECTION II FOR DEFINITIONS OF ELASTIC CONSTANTS	
⑥	NØDESC	I5
	NØDESC = NO. OF DEGREES OF FREEDOM TO BE CONSTRAINED	
⑦	$NØDE_1$ | $NDØF_1$ | $NØDE_2$ | $NDØF_2$ | $NØDE_3$ | $NDØF_3$ | $NØDE_4$ | $NDØF_4$ | $NØDE_5$ | $NDØF_5$ | $NØDE_6$ | $NDØF_6$ | $NØDE_7$ | $NDØF_7$ | $NØDE_8$ | $NDØF_8$	
	$NØDE_9$ | $NDØF_9$ | ...	16I5
	$NØDE_i$ = GLOBAL NODE NO. AT WHICH CONSTRAINT IS APPLIED	
	$NDØF_i$ = LOCAL DEGREE-OF-FREEDOM NO. TO BE CONSTRAINED, AS FOLLOWS: $\{1\,2\,3\,4\,5\} = \{u\ v\ w\ \theta_x\ \theta_y\}$	
	EIGHT PAIRS OF DATA PER CARD; REPEAT CARD #⑦ AS MANY TIMES AS REQUIRED TO AGREE WITH NØDESC ON CARD #⑥	

TABLE 13

INPUT CONVENTIONS FOR SUBROUTINE VIBEPT

AEROELASTIC AND STRUCTURES RESEARCH LABORATORY

JOB TITLE SUBROUTINE VIBEPT ENGINEER SPILKER /ORRINGER

JOB NO. 82619 PROGRAMMER FRENCH DATE 12 MAY 1976 SHEET 2 OF 2

CARD #		FORMAT
8	← PZERØ →	E15.5
	PZERØ = TRANSVERSE LOADING INTENSITY p_0 LOAD $p(X,Y,t) = p_0 \sin\left(\frac{\pi X}{2^{*}WIDTH}\right) \sin\left(\frac{\pi Y}{2^{*}LENGTH}\right) \sin(\omega t)$	
9	NØMK	I5
	NØMK = No. OF TRANSIENT RESPONSE SUB-CASES TO BE RUN AFTER ONE EIGENVALUE ANALYSIS	
10	← FACTØR → KØMG	E15.5, I5
	FACTØR = FRACTION OF NATURAL FREQUENCY; KØMG = NATURAL FREQUENCY NUMBER } LOAD TIME-HISTORY WILL BE SINUSOIDAL AT FREQUENCY $\omega = FACTØR^{*}\,\omega_{KØMG}$	

GENERAL NOTES: CARD #10 - ONE CARD PER SUB-CASE TO AGREE WITH NØMK ON CARD #9

CARDS #4 AND 5 - ONE PAIR PER LAYER; BOTTOM LAYER FIRST, TOP LAYER LAST; CARDS MUST BE IN SEQUENCE 4 5 4 5 ...; TOTAL NO. OF PAIRS TO AGREE WITH NLAY ON CARD #2

REPEAT CARDS #2, 3, CARD SET #4-5, CARDS #6, 7, 8, 9 AND CARD SET #10 FOR SUCCEEDING CASES

E10.3 FORMATS MAY BE OVERRIDDEN BY F10 FORMATS

E15.5 FORMATS MAY BE OVERRIDDEN BY F15 FORMATS

TABLE 13 (Concluded)

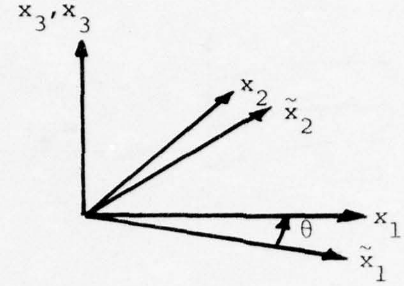

FIG. 1 POSITIVE CONVENTION FOR SINGLE-ROTATION AXIS TRANSFORMATION

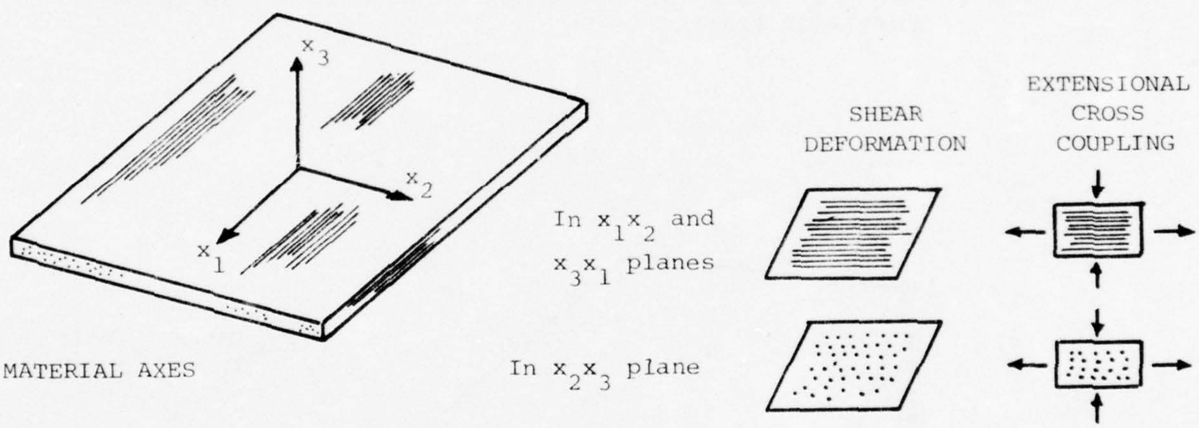

FIG. 2 PHYSICAL SYMMETRIES IN A TYPICAL FIBER-COMPOSITE PLY

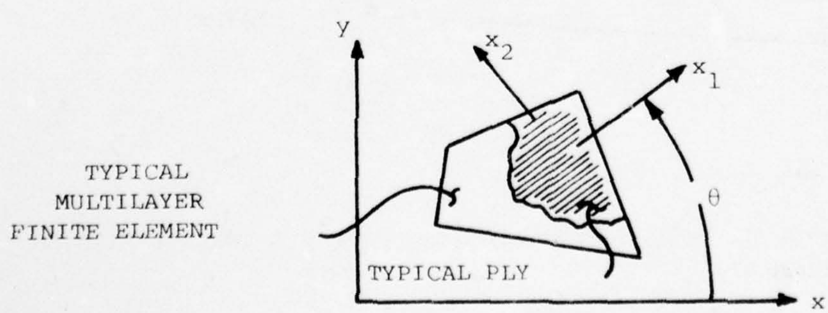

FIG. 3 POSITIVE CONVENTION FOR TRANSFORMATION OF TYPICAL PLY PROPERTIES

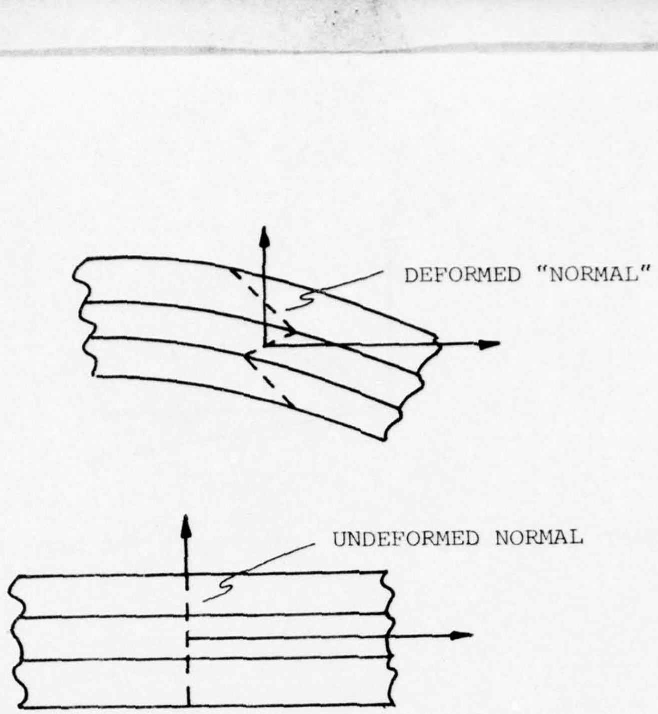

FIG. 4 POSSIBLE SEVERE CROSS-SECTIONAL WARPING EFFECT IN THICK MULTILAYER PLATES

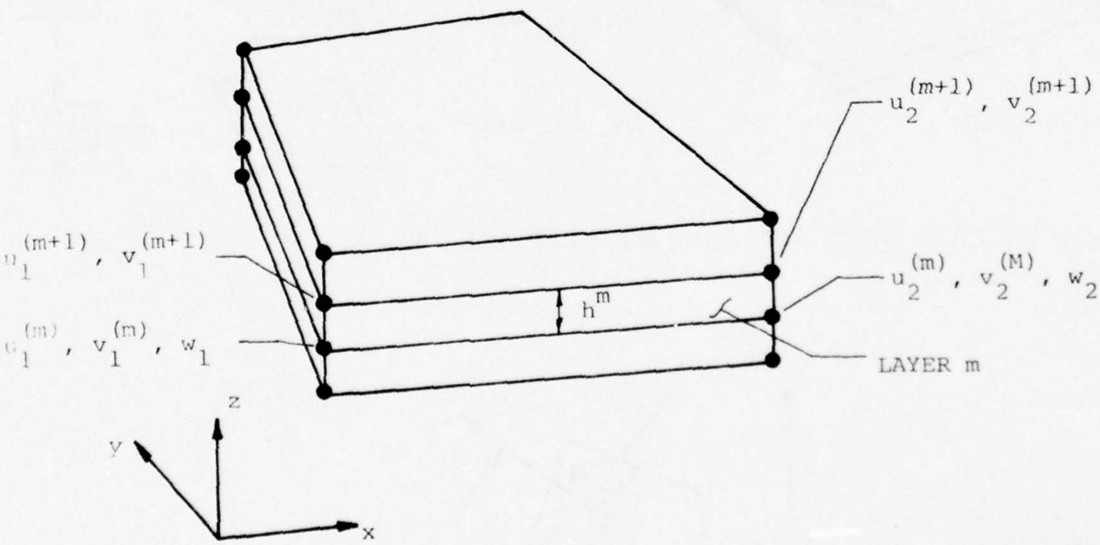

FIG. 5 DEFINITION OF NODAL DEGREES OF FREEDOM FOR A THICK LAMINATED PLATE ELEMENT

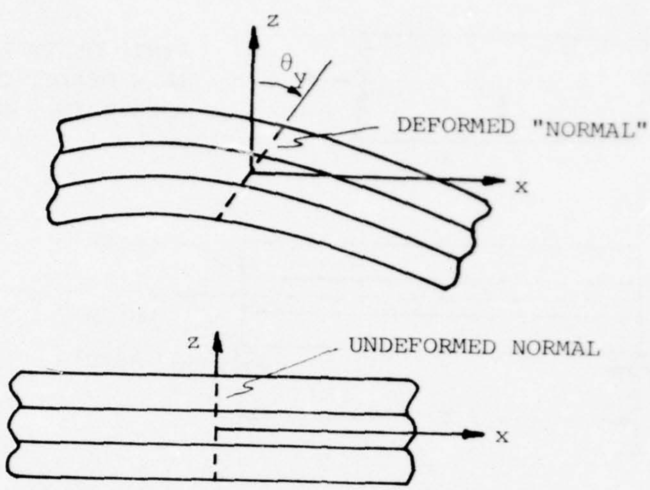

FIG. 6 DEFORMATION OF NORMAL TO THE PLATE MIDSURFACE FOR MODERATELY-THICK LAMINATE

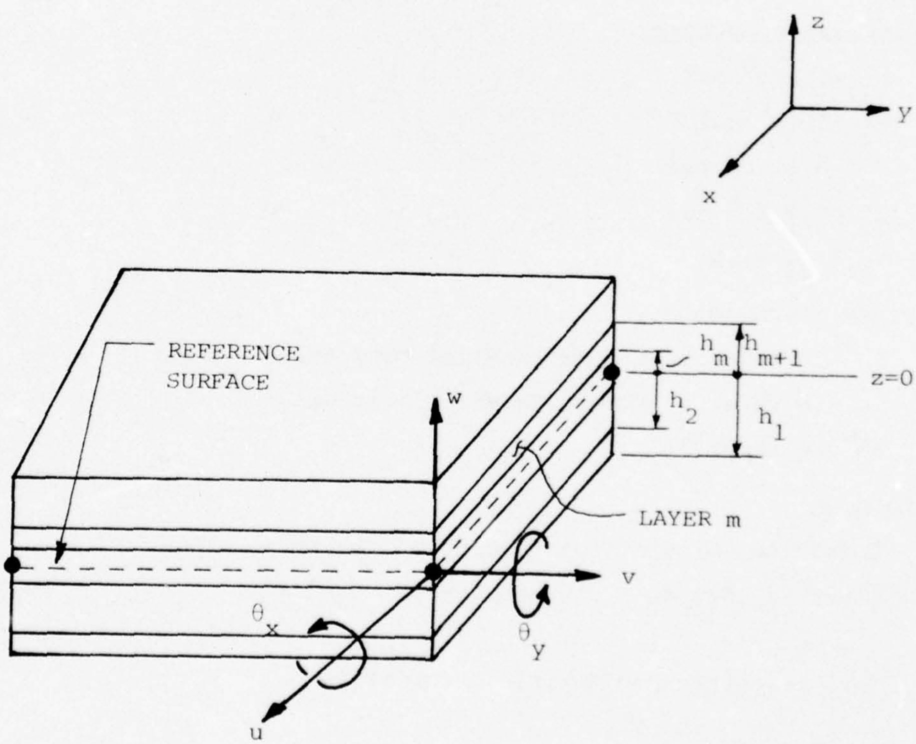

FIG. 7 DEFINITION OF NODAL DEGREES OF FREEDOM FOR A MODERATELY-THICK LAMINATED PLATE ELEMENT

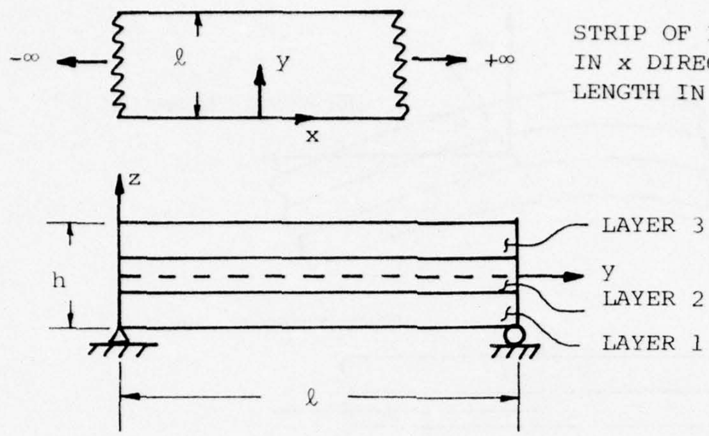

STRIP OF INFINITE LENGTH IN x DIRECTION, FINITE LENGTH IN y DIRECTION

GEOMETRIC PROPERTIES:

$\ell=24$, $h=6$ for $S=\ell/h4$

$\ell=60$, $h=6$ for $S=10$

MATERIAL PROPERTIES:

$E_{11}=25\times10^{6}$ psi

$E_{22}=1\times10^{6}$ psi

$G_{12}=0.5\times10^{6}$ psi

$G_{23}=0.2\times10^{6}$ psi

$\nu_{21}=\nu_{23}=0.25$

FIBER ORIENTATIONS:

90° In Layer 1 (Fibers Parallel to y Axis)

0° In Layer 2 (Fibers Parallel to x Axis)

90° In Layer 3

LOADING:

Transverse Sinuisoidal Loading of the Form

$q(x,y)=q_{o}\ \sin\ (\frac{\pi y}{\ell})$ where $q_{o}\approx100$

(a) Geometric and Material Properties

FIG. 8 NOMENCLATURE AND PROPERTY DEFINITIONS FOR 3-LAYER CROSS PLY CYLINDRICAL BENDING PROBLEM

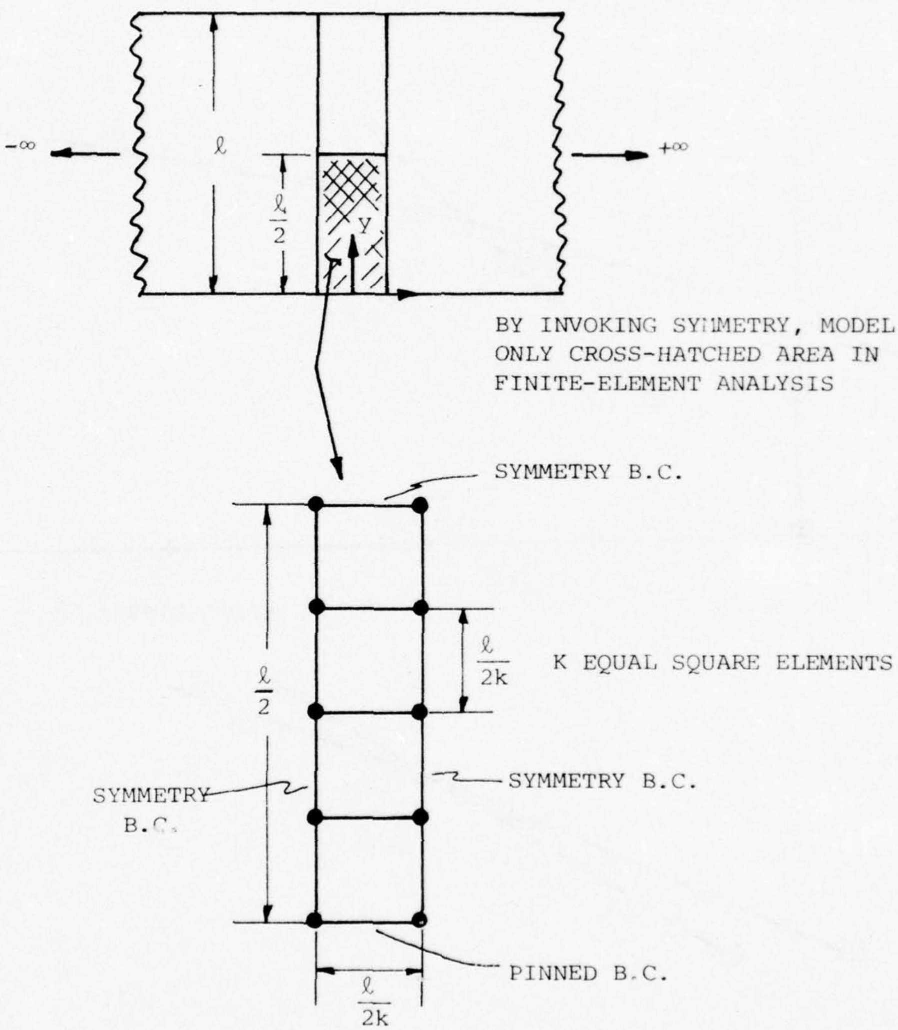

(b) Finite-Element Mesh and Required Boundary Conditions

FIG. 8 CONCLUDED

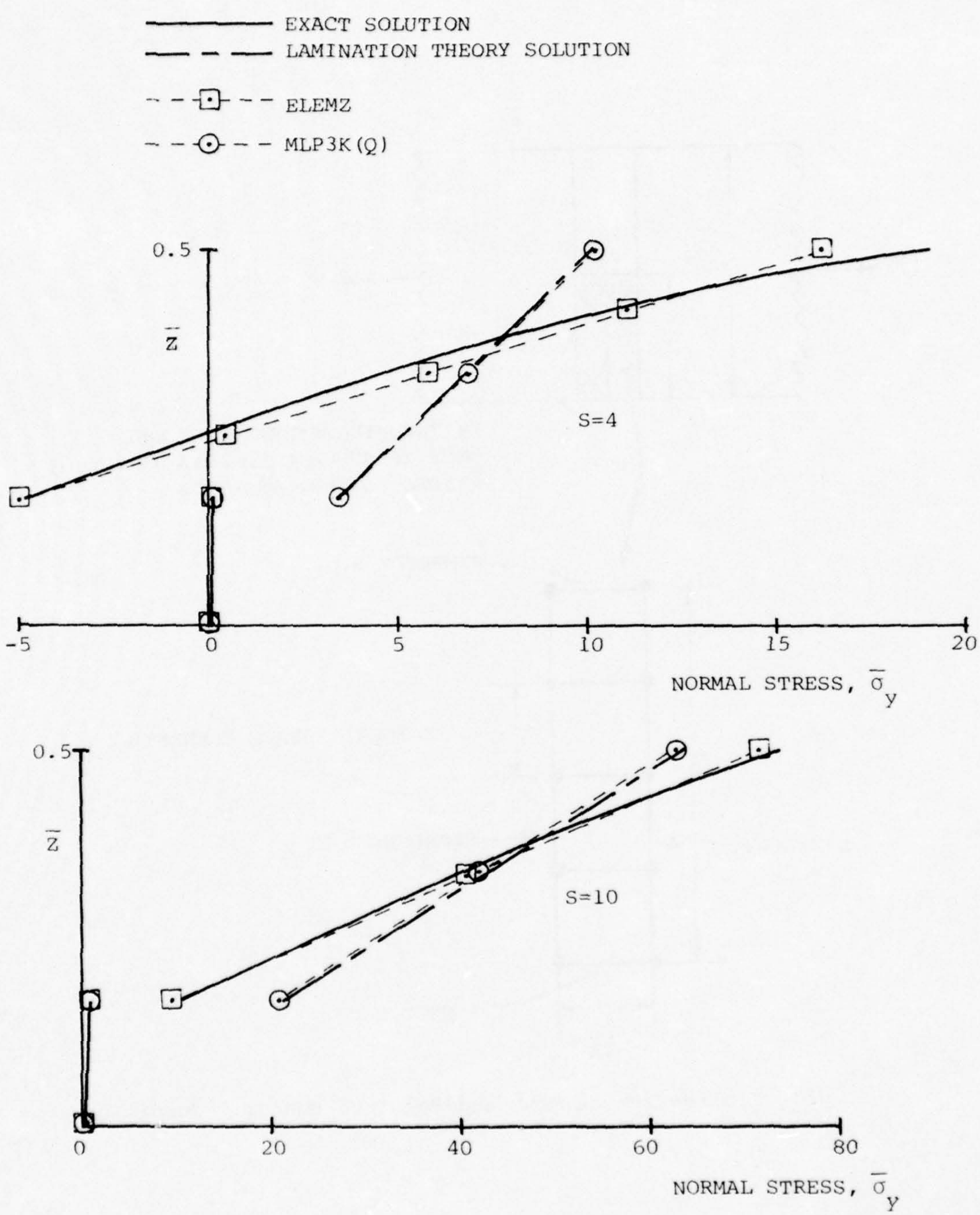

(a) Normal Stress, $\bar{\sigma}_y$, at the Center of the Strip

FIG. 9 ANALYTIC SOLUTIONS AND FINITE-ELEMENT RESULTS FOR THE PROBLEM OF THE CYLINDRICAL BENDING OF A THREE-LAYER (CROSS-PLY) INFINITE STRIP

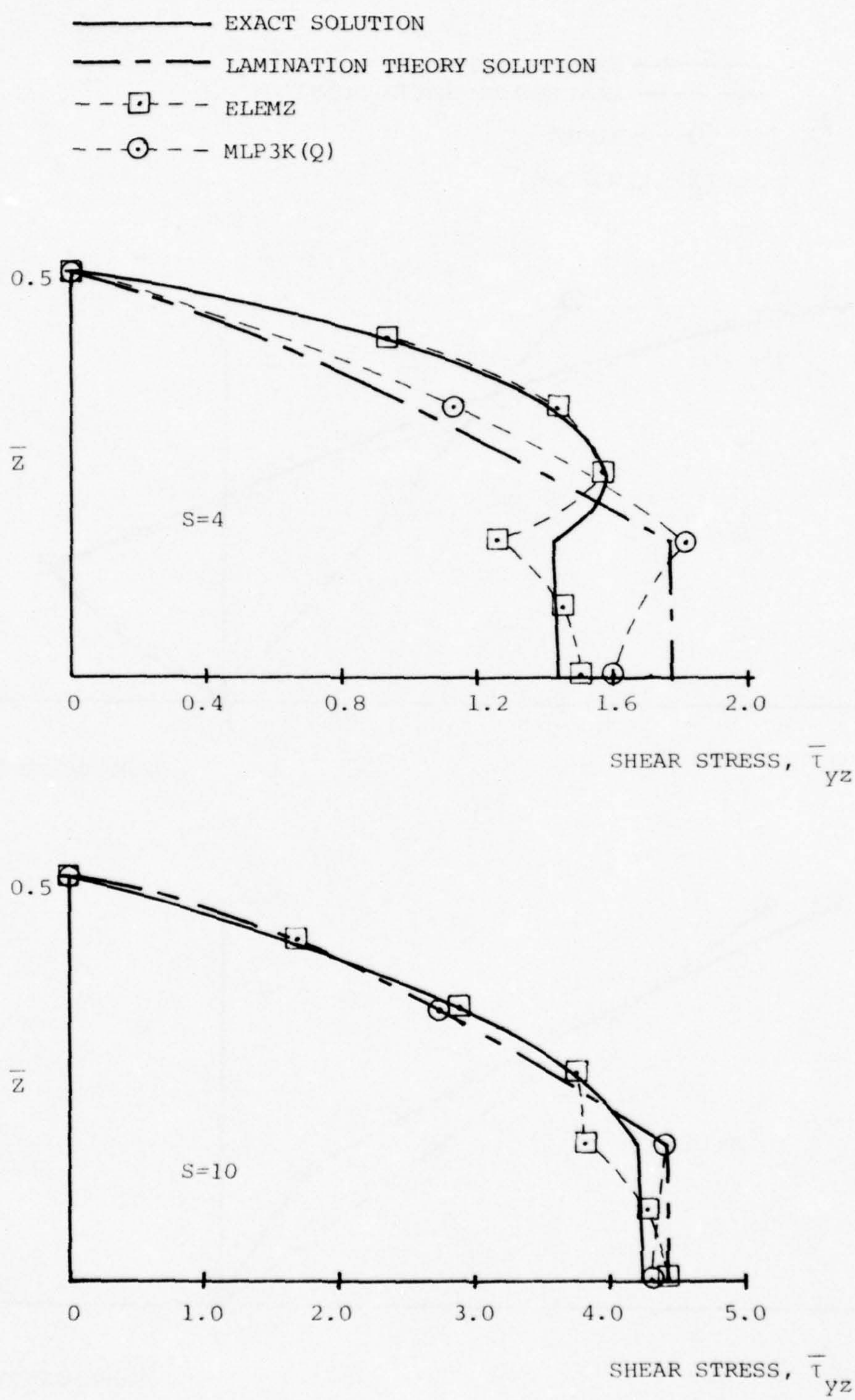

(b) Transverse Shear Stress, $\bar{\tau}_{yz}$, at the Boundary

FIG. 9 CONTINUED

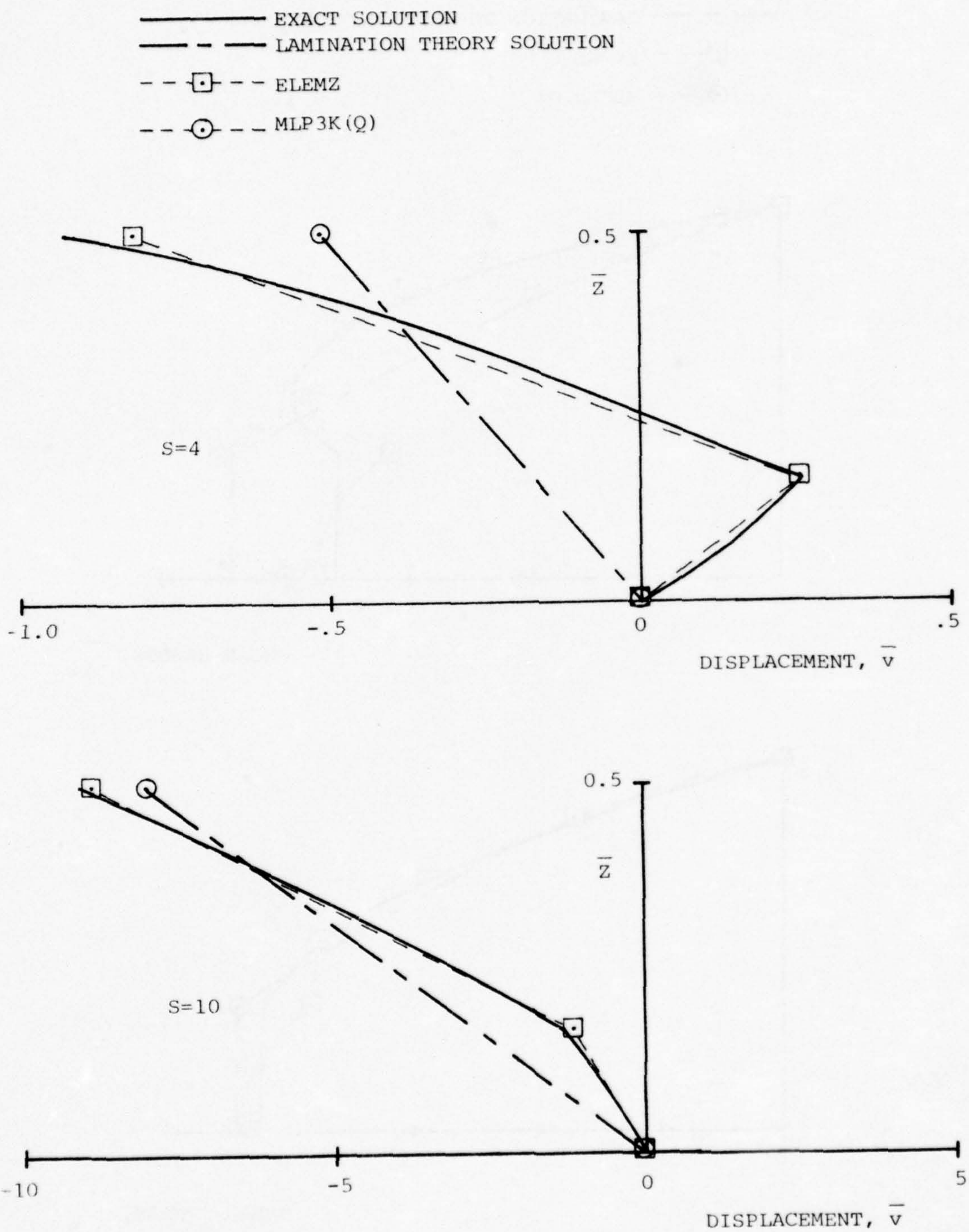

(c) Inplane Displacement, $\overline{v}$, in y Direction at the Boundary of of the Strip

FIG. 9 CONCLUDED

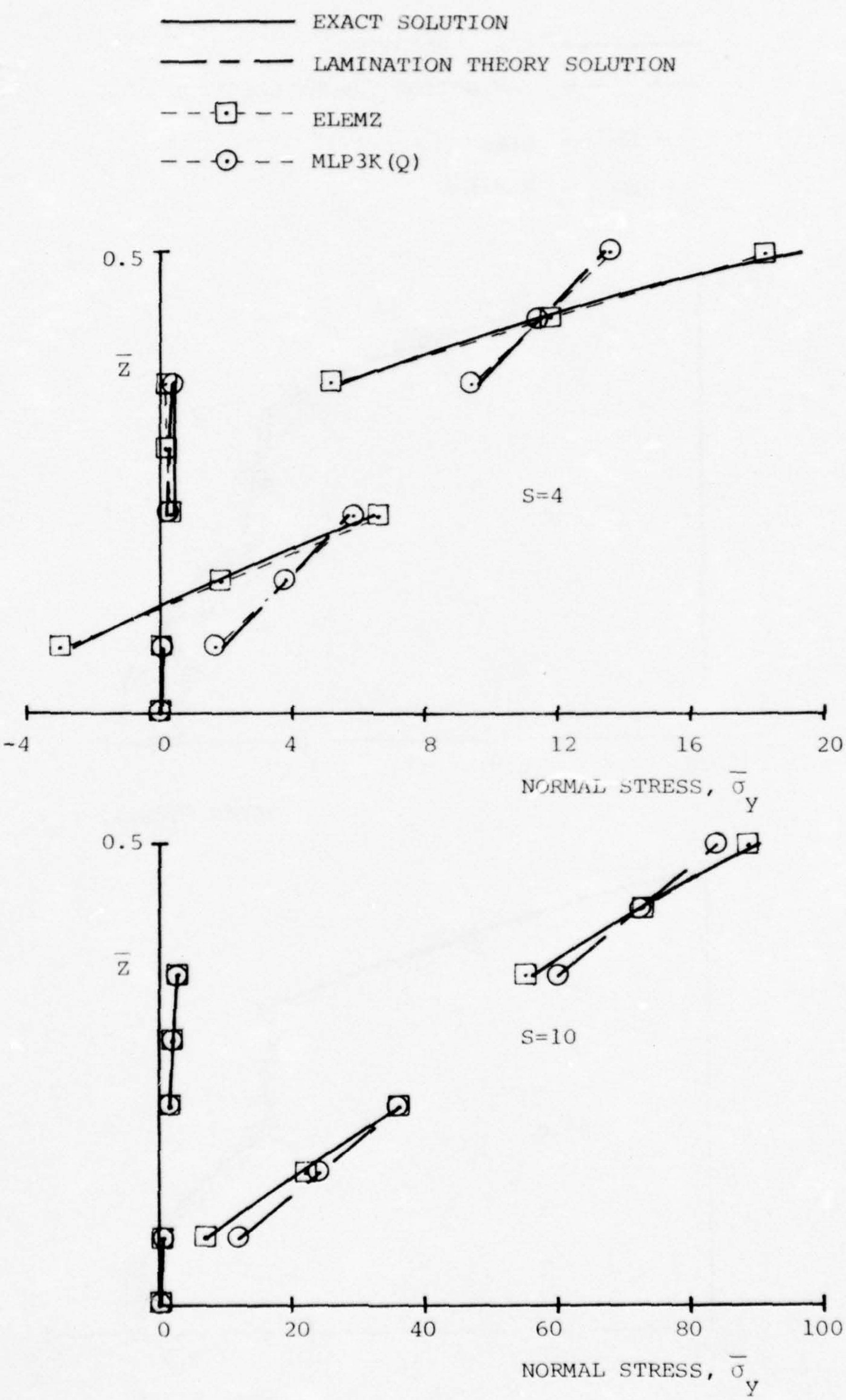

(a) Normal Stress, $\bar{\sigma}_y$, at the Center of the Strip

FIG. 10 ANALYTIC SOLUTIONS AND FINITE-ELEMENT RESULTS FOR THE PROBLEM OF THE CYLINDRICAL BENDING OF A SEVEN-LAYER (CROSS-PLY) INFINITE STRIP

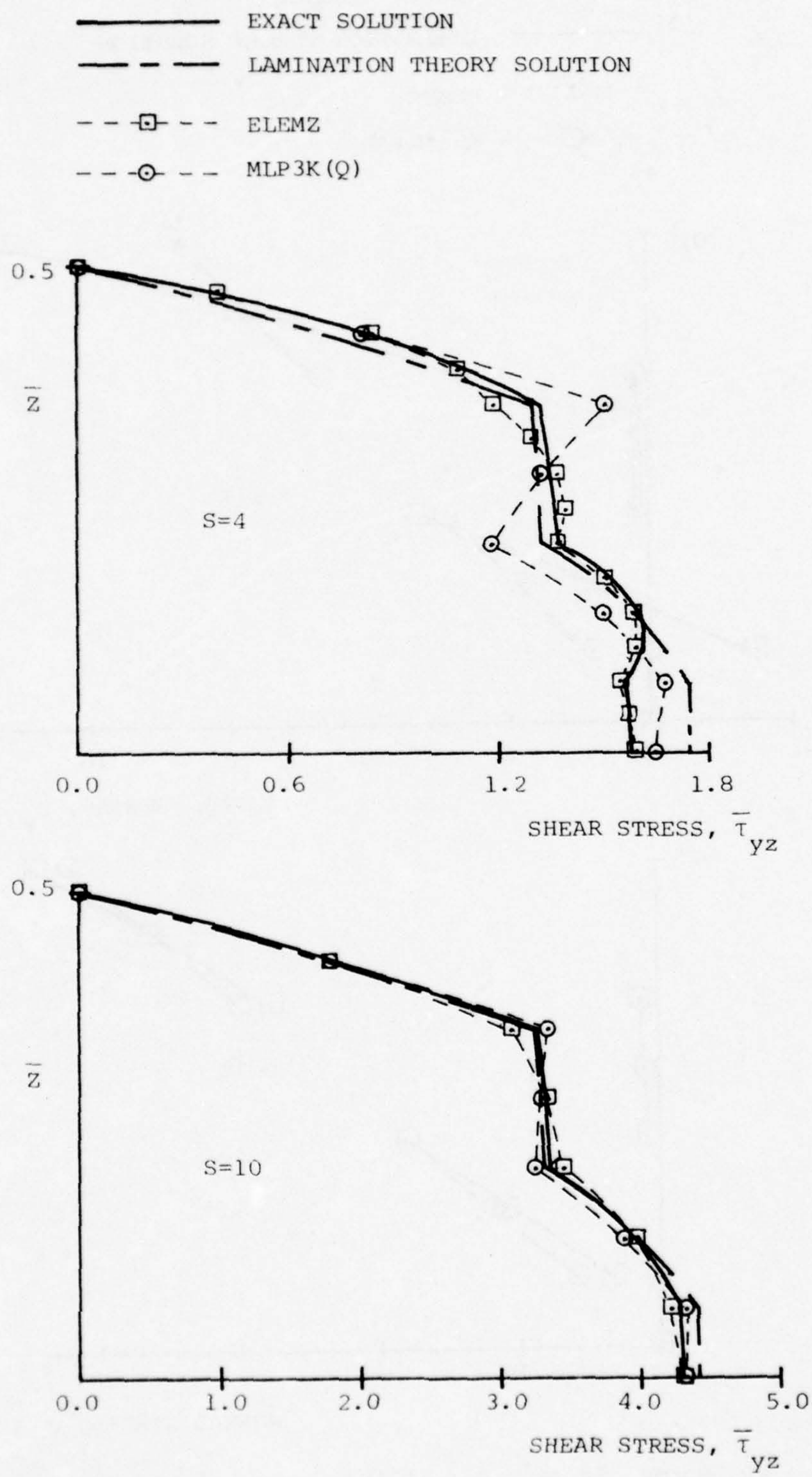

(b) Transverse Shear Stress, $\overline{\tau}_{yz}$, at the Boundary

FIG. 10 CONTINUED

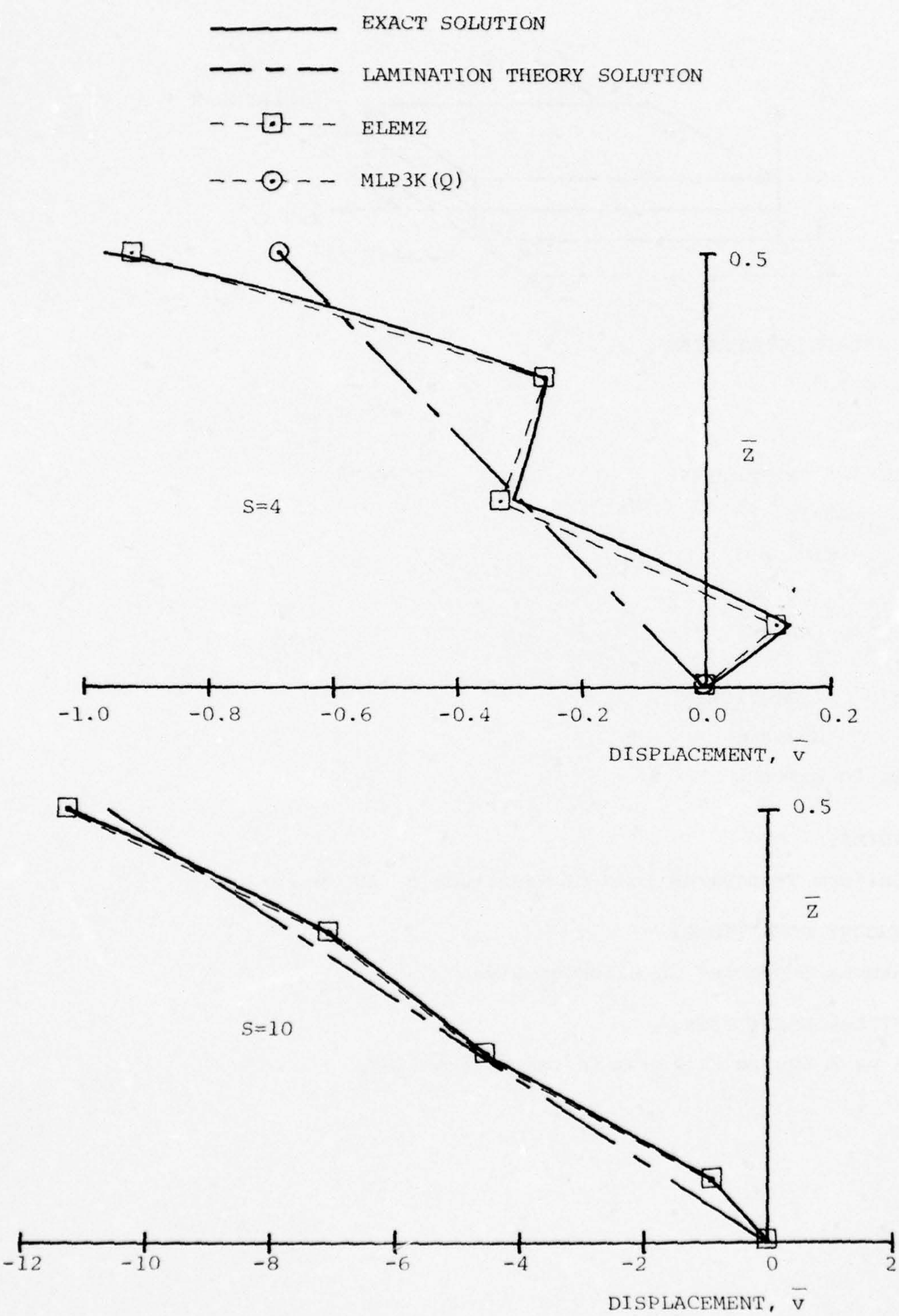

(c) Inplane Displacement, $\bar{v}$, in the y direction at the Boundary of the Strip

FIG. 10 CONCLUDED

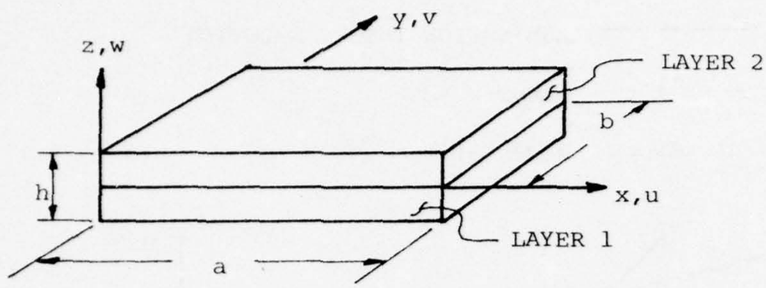

GEOMETRIC PROPERTIES:

$a=b=10''$

$h=0.2''$

MATERIAL PROPERTIES:

$E_{11}=40\times10^{6}$ psi

$E_{22}=1\times10^{6}$ psi

$G_{12}=G_{23}=0.5\times10^{6}$ psi

$\nu_{12}=\nu_{23}=0.25$

FIBER ORIENTATIONS:

$-\theta$ In Layer 1

$+\theta$ In Layer 2

LOADING:

Uniform Transverse Load of Magnitude $q_o=100$ psi

BOUNDARY CONDITIONS:

Simply Supported on all Four Sides

FINITE-ELEMENT MESH:

K by K Square Elements in the Entire Plate

FIG. 11 NOMENCLATURE AND PROPERTY DEFINITIONS FOR 2-LAYER ANGLE PLY UNDER UNIFORM TRANSVERSE LOADING

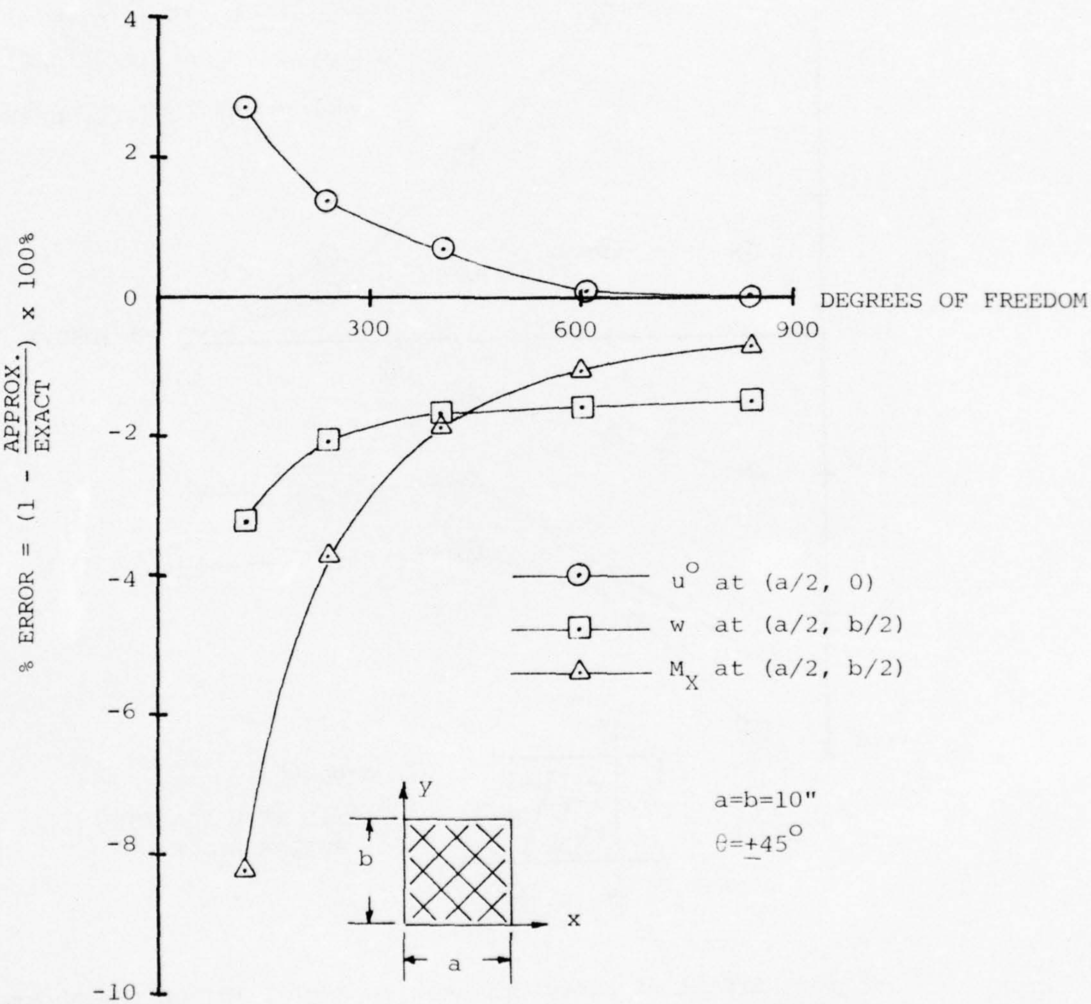

(a) Convergence Behavior of Finite-Element Solution Using Element MLP3K(Q)

FIG. 12 FINITE-ELEMENT RESULTS FOR A TWO-LAYER LAMINATE OF ANGLE-PLY ($\pm\theta$) CONSTRUCTION

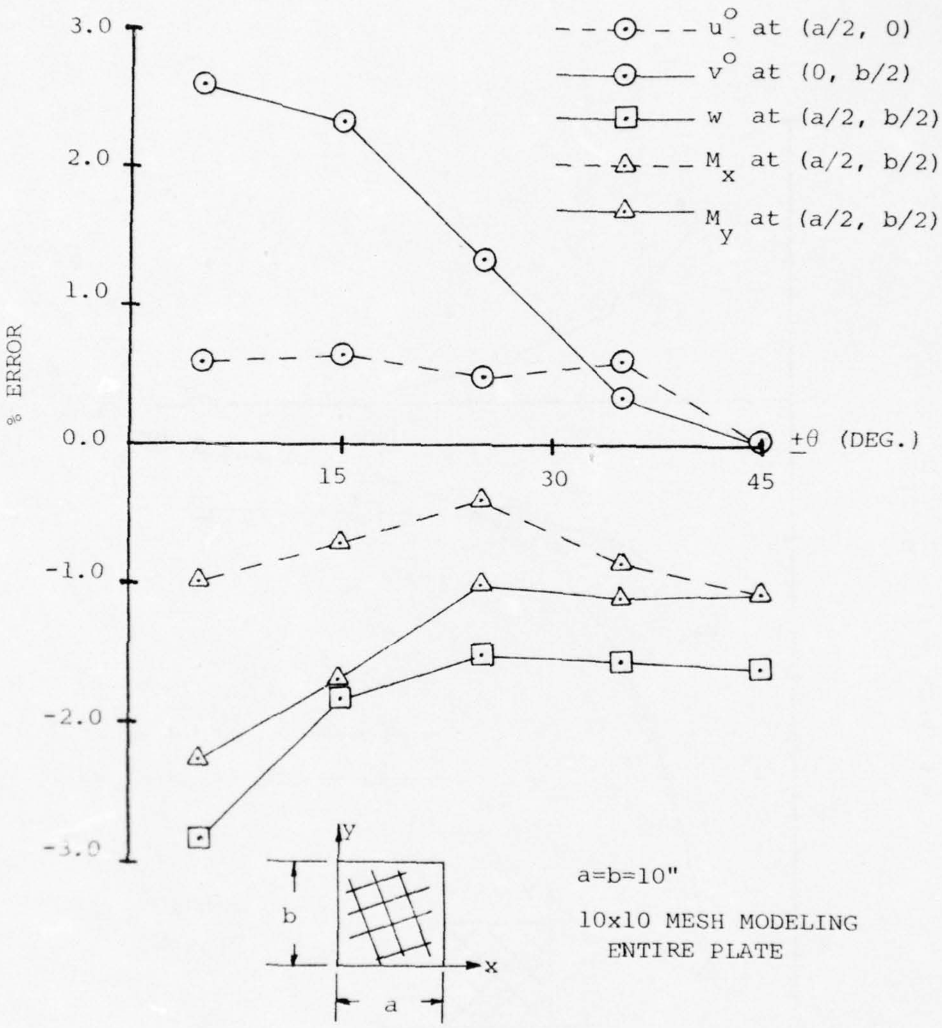

(b) Effect of Fiber Orientation Angle, $\pm\theta$, on the Accuracy of the Finite-Element Solution Using Element MLP3K(Q)

FIG. 12 CONTINUED

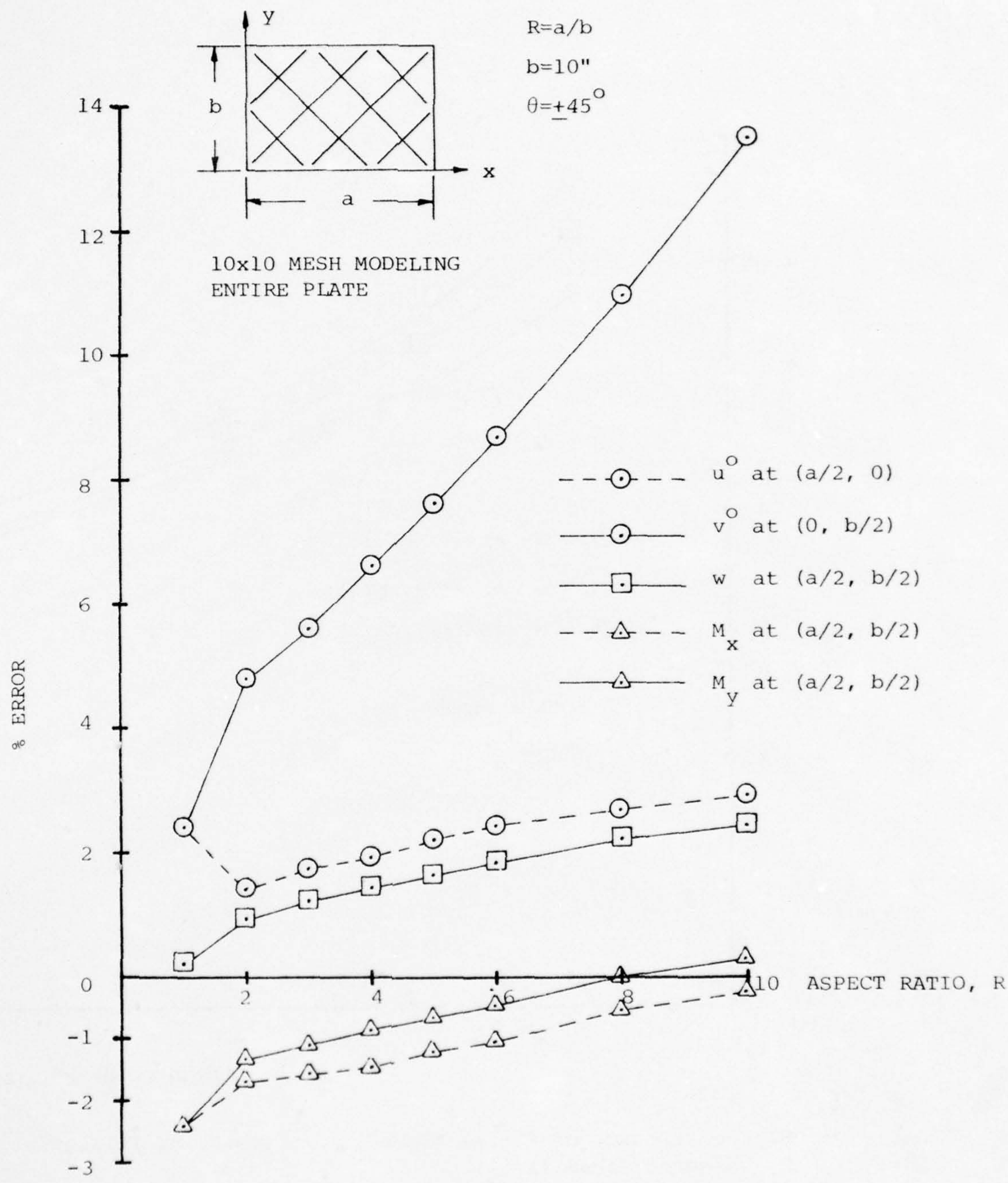

(c) Effect of Element Aspect Ratio on the Accuracy of the Finite-Element Solution Using Element MLP3K(Q)

FIG. 12 CONTINUED

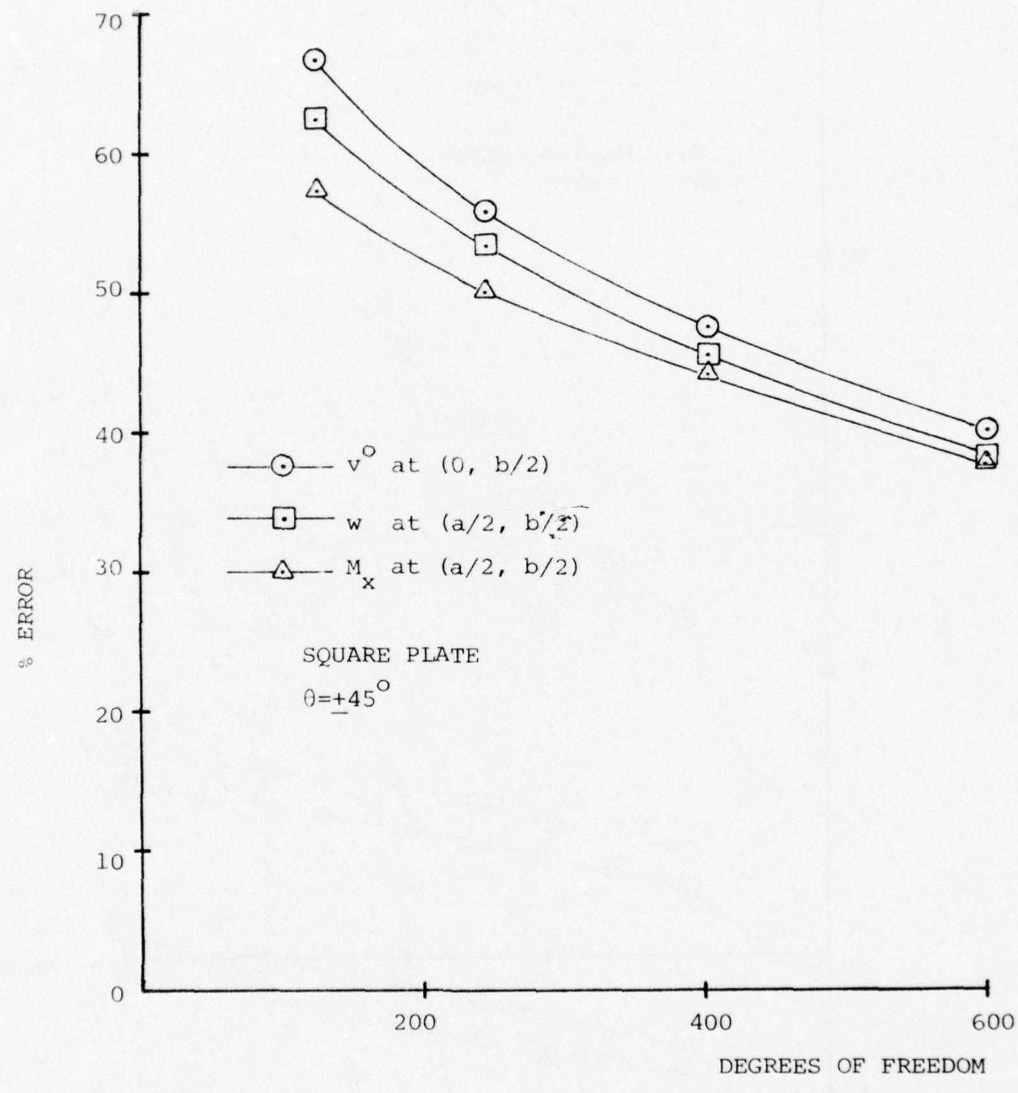

(d) Convergence of Finite-Element Solution Using Triangular Element MLP3K(T)

FIG. 12 CONTINUED

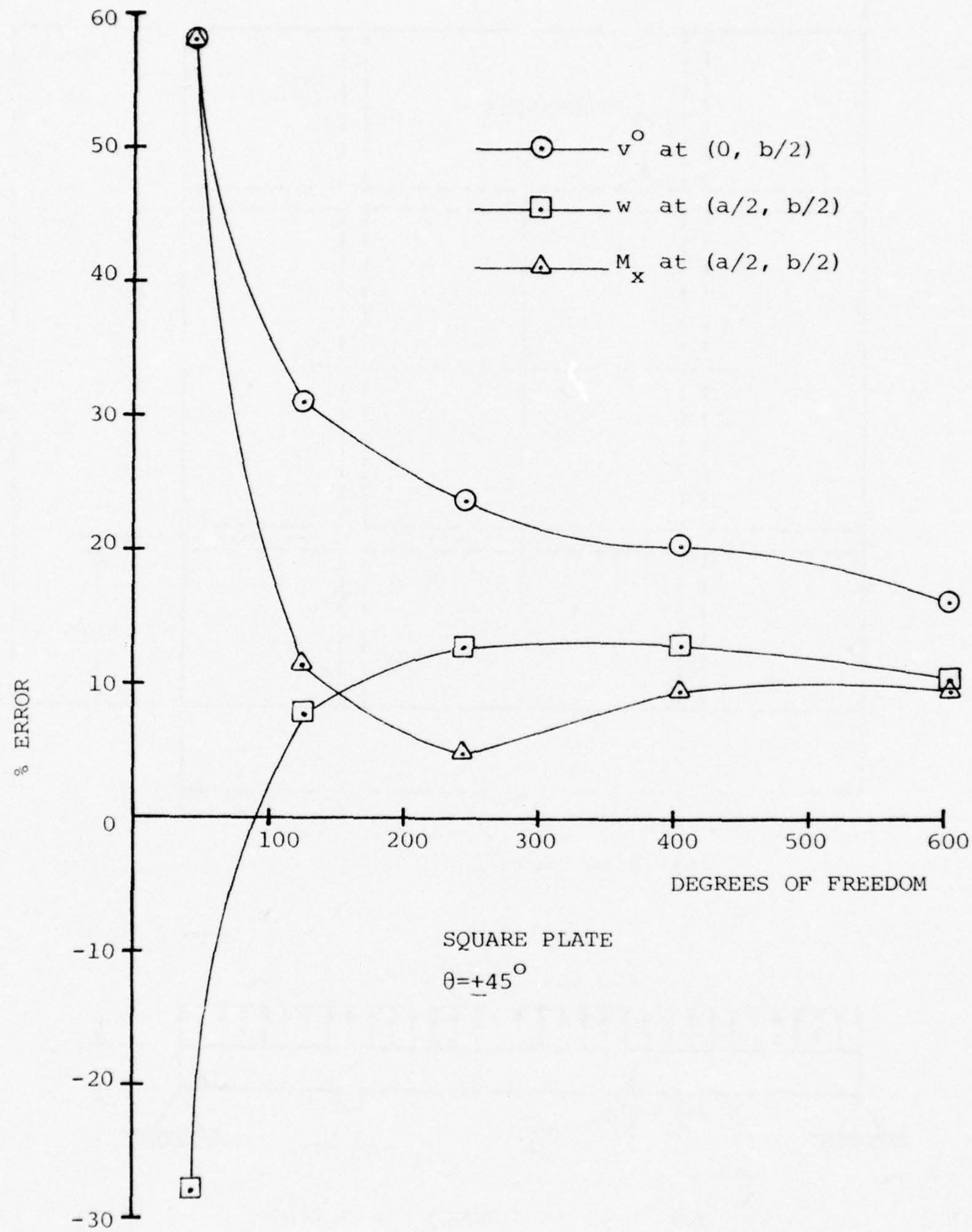

(e) Convergence of Finite-Element Solution Using Triangular Element MLTPK

FIG. 12 CONCLUDED

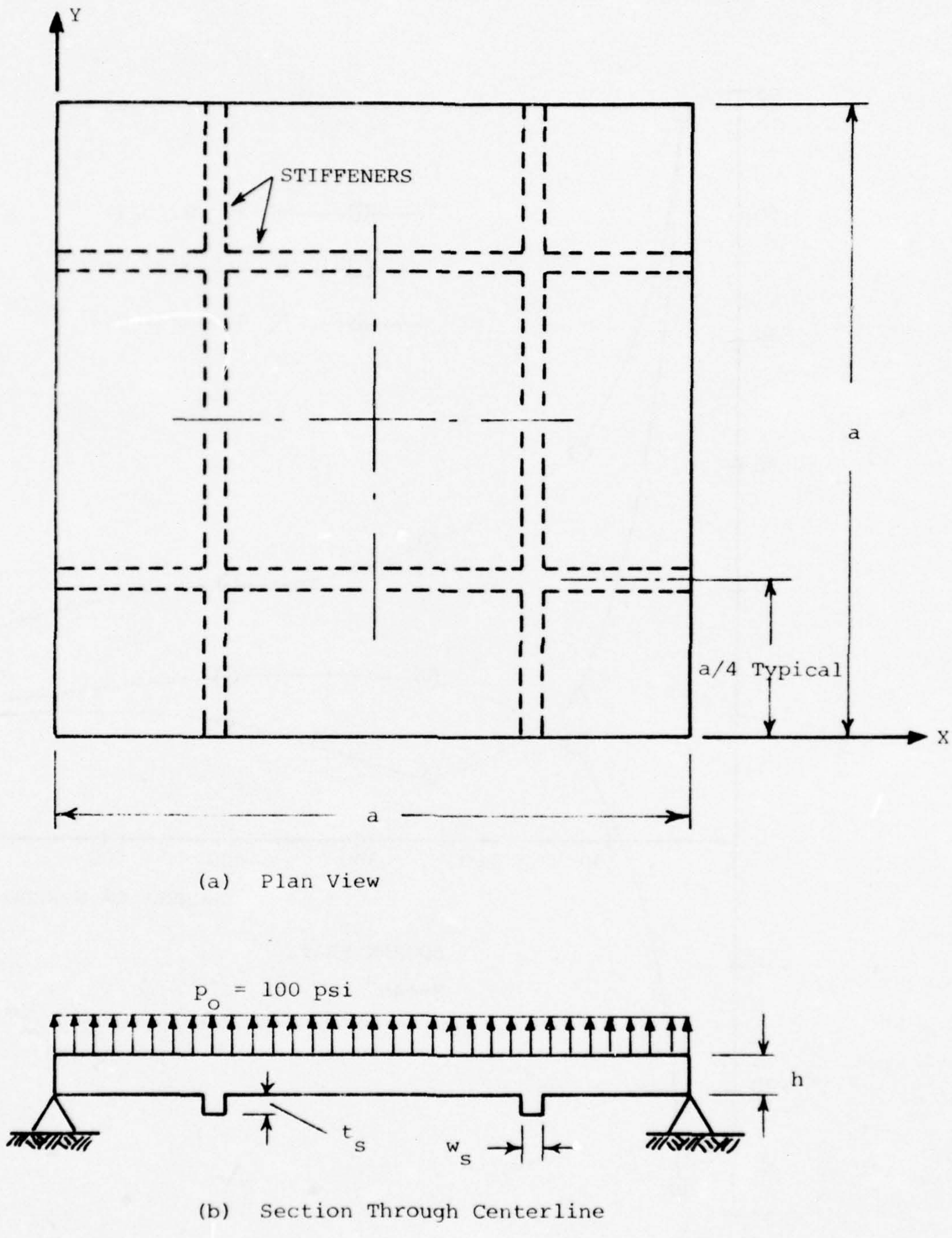

a = 12.0 in. $\quad$ $\left.\begin{array}{l} t_s \\ w_s \end{array}\right\}$ - Variable $\quad$ E = 0.4×10^8 psi

h = 0.2 in. $\quad$ $\nu = 0.25$

FIG. 13 EXAMPLE PROBLEM - SIMPLY SUPPORTED ISOTROPIC STIFFENED PLATE

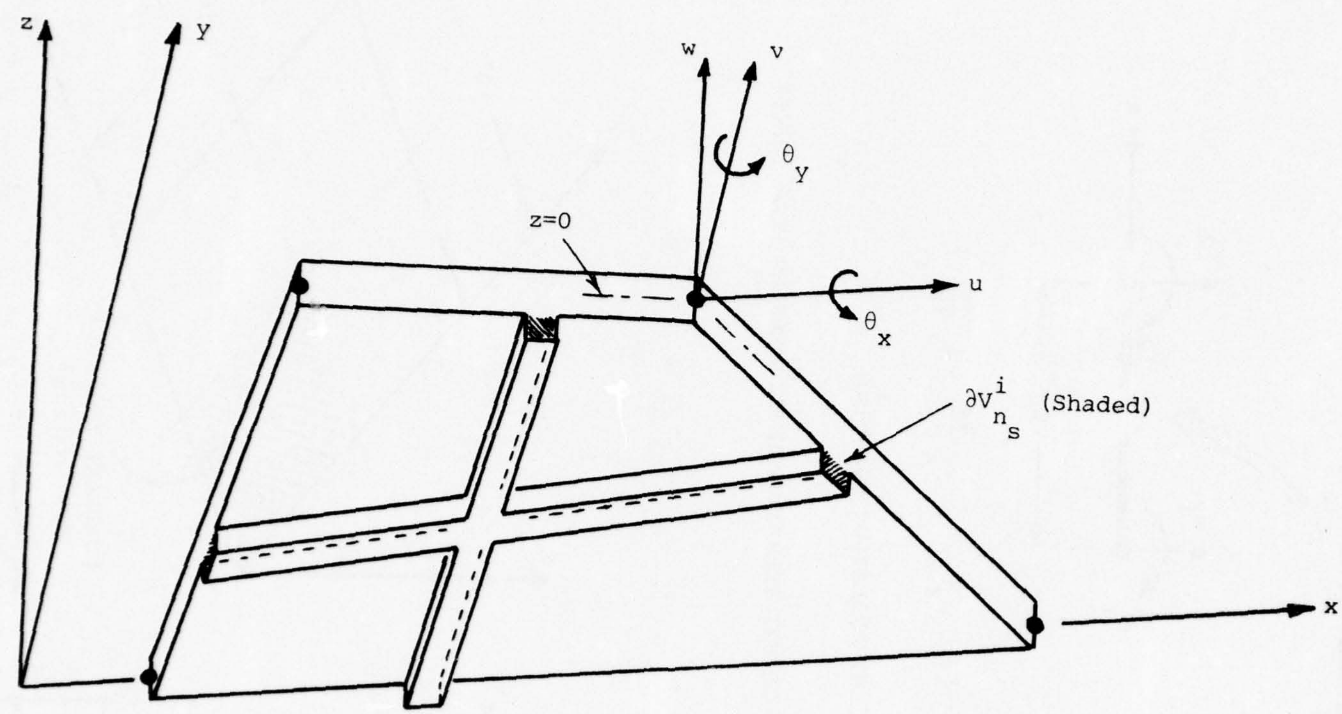

FIG. 14 PERSPECTIVE VIEW OF TYPICAL INTEGRALLY STIFFENED PLATE ELEMENT (VIEWED FROM BELOW)

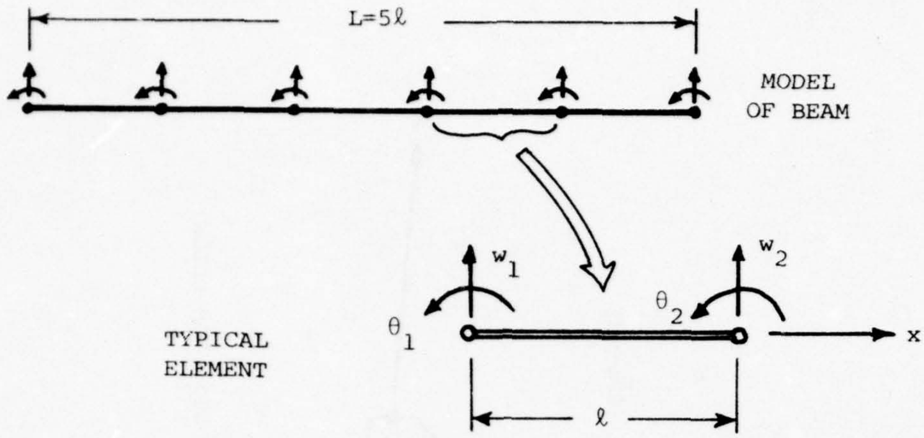

$$\underset{\sim}{q} = \{q_1 q_2 q_3 q_4\} = \{w_1 \theta_1 w_2 \theta_2\} = \{w_1 \left.\frac{\partial w}{\partial x}\right|_1 \; w_2 \left.\frac{\partial w}{\partial x}\right|_2\}$$

CUBIC INTERPOLATION FOR w(x)

FIG. 15 ASSUMED-DISPLACEMENT ELEMENT FOR ENGINEERING BEAM THEORY

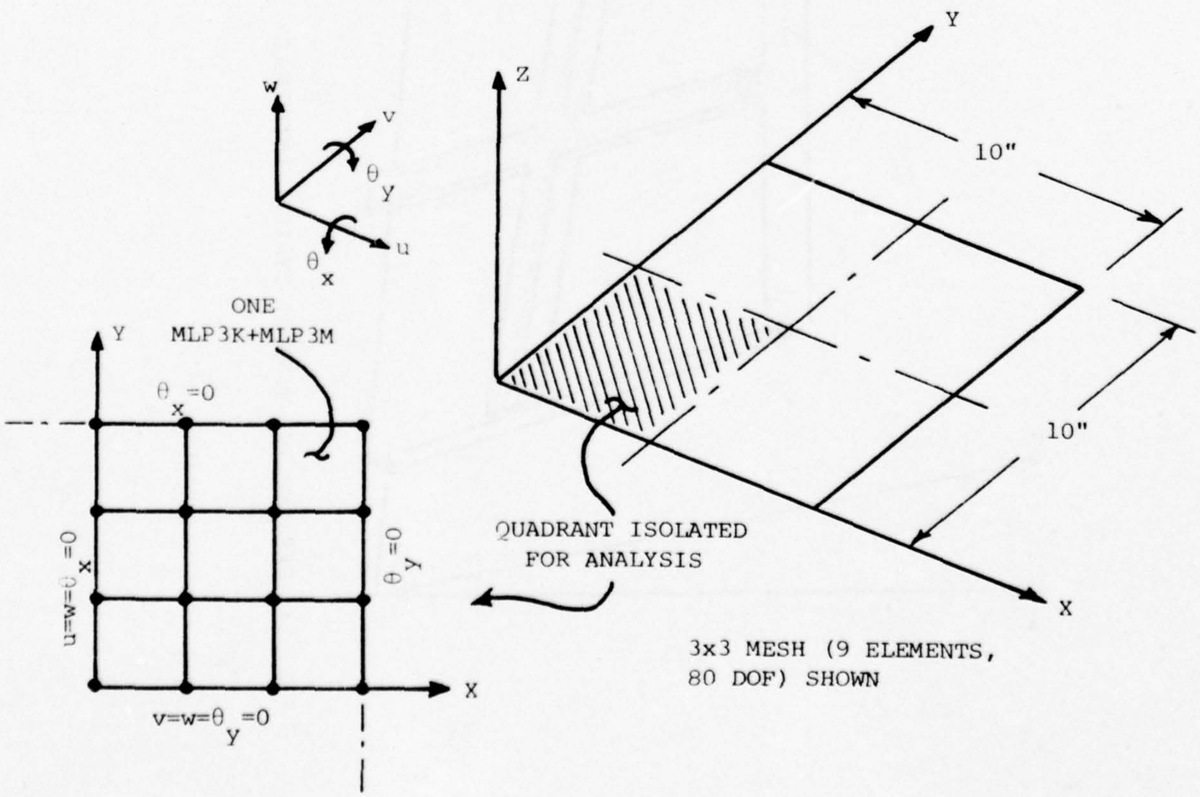

FIG. 16 FINITE-ELEMENT MODEL OF SIMPLY SUPPORTED SQUARE PLATE

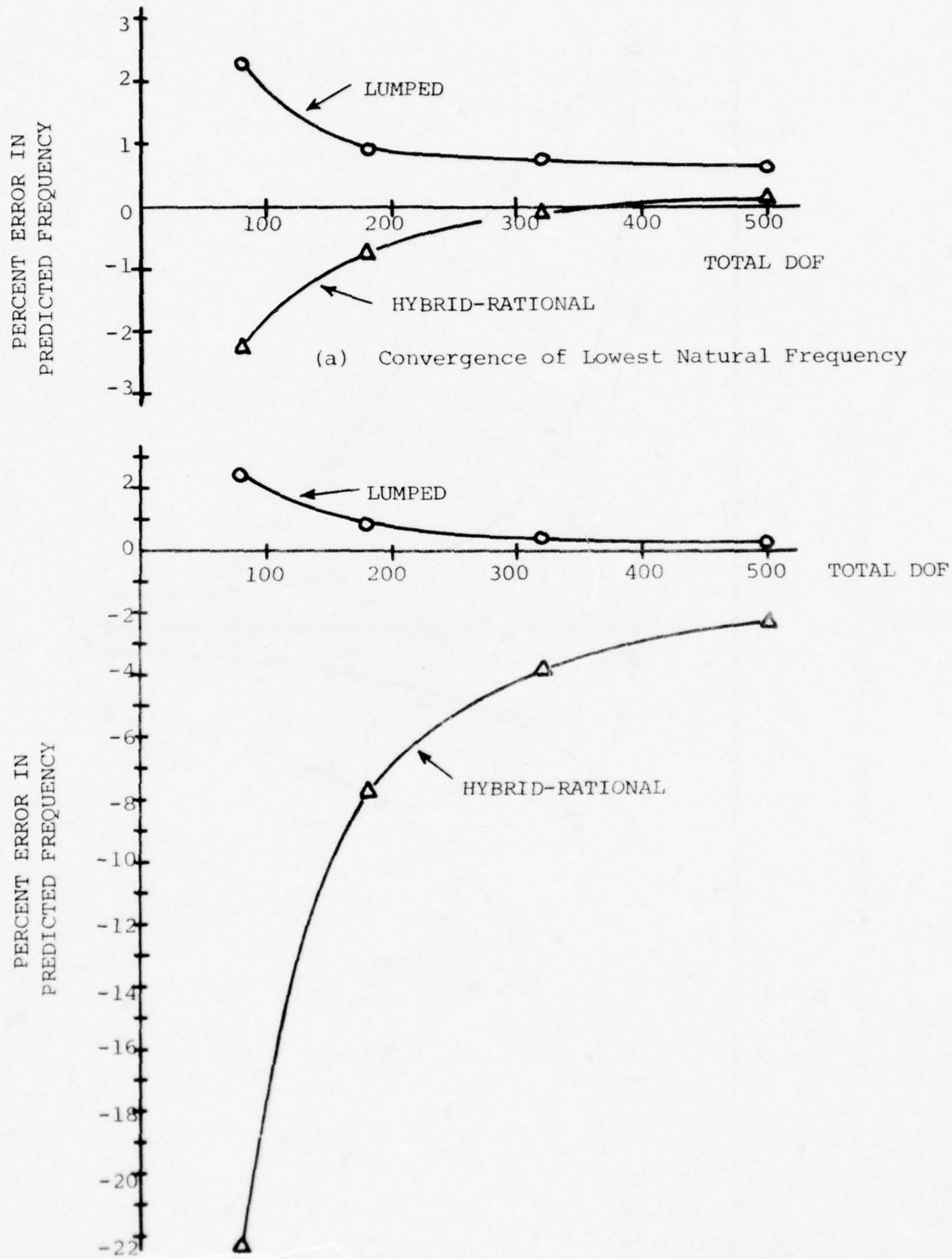

(b) Convergence of Symmetric Second and Third (Equal) Natural Frequencies

FIG. 17 EIGENVALUE CONVERGENCE RATES FOR SIMPLY SUPPORTED SQUARE PLATE

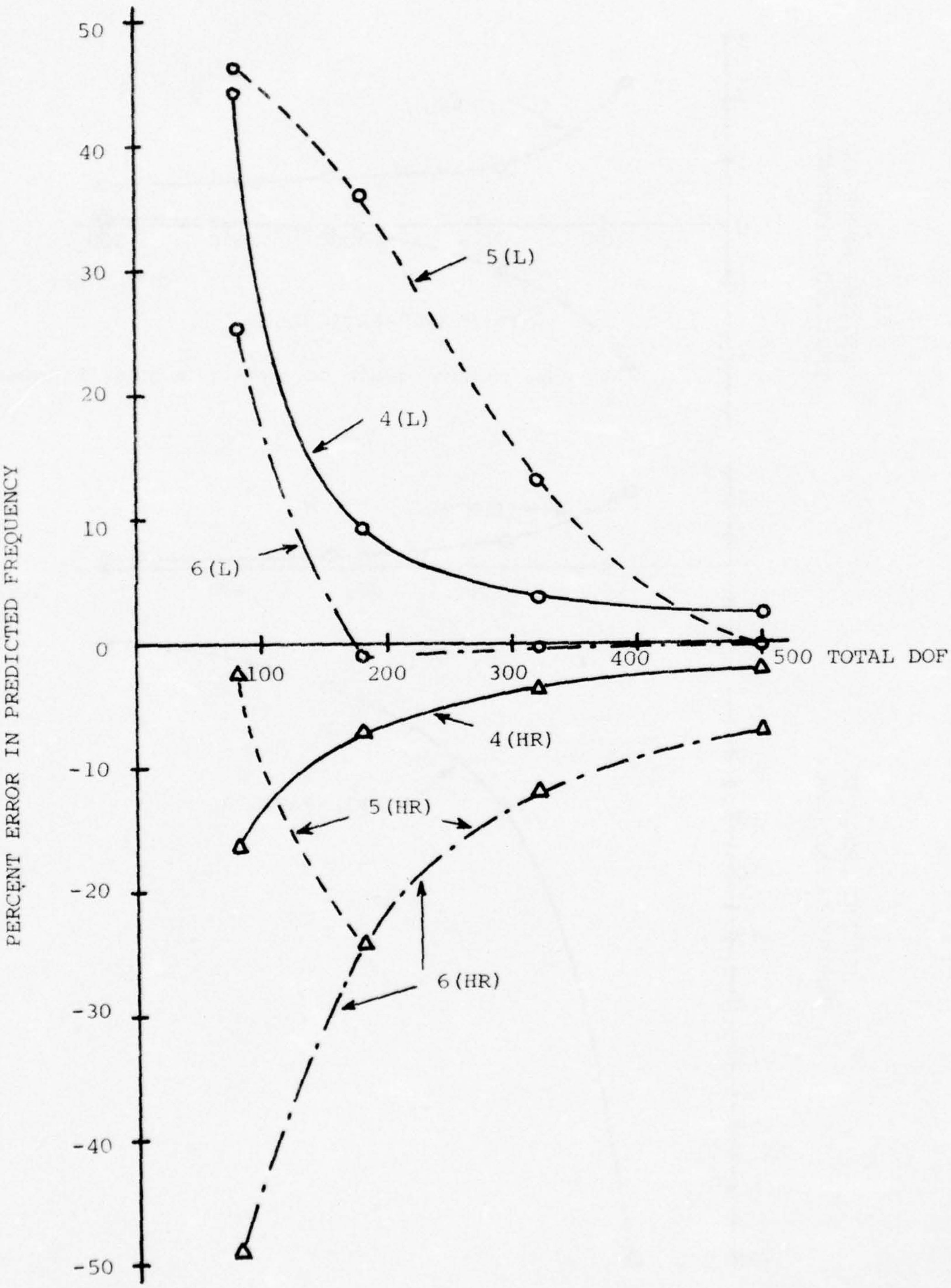

(c) Convergence of Symmetric Natural Frequencies 4 Through 6

FIG. 17 (CONCLUDED)

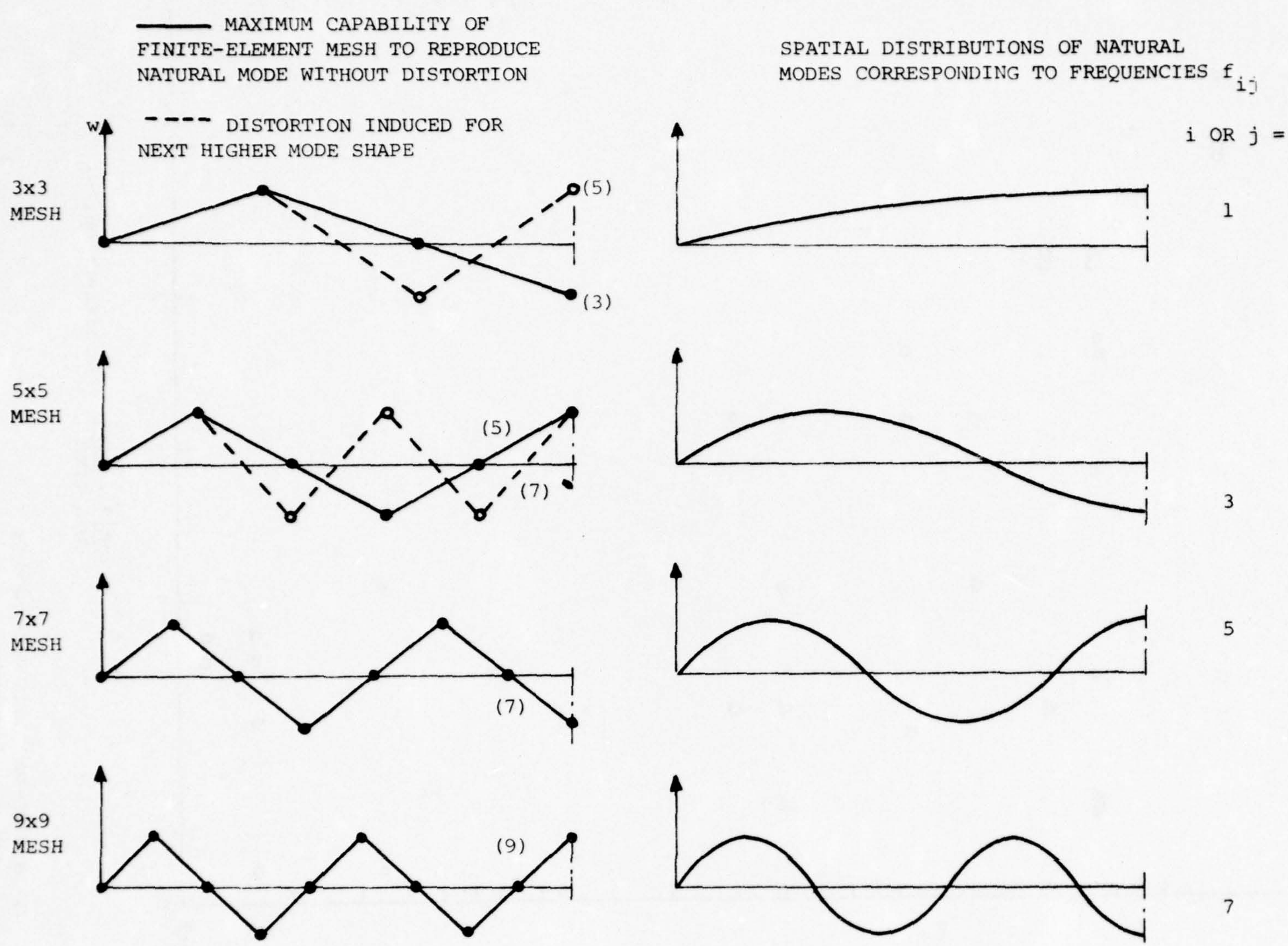

FIG. 18 LIMITING EFFECT OF ELEMENT MODE-SHAPE REPRODUCTION CAPABILITY ON SOLUTION CONVERGENCE

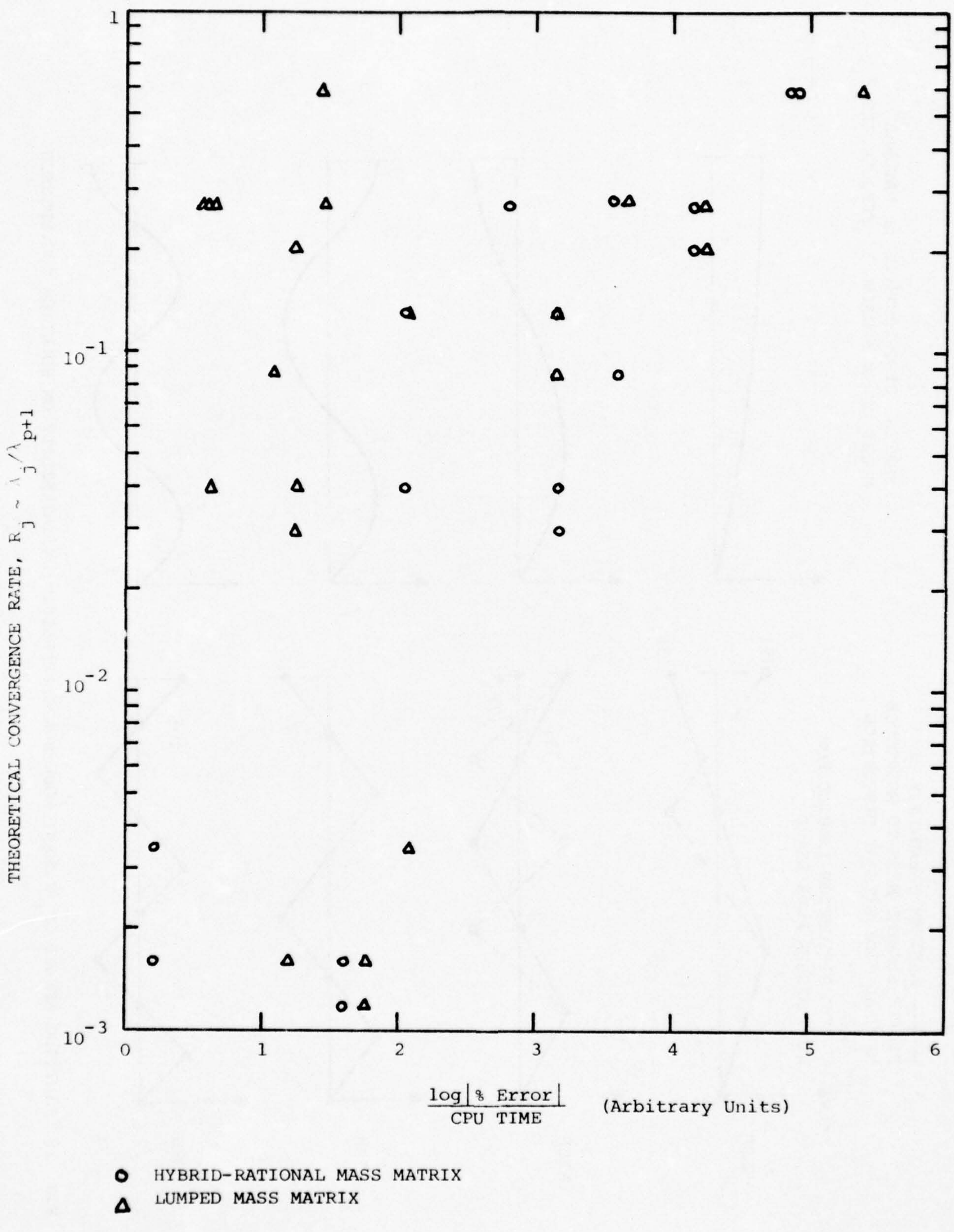

FIG. 19 CORRELATION OF COMPUTING EFFICIENCY WITH CONVERGENCE RATE

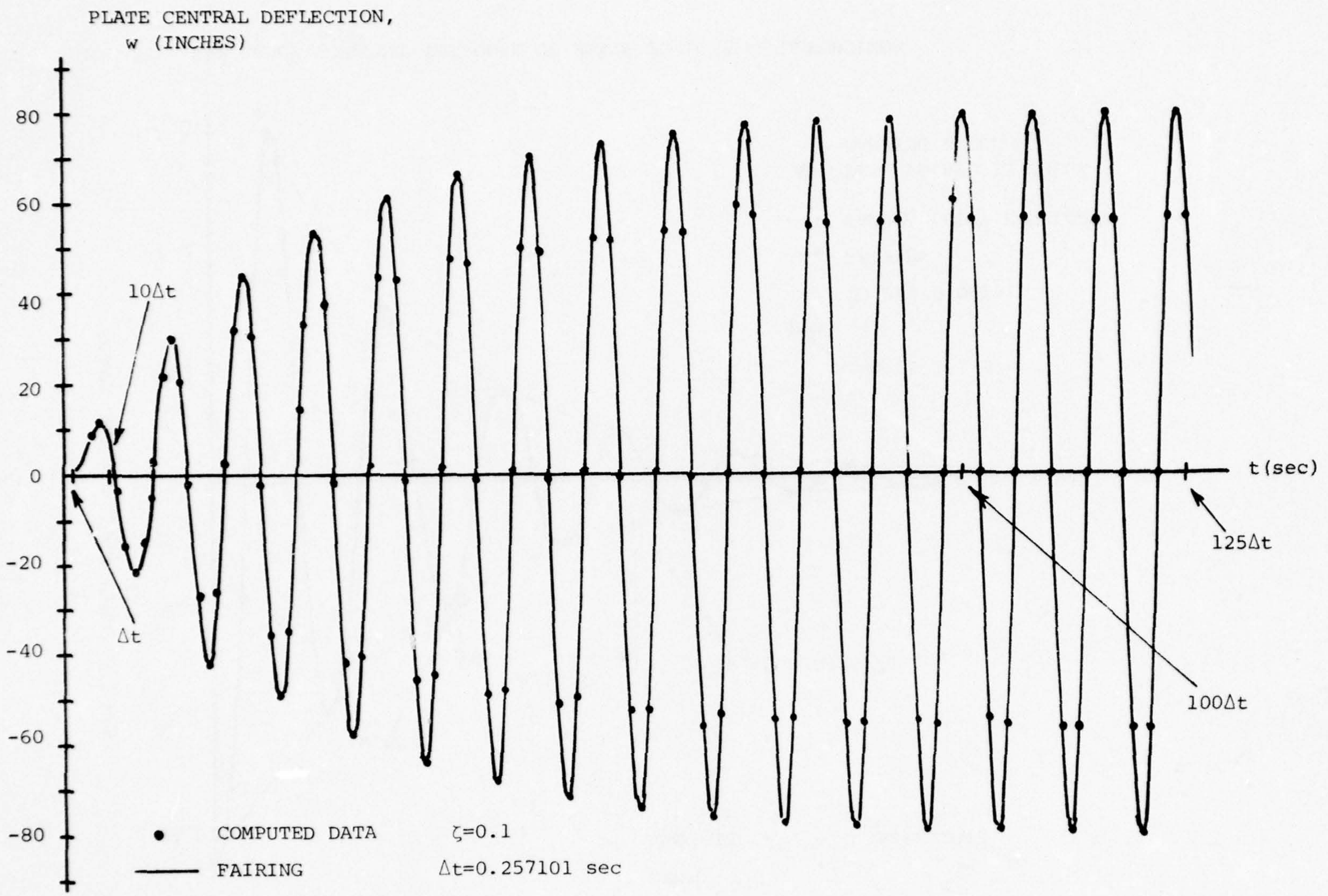

FIG. 20 EXAMPLE OF COMPUTED RESPONSE OF PLATE TO STEADY SINUSOIDAL LOAD

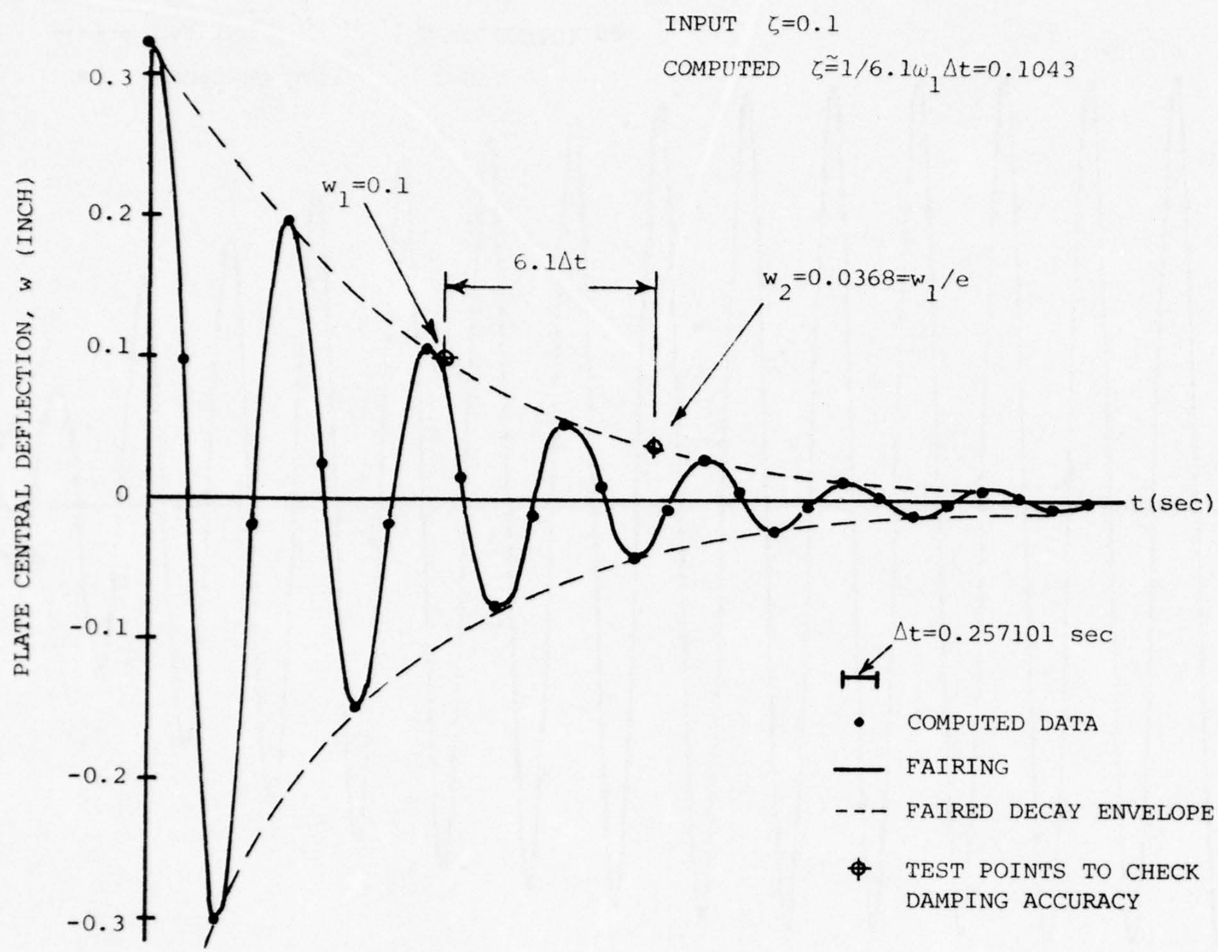

FIG. 21 EXAMPLE OF COMPUTED RESPONSE OF PLATE TO INITIAL DEFLECTION

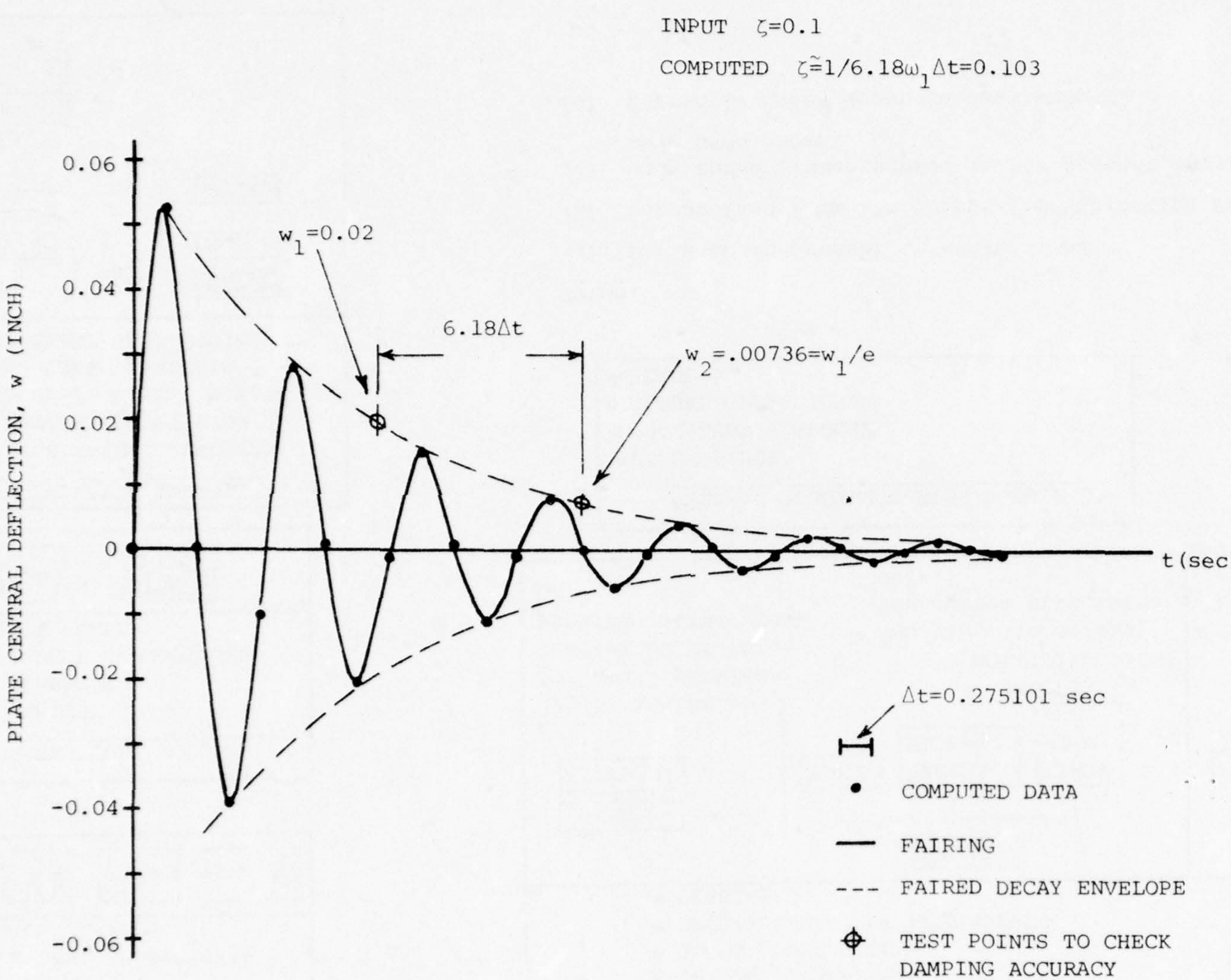

FIG. 22 EXAMPLE OF COMPUTED RESPONSE OF PLATE TO INITIAL VELOCITY

ROOT MODULE

- STATIC ANALYSIS
- GLOBAL OPERATIONS
- 8 INDEPENDENT SUBROUTINES
- FEABL-2 OR FEABL-5

ASEMBL, BCON, ORK, SIMULQ
ASMLTV, FACT, SETUP, XTRACT

SUBSTRUCTURE MODULE (1)

- STATIC ANALYSIS
- GLOBAL OPERATIONS
- 4 INDEPENDENT SUBROUTINES
- FEABL-2 OR FEABL-5

ASMSUB, STACON
QBACK, SUPERL

ELEMENT GENERATOR LIBRARY (3)

- STIFFNESS MATRIX COMPUTATION
- MASS MATRIX COMPUTATION
- STRESS-DISPLACEMENT MATRIX
- STRESS/STRAIN ANALYSIS
- EACH ELEMENT SELF-CONTAINED

MLP3K
PROD, SINV(2)
MFSD(2)

MLTPK
PROD, SINV(2)
MFSD(2)

MLP3M
MLP3S
STIF2

DYNAMIC ANALYSIS MODULE

- EIGENVALUES
- TRANSIENT RESPONSE
- GLOBAL OPERATIONS
- REQUIRES PART OF ROOT MODULE
- FEABL-5

JACKM1
EIGEN(2)

- Jacobi iteration for small problems; restrained or unrestrained structures.

SSPACE
FACT, JACKM1 EIGEN(2), KINXV UTXV MXU
(MATRIX MULTIPLICATION)

- Subspace iteration; restrained structures only.

TSTEP
ELAPSE, INPUT
Temporary subroutine

- Transient response by modal superposition.

DYNAMIC SUBSTRUCTURING MODULE (4)

- EIGENVALUES
- TRANSIENT RESPONSE
- GLOBAL OPERATIONS
- FEABL-5

Notes:

(1) Not used in present investigation.

(2) Subroutines from IBM Scientific Subroutine Package

(3) Only those elements used in the present investigation have been shown.

(4) Currently under separate development.

FIG. 23 SUMMARY OF FEABL-2 AND FEABL-5 SOFTWARE MODULES

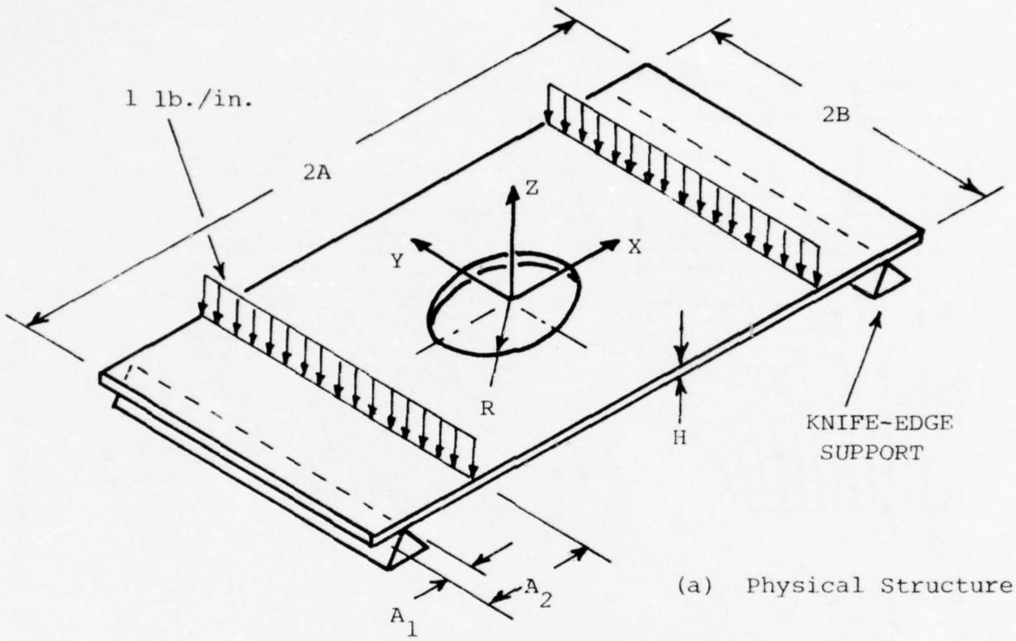

(a) Physical Structure

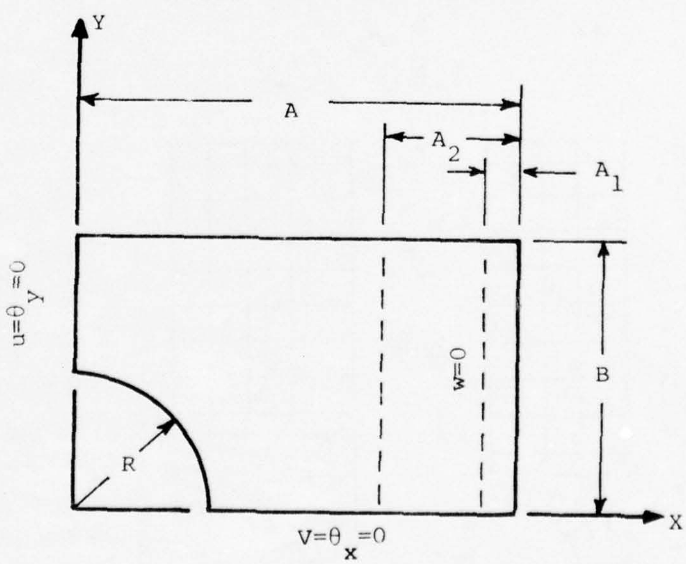

(b) Quadrant Isolated for Finite-Element Analysis, with Physical and Symmetry Boundary Conditions Indicated

FIG. 24 FOUR-POINT BENDING EXPERIMENT ON PLATE WITH CIRCULAR HOLE

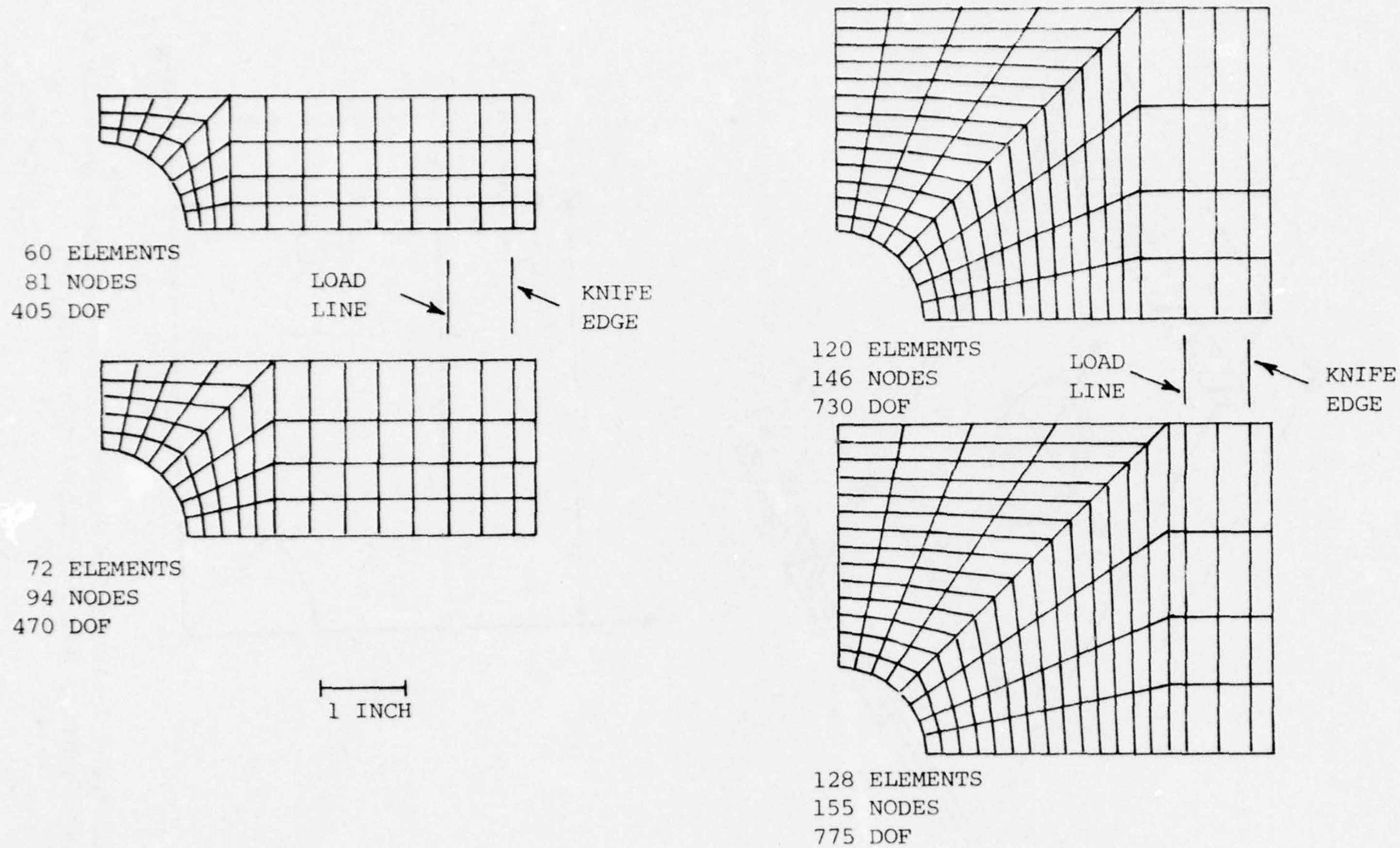

FIG. 25 SCALE PLANES OF TYPICAL MESHES GENERATED BY SUBROUTINE AMMRC2

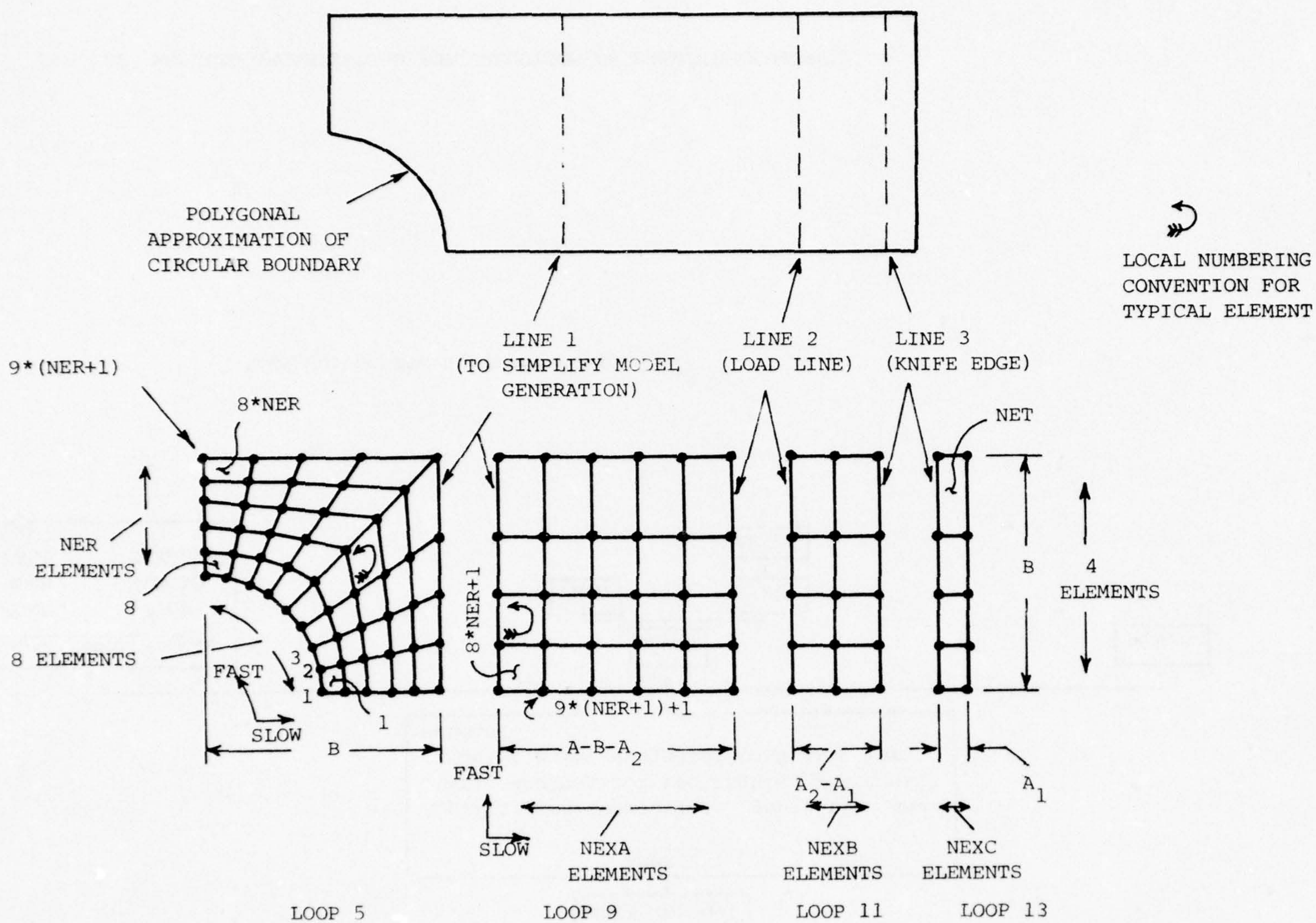

FIG. 26 DIVISION OF QUADRANT INTO REGIONS FOR AUTOMATIC MESH GENERATION

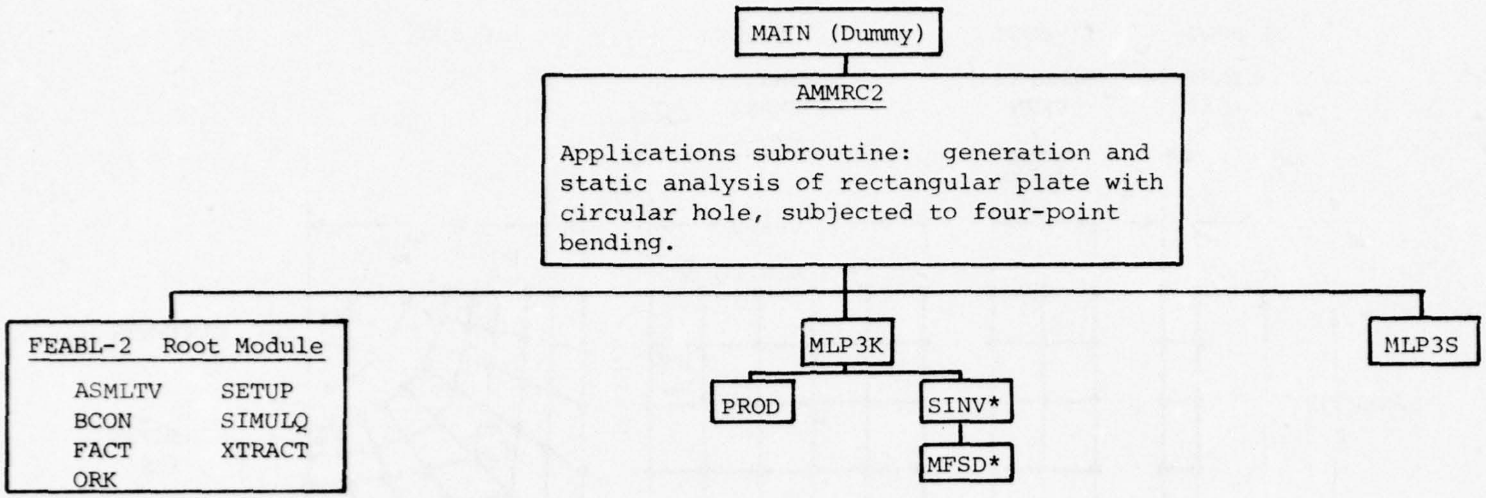

*IBM Scientific Subroutine Package.

FIG. 27 MODULAR ORGANIZATION FOR EXECUTION OF SUBROUTINE AMMRC2

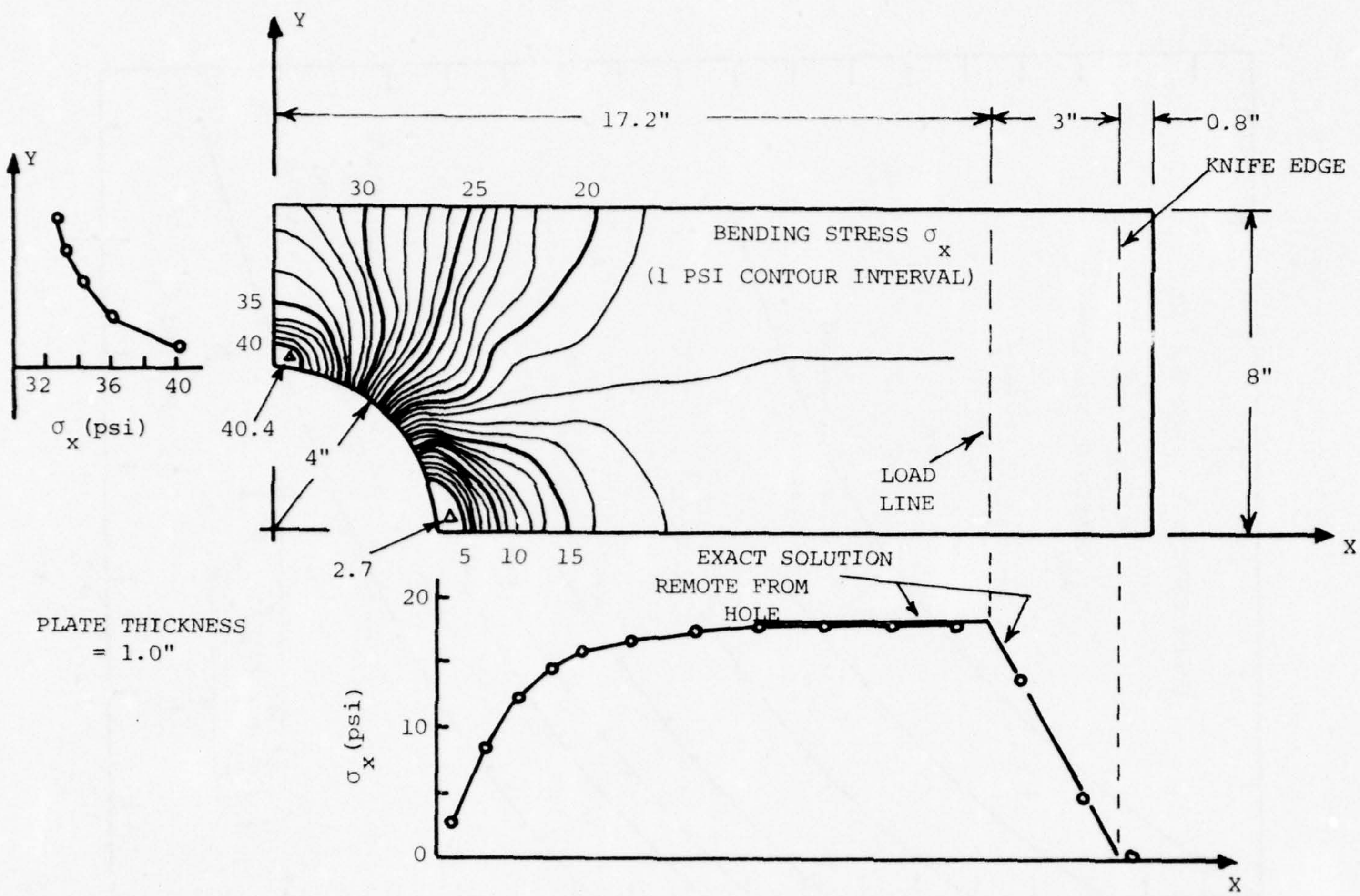

FIG. 28 BENDING STRESSES COMPUTED BY SUBROUTINE AMMRC2 FOR A SINGLE-LAYER ISOTROPIC PLATE

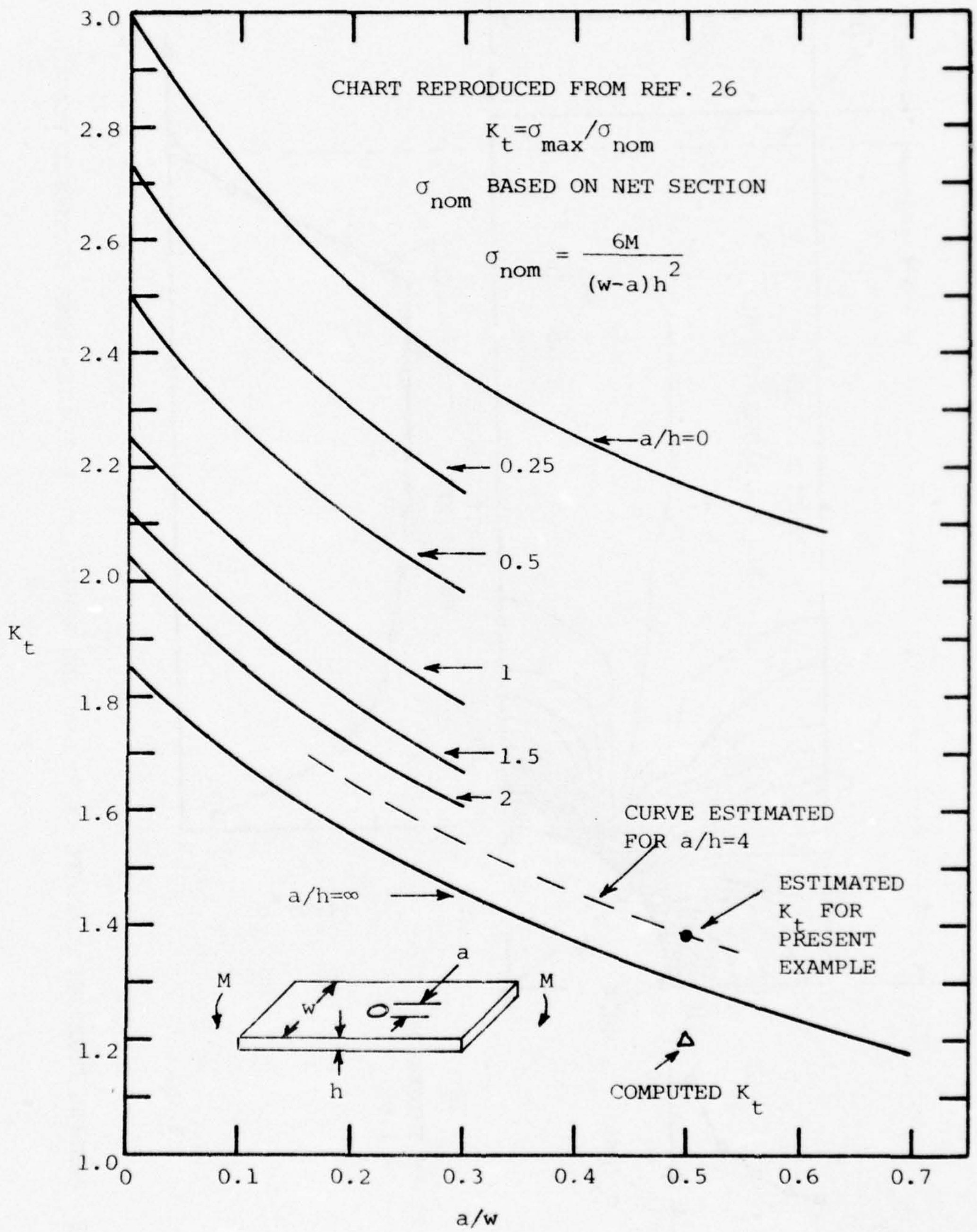

FIG. 29 COMPARISON OF COMPUTED AND EXPERIMENTAL STRESS CONCENTRATION FACTORS

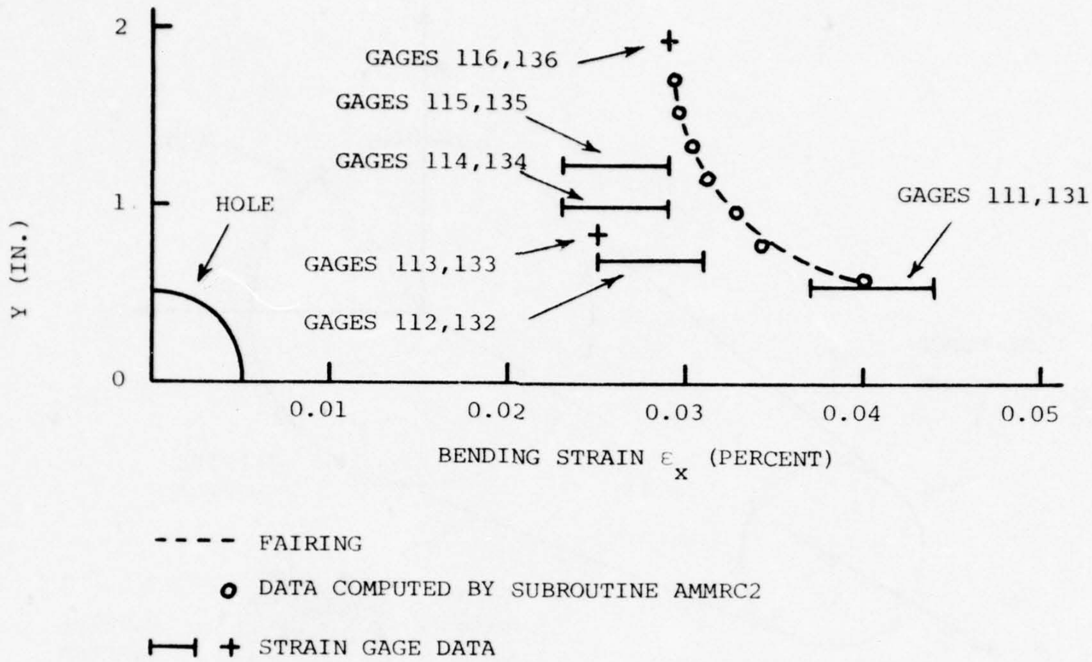

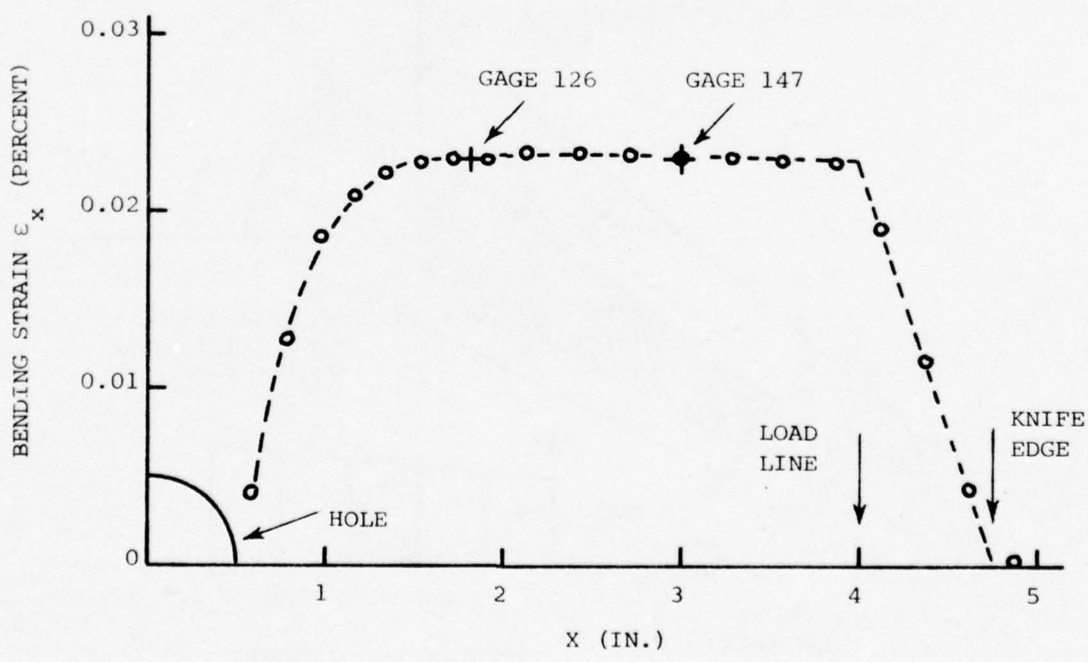

FIG. 30 COMPARISON OF COMPUTED AND EXPERIMENTAL RESULTS FOR BENDING STRAIN

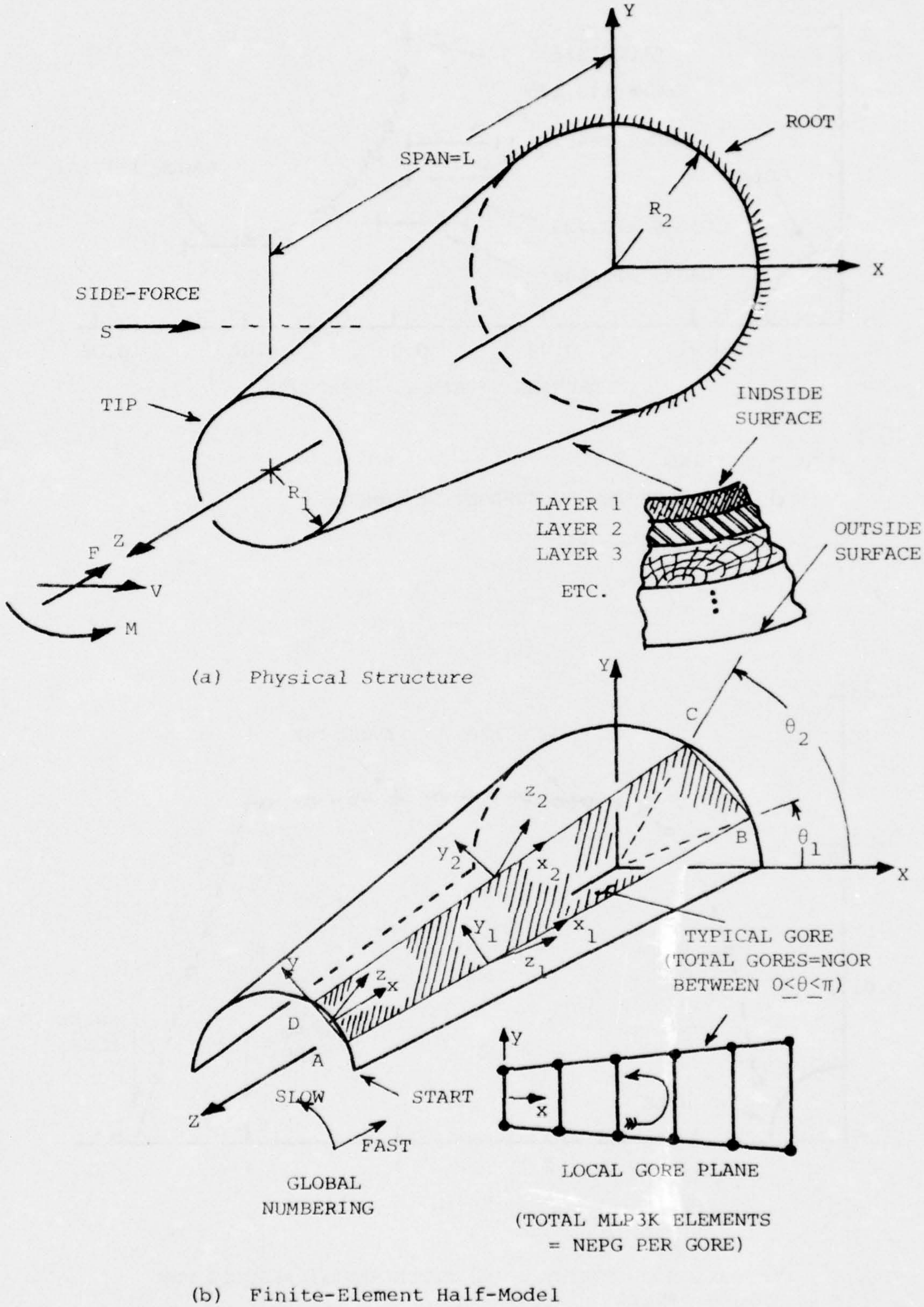

FIG. 31 LAMINATED CONICAL SHELL AND FINITE-ELEMENT MODEL

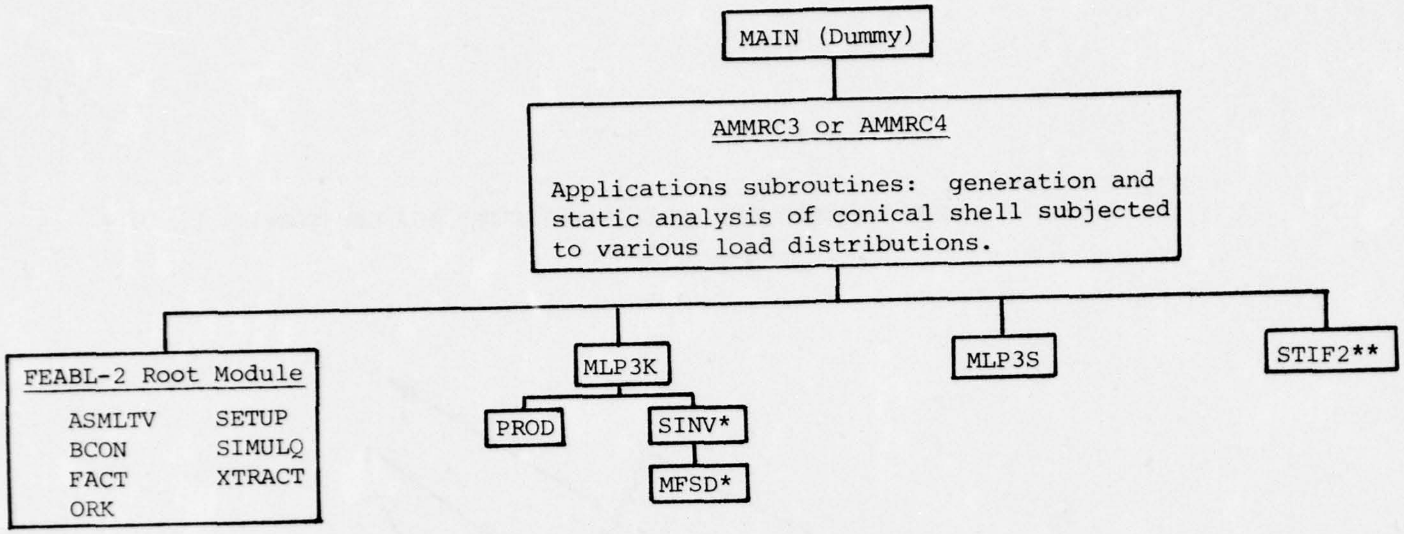

*IBM Scientific Subroutine Package.

**Required by AMMRC4 only.

FIG. 32 MODULAR ORGANIZATION FOR EXECUTION OF SUBROUTINES AMMRC3 AND AMMRC4

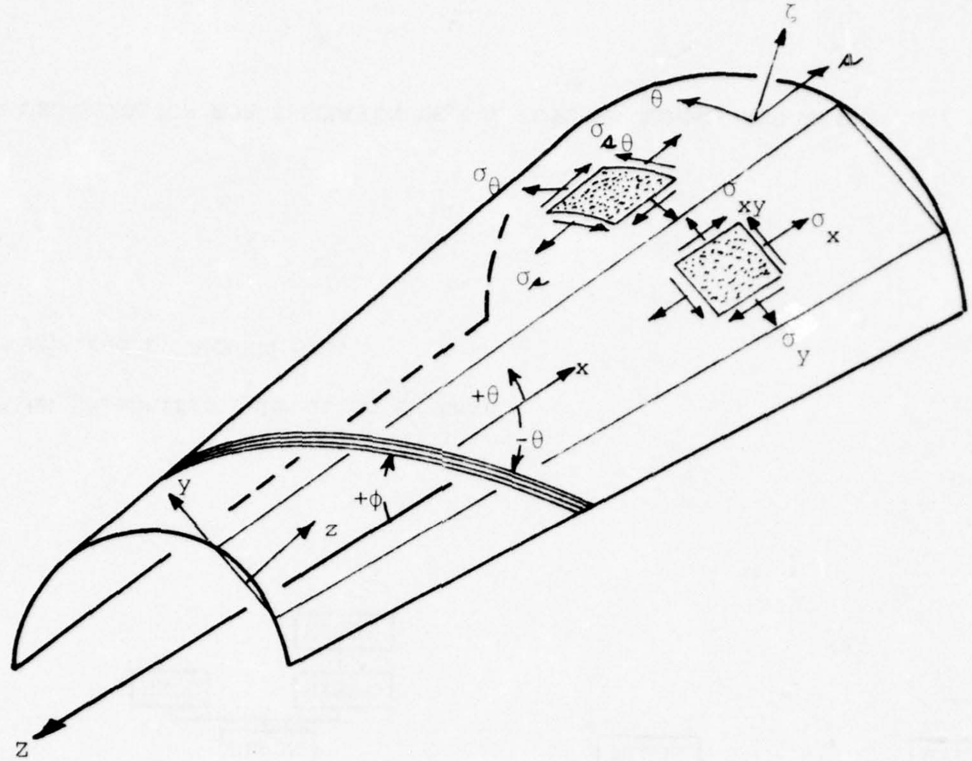

FIG. 33 STRESS AND PLY ANGLE CONVENTIONS FOR CONICAL SHELL

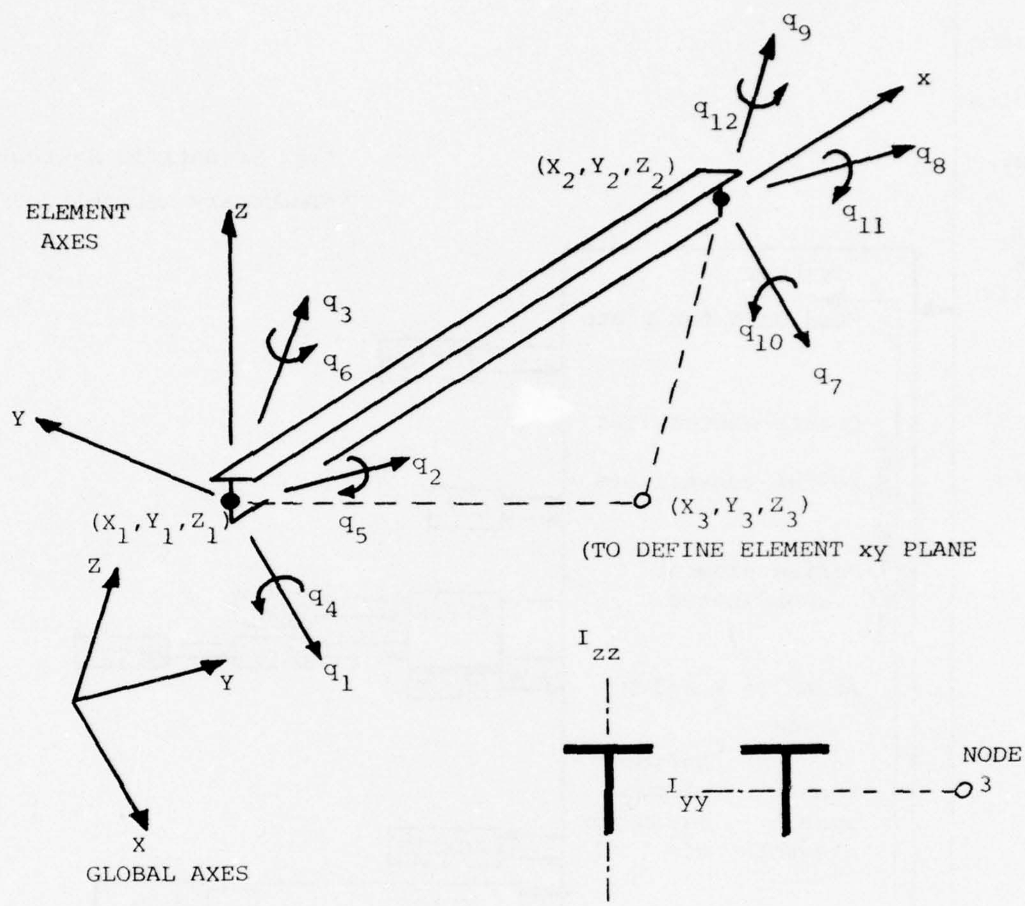

REQUIRED ELEMENT PROPERTIES:

E,G = Young's modulus, shear modulus

A = Cross section area

I_{yy}, I_{zz}, I_{yz} = Cross section inertias for bending

J = Torsion Constant

FIG. 34 CONVENTIONS FOR ELEMENT STIF2

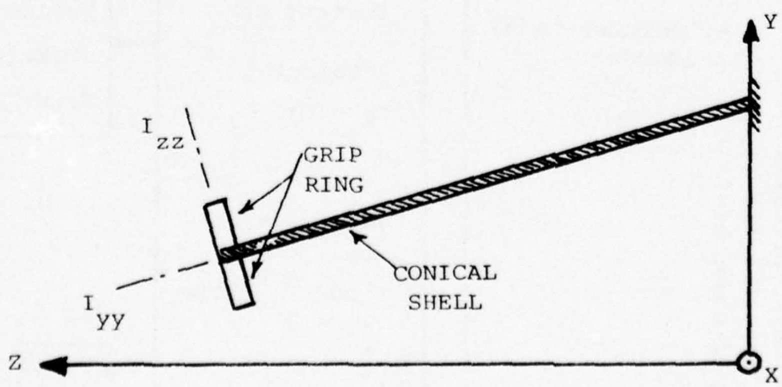

FIG. 35 ORIENTATION OF GRIP RING STIFFENERS ASSUMED IN SUBROUTINE AMMRC4

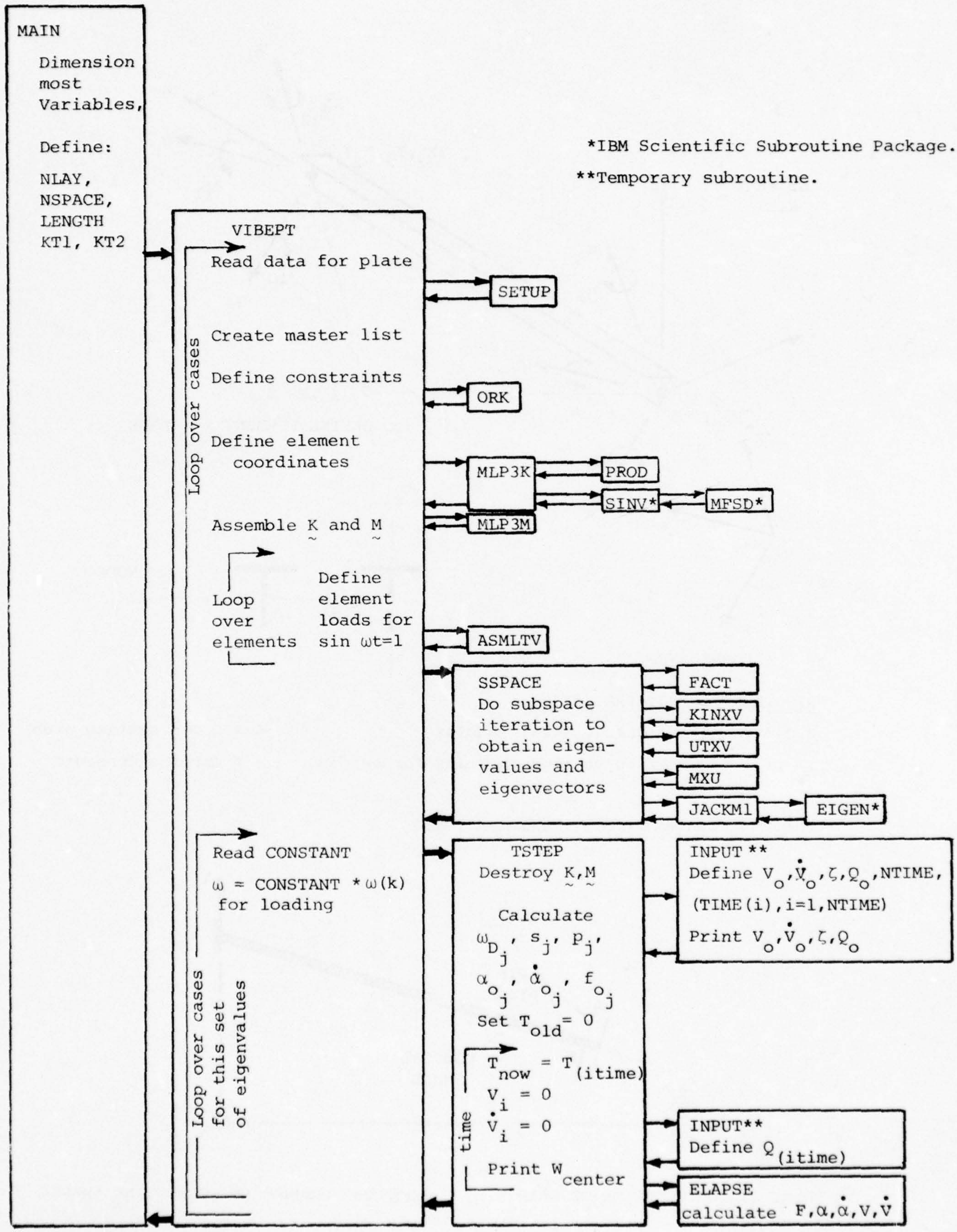

FIG. 36 FLOW DIAGRAM FOR SUBROUTINE VIBEPT

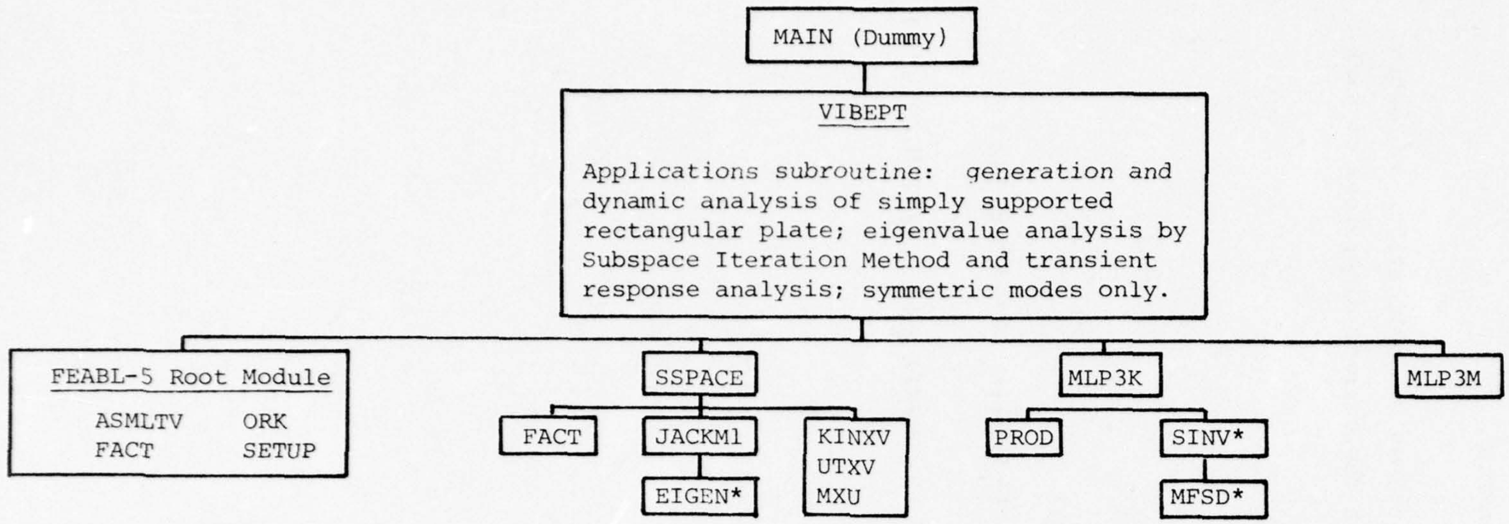

*IBM Scientific Subroutine Package.

FIG. 37 MODULAR ORGANIZATION FOR EXECUTION OF SUBROUTINE VIBEPT

APPENDIX A

SUBROUTINE AMMRC2

This appendix contains FORTRAN-IV listings of applications subroutine AMMRC2 and the dummy MAIN program in which the correct dimensions of variables are established.

```
C MAIN FOR AMMRC2
      DIMENSION RE(35000), IN(35000)
      EQUIVALENCE (RE(1), IN(1))
      DIMENSION XEL(1,9),XR(1),CMC(1,3,3),HI(2),XEL2(1,6)
      DATA LENGTH,NLY/35000,1/
      NLYP1=NLY+1
      CALL AMMRC2(LENGTH,NLY,NLYP1,RE,IN,XEL,XEL2,XR,CMC,HI,IP)
      STOP
      END
```

```
      SUBROUTINE AMMRC2(LENGTH,NLY,NLY1,RE,IN,XEL,XEL2,XR,CMC,HI,IP)      AMM20001
C FEABL-4 MAIN FOR ASRL & AMMRC PLATE BENDING WITH CUTOUT EXPERIMENTS    AMM20002
C                                                                         AMM20003
C                                                                         AMM20004
C                                                                         AMM20005
C                                                                         AMM20006
C                                                                         AMM20007
C                                                                         AMM20008
C                                                                         AMM20009
C                                                                         AMM20010
C                                                                         AMM20011
C                                                                         AMM20012
C THIS VERSION USES SPILKER MLP3K ELEMENT AND DOES NOT REQUIRE CONVT     AMM20013
C SINGLE PRECISION VERSION FOR USE AT AMMRC WATERTOWN........            AMM20014
      DIMENSION RE(1),IN(1)                                               AMM20015
      COMMON /IO/ KR, KW, KP, KT1, KT2, KT3                               AMM20016
      COMMON /SIZE/ NET, NDT                                              AMM20017
      COMMON /BEGIN/ ICON,IKCUNT,ILNZ,IMASTR,IQ,IK                        AMM20018
      COMMON /END/ LCON,LKCUNT,LLNZ,LMASTR,LQ,LK                          AMM20019
      DIMENSION X(5),Y(5),Q(20),LINE1(45),LINE2(45),LINE3(45),DY(4),      AMM20020
     &          BETA(352),XSP(5),YSP(5),ELK(210)                          AMM20021
      DIMENSION XEL(NLY,9),XR(NLY),XEL2(NLY,6),HI(NLY1),CMC(NLY,3,3)      AMM20022
      DATA PI/3.141593/                                                   AMM20023
      KR = 5                                                              AMM20024
      KW = 6                                                              AMM20025
      READ (KR,5000) NCASES, KT1                                          AMM20026
 5000 FORMAT(2I5)                                                         AMM20027
      WRITE (KW,800) NCASES, NLY, KT1                                     AMM20028
  800 FORMAT(13H0AMMRC ANALYSIS OF,I4,11H CASES WITH,I3,16H LAYERS AND KAMM20029
     &T1=,I2,/,28H ANALYSIS WITH MLP3K ELEMENT)                           AMM20030
      DO 1000 ICASE = 1,NCASES                                            AMM20031
      DO 100 I = 1,20                                                     AMM20032
  100 Q(I) = 0.                                                           AMM20033
      READ (KR,500) R, A, B, A1, A2, H, OPTION                            AMM20034
      DO 1 I = 1,NLY                                                      AMM20035
      READ (KR,500) XR(I), HI(I), (XEL(I,J), J = 1,9)                     AMM20036
```

```
      HI(I) = HI(I)-0.5*H                                              AMM20037
      XEL2(I,1) = XEL(I,1)                                             AMM20038
      XEL2(I,2) = XEL(I,2)                                             AMM20039
      XEL2(I,3) = XEL(I,6)                                             AMM20040
      XEL2(I,4) = XEL(I,4)                                             AMM20041
      XEL2(I,5) = XEL(I,9)                                             AMM20042
    1 XEL2(I,6) = XEL(I,7)                                             AMM20043
  500 FORMAT(8E10.3)                                                   AMM20044
      HI(NLY+1) = 0.5*H                                                AMM20045
C MESH SIZING CALCULATIONS & AUXILIARY COUNTERS                        AMM20046
      EDGE = PI*R/16.                                                  AMM20047
      EE = (B-R)/EDGE+0.5                                              AMM20048
      NER = EE                                                         AMM20049
      NNR = NER+1                                                      AMM20050
      EE = (A-B-A2)/(2.*EDGE)+0.5                                      AMM20051
      NEXA = EE                                                        AMM20052
      IF (NEXA .EQ. 0) NEXA = 1                                        AMM20053
      EE = (A2-A1)/(2.*EDGE)+0.5                                       AMM20054
      NEXB = EE                                                        AMM20055
      IF (NEXB .EQ. 0) NEXB = 1                                        AMM20056
      EE = A1/(2.*EDGE)+0.5                                            AMM20057
      NEXC = EE                                                        AMM20058
      IF (NEXC .EQ. 0) NEXC = 1                                        AMM20059
      DXA = (A-B-A2)/NEXA                                              AMM20060
      DXB = (A2-A1)/NEXB                                               AMM20061
      DXC = A1/NEXC                                                    AMM20062
      NET = 8*NER+4*(NEXA+NEXB+NEXC)                                   AMM20063
      NNT = 9*NNR+5*(NEXA+NEXB+NEXC)                                   AMM20064
      NDPN = 5                                                         AMM20065
      NDT = NDPN*NNT                                                   AMM20066
      NCON = 4*NNR+2*(NEXA+NEXB+NEXC)+5                                AMM20067
      NDOFT = 9*NDPN                                                   AMM20068
      NDPE = 4*NDPN                                                    AMM20069
      LIST = NET*(NDPE+1)                                              AMM20070
      NDOFB = 5*NDPN                                                   AMM20071
      WRITE (KW,801) ICASE, R, A, B, A1, A2, H, OPTION                 AMM20072
```

```
801 FORMAT(15HIINPUT FOR CASE,I4,//,4H R =,E10.3,/,4H A =,E10.3,/,4H B
   & =,E10.3,/,4H A1=,E10.3,/,4H A2=,E10.3,/,4H H =,E10.3,/,4H CP=,
   &F10.1)
    WRITE (KW,802) NLY
802 FORMAT(15HCPROPERTIES FOR,I3,7H LAYERS,/,1X,10HRCTA ANGLE,1X,10HIN
   &TRLYR HT,5X,2HE1,9X,2HE2,9X,2HE3,8X,4HNU23,7X,4HNU13,7X,4HNU12,7X,
   &4HG 23,7X,4HG 13,7X,4HG 12,/,11(1X,10H----------))
    DO 83 I = 1,NLY
 83 WRITE (KW,803) XR(I), HI(I), (XEL(I,J), J = 1,9)
803 FORMAT(11(1X,E10.3))
    WRITE (KW,804) NER, NEXA, NEXB, NEXC, NET, NNT, NDPN, NDT, NCCN,
   &                NDOFT, NDOFB, LIST
804 FORMAT(21HOMESH SIZING RESULTS:,//,7H   NER=,I6,/,7H  NEXA=,I6,/,
   &7H  NEXB=,I6,/,7H  NEXC=,I6,/,7H   NET=,I6,/,7H   NNT=,I6,/,7H  ND
   &PN=,I6,/,7H   NDT=,I6,/,7H  NCCN=,I6,/,7H NDOFT=,I6,/,7H NDOFB=,I6
   &,/,7H  LIST=,I6)
    CALL SETUP(LENGTH,NCON,LIST,RE,IN)
    ND1 = NDPN*9*NNR
    NSTO = NDOFT*ND1+NDOFB*(NDT-ND1)
    LK = IK+NSTO
    WRITE (KW,805) IK, NSTO, LK
805 FORMAT(18HOSTORAGE ESTIMATE:,//,6H   IK=,I6,/,6H NSTO=,I6,/,6H   L
   &K=,I6,/,32H USE 1.2XLK IF RUN BOMBS IN CORK,//)
C ASSEMBLY LIST IN DATA VECTOR; STORE ELEMENT COORDINATES, TYPE AND
C CENTROID IN FILE 20
    REWIND 20
    LP = IMASTR
    L = LP+NET
    DO 5 I = 1,NER
    DO 5 J = 1,8
    T2 = J*PI/16.
    T1 = T2-PI/16.
    IF (J .GT. 4) GO TO 2
    SR1 = (B/COS(T1)-R)/NER
    SR2 = (B/COS(T2)-R)/NER
    GO TO 3
```

```
2 SR1 = (B/SIN(T1)-R)/NER                                        AMM20109
  SR2 = (B/SIN(T2)-R)/NER                                        AMM20110
3 X(1) = (R+(I-1)*SR1)*COS(T1)                                   AMM20111
  X(2) = (R+I*SR1)*COS(T1)                                       AMM20112
  X(3) = (R+I*SR2)*COS(T2)                                       AMM20113
  X(4) = (R+(I-1)*SR2)*COS(T2)                                   AMM20114
  Y(1) = (R+(I-1)*SR1)*SIN(T1)                                   AMM20115
  Y(2) = (R+I*SR1)*SIN(T1)                                       AMM20116
  Y(3) = (R+I*SR2)*SIN(T2)                                       AMM20117
  Y(4) = (R+(I-1)*SR2)*SIN(T2)                                   AMM20118
  IF (I .EQ. NER .AND. J .LE. 4) DY(J) = Y(3)-Y(2)               AMM20119
  IN(LP) = L                                                     AMM20120
  KM1 = (I-1)*NDOFT+(J-1)*NDPN                                   AMM20121
  DO 4 K = 1,NDPN                                                AMM20122
  IN(L+K-1) = KM1+K                                              AMM20123
  IN(L+NDPN+K-1) = KM1+NDOFT+K                                   AMM20124
  IN(L+2*NDPN+K-1) = KM1+NDOFT+NDPN+K                            AMM20125
  IN(L+3*NDPN+K-1) = KM1+NDPN+K                                  AMM20126
  IF (I .LT. NER) GO TO 4                                        AMM20127
  IF (J .GT. 4) GO TO 4                                          AMM20128
  LINE3(NDPN*J-NDPN+K) = KM1+NDOFT+K                             AMM20129
  LINE3(NDPN*J+K) = KM1+NDOFT+NDPN+K                             AMM20130
4 CONTINUE                                                       AMM20131
  LIST = KM1+NDOFT+2*NDPN                                        AMM20132
  WRITE (20) X, Y                                                AMM20133
  LP = LP+1                                                      AMM20134
5 L = L+NDPE                                                     AMM20135
  DO 6 I = 2,4                                                   AMM20136
6 DY(I) = DY(I)+DY(I-1)                                          AMM20137
  DO 9 I = 1,NEXA                                                AMM20138
  X(1) = B+(I-1)*DXA                                             AMM20139
  X(2) = X(1)+DXA                                                AMM20140
  X(3) = X(2)                                                    AMM20141
  X(4) = X(1)                                                    AMM20142
  DO 9 J = 1,4                                                   AMM20143
  IF (J .EQ. 1) Y(1) = 0.                                        AMM20144
```

```
      IF (J .GT. 1) Y(1) = DY(J-1)                                      AMM20145
      Y(2) = Y(1)                                                       AMM20146
      Y(3) = DY(J)                                                      AMM20147
      Y(4) = DY(J)                                                      AMM20148
      KM1 = LIST+(I-1)*NDOFB+(J-1)*NDPN                                 AMM20149
      IN(LP) = L                                                        AMM20150
      DO 8 K = 1,NDPN                                                   AMM20151
      IN(L+K-1) = KM1-NDOFB+K                                           AMM20152
      IN(L+NDPN+K-1) = KM1+K                                            AMM20153
      IN(L+2*NDPN+K-1) = KM1+NDPN+K                                     AMM20154
      IN(L+3*NDPN+K-1) = KM1-NDOFB+NDPN+K                               AMM20155
      IF (I .GT. 1) GO TO 7                                             AMM20156
      IN(L+K-1) = LINE3(NDPN*J-NDPN+K)                                  AMM20157
      IN(L+3*NDPN+K-1) = LINE3(NDPN*J+K)                                AMM20158
    7 IF (I .LT. NEXA) GO TO 8                                          AMM20159
      LINE2(NDPN*J-NDPN+K) = KM1+K                                      AMM20160
      LINE2(NDPN*J+K) = KM1+NDPN+K                                      AMM20161
    8 CONTINUE                                                          AMM20162
      NNT = KM1+2*NDPN                                                  AMM20163
      WRITE (20) X, Y                                                   AMM20164
      LP = LP+1                                                         AMM20165
    9 L = L+NDPE                                                        AMM20166
      DO 11 I = 1,NEXB                                                  AMM20167
      X(1) = A-A2+(I-1)*DXB                                             AMM20168
      X(2) = X(1)+DXB                                                   AMM20169
      X(3) = X(2)                                                       AMM20170
      X(4) = X(1)                                                       AMM20171
      DO 11 J = 1,4                                                     AMM20172
      IF (J .EQ. 1) Y(1) = 0.                                           AMM20173
      IF (J .GT. 1) Y(1) = DY(J-1)                                      AMM20174
      Y(2) = Y(1)                                                       AMM20175
      Y(3) = DY(J)                                                      AMM20176
      Y(4) = DY(J)                                                      AMM20177
      KM1 = NNT+(I-1)*NDOFB+(J-1)*NDPN                                  AMM20178
      IN(LP) = L                                                        AMM20179
      DO 10 K = 1,NDPN                                                  AMM20180
```

```
      IN(L+K-1) = KM1-NDOFB+K                                           AMM20181
      IN(L+NDPN+K-1) = KM1+K                                            AMM20182
      IN(L+2*NDPN+K-1) = KM1+NDPN+K                                     AMM20183
      IN(L+3*NDPN+K-1) = KM1-NDOFB+NDPN+K                               AMM20184
      IF (I .LT. NEXB) GO TO 10                                         AMM20185
      LINE1(NDPN*J-NDPN+K) = KM1+K                                      AMM20186
      LINE1(NDPN*J+K) = KM1+NDPN+K                                      AMM20187
   10 CONTINUE                                                          AMM20188
      LIST = KM1+2*NDPN                                                 AMM20189
      WRITE (20) X, Y                                                   AMM20190
      LP = LP+1                                                         AMM20191
   11 L = L+NDPE                                                        AMM20192
      DO 13 I = 1,NEXC                                                  AMM20193
      X(1) = A-A1+(I-1)*DXC                                             AMM20194
      X(2) = X(1)+DXC                                                   AMM20195
      X(3) = X(2)                                                       AMM20196
      X(4) = X(1)                                                       AMM20197
      DO 13 J = 1,4                                                     AMM20198
      IF (J .EQ. 1) Y(1) = 0.                                           AMM20199
      IF (J .GT. 1) Y(1) = DY(J-1)                                      AMM20200
      Y(2) = Y(1)                                                       AMM20201
      Y(3) = DY(J)                                                      AMM20202
      Y(4) = DY(J)                                                      AMM20203
      KM1 = LIST+(I-1)*NDOFB+(J-1)*NDPN                                 AMM20204
      IN(LP) = L                                                        AMM20205
      DO 12 K = 1,NDPN                                                  AMM20206
      IN(L+K-1) = KM1-NDOFB+K                                           AMM20207
      IN(L+NDPN+K-1) = KM1+K                                            AMM20208
      IN(L+2*NDPN+K-1) = KM1+NDPN+K                                     AMM20209
   12 IN(L+3*NDPN+K-1) = KM1-NDOFB+NDPN+K                               AMM20210
      WRITE (20) X, Y                                                   AMM20211
      LP = LP+1                                                         AMM20212
   13 L = L+NDPE                                                        AMM20213
      IF (KT1 .EQ. KW) GO TO 15                                         AMM20214
      LP = IMASTR                                                       AMM20215
      L = LP+NET                                                        AMM20216
```

```
      LIST = L+NDPE-1                                                   AMM20217
      DO 14 I = 1,NET                                                   AMM20218
      WRITE (KW,600) IN(LP), (IN(J), J = L,LIST)                        AMM20219
  600 FORMAT(1X,26I5)                                                   AMM20220
      LP = LP+1                                                         AMM20221
      L = L+NDPE                                                        AMM20222
   14 LIST = LIST+NDPE                                                  AMM20223
   15 CALL ORK(LENGTH,RE,IN)                                            AMM20224
C ASSEMBLY; STOR B-MATRICES IN FILE 30                                  AMM20225
      REWIND 20                                                         AMM20226
      REWIND 30                                                         AMM20227
      DO 16 L = 1,NET                                                   AMM20228
      READ (20) X, Y                                                    AMM20229
      CALL MLP3K(ELK,NLY,XEL2,HI,XR,X,Y,BETA,CMC,NLY,4,IP,KW)           AMM20230
      WRITE (30) BETA, CMC                                              AMM20231
      CALL ASMLTV(L,NDPE,ELK,Q,RE,IN)                                   AMM20232
   16 CONTINUE                                                          AMM20233
C CONSTRAINTS ALGORITHM                                                 AMM20234
      NNT = 2                                                           AMM20235
      L = ICON                                                          AMM20236
      DO 17 I = 1,NNR                                                   AMM20237
      KM1 = NDPN*(I-1)*9                                                AMM20238
      K = NDPN*(9*(I-1)+8)                                              AMM20239
      DO 17 J = 2,NNT,2                                                 AMM20240
      IN(L) = KM1+J                                                     AMM20241
      IN(L+1) = K+J-1                                                   AMM20242
C CONSTRAIN THETA Y                                                     AMM20243
      IN(L+2) = KM1+J+2                                                 AMM20244
C CONSTRAIN THETA X                                                     AMM20245
      IN(L+3) = K+J+3                                                   AMM20246
   17 L = L+4                                                           AMM20247
      LP = NEXA+NEXB+NEXC                                               AMM20248
      LIST = 9*NNR                                                      AMM20249
      DO 18 I = 1,LP                                                    AMM20250
      KM1 = NDPN*(LIST+5*(I-1))                                         AMM20251
      DO 18 J = 2,NNT,2                                                 AMM20252
```

```
      IN(L) = KM1+J                                                     AMM20253
C CONSTRAIN THETA X                                                     AMM20254
      IN(L+1) = KM1+J+2                                                 AMM20255
   18 L = L+2                                                           AMM20256
      DO 19 I = 1,5                                                     AMM20257
      KM1 = LINE1(NDPN*I)-2                                             AMM20258
      IN(L) = KM1                                                       AMM20259
   19 L = L+1                                                           AMM20260
      CALL BCON(RE,IN)                                                  AMM20261
C FORCES ON LINE2 (UNIT LINE LOAD = 1 LB/IN)                            AMM20262
      DO 20 I = 1,3                                                     AMM20263
   20 DY(5-I) = DY(5-I)-DY(4-I)                                         AMM20264
      DO 24 J = 1,5                                                     AMM20265
      KM1 = IQ+LINE2(J*NDPN)-3                                          AMM20266
      GO TO (21,22,22,22,23), J                                         AMM20267
   21 RE(KM1) = -0.5*DY(1)                                              AMM20268
      GO TO 24                                                          AMM20269
   22 RE(KM1) = -0.5*(DY(J-1)+DY(J))                                    AMM20270
      GO TO 24                                                          AMM20271
   23 RE(KM1) = -0.5*DY(4)                                              AMM20272
   24 CONTINUE                                                          AMM20273
      CALL FACT(1,RE,IN)                                                AMM20274
      CALL SIMULQ(EE,RE,IN)                                             AMM20275
C STRESS ANALYSIS                                                       AMM20276
      DO 30 ITIME = 1,2
      ISDIR = ITIME-1
      NNT = NLY+1                                                       AMM20277
      REWIND 20                                                         AMM20278
      REWIND 30                                                         AMM20279
      DO 25 L = 1,NET                                                   AMM20280
      READ (20) X, Y                                                    AMM20281
      READ (30) BETA, CMC                                               AMM20282
      CALL XTRACT(L,NDPE,Q,RE,IN)                                       AMM20283
      CALL MLP3S(L,Q,BETA,CMC,NLY,HI,NLY,4,0,XSP,YSP,X,Y,XEL2,XR,ISDIR, AMM2284A
     +KW)                                                               AMM2284B
   25 CONTINUE                                                          AMM20285
```

```
C STRESSES ALONG VERTICAL CL                                            AMM20286
      REWIND 20                                                         AMM20287
      REWIND 30                                                         AMM20288
      LP = 8*NER                                                        AMM20289
      WRITE (KW,901)                                                    AMM20290
  901 FORMAT(22H0STRESSES ALONG Y AXIS)                                 AMM20291
      XSP(1) = 0.E0                                                     AMM20292
      DO 27 L = 1,LP                                                    AMM20293
      READ (20) X, Y                                                    AMM20294
      READ (30) BETA, CMC                                               AMM20295
      IF (8*(L/8) .NE. L) GO TO 27                                      AMM20296
      CALL XTRACT(L,NDPE,Q,RE,IN)                                       AMM20297
      YSP(1) = 0.5*(Y(3)+Y(4))                                          AMM20298
      CALL MLP3S(L,Q,BETA,CMC,NLY,HI,NLY,4,0,XSP,YSP,X,Y,XEL2,XR,ISDIR, AMM2299A
     +KW)                                                               AMM2299B
   27 CONTINUE                                                          AMM20300
C STRESSES ALONG HORIZONTAL CL                                          AMM20301
      REWIND 20                                                         AMM20302
      REWIND 30                                                         AMM20303
      LP = 8*NER-7                                                      AMM20304
      WRITE (KW,902)                                                    AMM20305
  902 FORMAT(22H0STRESSES ALONG X AXIS)                                 AMM20306
      YSP(1) = 0.E0                                                     AMM20307
      DO 29 L = 1,NET                                                   AMM20308
      READ (20) X, Y                                                    AMM20309
      READ (30) BETA, CMC                                               AMM20310
      IF (L .GT. LP) GO TO 28                                           AMM20311
      IF (8*((L-1)/8) .NE. L-1) GO TO 29                                AMM20312
      XSP(1) = 0.5*(X(1)+X(2))                                          AMM20313
      CALL XTRACT(L,NDPE,Q,RE,IN)                                       AMM20314
      CALL MLP3S(L,Q,BETA,CMC,NLY,HI,NLY,4,0,XSP,YSP,X,Y,XEL2,XR,ISDIR, AMM2315A
     +KW)                                                               AMM2315B
      GO TO 29                                                          AMM20316
   28 IF (4*((L-8*NER-1)/4) .NE. L-8*NER-1) GO TO 29                    AMM20317
      IF (L-8*NER-1 .LT. 0) GO TO 29                                    AMM20318
      XSP(1) = 0.5*(X(1)+X(2))                                          AMM20319
```

```
      CALL XTRACT(L,NDPE,Q,RE,IN)                                       AMM20320
      CALL MLP3S(L,Q,BETA,CMC,NLY,HI,NLY,4,0,XSP,YSP,X,Y,XEL2,XR,ISDIR, AMM2321A
     +KW)                                                               AMM2321B
   29 CONTINUE                                                          AMM20322
   30 CONTINUE
 1000 CONTINUE                                                          AMM20323
      RETURN                                                            AMM20324
      END                                                               AMM20325
```

APPENDIX B

SUBROUTINE AMMRC3

This appendix contains FORTRAN-IV listings of applications subroutine AMMRC3 and the dummy MAIN program in which the correct dimensions of variables are established.

```
C MAIN FOR AMMRC3
      DIMENSION RE(10000), IN(10000)
      DIMENSION CM(1,3,3,10), CMC(1,3,3), H(1), XEL(1,6), XR(1), Z(1)
      EQUIVALENCE(RE(1), IN(1))
      DATA LENGTH,NLY,NLYP1/10000,1,2/
      CALL AMMRC3(LENGTH,NLY,NLYP1,RE,IN,CM,CMC,H,XEL,XR,Z)
      STOP
      END
```

```
      SUBROUTINE AMMRC3(LENGTH,NLY,NLYP1,RE,IN,CM,CMC,H,XEL,XR,Z)        AMM30001
C SUB-MAIN FOR ANALYSIS OF HALF-MODEL OF CONICAL SHELL                    AMM30002
C REQUIRES FOLLOWING ITEMS TO FORM EXECUTABLE LOAD MODULE:                AMM30003
C    1. ASRL/FEABL-2 SUBRS ASMLTV,ECON,FACT,CRK,SETUP,SIMULT,XTRACT       AMM30004
C    2. ASRL/EGL SUBRS MLP3K,MLP3S,PROD                                   AMM30005
C    3. IBM/SSP SUBRS MFSD,SINV                                           AMM30006
C    4. DUMMY MAIN PROGRAM WITH CORRECT DIMENSION DECLARATIONS            AMM30007
C    5. SEQUENTIAL-ACCESS SCRATCH FILE (FORTRAN UNIT NO. = 20): WITH      AMM30008
C       418 UNFORMATTED SGL-PREC WORDS PER RECORD; NO. OF RECORDS .GE.    AMM30009
C       NO. OF CORE PLANES INTO WHICH FINITE-ELEMENT MODEL IS DIVIDED     AMM30010
C COPYRIGHT (C) 1975  MASSACHUSETTS INSTITUTE OF TECHNOLOGY               AMM30011
C SINGLE PRECISION VERSION FOR AMMRC WATERTOWN.............               AMM30012
      DIMENSION CM(NLY,3,3,10), CMC(NLY,3,3), H(NLY), XEL(NLY,6),         AMM30013
     &          XR(NLY), Z(NLYP1)                                         AMM30014
      DIMENSION RE(1), IN(1)                                              AMM30015
      COMMON /IO/ KR, KW, KP, KT1,KT2,KT3                                 AMM30016
      COMMON /SIZE/ NET, NDT                                              AMM30017
      COMMON /BEGIN/ ICON,IKOUNT,ILNZ,IMASTR,IQ,IK                        AMM30018
      COMMON /END/ LCON,LKOUNT,LLNZ,LMASTR,LQ,LK                          AMM30019
      DIMENSION X(5), Y(5), Q(20), QL(20), BMTRX(352), E(352,10),         AMM30020
     &          XS(5), YS(5), EKL(210,10), EKR(20,20), EKG(210),          AMM30021
     &          D(3,3), D1(3,3), D2(3,3), DIR1(3,3), DIR2(3,3),           AMM30022
     &          DE(20,20), XX(4,10), YY(4,10)                             AMM30023
      DATA PI/3.141593/, DE/400*0.E0/, Q/20*0.E0/                         AMM30024
      KR = 5                                                              AMM30025
      KW = 6                                                              AMM30026
      KT1 = KW                                                            AMM30027
      READ (KR,500) NCASES                                                AMM30028
  500 FORMAT(16I5)                                                        AMM30029
      WRITE (KW,600) NLY, NCASES                                          AMM30030
  600 FORMAT(19H0ENTRY AMMRC PGM 3:,/,12H0ANALYSIS OF,I3,21H-LAYER CONICAMM30031
     &AL SHELLS,/,9H0TOTAL OF,I4,6H CASES)                                AMM30032
      DO 1000 ICASE = 1,NCASES                                            AMM30033
C INPUT GEOMETRY                                                          AMM30034
      READ (KR,500) NGOR, NEPG                                            AMM30035
      READ (KR,501) R1, R2, SPAN                                          AMM30036
```

```
  501 FORMAT(8E10.3)                                                    AMM30037
C INPUT LOADS                                                           AMM30038
      READ (KR,501) BENDMT, COMP, SHEAR                                 AMM30039
C INPUT LAYER PROPERTIES                                                AMM30040
      HTOT = 0.                                                         AMM30041
      DO 1 I = 1,NLY                                                    AMM30042
      READ (KR,501) H(I), XR(I), (XEL(I,J), J = 1,6)                    AMM30043
    1 HTOT = HTOT+H(I)                                                  AMM30044
      Z(1) = -0.5*HTOT                                                  AMM30045
      DO 2 I = 1,NLY                                                    AMM30046
    2 Z(I+1) = Z(I)+H(I)                                                AMM30047
C DUMP INPUT DATA                                                       AMM30048
      WRITE (KW,601) ICASE, NGOR, NEPG, R1, R2, SPAN,                   AMM30049
     &                  BENDMT, COMP, SHEAR                             AMM30050
  601 FORMAT(5HICASE,I4,11X,12HTOTAL GORES=,12X,I10,/,20X,24HTOTAL ELEMEAMM30051
     &NTS PER GORE=,I10,/,20X,14HTIP RADIUS R1=,10X,E10.3,/,20X,15HROOT AMM30052
     &RADIUS R2=,9X,E10.3,/,20X,5HSPAN=,19X,E10.3,/,20X,15HBENDING MOMENAMM30053
     &T=,9X,E10.3,/,20X,18HAXIAL COMPRESSION=,6X,E10.3,/,20X,6HSHEAR=,18AMM30054
     &X,E10.3,//,50HCTABLE OF LAYER PROPERTIES FROM INSIDE TO OUTSIDE:,/AMM30055
     &/,1X,5HLAYER,1X,10H THICKNESS,1X,10HPLY  ANGLE,5X,2HE1,9X,2HE2,8X,AMM30056
     &4HNU12,7X,4HNU23,7X,4HG 12,7X,4HG 23,/,1X,5H-----,8(1X,10H--------AMM30057
     &--))                                                              AMM30058
      DO 3 I = 1,NLY                                                    AMM30059
    3 WRITE (KW,602) I, H(I), XR(I), (XEL(I,J), J = 1,6)                AMM30060
  602 FORMAT(1X,I5,8(1X,E10.3))                                         AMM30061
C SIZING                                                                AMM30062
      NET = NGOR*NEPG                                                   AMM30063
      NOT = 5*(NGOR+1)*(NEPG+1)                                         AMM30064
      NDL = 5*(NEPG+1)                                                  AMM30065
      NCON = 5*(NGOR+1)+4*NEPG                                          AMM30066
      LIST = 21*NET                                                     AMM30067
      CALL SETUP(LENGTH,NCON,LIST,RE,IN)                                AMM30068
C COUPLING                                                              AMM30069
      LP = IMASTR                                                       AMM30070
      L = LP+NET-1                                                      AMM30071
      DO 6 I = 1,NGOR                                                   AMM30072
```

```
      DO 6 J = 1,NEPG                                                   AMM30073
      IN(LP) = L+1                                                      AMM30074
      K = NDL*(I-1)+5*(J-1)                                             AMM30075
      DO 4 KK = 1,10                                                    AMM30076
    4 IN(L+KK) = K+KK                                                   AMM30077
      DO 5 KK = 1,5                                                     AMM30078
      IN(L+10+KK) = K+5+KK+NDL                                          AMM30079
    5 IN(L+15+KK) = K+KK+NDL                                            AMM30080
      LP = LP+1                                                         AMM30081
    6 L = L+20                                                          AMM30082
      CALL DRK(LENGTH,RE,IN)                                            AMM30083
C ELEMENT GENERATION IN GORE PLANE                                      AMM30084
      BETA2 = PI/NGOR                                                   AMM30085
      BETA = 0.5*BETA2                                                  AMM30086
      DCB = COS(BETA)                                                   AMM30087
      DSB = SIN(BETA)                                                   AMM30088
      AL = SQRT(((R2-R1)*DCB)**2+SPAN**2)                               AMM30089
      DX = AL/NEPG                                                      AMM30090
      DY = (R2-R1)*DSB/NEPG                                             AMM30091
      DO 10 L = 1,NEPG                                                  AMM30092
      X(1) = (L-1)*DX                                                   AMM30093
      X(2) = L*DX                                                       AMM30094
      X(3) = X(2)                                                       AMM30095
      X(4) = X(1)                                                       AMM30096
      Y(4) = R1*DSB+(L-1)*DY                                            AMM30097
      Y(3) = R1*DSB+L*DY                                                AMM30098
      Y(2) = -Y(3)                                                      AMM30099
      Y(1) = -Y(4)                                                      AMM30100
      CALL MLP3K(EKG,NLY,XEL,Z,XR,X,Y,BMTRX,CMC,NLY,4,1,KW)             AMM30101
      DO 7 I = 1,210                                                    AMM30102
    7 EKL(I,L) = EKG(I)                                                 AMM30103
      DO 8 I = 1,352                                                    AMM30104
    8 B(I,L) = BMTRX(I)                                                 AMM30105
      DO 9 I = 1,NLY                                                    AMM30106
      DO 9 J = 1,3                                                      AMM30107
      DO 9 K = 1,3                                                      AMM30108
```

AD-A031 361 MASSACHUSETTS INST OF TECH CAMBRIDGE AEROELASTIC AND--ETC F/G 20/11
USE OF THE HYBRID-STRESS FINITE-ELEMENT MODEL FOR THE STATIC AN--ETC(U)
SEP 76 R L SPILKER, O ORRINGER, E A WITMER DAAG46-75-C-0055
UNCLASSIFIED ASRL-TR-181-2 AMMRC-CTR-76-29 NL

3 OF 3
AD
A031361

END
DATE
FILMED
11 — 76

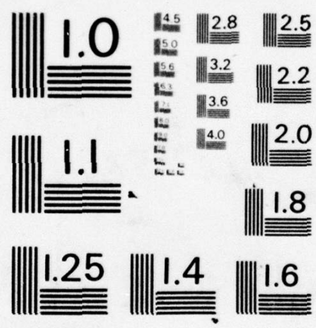

MICROCOPY RESOLUTION TEST CHART

NATIONAL BUREAU OF STANDARDS-1963-A

```
    9 CM(I,J,K,L) = CMC(I,J,K)                                        AMM30109
      DO 10 I = 1,4                                                   AMM30110
      XX(I,L) = X(I)                                                  AMM30111
   10 YY(I,L) = Y(I)                                                  AMM30112
C TRANSFORMATION/ASSEMBLY                                             AMM30113
      REWIND 20                                                       AMM30114
      AL12 = SQRT((R2-R1)**2+SPAN**2)                                 AMM30115
      LP = 1                                                          AMM30116
      DO 17 N = 1,NGOR                                                AMM30117
      T1 = (N-1)*BETA2                                                AMM30118
      T2 = N*BETA2                                                    AMM30119
      ALFA = 0.5*(T1+T2)                                              AMM30120
C GORE PLANE DIRECTION COSINES                                        AMM30121
      D(1,1) = (R2-R1)*DCB*COS(ALFA)/AL                               AMM30122
      D(1,2) = (R2-R1)*DCB*SIN(ALFA)/AL                               AMM30123
      D(1,3) = -SPAN/AL                                               AMM30124
      D(2,1) = 0.5*(COS(T2)-COS(T1))/DSB                              AMM30125
      D(2,2) = 0.5*(SIN(T2)-SIN(T1))/DSB                              AMM30126
      D(2,3) = 0.                                                     AMM30127
      D(3,1) = 0.5*SPAN*(SIN(T2)-SIN(T1))/(AL*DSB)                    AMM30128
      D(3,2) = -.5*SPAN*(COS(T2)-COS(T1))/(AL*DSB)                    AMM30129
      D(3,3) = (R2-R1)*DCB/AL                                         AMM30130
C CONE GENERATOR DIRECTION COSINES                                    AMM30131
      D1(1,1) = (R2-R1)*COS(T1)/AL12                                  AMM30132
      D2(1,1) = (R2-R1)*COS(T2)/AL12                                  AMM30133
      D1(1,2) = (R2-R1)*SIN(T1)/AL12                                  AMM30134
      D2(1,2) = (R2-R1)*SIN(T2)/AL12                                  AMM30135
      D1(1,3) = -SPAN/AL12                                            AMM30136
      D2(1,3) = -SPAN/AL12                                            AMM30137
      D1(2,1) = -SIN(T1)                                              AMM30138
      D2(2,1) = -SIN(T2)                                              AMM30139
      D1(2,2) = COS(T1)                                               AMM30140
      D2(2,2) = COS(T2)                                               AMM30141
      D1(2,3) = 0.                                                    AMM30142
      D2(2,3) = 0.                                                    AMM30143
      D1(3,1) = SPAN*COS(T1)/AL12                                     AMM30144
```

```
      D2(3,1) = SPAN*COS(T2)/AL12                                         AMM30145
      D1(3,2) = SPAN*SIN(T1)/AL12                                         AMM30146
      D2(3,2) = SPAN*SIN(T2)/AL12                                         AMM30147
      D1(3,3) = (R2-R1)/AL12                                              AMM30148
      D2(3,3) = (R2-R1)/AL12                                              AMM30149
C DIRECT TRANSFORMS SKIPPING REFERENCE SYSTEM                             AMM30150
      DO 12 I = 1,3                                                       AMM30151
      DO 12 J = 1,3                                                       AMM30152
      DIR1(I,J) = 0.                                                      AMM30153
      DIR2(I,J) = 0.                                                      AMM30154
      DO 12 K = 1,3                                                       AMM30155
      DIR1(I,J) = DIR1(I,J)+D1(I,K)*D(J,K)                                AMM30156
   12 DIR2(I,J) = DIR2(I,J)+D2(I,K)*D(J,K)                                AMM30157
C ELEMENT TRANSFORM                                                       AMM30158
      DO 13 I = 1,3                                                       AMM30159
      DO 13 J = 1,3                                                       AMM30160
      DE(I,J) = DIR1(I,J)                                                 AMM30161
      DE(I+5,J+5) = DIR1(I,J)                                             AMM30162
      DE(I+10,J+10) = DIR2(I,J)                                           AMM30163
   13 DE(I+15,J+15) = DIR2(I,J)                                           AMM30164
      DO 14 I = 1,2                                                       AMM30165
      DO 14 J = 1,2                                                       AMM30166
      DE(I+3,J+3) = DIR1(I,J)                                             AMM30167
      DE(I+8,J+8) = DIR1(I,J)                                             AMM30168
      DE(I+13,J+13) = DIR2(I,J)                                           AMM30169
   14 DE(I+18,J+18) = DIR2(I,J)                                           AMM30170
      WRITE (20) D1, D2, DE                                               AMM30171
C SWEEP THE GORE FROM TIP TO ROOT                                         AMM30172
      DO 17 L = 1,NEPG                                                    AMM30173
      K = 0                                                               AMM30174
      DO 15 I = 1,20                                                      AMM30175
      DO 15 J = 1,I                                                       AMM30176
      K = K+1                                                             AMM30177
      EKR(I,J) = EKL(K,L)                                                 AMM30178
   15 EKR(J,I) = EKR(I,J)                                                 AMM30179
      K = 0                                                               AMM30180
```

```
      DO 16 I = 1,20                                                    AMM30181
      DO 16 J = 1,I                                                     AMM30182
      K = K+1                                                           AMM30183
      EKG(K) = 0.                                                       AMM30184
      DO 16 KK = 1,20                                                   AMM30185
      DO 16 LL = 1,20                                                   AMM30186
   16 EKG(K) = EKG(K)+DE(I,KK)*EKR(KK,LL)*DE(J,LL)                      AMM30187
      CALL ASMLTV(LP,20,EKG,Q,RE,IN)                                    AMM30188
   17 LP = LP+1                                                         AMM30189
C CONSTRAINTS: ROOT                                                     AMM30190
      L = 1                                                             AMM30191
      LP = NGOR+1                                                       AMM30192
      DO 18 I = 1,LP                                                    AMM30193
      K = I*NDL-5                                                       AMM30194
      DO 18 J = 1,5                                                     AMM30195
      IN(L) = K+J                                                       AMM30196
   18 L = L+1                                                           AMM30197
C SYMMETRY CONSTRAINTS: EDGES                                           AMM30198
      LP = (NEPG+1)*NGOR                                                AMM30199
      DO 19 J = 1,NEPG                                                  AMM30200
C TOP                                                                   AMM30201
      IN(L) = 5*J-3                                                     AMM30202
      IN(L+1) = 5*J-1                                                   AMM30203
C BOTTOM                                                                AMM30204
      IN(L+2) = 5*(LP+J)-3                                              AMM30205
      IN(L+3) = 5*(LP+J)-1                                              AMM30206
   19 L = L+4                                                           AMM30207
      CALL BCON(RE,IN)                                                  AMM30208
C LOADS                                                                 AMM30209
      REWIND 20                                                         AMM30210
      BO2P = 0.25/NGOR                                                  AMM30211
      LP = NEPG+1                                                       AMM30212
      DO 21 N = 1,NGOR                                                  AMM30213
      T1 = (N-1)*BETA2                                                  AMM30214
      T2 = N*BETA2                                                      AMM30215
      Q(1) = BO2P*SHEAR*(SIN(T1)**2+SIN(T2)**2)                         AMM30216
```

```
      Q(3) = -BO2P*(BENDMT*(COS(T1)+COS(T2))/R1+COMP)                  AMM30217
      READ (20) D1, D2                                                  AMM30218
      DO 20 I = 1,3                                                     AMM30219
      Q(I+3) = 0.                                                       AMM30220
      Q(I+6) = 0.                                                       AMM30221
      DO 20 J = 1,3                                                     AMM30222
      Q(I+3) = Q(I+3)+D1(I,J)*Q(J)                                      AMM30223
   20 Q(I+6) = Q(I+6)+D2(I,J)*Q(J)                                      AMM30224
      K = (N-1)*NDL-1                                                   AMM30225
      DO 21 KK = 1,3                                                    AMM30226
      RE(IQ+K+KK) = RE(IQ+K+KK)+Q(KK+3)                                 AMM30227
   21 RE(IQ+K+KK+NDL) = RE(IQ+K+KK+NDL)+Q(KK+6)                         AMM30228
      ISGN = 0                                                          AMM30229
      CALL FACT(ISGN,RE,IN)                                             AMM30230
      IF (ISGN .EQ. 1) GO TO 22                                         AMM30231
      WRITE (KW,603) ICASE                                              AMM30232
  603 FORMAT(5HOCASE,I4,17H FAILED INVERSION)                           AMM30233
      GO TO 28                                                          AMM30234
   22 KT1 = 0                                                           AMM30235
      CALL SIMULQ(BO2P,RE,IN)                                           AMM30236
      KT1 = KW                                                          AMM30237
C STRESS SOLUTION                                                       AMM30238
      DO 27 ITIME = 1,2
      ISDIR = ITIME-1
      LP = 0                                                            AMM30239
      REWIND 20                                                         AMM30240
      DO 27 N = 1,NGOR                                                  AMM30241
      READ (20) D1, D2, DE                                              AMM30242
      DO 27 L = 1,NEPG                                                  AMM30243
      LP = LP+1                                                         AMM30244
      CALL XTRACT(LP,20,Q,RE,IN)                                        AMM30245
      DO 23 I = 1,20                                                    AMM30246
      QL(I) = 0.                                                        AMM30247
      DO 23 J = 1,20                                                    AMM30248
   23 QL(I) = QL(I)+DE(J,I)*Q(J)                                        AMM30249
      DO 24 I = 1,352                                                   AMM30250
```

```
   24 BMTRX(I) = B(I,L)                                                    AMM30251
      DO 25 I = 1,NLY                                                      AMM30252
      DO 25 J = 1,3                                                        AMM30253
      DO 25 K = 1,3                                                        AMM30254
   25 CMC(I,J,K) = CM(I,J,K,L)                                             AMM30255
      DO 26 I = 1,4                                                        AMM30256
      X(I) = XX(I,L)                                                       AMM30257
   26 Y(I) = YY(I,L)                                                       AMM30258
      CALL MLP3S(LP,QL,BMTRX,CMC,NLY,Z,NLY,4,0,XS,YS,X,Y,XEL,XR,ISDIR,     AMM3259A
     +KW)                                                                  AMM3259B
   27 CONTINUE                                                             AMM30260
   28 DO 1000 I = 1,20                                                     AMM30261
 1000 Q(I) = 0.                                                            AMM30262
      RETURN                                                               AMM30263
      END                                                                  AMM30264
```

APPENDIX C

SUBROUTINE AMMRC4

This appendix contains FORTRAN-IV listings of applications subroutine AMMRC4 and the dummy MAIN program in which the correct dimensions of variables are established.

```
C MAIN FOR AMMRC4 (SINGLE PRECISION)
      DIMENSION CM(1,3,3,10),CMC(1,3,3),H(1),XEL(1,6),XR(1),Z(2),RE(9000
     +),IN(9000)
      EQUIVALENCE(RE(1),IN(1))
      DATA LENGTH,NLY,NLYP1/9000,1,2/
      CALL AMMRC4(LENGTH,NLY,NLYP1,RE,IN,CM,CMC,H,XEL,XR,Z)
      STOP
      END
```

```
      SUBROUTINE AMMRC4(LENGTH,NLY,NLYP1,RE,IN,CM,CMC,H,XEL,XR,Z)        AMM40001
C SUB-MAIN FOR ANALYSIS OF HALF-MODEL OF CONICAL SHELL WITH STIFFENERS  AMM40002
C AND COSINE LOADING                                                    AMM40003
C REQUIRES FOLLOWING ITEMS TO FORM EXECUTABLE LOAD MODULE:              AMM40004
C    1. ASRL/FEABL-2 SUBRS ASMLTV,BCON,FACT,CRK,SETUP,SIMULQ,XTRACT     AMM40005
C    2. ASRL/EGL SUBRS MLP3K,MLP3S,PROD                                 AMM40006
C    3. IBM/SSP SUBRS MFSD,SINV                                         AMM40007
C    4. DUMMY MAIN PROGRAM WITH CORRECT DIMENSION DECLARATIONS          AMM40008
C    5. SEQUENTIAL-ACCESS SCRATCH FILE (FORTRAN UNIT NO. = 20): WITH    AMM40009
C       418 UNFORMATTED SGL-PREC WORDS PER RECORD; NO. OF RECORDS .GE.  AMM40010
C       NO. OF CORE PLANES INTO WHICH FINITE-ELEMENT MODEL IS DIVIDED   AMM40011
C COPYRIGHT (C) 1976  MASSACHUSETTS INSTITUTE OF TECHNOLOGY             AMM40012
C SINGLE PRECISION VERSION FOR AMMRC WATERTOWN.............             AMM40013
      DIMENSION CM(NLY,3,3,10), CMC(NLY,3,3), H(NLY), XEL(NLY,6),       AMM40014
     &          XR(NLY), Z(NLYP1)                                       AMM40015
      DIMENSION RE(1), IN(1)                                            AMM40016
      COMMON /IO/ KR, KW, KP, KT1,KT2,KT3                               AMM40017
      COMMON /SIZE/ NET, NDT                                            AMM40018
      COMMON /BEGIN/ ICON,IKOUNT,ILNZ,IMASTR,IQ,IK                      AMM40019
      COMMON /END/ LCON,LKOUNT,LLNZ,LMASTR,LQ,LK                        AMM40020
      DIMENSION X(5), Y(5), Q(20), QL(20), BMTRX(352), B(352,10),       AMM40021
     &          XS(5), YS(5), EKL(210,10), EKR(20,20), EKG(210),        AMM40022
     &          D(3,3), D1(3,3), D2(3,3), DIR1(3,3), DIR2(3,3),         AMM40023
     &          DE(20,20), XX(4,10), YY(4,10), SPROP(8), COORD(9), DUM(2AMM40024
     &          ), NODE(2), QQ(20), EKST(78), RT(12,12), ELOAD(10)      AMM40025
      DATA PI/3.141593/, DE/400*0.E0/, Q/20*0.E0/, DUM/2*0.E0/          AMM40026
      KR = 5                                                            AMM40027
      KW = 6                                                            AMM40028
      KT1 = KW                                                          AMM40029
      READ (KR,500) NCASES                                              AMM40030
  500 FORMAT(16I5)                                                      AMM40031
      WRITE (KW,600) NLY, NCASES                                        AMM40032
  600 FORMAT(19H0ENTRY AMMRC PGM 4:,/,12HCANALYSIS OF,I3,37H-LAYER CONICAMM40033
     &AL SHELLS WITH STIFFENERS,/,9H0TOTAL OF,I4,6H CASES)              AMM40034
      DO 1000 ICASE = 1,NCASES                                          AMM40035
C INPUT GEOMETRY                                                        AMM40036
```

```
      READ(KR,500) NGOR, NEPG, NSTIF                                    AMM40037
      READ (KR,501) R1, R2, SPAN                                        AMM40038
  501 FORMAT(8E10.3)                                                    AMM40039
C INPUT LOADS                                                           AMM40040
      READ (KR,501) BENDMT, COMP, SHEAR, SIDEF                          AMM40041
C INPUT LAYER PROPERTIES                                                AMM40042
      HTOT = 0.                                                         AMM40043
      DO 1 I = 1,NLY                                                    AMM40044
      READ (KR,501) H(I), XR(I), (XEL(I,J), J = 1,6)                    AMM40045
    1 HTOT = HTOT+H(I)                                                  AMM40046
      Z(1) = -0.5*HTOT                                                  AMM40047
      DO 2 I = 1,NLY                                                    AMM40048
    2 Z(I+1) = Z(I)+H(I)                                                AMM40049
      IF(NSTIF .NE. 0) READ(KR,501) (SPROP(J), J = 1,8)                 AMM40050
C DUMP INPUT DATA                                                       AMM40051
      WRITE (KW,601) ICASE, NGOR, NEPG, R1, R2, SPAN,                   AMM40052
     &              BENDMT, COMP, SHEAR, SIDEF                          AMM40053
  601 FORMAT(5H1CASE,I4,11X,12HTOTAL GORES=,12X,I10,/,20X,24HTOTAL ELEMEAMM40054
     &NTS PER GORE=,I10,/,20X,14HTIP RADIUS R1=,10X,E10.3,/,20X,15HROOT AMM40055
     &RADIUS R2=,9X,E10.3,/,20X,5HSPAN=,19X,E10.3,/,20X,15HBENDING MOMENAMM40056
     &T=,9X,E10.3,/,20X,18HAXIAL COMPRESSION=,6X,E10.3,/,20X,6HSHEAR=,18AMM40057
     &X,E10.3/,20X,11HSIDE FORCE=,13X,E10.3,//,50H TABLE OF LAYER PROPERAMM40058
     &TIES FROM INSIDE TO OUTSIDE: ,//,1X,5HLAYER,1X,10H THICKNESS,1X,10AMM40059
     &HPLY  ANGLE,5X,2HE1,9X,2HE2,8X,4HNU12,7X,4HNU23,7X,4HG 12,7X,4HG 2AMM40060
     &3,/,1X,5H-----,8(1X,10H----------))                               AMM40061
      DO 3 I = 1,NLY                                                    AMM40062
    3 WRITE (KW,602) I, H(I), XR(I), (XEL(I,J), J = 1,6)                AMM40063
  602 FORMAT(1X,I5,8(1X,E10.3))                                         AMM40064
      IF(NSTIF .NE. 0) WRITE(KW,603) (SPROP(J), J = 1,8)                AMM40065
  603 FORMAT (1H0,40X,                    38HTWO-NODE STIFFENERS SECTION PROAMM40066
     2PERTIES,/,14X,94HYOUNGS MOD  SHEAR  MOD  ---AREA---  J(TORSION)  -AMM40067
     3--I YY---  ---I ZZ---  ---I YZ---  -UNIT WGT-,/,14X,8(E10.3,2X))  AMM40068
C SIZING                                                                AMM40069
      IF(NSTIF .EQ. 0) WRITE(6,606)                                     AMM40070
  606 FORMAT(1H0,22(1H-),28HTHIS SHELL HAS NO STIFFENERS,22(1H-))       AMM40071
      IF(NEPG .LE. 10) GO TO 31                                         AMM40072
```

```
      WRITE(KW,604)                                                     AMM40073
  604 FORMAT(1H0,20(1H*),110HNEPG EXCEEDS 10, THE MAXIMUM VALUE ALLOWED AMM40074
     &BY THE DIMENSIONING OF THE VARIABLES: CM, EKL, B, XX, YY, AND ELOAAMM40075
     &D)                                                                AMM40076
      GO TO 1000                                                        AMM40077
   31 NPLT = NGOR*NEPG                                                  AMM40078
      NGOR1 = NGOR+1                                                    AMM40079
      NEPG1 = NEPG+1                                                    AMM40080
      NET = NPLT+NGOR                                                   AMM40081
      NDL = 5*NEPG1                                                     AMM40082
      NDT = NGOR1*(NDL+1)                                               AMM40083
      NCON = 5*NGOR1+4*NEPG+2                                           AMM40084
      IF(NSTIF .EQ. 0) NCON = NCON+NGOR1-2                              AMM40085
      LIST = 21*NGOR*NEPG+13*NGOR                                       AMM40086
      CALL SETUP(LENGTH,NCON,LIST,RE,IN)                                AMM40087
C COUPLING                                                              AMM40088
      LP = IMASTR                                                       AMM40089
      L = LP+NET-1                                                      AMM40090
      DO 6 I = 1,NGOR                                                   AMM40091
      KAY = NDL*(I-1)+NGOR1                                             AMM40092
      DO 6 J = 1,NEPG                                                   AMM40093
      IN(LP) = L+1                                                      AMM40094
      K = 5*(J-1)+KAY                                                   AMM40095
      DO 4 KK = 1,10                                                    AMM40096
    4 IN(L+KK) = K+KK                                                   AMM40097
      DO 5 KK = 1,5                                                     AMM40098
      IN(L+10+KK) = K+5+KK+NDL                                          AMM40099
    5 IN(L+15+KK) = K+KK+NDL                                            AMM40100
      LP = LP+1                                                         AMM40101
    6 L = L+20                                                          AMM40102
C STIFFENERS                                                            AMM40103
      DO 63 I = 1,NGOR                                                  AMM40104
      IN(LP) = L+1                                                      AMM40105
      IP1 = I+1                                                         AMM40106
      DO 62 K = I,IP1                                                   AMM40107
      J = NGOR1+NDL*(K-1)                                               AMM40108
```

```
      DO 61 KK = 1,5                                                    AMM40109
   61 IN(L+KK) = J+KK                                                   AMM40110
      L = L+6                                                           AMM40111
   62 IN(L) = K                                                         AMM40112
   63 LP = LP+1                                                         AMM40113
      CALL ORK(LENGTH,RE,IN)                                            AMM40114
C ELEMENT GENERATION IN GORE PLANE                                       AMM40115
      BETA2 = PI/NGOR                                                   AMM40116
      BETA = 0.5*BETA2                                                  AMM40117
      DCB = COS(BETA)                                                   AMM40118
      DSB = SIN(BETA)                                                   AMM40119
      R11 = (R2-R1)/NEPG                                                AMM40120
      RR = R1+R11                                                       AMM40121
      CO = (R2-R1)*DCB                                                  AMM40122
      AL = SQRT(CO*CO+SPAN*SPAN)                                        AMM40123
      CO = CO/AL                                                        AMM40124
      DX = AL/NEPG                                                      AMM40125
      DY = R11*DSB                                                      AMM40126
      DO 10 L = 1,NEPG                                                  AMM40127
      X(1) = (L-1)*DX                                                   AMM40128
      X(2) = L*DX                                                       AMM40129
      X(3) = X(2)                                                       AMM40130
      X(4) = X(1)                                                       AMM40131
      Y(4) = R1*DSB+(L-1)*DY                                            AMM40132
      Y(3) = R1*DSB+L*DY                                                AMM40133
      Y(2) = -Y(3)                                                      AMM40134
      Y(1) = -Y(4)                                                      AMM40135
      CALL MLP3K(EKG,NLY,XEL,Z,XR,X,Y,BMTRX,CMC,NLY,4,1,KW)             AMM40136
      DO 7 I = 1,210                                                    AMM40137
    7 EKL(I,L) = EKG(I)                                                 AMM40138
      DO 8 I = 1,352                                                    AMM40139
    8 B(I,L) = BMTRX(I)                                                 AMM40140
      DO 9 I = 1,NLY                                                    AMM40141
      DO 9 J = 1,3                                                      AMM40142
      DO 9 K = 1,3                                                      AMM40143
    9 CM(I,J,K,L) = CMC(I,J,K)                                          AMM40144
```

```
      DO 10 I = 1,4                                                     AMM40145
      XX(I,L) = X(I)                                                    AMM40146
   10 YY(I,L) = Y(I)                                                    AMM40147
C TRANSFORMATION/ASSEMBLY                                               AMM40148
      REWIND 20                                                         AMM40149
      AL12 = SQRT((R2-R1)**2+SPAN**2)                                   AMM40150
      LP = 1                                                            AMM40151
      DO 11 I = 1,20                                                    AMM40152
      PMTRX(I) = 0.                                                     AMM40153
   11 QQ(I) = 0.                                                        AMM40154
      CONST = -SIDEF*AL12*BETA2/(SPAN*(R1+R2)*NEPG)                     AMM40155
      COORD(3) = SPAN                                                   AMM40156
      COORD(6) = SPAN                                                   AMM40157
      COORD(9) = SPAN-SPAN/NEPG                                         AMM40158
      MID=NGOR/2                                                        AMM40159
      IF(MID*2-NGOR .LT. 0) GO TO 112                                   AMM40160
      IND=0                                                             AMM40161
      GO TO 114                                                         AMM40162
  112 IND=1                                                             AMM40163
  114 MID=MID+1                                                         AMM40164
      DO 17 N = 1,NGOR                                                  AMM40165
      T1 = (N-1)*BETA2                                                  AMM40166
      T2 = N*BETA2                                                      AMM40167
      ALFA = 0.5*(T1+T2)                                                AMM40168
      SINT1 = SIN(T1)                                                   AMM40169
      COST1 = COS(T1)                                                   AMM40170
      SINT2 = SIN(T2)                                                   AMM40171
      COST2 = COS(T2)                                                   AMM40172
      COSAV = COST1+COST2                                               AMM40173
      IF(IND .EQ. 1 .AND. N .EQ. MID) COSAV=COST2                       AMM40174
C GORE PLANE DIRECTION COSINES                                          AMM40175
      D(1,1) = CO*COS(ALFA)                                             AMM40176
      D(1,2) = CO*SIN(ALFA)                                             AMM40177
      D(1,3) = -SPAN/AL                                                 AMM40178
      D(2,1) = 0.5*(COST2-COST1)/DSB                                    AMM40179
      D(2,2) = 0.5*(SINT2-SINT1)/DSB                                    AMM40180
```

```
      D(2,3) = 0.                                                       AMM40181
      D(3,1) = -D(2,2)*D(1,3)                                           AMM40182
      D(3,2) = D(2,1)*D(1,3)                                            AMM40183
      D(3,3) = CO                                                       AMM40184
C CONE GENERATOR DIRECTION COSINES                                      AMM40185
      D1(3,3) = (R2-R1)/AL12                                            AMM40186
      D1(1,1) = D1(3,3)*COST1                                           AMM40187
      D2(1,1) = D1(3,3)*COST2                                           AMM40188
      D1(1,2) = D1(3,3)*SINT1                                           AMM40189
      D2(1,2) = D1(3,3)*SINT2                                           AMM40190
      CON = SPAN/AL12                                                   AMM40191
      D1(1,3) = -CON                                                    AMM40192
      D2(1,3) = -CON                                                    AMM40193
      D1(2,1) = -SINT1                                                  AMM40194
      D2(2,1) = -SINT2                                                  AMM40195
      D1(2,2) = COST1                                                   AMM40196
      D2(2,2) = COST2                                                   AMM40197
      D1(2,3) = 0.                                                      AMM40198
      D2(2,3) = 0.                                                      AMM40199
      D1(3,1) = CON*COST1                                               AMM40200
      D2(3,1) = CON*COST2                                               AMM40201
      D1(3,2) = CON*SINT1                                               AMM40202
      D2(3,2) = CON*SINT2                                               AMM40203
      D2(3,3) = D1(3,3)                                                 AMM40204
C DIRECT TRANSFORMS SKIPPING REFERENCE SYSTEM                           AMM40205
      DO 12 I = 1,3                                                     AMM40206
      DO 12 J = 1,3                                                     AMM40207
      DIR1(I,J) = 0.                                                    AMM40208
      DIR2(I,J) = 0.                                                    AMM40209
      DO 12 K = 1,3                                                     AMM40210
      DIR1(I,J) = DIR1(I,J)+D1(I,K)*D(J,K)                              AMM40211
   12 DIR2(I,J) = DIR2(I,J)+D2(I,K)*D(J,K)                              AMM40212
C ELEMENT TRANSFORM                                                     AMM40213
      DO 13 I = 1,3                                                     AMM40214
      DO 13 J = 1,3                                                     AMM40215
      DE(I,J) = DIR1(I,J)                                               AMM40216
```

```
      DE(I+5,J+5) = DIR1(I,J)                                           AMM40217
      DE(I+10,J+10) = DIR2(I,J)                                         AMM40218
   13 DE(I+15,J+15) = DIR2(I,J)                                         AMM40219
      DO 14 I = 1,2                                                     AMM40220
      DO 14 J = 1,2                                                     AMM40221
      DE(I+3,J+3) = DIR1(I,J)                                           AMM40222
      DE(I+8,J+8) = DIR1(I,J)                                           AMM40223
      DE(I+13,J+13) = DIR2(I,J)                                         AMM40224
   14 DE(I+18,J+18) = DIR2(I,J)                                         AMM40225
      WRITE (20) D1, D2, DE                                             AMM40226
      IF(NSTIF .EQ. 0) GO TO 141                                        AMM40227
      COORD(1) = R1*COST1                                               AMM40228
      COORD(2) = R1*SINT1                                               AMM40229
      COORD(4) = R1*COST2                                               AMM40230
      COORD(5) = R1*SINT2                                               AMM40231
      COORD(7) = RR*COST1                                               AMM40232
      COORD(8) = RR*SINT1                                               AMM40233
      LLL = NPLT+N                                                      AMM40234
      CALL STIF2(COORD,DUM,SPROP,0,NODE,DUM(1),DUM(1),DUM(1),EKG,EKST,  AMM40235
     & RT,LLL,KW)                                                       AMM40236
      CALL ASMLTV(LLL,12,EKST,BMTRX,RE,IN)                              AMM40237
C SWEEP THE GORE FROM TIP TO ROOT                                       AMM40238
  141 DO 17 L = 1,NEPG                                                  AMM40239
      IF(SIDEF .EQ. 0. .OR. N .LT. MID) GO TO 143                       AMM40240
      IF(N .GT. MID) GO TO 142                                          AMM40241
      ELOAD(L) = (R2-RI1*(NEPG-L+.5))*CONST                             AMM40242
  142 QQ(13)=-.25*ELOAD(L)*COSAV                                        AMM40243
      QQ(18)=QQ(13)                                                     AMM40244
      IF(IND .EQ. 1 .AND. N .EQ. MID) GO TO 143                         AMM40245
      QQ(3)=QQ(13)                                                      AMM40246
      QQ(8)=QQ(13)                                                      AMM40247
  143 K = 0                                                             AMM40248
      DO 15 I = 1,20                                                    AMM40249
      DO 15 J = 1,I                                                     AMM40250
      K = K+1                                                           AMM40251
      EKR(I,J) = EKL(K,L)                                               AMM40252
```

```
   15 EKR(J,I) = EKR(I,J)                                               AMM40253
      K = 0                                                             AMM40254
      DO 16 I = 1,20                                                    AMM40255
      DO 16 J = 1,I                                                     AMM40256
      K = K+1                                                           AMM40257
      EKG(K) = 0.                                                       AMM40258
      DO 16 KK = 1,20                                                   AMM40259
      DO 16 LL = 1,20                                                   AMM40260
   16 EKG(K) = EKG(K)+DE(I,KK)*EKR(KK,LL)*DE(J,LL)                     AMM40261
      CALL ASMLTV(LP,20,EKG,QQ,RE,IN)                                   AMM40262
   17 LP = LP+1                                                         AMM40263
C CONSTRAINTS: ROOT                                                     AMM40264
      L = 1                                                             AMM40265
      LP = NGOR1                                                        AMM40266
      DO 18 I = 1,LP                                                    AMM40267
      K = I*NDL-5+NGOR1                                                 AMM40268
      DO 18 J = 1,5                                                     AMM40269
      IN(L) = K+J                                                       AMM40270
   18 L = L+1                                                           AMM40271
C SYMMETRY CONSTRAINTS: EDGES                                           AMM40272
      LP = NEPG1*NGOR                                                   AMM40273
      DO 19 J = 1,NEPG                                                  AMM40274
C TOP                                                                   AMM40275
      JAY5 = 5*J                                                        AMM40276
      IN(L) = JAY5-3+NGOR1                                              AMM40277
      IN(L+1) = JAY5-1+NGOR1                                            AMM40278
C BOTTOM                                                                AMM40279
      IN(L+2) = JAY5-3+NGOR1+5*LP                                       AMM40280
      IN(L+3) = JAY5-1+NGOR1+5*LP                                       AMM40281
   19 L = L+4                                                           AMM40282
      IN(L) = 1                                                         AMM40283
      IN(L+1) = NGOR1                                                   AMM40284
      IF(NSTIF .NE. 0) GO TO 192                                        AMM40285
      IF(NGOR .EQ. 1) GO TO 192                                         AMM40286
      DO 191 I = 2,NGOR                                                 AMM40287
  191 IN(L+I) = I                                                       AMM40288
```

```
  192 J = IQ-1                                                     AMM40289
      DO 193 I = 1,NCON                                            AMM40290
      KK = IN(I)+J                                                 AMM40291
  193 RE(KK) = 0.                                                  AMM40292
      CALL PCON(RE,IN)                                             AMM40293
C LOADS                                                             AMM40294
      REWIND 20                                                    AMM40295
      BO2P = 0.25/NGOR                                             AMM40296
      LP = NEPG1                                                   AMM40297
      JAY5 = IQ-1+NGOR1                                            AMM40298
      DO 21 N = 1,NGOR                                             AMM40299
      T1 = (N-1)*BETA2                                             AMM40300
      T2 = N*BETA2                                                 AMM40301
      Q(1) = BO2P*SHEAR*(SIN(T1)**2+SIN(T2)**2)                    AMM40302
      Q(3) = -BO2P*(BENDMT*(COS(T1)+COS(T2))/R1+COMP)              AMM40303
      READ (20) D1, D2                                             AMM40304
      DO 20 I = 1,3                                                AMM40305
      IP3 = I+3                                                    AMM40306
      IP6 = I+6                                                    AMM40307
      Q(IP3) = 0.                                                  AMM40308
      Q(IP6) = 0.                                                  AMM40309
      DO 20 J = 1,3                                                AMM40310
      Q(IP3) = Q(IP3)+D1(I,J)*Q(J)                                 AMM40311
   20 Q(IP6) = Q(IP6)+D2(I,J)*Q(J)                                 AMM40312
      K = (N-1)*NDL+JAY5                                           AMM40313
      DO 21 KK = 1,3                                               AMM40314
      KON = K+KK                                                   AMM40315
      RE(KON) = RE(KON)+Q(KK+3)                                    AMM40316
   21 RE(KON+NDL) = RE(KON+NDL)+Q(KK+6)                            AMM40317
      ISGN = 0                                                     AMM40318
      CALL FACT(ISGN,RE,IN)                                        AMM40319
      IF (ISGN .EQ. 1) GO TO 22                                    AMM40320
      WRITE (KW,605) ICASE                                         AMM40321
  605 FORMAT(5HOCASE,I4,17H FAILED INVERSION)                      AMM40322
      GO TO 28                                                     AMM40323
   22 KT1 = 0                                                      AMM40324
```

```
      CALL SIMULQ(BO2P,RE,IN)                                           AMM40325
      KT1 = KW                                                          AMM40326
C STRESS SOLUTICN                                                       AMM40327
      DC 27 ITIME = 1,2                                                 AMM40328
      ISDIR = ITIME-1                                                   AMM40329
      LP = 0                                                            AMM40330
      REWIND 20                                                         AMM40331
      DO 27 N = 1,NGOR                                                  AMM40332
      READ (20) D1, D2, DE                                              AMM40333
      DO 27 L = 1,NEPG                                                  AMM40334
      LP = LP+1                                                         AMM40335
      CALL XTRACT(LP,20,Q,RE,IN)                                        AMM40336
      DC 23 I = 1,20                                                    AMM40337
      QL(I) = 0.                                                        AMM40338
      DO 23 J = 1,20                                                    AMM40339
   23 QL(I) = QL(I)+DE(J,I)*Q(J)                                        AMM40340
      DO 24 I = 1,352                                                   AMM40341
   24 BMTRX(I) = B(I,L)                                                 AMM40342
      DO 25 I = 1,NLY                                                   AMM40343
      DO 25 J = 1,3                                                     AMM40344
      DO 25 K = 1,3                                                     AMM40345
   25 CMC(I,J,K) = CM(I,J,K,L)                                          AMM40346
      DO 26 I = 1,4                                                     AMM40347
      X(I) = XX(I,L)                                                    AMM40348
   26 Y(I) = YY(I,L)                                                    AMM40349
      CALL MLP3S(LP,QL,BMTRX,CMC,NLY,Z,NLY,4,0,XS,YS,X,Y,XEL,XR,ISDIR,  AMM40350
     +KW)                                                               AMM40351
   27 CONTINUE                                                          AMM40352
   28 DO 1000 I = 1,20                                                  AMM40353
 1000 0(I) = 0.                                                         AMM40354
      RETURN                                                            AMM40355
      END                                                               AMM40356
```

APPENDIX D

SUBROUTINE VIBEPT

This appendix contains FORTRAN-IV listings of applications subroutine VIBEPT and the dummy MAIN program in which the correct dimensions of variables are established.

```
C MAIN FOR VIBEPT                                                    MNVB0001
C COPYRIGHT (C) MASSACHUSETTS INSTITUTE OF TECHNOLOGY 1976
C THIS PROGRAM REQUIRES R. SPILKER'S SUBROUTINES: MLP3K,MLP3M, AND PROD MNVB0002
C  AND FEABL V5: ASMLTV, FACT, ORK AND SETUP                          MNVB0003
C THE SUBSPACE SUBROUTINES (SSPACE,JACKM1,MXU,KINXV,UTXV AND EIGEN) ARE MNVB0004
C REQUIRED FOR EXECUTION.                                             MNVB0005
C THE TRANSIENT RESPONSE IS OBTAINED USING SUBROUTINES:ELAPSE,INPUT,  MNVB0006
C TSTEP AND VIBEPT                                                    MNVB0007
      DOUBLE PRECISION DEMS,DELK,EV,ASQ,T,AM                          MNVB0008
      DIMENSION REAL(2496), INTGR(2496)                               MNVB0009
      EQUIVALENCE (REAL(1), INTGR(1))                                 MNVB0010
      DIMENSION CMC(1,3,3), H(1), DENS(1), XR(1), XEL(1,6), Z(2)      MNVB0011
      DIMENSION ELK(21), EMS(21), DELK(21), DEMS(21)                  MNVB0012
      DIMENSION   EV( 36), T( 6, 6), AM( 6,6 ), ICONV(6), ASQ(6)      MNVB0013
      DIMENSION ALOAD(500), TIME(1000)                                MNVB0014
      COMMON /S I Z E / NET,NDT,NUT,NSP,IODYN                         MNVB0015
      COMMON / I O / KR, KW, KP, KT1, KT2, KT3                        MNVB0016
      DATA NLY,  NSPACE, LENGTH/ 1, 6,2496/                           MNVB0017
      KT2=6                                                           MNVB0018
      CALL VIBEPT (LENGTH,NLY,REAL,INTGR,CMC,NSPACE,H,DENS,XR,XEL,Z,ELK,MNVB0019
     +EMS,DELK,DEMS,EV,T,AM,ICONV,ASQ,ALOAD,TIME)                     MNVB0020
      RETURN                                                          MNVB0021
      END                                                             MNVB0022
```

```
      SUBROUTINE VIBEPT (LENGTH,NLY,REAL,INTGR,CMC,NSPACE,H,DENS,XR,XEL,VIBE0001
     +Z,ELK,EMS,DELK,DEMS,EV,T,AM,ICONV,ASQ,ALOAD,TIME)                 VIBE0002
C COPYRIGHT (C) MASSACHUSETTS INSTITUTE OF TECHNOLOGY 1976
C PROGRAM FOR TRANSIENT DYNAMIC ANALYSIS OF A MULTI-LAYER  RECTANGULAR  VIBE0003
C PLATE. R. SPILKER'S SUBROUTINE MLP3K GENERATES THE ELEMENT STIFFNESS  VIBE0004
C MATRIX AND HIS SUBROUTINE MLP3M GENERATES THE ELEMENT MASS MATRIX     VIBE0005
      DOUBLE PRECISION DEMS, DELK, EV,ASQ, T, AM                        VIBE0006
      DIMENSION  CMC(NLY,3,3), H(1), DENS(1), XR(1), XEL(NLY,6),  Z(1)  VIBE0007
      DIMENSION T(NSPACE,NSPACE), AM(NSPACE,NSPACE), ALOAD(1), TIME(1)  VIBE0008
      DIMENSION REAL(1), INTGR(1)                                       VIBE0009
      DIMENSION ELK(1), EMS(1), DELK(1), DEMS(1), EV(1), ICONV(1),ASQ(1)VIBE0010
      DIMENSION STIF(210), BMTRX(352), EMASS(210), X(5), Y(5), NODE(120)VIBE0011
     +, NDOF(120), QLOAD(20)                                            VIBE0012
      COMMON /CONVRG/ MAXIT,EPS,NOEIG                                   VIBE0013
      COMMON /SIZE/ NET,NDT,NUT,NSP,IODYN                               VIBE0014
      COMMON/BEGIN/ICON,IKOUNT,ILNZ,IMASTR,IQ,IK,IM,IV,IVB,IU           VIBE0015
      COMMON/IO/ KR,KW,KP,KT1,KTI,KT3                                   VIBE0016
      COMMON/END/LCON,LKOUNT,LLNZ,LMASTR,LQ,LK,LM,LV,LVB,LU             VIBE0017
      DATA X/5*0./,Y/5*0./                                              VIBE0018
      KT1=0                                                             VIBE0019
      KR=5                                                              VIBE0020
      KW=6                                                              VIBE0021
      READ(KR,100) NCASES                                               VIBE0022
      DO 70 ICASE=1,NCASES                                              VIBE0023
      READ(KR,100) IODYN,NW,NL,NLAY,WIDTH,EL,MAXIT,NOEIG,EPS            VIBE0024
  100 FORMAT(4I5,2F15.5/      2I5,F15.5)                                VIBE0025
      NSP=NSPACE                                                        VIBE0026
      WRITE(KW,1000) ICASE,IODYN,NW,NL,NLAY,WIDTH,EL,NSPACE,MAXIT,      VIBE0027
     +NOEIG,EPS                                                         VIBE0028
 1000 FORMAT(23H1VIBE PLATE CASE      ,I2,8H  IODYN=,I2,6H,  NW=,I3,6H,VIBE0029
     +  NL=,I3,8H,  NLAY=,I2,9H,  WIDTH=,E10.3,10H,  LENGTH=,E10.3/    VIBE0030
     +                                  14H0 SUBSPACE HAS,I3,14H DOFSVIBE0031
     +. AT MOST,I3,34H ITERATIONS WILL BE DONE TO OBTAIN,I3,33H OF THE EVIBE0032
     +IGENVALUES. TOLERENCE IS,E10.3)                                   VIBE0033
      HTOT=0.                                                           VIBE0034
      DO 5 I=1,NLAY                                                     VIBE0035
```

```
      READ(KR,101) H(I),DENS(I),XR(I),(XEL(I,J),J=1,6)                  VIBE0036
  101 FORMAT(3E15.5/6E10.5)                                              VIBE0037
    5 HTOT=HTOT+H(I)                                                     VIBE0038
      Z(1)=-0.5*HTOT                                                     VIBE0039
      WRITE(6,1001)                                                      VIBE0040
 1001 FORMAT(1H0, 5HLAYER,1X, 9HTHICKNESS,4X,7HDENSITY,4X,9HPLY ANGLE,7XVIBE0041
     +,2HE1,10X,2HE2,9X,4HNU12,8X,4HNU23,8X,4HG 12,8X,4HG 23)            VIBE0042
      DO 10 I=1,NLAY                                                     VIBE0043
      Z(I+1)=Z(I)+H(I)                                                   VIBE0044
   10 WRITE(KW,1002) I,H(I),DENS(I),XR(I),(XEL(I,J),J=1,6)               VIPE0045
 1002 FORMAT(1H ,I3,1X,9(E12.5))                                         VIBE0046
C INPUT CONSTRAINTS                                                      VIBE0047
      READ(KR,100) NODESC                                                VIBE0048
      READ(KR,103) (NODE(I),NDOF(I),I=1,NODESC)                          VIBE0049
  103 FORMAT(16I5)                                                       VIBE0050
      READ(KR,101) PZERO                                                 VIBE0051
      WRITE(KW,1004) PZERO                                               VIBE0052
 1004 FORMAT(1H0,'PZERO=',E12.5)                                         VIBE0053
C LOADING FOR THESE CASES IS :                                           VIBE0054
C         P(X,Y,T)=PZERO*SIN(.5*PI*X/WIDTH)*SIN(.5*PI*Y/EL)*SIN(OMEGA*T) VIBE0055
C OMEGA IS A FACTOR LESS THAN ONE TIMES AN EIGENVALUE FREQUENCY          VIBEC056
C AND T IS TIME                                                          VIBECC57
      NCON=NODESC                                                        VIBE0058
      NWP1=NW+1                                                          VIBE0059
      NLP1=NL+1                                                          VIBE0060
      NET=NW*NL                                                          VIBE0061
      NDT=5*NWP1*NLP1                                                    VIBE0062
      MASTRL=NET*21                                                      VIBE0063
      NSP=NSPACE                                                         VIBE0064
      CALL SETUP(LENGTH,NCON,MASTRL,REAL,INTGR)                          VIBE0065
      NL5=5*NLP1                                                         VIBE0066
C MASTER ASSEMBLY LIST                                                   VIBE0067
      KADD=IMASTR-1                                                      VIBE0068
      MADD=IMASTR+NET-20                                                 VIBE0069
      DO 25 J=1,NW                                                       VIBE0070
      J1=J*NL5                                                           VIBE0071
```

```
      J2=J1-NL5                                                         VIBE0072
      DO 20 I=1,NL                                                      VIBE0073
      MADD=MADD+20                                                      VIBE0074
      KADD=KADD+1                                                       VIBE0075
      INTGR(KADD)=MADD                                                  VIBE0076
      J3=J1+5*(I-1)                                                     VIBE0077
      J4=J3-NL5                                                         VIBE0078
      DO 15 L=1,5                                                       VIBE0079
      K=L-1                                                             VIBE0080
      LADD=MADD+K                                                       VIBE0081
      INTGR(LADD)=J3+L                                                  VIBE0082
      INTGR(LADD+5)=J4+L                                                VIBE0083
      INTGR(LADD+10)=J4+L+5                                             VIBE0084
   15 INTGR(LADD+15)=J3+L+5                                             VIBE0085
   20 CONTINUE                                                          VIBE0086
   25 CONTINUE                                                          VIBE0087
C DEFINE CONSTRAINTS                                                    VIBE0088
      DO 30 I=1,NCON                                                    VIBE0089
   30 INTGR(I)=5*(NODE(I)-1)+NDOF(I)                                    VIBE0090
C ORGANIZE K                                                            VIBE0091
      KT1=KW                                                            VIBE0092
      CALL ORK(LENGTH,REAL,INTGR)                                       VIBE0093
      KT1=0                                                             VIBE0094
      DX=WIDTH/NW                                                       VIBE0095
      DY=EL/NL                                                          VIBE0096
      X(2)=DX                                                           VIBE0097
      X(3)=DX                                                           VIBE0098
      Y(3)=DY                                                           VIBE0099
      Y(4)=DY                                                           VIBE0100
C ELEMENT LOADS                                                         VIBE0101
      DO 35 I=1,20                                                      VIBE0102
   35 QLOAD(I)=0.                                                       VIBE0103
C ELEMENT STIFFNESS MATRIX                                              VIBE0104
      CALL MLP3K(STIF,NLAY,XEL,Z,XR,X,Y,BMTRX,CMC,NLY,4,1,KW)           VIBE0105
      IF(IODYN .LT. 2) STOP                                             VIBE0106
      IF(IODYN .EQ. 2) ILC=1                                            VIBE0107
```

```
      IF(IODYN .EQ. 3) ILC=0                                            VIBE0108
C ELEMENT MASS MATRIX                                                   VIBE0109
      CALL MLP3M(EMASS,NLAY,X,Y,Z,DENS,ILC,4)                           VIBE0110
C ASSEMBLE GLOBAL MASS AND STIFFNESS MATRICES                           VIBE0111
C CALCULATE LOADING AT THE CORNERS OF EACH ELEMENT                      VIBE0112
      I=0                                                               VIBE0113
      CON=.0625*PZERO*DX*DY                                             VIBE0114
      DO 40 IX=1,NW                                                     VIBE0115
      X2=WIDTH*(NW-IX+1)/NW                                             VIBE0116
      X1=WIDTH*(NW-IX)/NW                                               VIBE0117
      SIN1=SIN(1.570796*X1/WIDTH)                                       VIBE0118
      SIN2=SIN(1.570796*X2/WIDTH)                                       VIBE0119
      DO 40 IY=1,NL                                                     VIBE0120
      I=I+1                                                             VIBE0121
      Y1=EL*(NL-IY)/NL                                                  VIBE0122
      Y3=EL*(NL-IY+1)/NL                                                VIBE0123
      SIN3=SIN(1.570796*Y1/EL)                                          VIBE0124
      SIN4=SIN(1.570796*Y3/EL)                                          VIBE0125
      QLOAD(3)=CON*(SIN1+SIN2)*(SIN3+SIN4)                              VIBE0126
      QLOAD(8)=QLOAD(3)                                                 VIBE0127
      QLOAD(13)=QLOAD(3)                                                VIBE0128
      QLOAD(18)=QLOAD(3)                                                VIBE0129
      KT1=KW                                                            VIBE0130
   40 CALL ASMLTV(I,20,STIF,EMASS,QLOAD,REAL,INTGR)                     VIBE0131
C SAVE THE NDT LOADS WHICH WERE ASSEMBLED IN REAL(IQ) TO REAL(LQ)       VIBE0132
      IQM1=IQ-1                                                         VIBE0133
      DO 53 I=1,NDT                                                     VIBE0134
   53 ALOAD(I)=REAL(IQM1+I)                                             VIBE0135
      CALL SSPACE(ELK,EMS,DELK,DEMS,EV,T,AM,ASQ,NSPACE,ICONV,REAL,INTGR)VIBE0136
      DO 55 J=1,NSPACE                                                  VIBE0137
      JJ=J*(J+1)/2                                                      VIBE0138
      WRITE(KW,601) J,DEMS(JJ),ASQ(J),T(J,I)                            VIBE0139
  601 FORMAT(4HON =,2X,10HEIGENVALUE,3X,12HFREQ,RAD/SEC,3X,10HFREQ IN HZVIBE0140
     &,/,1X,I3,D12.5,2X,D12.5,2X,D12.5,/,13HOEIGENVECTOR:)              VIBE0141
   55 WRITE (6,602) (AM(I,J), I = 1,NSPACE)                             VIBE0142
  602 FORMAT(1X,10D12.5)                                                VIBE0143
```

```
C INPUT DATA FOR TRANSIENT ANALYSIS FCR THIS SET OF FIGENVALUES         VIBF0144
      READ(KR,103) NOMK                                                 VIBE0145
      DO 58 IRUN=1,NOMK                                                 VIBE0146
      READ(KR,105) FACTOR,KOMG                                          VIBE0147
  105 FORMAT(F15.5,I5)                                                  VIBE0148
      OM=FACTOR*ASQ(KOMG)                                               VIBE0149
      WRITE(KW,1005) IRUN,FACTOR,KOMG   ,OM                             VIBE0150
 1005 FORMAT(12HORUN NUMBER ,I3,8H   OMEGA=,F7.4,13H TIMES OMEGA(,I1,1H),VIBE0151
     +F15.7)                                                            VIBE0152
      CALL TSTEP(ASQ,ELK ,LENGTH,TIME,NL,CM,ALOAD,REAL,INTGR)           VIBE0153
   58 CONTINUE                                                          VIBE0154
   70 CONTINUE                                                          VIBE0155
      RETURN                                                            VIBE0156
      END                                                               VIBE0157
```

DISTRIBUTION

No. of Copies	To
	Office of Secretary of Defense, Office of the Director of Defense Research and Engineering
1	ATTN: Mr. J. Persh, Staff Specialist for Materials and Structures
	The Pentagon, Washington, D.C. 20301
	Commander, U.S. Army Materiel Command
1	ATTN: AMCRD-TT, Dr. R. Zentner
	5001 Eisenhower Avenue, Alexandria, VA 22333
	Ballistic Missile Defense Program Office, ABMDA/W (Provisional)
1	ATTN: DACS-BMT, Mr. C. McLain
1	DACS-BMT, Mr. V. Kupelian
	Commonwealth Bldg., Room 1100, 1300 Wilson Blvd., Arlington, VA 22209
	Director, Ballistic Missile Defense Advanced Technology Center
1	ATTN: ATC-M, Mr. M. Whitfield
1	ATC-M, Dr. D. Harmon
1	ATC-X, Mr. W. Davis
	P.O. Box 1500, Huntsville, AL 35807
	Commander, Ballistic Missile Defense Systems Command
1	ATTN: BMDSC-TEN, Mr. N.J. Hurst
	P.O. BOX 1500, Huntsville, AL 35807
	Director, Defense Nuclear Agency
1	ATTN: SPAS, Mr. J.F. Moulton, Jr.
1	SPAS, Mr. M. Rubenstein
	Washington, D.C. 20305
	Office of Chief of Research Development and Acquisition, Department of the Army
1	ATTN: DAMA-CSS, Dr. J. Bryant
	Washington, D.C. 20310
	Director, Army Ballistic Research Laboratory
1	ATTN: Mr. J. Meszaros
1	Dr. N.J. Huffington, Jr.
1	Dr. J. Santiago
	Aberdeen Proving Ground, MD 21005
	Commander, U. S. Army Missile Command
1	ATTN: Dr. R. Rhodes
1	Dr. S. Smith
	Huntsville, AL 35809
	Commander, Harry Diamond Laboratories
1	ATTN: AMXDO-RBF, Dr. R. Oswald
1	AMXDO-NP, Dr. F. Wimenitz
	2800 Powder Mill Road, Adelphi, MD 20783

Commander, Picatinny Arsenal
1 ATTN: Mr. M. Allen
1 Mr. M. Weinstein
1 Mr. B. Frank
Dover, NJ 07801

Commander, U.S. Army Combat Development Command
1 ATTN: Technical Library
Institute of Nuclear Studies, Fort Bliss, Texas 79916

Commander, Air Force Materials Laboratory, Air Force Systems Command
1 ATTN: LNE/Major H. Keck
1 LNC/Dr. D. Schmidt
Wright-Patterson Air Force Base, Ohio 45433

Department of the Navy, Naval Ordnance Systems Command
1 ATTN: ORD-03331, Mr. M. Kinna
Washington, D.C. 20360

Commander, Naval Surface Weapons Center
1 ATTN: Mr. L. Gowen
1 Mr. F. Koubek
Silver Springs, MD 20910

Los Alamos Scientific Laboratory
1 ATTN: GMX-6, Dr. J.W. Taylor
P.O. Box 1663, Los Alamos, NM 87544

Space and Missile Systems Organization
1 ATTN: RSSE/Major J. McCormack
P.O. Box 92960, World Way Postal Center, Los Angeles, CA 90009

Sandia Laboratories
1 ATTN: Dr. D. Munson
1 Dr. W. Herrmann
1 Dr. L.D. Bertholf
1 Dr. B. Butcher
1 Dr. J. Lipkin
P.O. Box 5800, Albuquerque, NM 87115

Aerospace Corporation
1 ATTN: Dr. R. Cooper
1 Dr. W. Barry
P.O. Box 92957, Los Angeles, CA 90009

AVCO Corporation, Government Products Group
1 ATTN: Dr. W. Reinecke
1 Mr. P. Rolincik
201 Lowell Street, Wilmington, MA 01997

Bell Telephone Laboratories, Inc.
1 ATTN: Mr. E.G. Denigris
1 Mr. M.F. Stevens
Murray Hill, NJ 07871

Effects Technology, Inc.
1 ATTN: Dr. R. Wengler
1 Mr. E. Steele
P.O. Box 30400, Santa Barbara, CA 93105

Fiber Materials, Inc.
1 ATTN: Mr. Maurice Subilia, Jr.
1 Mr. L. Landers
Biddeford Industrial Park, Biddeford, ME 04005

General Electric Company, Valley Forge Space Technology Center
1 ATTN: Mr. K. Hall
1 Mr. R. Sullivan
1 Mr. J. Brazel
P.O. Box 8555, Philadelphia, PA 19101

Kaman Sciences Corporation
1 ATTN: Mr. F. Shelton
P.O. Box 7463, Colorado Springs, CO 80933

Ktech
1 ATTN: Dr. D. Keller
1 Mr. N.H. Froula
911 Pennsylvania Avenue, N.E., Albuquerque, NM 87110

Lockheed Missiles and Space Company
1 ATTN: Mr. D. Aspinwall
P.O. Box 504, Sunnyvale, CA 94088

Lawrence Livermore Laboratory
1 ATTN: Dr. E.M. Wu
P.O. Box 808, L-421, University of California, Livermore, CA 94550

Martin Marietta Aerospace
1 ATTN: Mr. M. Hendricks
1 Mr. L. Kinnaird
1 Mr. F. Koo
P.O. Box 5837, Orlando, Florida 32805

McDonnell Douglas Corporation
1 ATTN: Dr. H. Hurwicz
5301 Bolsa Avenue, Huntington Beach, CA 92647

Prototype Development Associates, Inc.
1 ATTN: Dr. J.I. Slaughter
1 Mr. J. Schutzler
1740 Garry Avenue, Suite 201, Santa Ana, CA 92705

R&D Associates
1 ATTN: Dr. A. Field
525 Wilshire Blvd., Santa Monica, CA 90025

Southwest Research Institute
1 ATTN: Mr. A. Wenzel
8500 Culebra Road, San Antonio, Texas 78206

Stanford Research Institute
1 ATTN: Dr. D. Curran
1 Dr. L. Seaman
333 Ravenswood Avenue, Menlo Park, CA 90250

Stanford University, Department of Applied Mechanics
1 ATTN: Prof. E.H. Lee
Stanford, CA 94305

TRW Systems Group
1 ATTN: Mr. D. Gamble
One Space Park, Redondo Beach, CA 90278

Terra Tek, Inc.
1 ATTN: Dr. A.H. Jones
420 Wakara Way, University Research Park, Salt Lake City, Utah 84108

2 Defense Documentation Center, Cameron Station, Bldg. 5
5010 Duke Station, Alexandria VA 22314

Director, Army Materials and Mechanics Research Center
1 ATTN: DRXMR-H, Mr. J. Dignam
1 DRXMR-H, Mr. L. Aronin
1 DRXMR-H, Dr. S.C. Chou
1 DRXMR-H, Dr. D. Dandekar
1 DRXMR-H, Major L. Abramson
1 DRXMR-AP
2 DRXMR-PL
1 DRXMR-PR
Watertown, MA 02172

Army Materials and Mechanics Research Center
Watertown, Massachusetts 02172

AD ____________

UNCLASSIFIED
UNLIMITED DISTRIBUTION

USE OF THE HYBRID-STRESS FINITE-ELEMENT MODEL FOR THE STATIC AND DYNAMIC ANALYSIS OF MULTILAYER COMPOSITE PLATES AND SHELLS

Robert L. Spilker, Oscar Orringer, Emmett A. Witmer
Samuel Verbiese, Susan E. French, and Alex Harris,
Aeroelastic and Structures Research Laboratory,
Department of Aeronautics and Astronautics, Massachusetts
Institute of Technology, Cambridge, Massachusetts 02139

Final Report AMMRC CTR 76-29, September 1976

(ASRL TR 181-2) 214 pp, illus. tables
Contract DAAG46-75-C-0055
D/A Project 1W362306AH72
AMCMS Code: 632306.11.117200

Key Words

Finite-Element Method
Static Response
Dynamic Response
Elastic Behavior
Structural Mechanics
Stress Analysis
Laminated Plates
Fiber Composites
Shell Structures

This report presents the results of an investigation into the formulation and application of assumed-stress hybrid finite-elements for bending of multilayer laminated plates and shells. Two families of hybrid-stress-based multilayer plate elements are considered; these elements are denoted as thick plate and moderately-thick plate elements. In the development of the thick plate elements, transverse shear deformation effects are included by allowing lines normal to the plate midsurface in the undeformed state to be piecewise linear from layer to layer in the deformed state. Transverse shear deformation effects are included in an average sense in the moderately-thick plate element family by assuming that straight lines normal to the plate midsurface prior to deformation remain straight but not necessarily normal to the plate midsurface after deformation. Comparison of the results obtained by using the thick plate and moderately-thick plate elements with independent analytical results shows that the moderately-thick plate elements are more efficient and practical for the analysis of multilayer structures having a large number of elastically dissimilar layers.

For dynamic analyses, the Modal Superposition Method (MSM) is employed to obtain the timewise solution, and the Subspace Iteration Method (SIM) is adopted as an efficient scheme for calculation of the lowest few eigenvalues and eigenvectors of the assembled structure. Both the SIM and MSM are programmed as modules to be compatible with a general modular finite-element computer code for static and dynamic analysis. The advantages of this modular approach are demonstrated in a series of static and dynamic applications analyses.

Army Materials and Mechanics Research Center
Watertown, Massachusetts 02172

AD ____________

UNCLASSIFIED
UNLIMITED DISTRIBUTION

USE OF THE HYBRID-STRESS FINITE-ELEMENT MODEL FOR THE STATIC AND DYNAMIC ANALYSIS OF MULTILAYER COMPOSITE PLATES AND SHELLS
Robert L. Spilker, Oscar Orringer, Emmett A. Witmer
Samuel Verbiese, Susan E. French, and Alex Harris,
Aeroelastic and Structures Research Laboratory,
Department of Aeronautics and Astronautics, Massachusetts
Institute of Technology, Cambridge, Massachusetts 02139

Final Report AMMRC CTR 76-29, September 1976

(ASRL TR 181-2) 214 pp, illus. tables
Contract DAAG46-75-C-0055
D/A Project 1W362306AH72
AMCMS Code: 632306.11.117200

Key Words

Finite-Element Method
Static Response
Dynamic Response
Elastic Behavior
Structural Mechanics
Stress Analysis
Laminated Plates
Fiber Composites
Shell Structures

This report presents the results of an investigation into the formulation and application of assumed-stress hybrid finite-elements for bending of multilayer laminated plates and shells. Two families of hybrid-stress-based multilayer plate elements are considered; these elements are denoted as thick plate and moderately-thick plate elements. In the development of the thick plate elements, transverse shear deformation effects are included by allowing lines normal to the plate midsurface in the undeformed state to be piecewise linear from layer to layer in the deformed state. Transverse shear deformation effects are included in an average sense in the moderately-thick plate element family by assuming that straight lines normal to the plate midsurface prior to deformation remain straight but not necessarily normal to the plate midsurface after deformation. Comparison of the results obtained by using the thick plate and moderately-thick plate elements with independent analytical results shows that the moderately-thick plate elements are more efficient and practical for the analysis of multilayer structures having a large number of elastically dissimilar layers.

For dynamic analyses, the Modal Superposition Method (MSM) is employed to obtain the timewise solution, and the Subspace Iteration Method (SIM) is adopted as an efficient scheme for calculation of the lowest few eigenvalues and eigenvectors of the assembled structure. Both the SIM and MSM are programmed as modules to be compatible with a general modular finite-element computer code for static and dynamic analysis. The advantages of this modular approach are demonstrated in a series of static and dynamic applications analyses.

Army Materials and Mechanics Research Center
Watertown, Massachusetts 02172

AD ____________

UNCLASSIFIED
UNLIMITED DISTRIBUTION

USE OF THE HYBRID-STRESS FINITE-ELEMENT MODEL FOR THE STATIC AND DYNAMIC ANALYSIS OF MULTILAYER COMPOSITE PLATES AND SHELLS
Robert L. Spilker, Oscar Orringer, Emmett A. Witmer
Samuel Verbiese, Susan E. French, and Alex Harris,
Aeroelastic and Structures Research Laboratory,
Department of Aeronautics and Astronautics, Massachusetts
Institute of Technology, Cambridge, Massachusetts 02139

Final Report AMMRC CTR 76-29, September 1976

(ASRL TR 181-2) 214 pp, illus. tables
Contract DAAG46-75-C-0055
D/A Project 1W362306AH72
AMCMS Code: 632306.11.117200

Key Words

Finite-Element Method
Static Response
Dynamic Response
Elastic Behavior
Structural Mechanics
Stress Analysis
Laminated Plates
Fiber Composites
Shell Structures

This report presents the results of an investigation into the formulation and application of assumed-stress hybrid finite-elements for bending of multilayer laminated plates and shells. Two families of hybrid-stress-based multilayer plate elements are considered; these elements are denoted as thick plate and moderately-thick plate elements. In the development of the thick plate elements, transverse shear deformation effects are included by allowing lines normal to the plate midsurface in the undeformed state to be piecewise linear from layer to layer in the deformed state. Transverse shear deformation effects are included in an average sense in the moderately-thick plate element family by assuming that straight lines normal to the plate midsurface prior to deformation remain straight but not necessarily normal to the plate midsurface after deformation. Comparison of the results obtained by using the thick plate and moderately-thick plate elements with independent analytical results shows that the moderately-thick plate elements are more efficient and practical for the analysis of multilayer structures having a large number of elastically dissimilar layers.

For dynamic analyses, the Modal Superposition Method (MSM) is employed to obtain the timewise solution, and the Subspace Iteration Method (SIM) is adopted as an efficient scheme for calculation of the lowest few eigenvalues and eigenvectors of the assembled structure. Both the SIM and MSM are programmed as modules to be compatible with a general modular finite-element computer code for static and dynamic analysis. The advantages of this modular approach are demonstrated in a series of static and dynamic applications analyses.

Army Materials and Mechanics Research Center
Watertown, Massachusetts 02172

AD ____________

UNCLASSIFIED
UNLIMITED DISTRIBUTION

USE OF THE HYBRID-STRESS FINITE-ELEMENT MODEL FOR THE STATIC AND DYNAMIC ANALYSIS OF MULTILAYER COMPOSITE PLATES AND SHELLS
Robert L. Spilker, Oscar Orringer, Emmett A. Witmer
Samuel Verbiese, Susan E. French, and Alex Harris,
Aeroelastic and Structures Research Laboratory,
Department of Aeronautics and Astronautics, Massachusetts
Institute of Technology, Cambridge, Massachusetts 02139

Final Report AMMRC CTR 76-29, September 1976

(ASRL TR 181-2) 214 pp, illus. tables
Contract DAAG46-75-C-0055
D/A Project 1W362306AH72
AMCMS Code: 632306.11.117200

Key Words

Finite-Element Method
Static Response
Dynamic Response
Elastic Behavior
Structural Mechanics
Stress Analysis
Laminated Plates
Fiber Composites
Shell Structures

This report presents the results of an investigation into the formulation and application of assumed-stress hybrid finite-elements for bending of multilayer laminated plates and shells. Two families of hybrid-stress-based multilayer plate elements are considered; these elements are denoted as thick plate and moderately-thick plate elements. In the development of the thick plate elements, transverse shear deformation effects are included by allowing lines normal to the plate midsurface in the undeformed state to be piecewise linear from layer to layer in the deformed state. Transverse shear deformation effects are included in an average sense in the moderately-thick plate element family by assuming that straight lines normal to the plate midsurface prior to deformation remain straight but not necessarily normal to the plate midsurface after deformation. Comparison of the results obtained by using the thick plate and moderately-thick plate elements with independent analytical results shows that the moderately-thick plate elements are more efficient and practical for the analysis of multilayer structures having a large number of elastically dissimilar layers.

For dynamic analyses, the Modal Superposition Method (MSM) is employed to obtain the timewise solution, and the Subspace Iteration Method (SIM) is adopted as an efficient scheme for calculation of the lowest few eigenvalues and eigenvectors of the assembled structure. Both the SIM and MSM are programmed as modules to be compatible with a general modular finite-element computer code for static and dynamic analysis. The advantages of this modular approach are demonstrated in a series of static and dynamic applications analyses.